Formation des aérosols organiques et inorganiques en Méditerranée

Mounir Chrit

THÈSE DE DOCTORAT DE L'UNIVERSITÉ PARIS EST

Spécialité

Science et Technologie de l'Environnement

École doctorale Sciences, Ingénierie et Environnement (Paris)

Présentée par

Mounir CHRIT

Pour obtenir le grade de

DOCTEUR DE l'UNIVERSITÉ PARIS EST

Sujet de thèse:
Formation des aérosols organiques et inorganiques en Méditerranée

Soutenue le 06 Avril 2018

devant le jury composé de:

Dr Virginie MARECAL	ENM Toulouse	Rapporteure
Dr Stéphane SAUVAGE	IMT Lille Douai	Rapporteur
Dr Matthias BEEKMANN	UPEC	Examinateur
Dr Sebnem AKSOYOGLU	Paul Scherrer Institut	Examinatrice
Dr Karine SARTELET	École des Ponts ParisTech, EDF R&D	Directrice de thèse

Résumé

Le but de cette thèse est de comprendre les origines et les processus de formation des aérosols organiques (AO) et inorganiques (AI) en Méditerranée durant différentes saisons en utilisant le modèle de chimie-transport de la plateforme de la modélisation de la qualité de l'air Polyphemus, et des comparaisons modèle-mesures.

Dans le cadre du projet de recherche ChArMEx (Chemistry-Aerosol Mediterranean Experiment), des mesures des concentrations des aérosols ainsi que de leurs propriétés ont été conduites à la station ERSA du Cap Corse (île de la Corse, France) dans le bassin ouest de la Méditerranée pendant les étés 2012 et 2013 et l'hiver 2014. Ce travail de thèse a également bénéficié de mesures effectuées durant des vols avions au sud de la France et au dessus de la Méditerranée pendant l'été 2014.

Le modèle est évalué pendant les différentes périodes simulées et des processus/paramétrisations ont été ajoutés ou modifiés afin d'avoir de bonnes comparaisons modèle/mesures, non seulement pour les concentrations, mais également pour les propriétés des aérosols. Des études de sensitivité à la météorologie, aux émissions anthropiques et aux émissions marines, en plus des différents paramètres d'entrée du modèle sont conduites pour comprendre les origines des aérosols.

Les émissions marines contribuent largement aux concentrations des AI en Méditerranée. La paramétrisation des émissions de sels marins est choisie de manière à avoir de bonnes comparaisons aux mesures de sodium, qui est un composé non volatil émis principalement par les sels marins. L'ajout au modèle d'une paramétrisation pour estimer la fraction organique des émissions marines à partir de la chlorophylle-a montre que les organiques marins contribuent à moins de 2% des AO.

L'évaluation du modèle montre l'importance de la description des émissions des bateaux pour la modélisation des concentrations du sulfate et des AO. Cependant, les hypothèses faites dans la modélisation de la condensation/évaporation ont beaucoup d'impact sur les concentrations simulées de nitrate et d'ammonium (équilibre thermodynamique, état de mélange).

Pendant les étés 2012 et 2013, les AO sont principalement d'origine biogénique, ce qui est bien reproduit par le modèle. Les mesures enregistrent d'importantes concentrations d'AO hautement oxydés et oxygénés. Pour que le modèle reproduise non seulement les concentrations, mais également les propriétés d'oxidation et d'hydrophilicité des AO, trois processus de formation d'aérosols organiques secondaires (AOS) à partir de monoterpènes sont ajoutés au modèle: l'autoxidation qui induit la formation de composés organiques d'extrêmement faible volatilité, un mécanisme de formation du nitrate organique, et un mécanisme de formation d'un produit d'oxydation de deuxième génération. Les états d'oxydation et d'oxygénation des AO à Ersa sont bien simulés en supposant de plus la formation d'organosulfates.

Des simulations hivernales montrent que les AO y sont principalement d'origine anthropique. Bien que les émissions des composés organiques semi-volatils et de volatilité intermédiaire (COVIS) qui sont manquants dans les inventaires d'émissions influencent peu les AO en été, leur influence est dominante en hiver. La contribution du secteur du chauffage résidentiel pendant la saison froide s'avère très importante. Différentes descriptions et paramétrisations des émissions et des schémas de vieillissement des COVIS sont ajoutées au modèle, c-à-d distribution de volatilité à l'émission, schéma à une étape d'oxydation vs schéma à plusieurs étapes d'oxydation et la prise en compte de composés organiques volatils non-traditionnels (COVNT). Bien que le modèle reproduise bien les concentrations des AO, les études de sensibilité révèlent que la distribution de volatilité à l'émission influence beaucoup les concentrations des AO. Néanmoins, les états d'oxydation et d'oxygénation des ces derniers restent sous-estimés par le modèle pendant l'hiver quelquesoit la paramétrisation utilisée, ce qui suggère la nécessité d'ajouter au modèle d'autres mécanismes de formation des AOS à partir des précurseurs anthropiques (autoxidation, formation du nitrate organique).

Abstract

This work aims at understanding the origins and processes leading to the formation of organic aerosols (OA) and inorganic aerosols (IA) over the western Mediterranean Sea during different seasons, using the air-quality model Polyphemus, and model to measurement comparisons. In the framework of ChArMEx (the Chemistry-Aerosol Mediterranean Experiment), measurements of both aerosol concentrations and properties are performed at a remote site (Ersa) on Corsica Island in the northwestern Mediterranean sea in the summers 2012, 2013 and the winter 2014. This thesis also benefits from measurements performed during flights above the western Mediterranean Sea in the summer 2014. The model is evaluated during these periods, and different processes/parameterizations are added or modified in order to have good model-to-measurements comparisons, not only of aerosol concentrations but also of their properties. Origins of aerosols are assessed through different sensitivity studies to the meteorological model, anthropogenic emissions inventory, sea-salt emissions and different input models.

The contribution of marine emissions to inorganic aerosols (IA) is important, and the parameterization of sea-salt emissions is chosen such as having good comparisons to sodium measurements, which is a non-volatile compound emitted mainly by sea salts. Marine organic aerosols (OA), which are added to the model with a parameterization that uses the chlorophyll-a concentration as a proxy parameter to model the marine chemistry, contribute to OA by only 2% at the maximum.

The ground-based and airborne model-to-measurements comparisons show the importance of an accurate description of shipping emissions to model sulfate and OA concentrations. However, this is not true for nitrate and ammonium concentrations, which are very dependent on the hypotheses used in the model for condensation/evaporation (thermodynamic equilibrium, mixing state).

During the summers 2012 and 2013, OA concentrations are mostly of biogenic origin, which is well reproduced by the model. Measurements show important concentrations of highly oxidized and oxygenated OA. For the model to reproduce not only the concentrations but also the oxidation and hydrophilicity properties of OA, three processes to form secondary organic aerosols (SOA) from monoterpenes are added to the model: the autoxidation process leading to the formation of extremely low volatility organic compounds, the organic nitrate formation mechanism and the second generational ageing. The high oxidation and oxygenation states of OA at Ersa are well modeled when organosulfate formation is also assumed.

Winter simulations show that OA are mainly of anthropogenic origin. The influence of the anthropogenic intermediate/semi-volatile organic compound (ISVOC) emissions, which are missing from emission inventories, is low in summer. Nonetheless, the role and the contribution of ISVOC appear very significant during the winter, with a large contribution from residential heating. Different parameterizations to represent the emissions and the ageing of ISVOC are implemented in the model, namely the volatility distribution of emissions, single-step vs multi-step oxidation scheme and non-traditional volatile organic compounds (NTVOC) chemistry. Sensitivity studies show that the volatility distribution at the emission is a key parameter to improve the modeling of OA concentrations. The model reproduces well the observed concentrations, but the observed organic oxidation and oxygenation states are strongly under-estimated, stressing the potential role of autoxidation and organic nitrate from anthropogenic precursors.

Sommaire

Chapitre 1

Introduction

Sommaire

1.1 Les aérosols

L'atmosphère désigne la fine couche de gaz qui enveloppe la Terre et qui permet d'y préserver la vie. Elle est principalement constituée d'azote (environ 78%), d'oxygène (environ 21%) et de vapeur d'eau (environ 0.33%), mais contient également d'autres espèces traces, comme par exemple certains gaz à effet de serre. En outre, l'atmosphère contient aussi des particules atmosphériques. Nous décrivons dans cette section l'impact de ces particules (section1.1.2) ainsi que leurs origines et compositions chimiques (section1.1.3).

1.1.1 Généralités

Les particules atmosphériques sont des petites particules de matière solide ou liquide, en suspension dans l'atmosphère. Elles se caractérisent par leur distribution en taille, en forme et en composition chimique. Ces particules et leurs origines peuvent ainsi être classées de plusieurs faiçons. Les particules sont dites primaires lorsqu'elles sont directement émises dans l'atmosphère en tant que telles. Il s'agit, par exemple, des sels marins, des poussières minérales et du carbone élémentaire (ou black carbon, noté BC). Les particules dites secondaires sont formées dans l'atmosphère par des réactions chimiques qui peuvent avoir lieu en phase aqueuse, en phase gazeuse, ou de manière hétérogène à la surface des particules ou des gouttelettes, mais également en phase particulaire. Elles comprennent notamment des composés inorganiques (sulfate, nitrate, ammonium, chlore, sodium ...), des composés organiques (formés par l'oxydation de nombreux composés organiques volatils et semi-volatils émis dans l'atmosphère), des poussières et du carbone élémentaire.

1.1.2 Impacts des particules

L'étude des aérosols se justifie par leur impacts sur: le climat, la santé et la qualité de l'air extérieur et intérieur, les impacts sur les écosystèmes, sur la visibilité, la détérioration des monuments, etc. Nous présentons ici succinctement les deux premiers.

Impact sur le climat

L'impact des aérosols sur le climat est aujourd'hui reconnu mais encore mal appréhendé (IPCC, 2013). Les aérosols, selon leur nature chimique ou leur diamètre, vont absorber ou diffuser le rayonnement solaire et occasionner différents types de forçages radiatifs (Bouvier, 2012) :
+ Effet direct. La rétrodiffusion vers l'espace du rayonnement solaire incident cause en moyenne un refroidissement du système climatique et une diminution de l'évaporation à la surface, moins éclairée (effet parasol).
+ Effets indirects. Les aérosols vont servir de noyau de condensation pour la vapeur d'eau et constituer des nuages. Les propriétés physiques et optiques des nuages vont dépendre de la nature et du nombre d'aérosols. L'augmentation du nombre de noyaux de condensation, notamment du fait de la présence d'aérosols de pollution en milieu marin, disperse la vapeur d'eau condensée sur d'avantage de gouttes, plus nombreuses et plus petites, ce qui augmente l'albédo des nuages et la durée de vie des gouttelettes, accentuant l'effet de refroidissement du système climatique et de ralentissement du cycle de l'eau. Un autre effet concerne le dépôt d'aérosols absorbants sur la neige ou sur la glace. Celles-ci vont devenir plus absorbantes, et vont réchauffer le système climatique.
+ Effet semi-direct. Les aérosols absorbants vont, quant à eux, générer un réchauffement dans la couche de l'atmosphère où ils sont présents, susceptible de limiter la formation des nuages.

A la différence des gaz à effet de serre, de fortes incertitudes sont associées à l'estimation du forçage radiatif induit par les aérosols. Ces incertitudes sont le reflet d'une forte variabilité spatio-temporelle dans la distribution des aérosols liée à leur courte durée de vie, à la disparité de leurs sources/puits et à leurs transformations dans l'atmosphère. Elles sont également dues à la difficulté d'appréhender les différents types d'effets, notamment semi-direct et indirects. Elles justifient la poursuite des efforts concernant la caractérisation des aérosols et de leurs impacts radiatifs. Le dernier rapport du GIEC (IPCC 2013) et en particulier la figure 1.1 confirme la complexité des impacts des aérosols sur le forçage radiatif terrestre, avec un forçage positif ou négatif selon leur nature chimique.

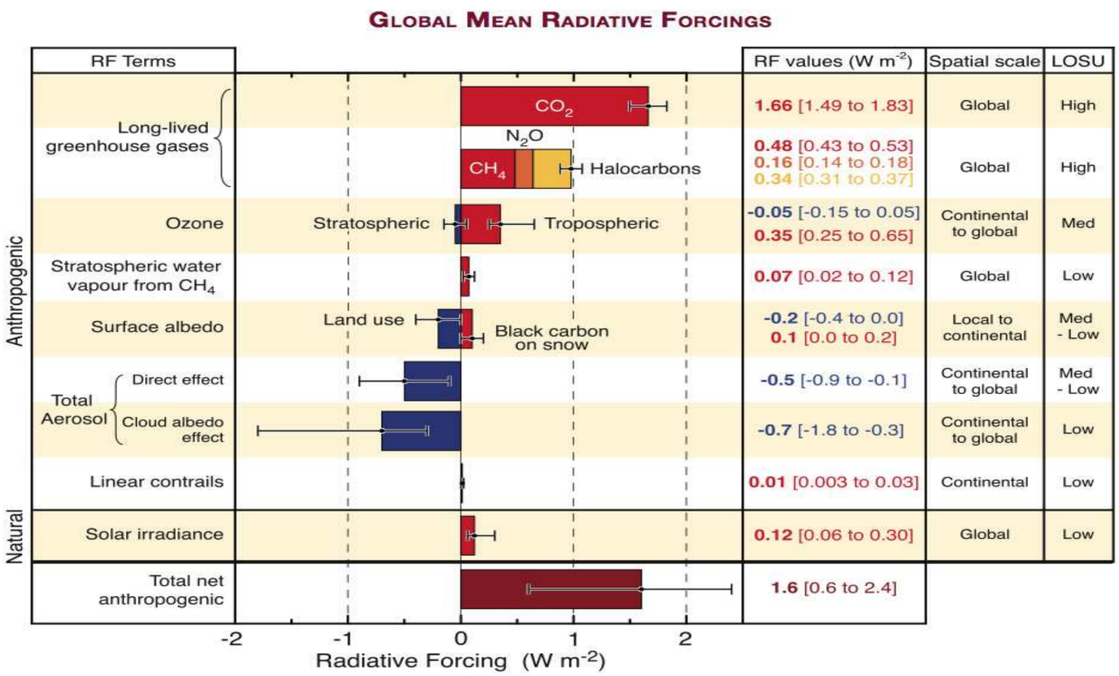

Figure 1.1: Forçage radiatif d'origine anthropique (et degré de confiance sur ces estimations) induit par différents types de composés traces de l'atmosphère (IPCC, 2013)

Sans forcément vouloir aller très loin dans la description des interactions aérosols-climat, la figure ci-dessus cache de fortes disparités au niveau régional qui sont le reflet de la forte hétérogénéité de la distribution spatiale des aérosols. Ainsi, dans certaines zones du globe où la charge des aérosols est particulièrement forte (comme c'est le cas en Méditerranée), leur impact sur le climat régional sera donc particulièrement fort, surpassant le réchauffement induit par les gaz à effet de serre.

Impacts sanitaires

En raison de leur taille, de leur forme et de leur nature chimique, les aérosols ont un impact avéré sur la santé humaine (Pope, 2000; Aphekom, 2011). Plus leur diamètre est petit, plus ils peuvent pénétrer profondément dans le système respiratoire humain, altérer les cellules, voire s'insérer dans la circulation sanguine. En octobre 2013, la pollution atmosphérique extérieure a été classée cancérigène (cancers du poumon et de la vessie) par le Centre International de Recherche sur le Cancer, imputant sa responsabilitéé dans le décès de 223 000 personnes en 2010 à travers le monde. Cette qualité de l'air extérieure impacte ensuite la qualité de l'air à l'intérieur des habitations. Pour ces raisons, des normes européennes réglementent aujourd'hui les concentrations de PM.

Les stratégies de réglementation de la pollution particulaire pourraient être plus efficaces si l'on parvenait à identifier des indicateurs directement reliés aux composés les plus toxiques des aérosols. Une voie de toxicité des particules est liée au stress oxydant. C'est un processus qui modifie l'équilibre redox pulmonaire soit en apportant directement des espèces réactives de l'oxygène (ROS) véhiculées par les particules, soit des espèces qui par leurs interactions avec notre organisme vont induire leur formation. Ce potentiel oxydant des particules semble être un facteur clé à l'origine des effets pathologiques dus à l'exposition à la pollution atmosphérique (Cho et al., 2005; Rattanavaraha et al., 2011). Il dépend de la composition chimique des particules (et est particulièrement élevé pour les composés organiques et des métaux traces), ainsi que des propriétés physiques des particules (taille, forme, etc) (Ayres et al., 2008; Goix et al., 2014; Jiang et al., 2016).

1.1.3 Origine et composition chimique des particules

Les particules peuvent être classées en fonction de leur source et de celle de leurs précurseurs. Parmi elles, il y a lieu de distinguer les sources naturelles des sources anthropiques. Les sources naturelles comprennent les émissions par l'océan, les sols, les volcans, les feux ou encore la végétation. Les sources anthropiques comprennent, quant à elles, la combustion des combustibles fossiles (charbon, pétrole), des biocarburants (agrocarburants, bois, déchets d'animaux), des feux de végétation provoqués par l'Homme, ainsi que des activités agricoles et industrielles.

Les particules peuvent également être classées "spatialement" car leurs caractéristiques peuvent varier sensiblement et de façon cohérente en fonction de leur environnement: on peut parler par exemple des particules urbaines, périurbaines, continentales, désertiques, marines, volcaniques, ou encore stratosphériques. Cependant, ces distinctions ne sont pas forcément rigoureuses. En effet, la durée de vie des particules étant généralement de plusieurs jours, elles sont transportées sur de longues distances durant ce temps et peuvent donc changer d'environnement.

Enfin, les particules peuvent être classées en fonction de leur taille. Elles sont alors notées PM_x , où x définit leur diamètre aérodynamique maximal en μm. On distingue notamment : les particules ultrafines, ou nanoparticules ($PM_{0.1}$), les particules très fines ($PM_{1.0}$), les particules fines ($PM_{2.5}$), et les PM_{10}, qui regroupent les particules fines et une partie des particules grossières ; certaines particules grossières pouvant avoir un diamètre aérodynamique supérieur à 10 μm. Les particules primaires sont principalement grossières, tandis que les particules secondaires sont principalement fines.

La composition chimique des particules dépend de leur environnement. Par exemple, à la station de fond urbaine de Villemomble, située dans la petite couronne de la région parisienne, les $PM_{2.5}$ sont composées de sels marins (3%), sulfate (13%), nitrate (19%), ammonium (10%), matière organique (39%), carbone élémentaire (BC, 8%), particules minérales (3%), autres ions (1%), les 4% restant étant non déterminés (Airparif, 2011).

1.2 Les modèles de chimie transport

Au début du XXe siècle, la combinaison de la fumée (smoke) et du brouillard (fog) a été observée et appelée smog. Ce smog était dû à la combustion du charbon et aux émissions des usines chimiques. Le grand smog de Londres du 5 au 9 décembre 1952 pourrait avoir causé jusqu'à 12 000 morts. La pollution due au charbon et aux usines émettant du dioxyde de soufre (SO_2) et en présence de brouillard est communément appelée le smog. L'utilisation généralisée de l'automobile et l'augmentation de l'activité industrielle ont augmenté la prévalence d'un autre type de pollution de l'air: le smog photochimique. Cette pollution était formée presque quotidiennement à Los Angeles, en Californie aux États-Unis. Elle est devenue si grave qu'un organisme, "Air Pollution Control District", a été formé à Los Angeles en 1947 pour lutter contre ce fléau. La composition du smog photochimique a été élucidée en 1951, quand Arie Haagen-Smit, professeur de biologie (chimie bio-organique) au California Institute of Technology (Caltech), a produit de l'ozone dans un laboratoire à partir d'oxydes d'azote et de gaz organiques réactifs, en présence de lumière et a suggéré que les gaz produits étaient les principaux constituants de la pollution atmosphérique à Los Angeles. Le smog photochimique a été observé dans la plupart des villes du monde. Suite aux travaux de laboratoire menés dans les années 1950 pour mieux comprendre la formation du smog photochimique, des modèles "boîte" pour simuler des réactions chimiques dans l'atmosphère ont été mis en œuvre. Dans les années 1960 et 1970, les modèles de pollution atmosphérique, appelés modèles de qualité de l'air, ont été élargis à deux et trois dimensions (Jacobson, 2005). Les modèles de qualité de l'air sont des implémentations numériques de modèles mathématiques de la physico-chimie de l'atmosphère qui décrivent l'évolution des polluants atmosphériques.

L'évolution de la concentration de polluants est donnée par une équation de type advection-diffusion-réaction, i.e., l'équation de dispersion réactive. L'advection correspond au transport par le champ de vent, la diffusion au mélange turbulent et la réaction aux processus physico-chimiques des transformations des polluants. Les modèles numériques tridimensionnels qui résolvent cette équation sont généralement appelés modèles de chimie-transport (CTM, Chemical-transport models). Les CTM sont utilisés de manière opérationnelle pour la prévision de qualité de l'air (e.g., PREV'AIR, ESMERALDA, AIRPARIF, AIRNOW, etc). Ils permettent également de tester l'impact de mesures affectant la qualité de l'air. Ils sont largement utilisés par les organismes (EEA, AASQA, US EPA, NOAA, NCAR, etc) chargés de lutter contre la pollution à la fois pour identifier la contribution de différentes sources aux problèmes de qualité de l'air et pour contribuer à la conception de stratégies efficaces pour réduire les concentrations de polluants atmosphériques nocifs. Les CTM peuvent également être utilisés pour prédire les concentrations futures de polluants après la mise en œuvre d'un nouveau programme de réglementations, afin d'estimer l'efficacité du programme pour réduire les concentrations (étude de prospective).

1.2.1 Les processus modélisés

On cherche à décrire l'évolution dans l'atmosphère de la concentration d'un ensemble d'espèces chimiques, radioactives ou biologiques, qui réagissent éventuellement entre elles. En toute rigueur, l'évolution du système couplé (fluide et espèces) est donnée par les équations de Navier-Stokes réactives. On parle alors de modèle intégré on line (MM5-CHEM (Grell et al., 2000), WRF-CHEM (Grell et al., 2005), GEM-MACH (Mnard, 2007), GATOR-GCMM (Jacobson, 2001), etc). Ce système de modélisation intégré permet de prendre en compte les rétroactions de la météorologie avec les constituants chimiques. Une approche plus commune parce que plus simple consiste à résoudre séparément la dynamique du fluide et les concentrations chimiques. Ce système de modélisation est appelé en série ("one-way") car la météorologie influence les concentrations des espèces chimiques mais la réciproque n'est pas vraie. Dans le cadre de l'approche en série, les champs dynamiques (vent, température, densité et humidité de l'air, diffusion, etc.) sont donc paramétrisés ou précalculés indépendamment par un code météorologique. Ils sont ensuite utilisés comme données d'entrée dans l'équation de dispersion pour les espèces étudiées. On parle souvent de couplage "off line" (e.g., CMAQ (Byun and Schere, 2006), CAMx (Morris et al., 2003), Chimere (Bessagnet et al., 2008), Polyphemus (Mallet et al., 2005), etc) (Sportisse, 2008). Les systèmes de modélisation "on line" ou "off line" comprennent les processus qui pilotent l'évolution des espèces ; ceux-ci sont présentés dans la figure 1.2.

Les CTM reconstituent l'information de la composition chimique de l'air en tout point d'une grille maillant le domaine d'étude grâce à la résolution des équations mathématiques pour reproduire les processus physiques et chimiques qui décrivent les phénomènes liés au transport, aux réactions en phase gazeuse et particulaire, ainsi qu'aux dépôts sec et humide. Les modèles découlent d'un système d'équations aux dérivées partielles décrit dans l'équation 1.1 et appelé plus communément équation d'advection-diffusion-réaction. Cette équation décrit le cycle de vie d'une espèce chimique i et représente les phénomènes physico-chimiques. L'évolution spatio-temporelle de la concentration de cette espèce i est:

$$\frac{\partial c_i}{\partial t} = -\underbrace{div(Vc_i)}_{Advection} - \underbrace{div(\overline{V'c'_i})}_{Diffusion} + \underbrace{\chi_i(c_i)}_{Réaction} + S_i - R_i \tag{1.1}$$

où c_i est la concentration de l'espèce i en moyenne, c'_i est la pertubation de la concentration de l'espèce i, V le champ de vent moyen, V' des perturbations du vent moyen, χ_i les réactions chimiques associées à l'espèce considérée, S_i le terme source (émission naturelle ou liée à une activité humaine) et R_i le terme perte (dépôts secs et humides). Le terme d'advection $div(Vc_i)$ représente le transport tridimensionnel par le vent, le terme de diffusion $div(\overline{V'c'_i})$ régit principalement le transport vertical en limite de zone de convection. Les quatre principaux modules qui constituent les CTM sont maintenant présentés en détails.

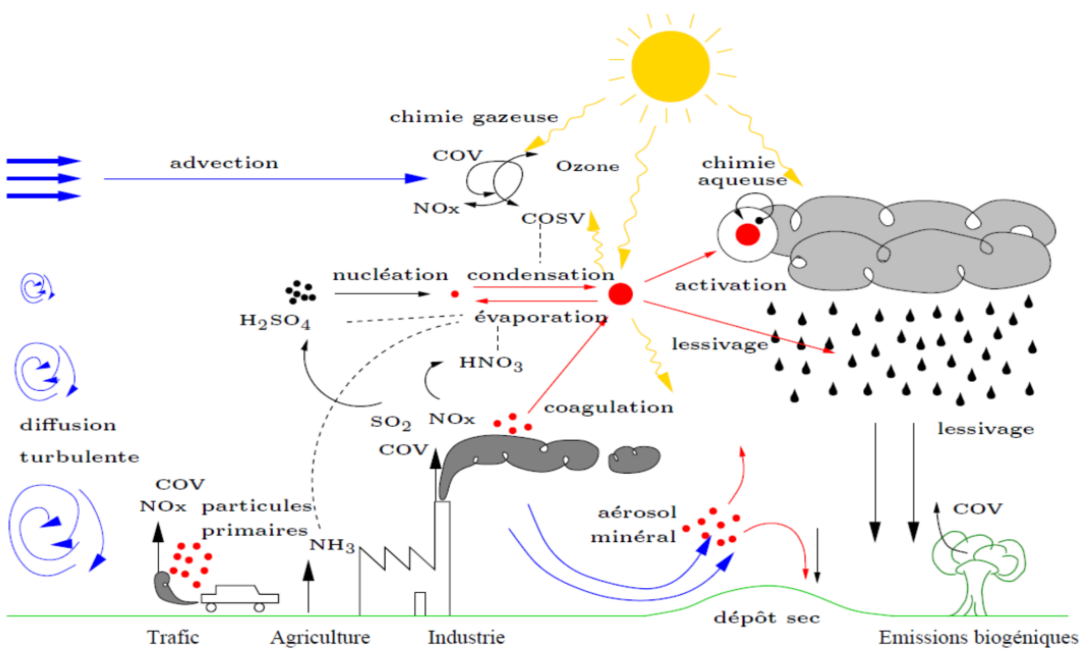

Figure 1.2: Processus décrits dans un modèle de chimie-transport (Sportisse, 2008)

Transport

Lorsqu'il s'agit du transport de polluants, on distingue généralement le transport dû à la convection thermique (diffusion) et celui dû aux vents (advection). Les principales composantes du vent sont horizontales. Dans la couche limite atmosphérique (CLA) - la partie de la troposphère directement soumise à l'influence de la surface terrestre et surtout du cycle diurne - les vents horizontaux sont typiquement de l'ordre de 2 à 10 m.s^{-1}. En revanche, les vents verticaux sont très faibles et habituellement de l'ordre de quelques millimètres à quelques centimètres par seconde (Stull, 1988). Ils sont donc généralement négligeables par rapport à la turbulence quand la surface est plate et uniforme.

Turbulence On peut représenter les mouvements turbulents par des tourbillons qui ont des dimensions couvrant un large spectre de taille et dont l'amplitude peut aller jusqu'à la hauteur de la couche limite (entre 100 et 3000 mètres). La turbulence naît d'une part de l'agitation de l'air due au frottement avec le sol (effet de cisaillement) : i.e., la turbulence mécanique. D'autre part, son origine peut être également le gradient vertical de température qui lui-même dépend des capacités d'absorption du rayonnement solaire par la surface. Le réchauffement au sol élève les masses d'air réchauffées au contact du sol : i.e., la turbulence thermique.

Fermeture turbulente Le nombre d'inconnues dans l'ensemble d'équations pour un écoulement turbulent est plus grand que le nombre d'équations. Quand les équations sont incluses pour ces inconnues, on découvre encore davantage de nouvelles inconnues. Donc, la description de la turbulence n'est pas fermée. Les paramétrisations utilisés afin de fermer les equations turbulentes sont classifiées par leur ordre (premier, second, etc.). Une paramétrisation qui a le premier ordre de la fermeture, utilise l'approximation des variables turbulentes ayant la double corrélation (e.g., $\overline{V'c_i'}$ où V' représente les perturbations du vent, c_i' est la perturbation des concentrations de l'espèce i et $\overline{V'c_i'}$ est la moyenne de $V'c_i'$). Les paramétrisations sont classifiées aussi comme la fermeture locale (une inconnue à un point paramétrisée par les valeurs connues à ce point) et la fermeture nonlocale (une inconnue à un point paramétrisée par les valeurs connues à plusieurs points). Si on utilise le premier ordre et la fermeture locale pour fermer le terme de diffusion dans l'equation 1.1, une fermeture possible et simple est:

$$\overline{V'c_i'} = -\rho K \nabla \frac{c_i}{\rho} \tag{1.2}$$

où ρ est la densité de l'air, K est une matrice de diffusion turbulente et c_i est la concentration moyenne. Si on reporte l'équation 1.2 dans l'équation 1.1, on obtient:

$$\frac{\partial c_i}{\partial t} = -\underbrace{div(Vc_i)}_{Advection} + \underbrace{div(\rho K \nabla \frac{c_i}{\rho})}_{Diffusion} + \underbrace{\chi_i(c_i)}_{Réaction} + S_i - R_i \tag{1.3}$$

La matrice K est prise diagonale : on note en général Kx, Ky et Kz les termes associés à la diffusion turbulente selon les directions x, y et z, respectivement. Les termes de diffusion horizontaux sont a priori négligeables par rapport à l'advection. Donc, on ne prend souvent en compte que la diffusion verticale, décrite par Kz. La diffusion verticale Kz est prépondérante et doit être paramétrisée en fonction de l'écoulement.

Photochimie

$\chi_i(c_i)$ dans l'équation 1.3 est le terme du bilan des productions et pertes par réactions chimiques de l'espèce i.

$$\chi_i(c_i) = P_i - L_i(c_i) \tag{1.4}$$

où c_i est la concentration de l'espèce i, P_i et L_i sont respectivement les termes de production et consommation (qui dépendent de l'ensemble des réactions). L_i est proportionnel à c_i (et parfois à c_i^2). En raison des nombreuses réactions et espèces chimiques impliquées dans la chimie atmosphèrique, un mécanisme cinétique chimique complet et détaillé n'est pas envisagé pour des simulations de qualité de l'air. Par conséquent, on utilise souvent un ensemble de réactions simplifié pour les espèces chimiques considérées. Le nombre des réactions dans les mécanismes peut varier de quelques centaines à plusieurs milliers. Les mécanismes chimiques avec quelques centaines de réactions sont souvent adaptés pour la formation des polluants atmosphériques dans les CTM. La production photochimique d'ozone résulte de la photo-oxydation des composés organiques volatils (COV) en présence de NO_x. La seule réaction de production de l'ozone est donnée par:

$$O_2 + O \rightarrow O_3 \tag{1.5}$$

Dans la troposphère, la source disponible d'oxygène atomique est la dissociation photolytique de NO_2,

$$NO_2 + h\nu(300nm \leq \lambda \leq 400nm) \rightarrow NO + O \tag{1.6}$$

L'oxydation des COV par OH va conduire à la formation des radicaux péroxyles (RO_2) qui oxydent NO en NO_2. Cette chaine contibue à la formation d'ozone par la formation de NO_2.

$$COV + OH \xrightarrow{O_2} RO_2 + H_2O \tag{1.7}$$

$$RO_2 + NO \rightarrow RO + NO_2 \tag{1.8}$$

où RO_2 et RO sont des radicaux organiques péroxyles et alcoxyle.

Il existe un grand nombre de COV dans la nature avec différentes vitesses de réaction par rapport à OH et des nombres de carbones et structures différents. La méthode de la classification des COV dans le mécanisme est importante et elle permet de diversifier le caractère des mécanismes. Par exemple, dans un mécanisme d'espèces moléculaires regroupées, un composé organique particulier ou une espèce chimique suppléante ("surrogate species") est utilisée afin de représenter plusieurs composés organiques de la même classe. Mais dans un mécanisme de structures regroupées, les composées organiques sont divisés en plus petits éléments (groupes fonctionnels) basés sur les types de liaisons carbones ("carbon-bond") dans chaque espèce. L'évolution de ces groupes fonctionnels lors de l'oxydation des COV est alors représentée afin de reproduire l'évolution de la composition chimique organique (section 1.4).

Dépôts

On dit que les polluants se déposent au sol lorsqu'ils sont absorbés par l'eau, le sol ou la végétation. Ce phénomène constitue un terme de perte. Son intensité dépend des polluants, des conditions météorologiques, du rayonnement, du lieu (type et densité de végétation), de la saison (état de la végétation). Le dépôt est plus fort en journée et il est accru par le rayonnement qui augmente le transport vertical turbulent. Au-dessus des masses d'eau, il croît avec la solubilité de l'espèce considérée.

Dépôt sec Le flux de dépôt sec est directement proportionnel la concentration au-dessus du sol de l'espèce qui se dépose.

$$F = -v_d C \tag{1.9}$$

où F représente le flux vertical de dépôt sec, i.e. la quantité de matière qui se dépose par unité de surface et unité de temps. La constante de proportionnalité, v_d, entre le flux et la concentration C a des unités de longueur par unité de temps et est appelée la vitesse de dépôt. Puisque C est une fonction de la hauteur z au-dessus du sol, vd est également une fonction de z et doit être liée à une hauteur de référence à laquelle C est spécifiée (Seinfeld and Pandis, 2006a). L'approximation classique consiste en une analogie électrique où apparait une résistance de transfert, composée de trois résistances en série :

$$v_d = \frac{1}{R_a + R_b + R_c} \tag{1.10}$$

où R_a est la résistance aérodynamique, R_b la résistance de couche quasi-laminaire et R_c la résistance de surface (végétation, sol, eau, etc.) (Wesely, 1989; Sportisse, 2007).

Dépôt humide On qualifie de dépôt humide ou de lessivage la perte due aux transferts de masse avec la phase aqueuse (nuages ou pluies). Les polluants solubles peuvent pénétrer les gouttes de pluie lors de leur chute et sont ainsi précipités au sol (below-cloud scavenging). Le taux de transfert d'un gaz à la surface d'une goutte en suspension ou en chute libre peut être calculée par

$$W_t(z,t) = K_c(C_g(z,t) - C_{eq}(z,t)) \tag{1.11}$$

où K_c est le coefficient de transfert de masse des espèces (m/s), C_g est la concentration de l'espèce dans la phase gazeuse, et C_{eq} est la concentration de l'espèce à la surface des gouttes en équilibre avec la concentration en phase aqueuse du gaz dissous (Seinfeld and Pandis, 2006a). Une autre forme de lessivage a lieu dans les nuages où les polluants solubles ont des échanges (transferts de masse) avec les gouttes d'eau (in-cloud scavenging). Les gaz comme HNO_3, NH_3 et SO_2 peuvent être dissous partiellement dans les gouttes des nuages. Le taux local du lessivage d'un gaz soluble avec la concentration C_g est donnée par

$$W_{ic} = \Lambda C_g \tag{1.12}$$

où Λ est le coefficient de lessivage (s^{-1}). Pour le lessivage d'un gaz très soluble comme HNO_3 dans un nuage typique, Λ est une fonction de K_c et de la distribution des gouttes de nuage. Par contre, pour un gaz modérément soluble comme SO_2, il faut tenir compte des variables supplémentaires pour calculer Λ (e.g., le pH). Le lessivage des particules est une fonction des tailles des particules et des tailles des gouttes de pluie (Seinfeld and Pandis, 2006a; Duhanian and Roustan, 2011).

Aérosol

L'évolution de la distribution en taille et de la compostion chimique des aérosols est gouvernée par de nombreux processus (Debry et al., 2007a).

Nucléation De très petits aérosols, de diamètre de l'ordre du nanomètre, se forment à partir de l'agrégation de molécules gazeuses menant à des agrégats stables thermodynamiquement. Le mécanisme et les espèces en jeux ne sont pas encore bien élucidés et des paramétrisations sont nécessaires pour représenter la nucléation binaire homogène de l'acide sulfurique et de l'eau (H_2O-H_2SO_4) ou la nucléation ternaire en incluant l'ammoniac (H_2O-H_2SO_4-NH_3) (Zhang et al., 2010b,a).

Condensation/évaporation Des composés gazeux à faible pression de vapeur saturante peuvent condenser sur les aérosols existants. A l'inverse, des composés condensés dans la matière particulaire peuvent s'évaporer. Ce transfert de masse est déterminé par le gradient entre la concentration moyenne en phase gazeuse et la concentration de l'espèce gazeuse à la surface des particules qui est en équilibre thermodynamique avec la concentration de l'espèce considérée (Pilinis et al., 2000).

Coagulation La coagulation des aérosols est principalement brownienne, c'est-à-dire elle est due à l'agitation thermique des aérosols. D'autres processus (turbulence, force de van der Waals et thermophorèse) ne sont importants que dans des cas particuliers. La coagulation est souvent négligée parce que son effet sur la distribution en masse est petit par rapport à l'effet de la condensation/évaporation loin des sources de particules. Mais la coagulation peut avoir un impact substantiel sur la distribution en taille pour les particules ultrafines après leur génération (Finlayson-Pitts and Pitts, Jr., 2000).

1.2.2 les entrées du modèles

De nombreuses données d'entrées sont nécessaires pour initier les processus précédemment exposés. Les résultats de simulation sont très sensibles à certaine de ces données. Or la plupart d'entre elles sont fortement entachées d'incertitudes. Elles jouent donc un rôle important dans la qualité des résultats. Certaines données d'entrée sont fixes et d'autres données varient dans l'espace et le temps. Les principales données sont listées dans cette section.

Données topographiques

Les données topographiques sont fixes dans l'espace et le temps. Elles sont utilisées pour spécifier la hauteur géopotentielle à la surface.

Occupation des sols

L'occupation des sols, souvent appelé avec l'acronyme anglais LUC (Land use cover), décrit les différents types de terrain, souvent avec une résolution de l'ordre du kilomètre carré. Cette donnée permet de distinguer les terres des étendues d'eau. Sur terre, plusieurs types de terrain sont aussi identifiés, selon le type de culture agricole, le type de forêt, l'étendue urbaine. L'occupation des sols est aussi utilisée pour estimer la longueur de rugosité de surface pour la vitesse du vent, la chaleur spécifique du sol, la densité du sol, la porosité du sol, etc. Elle peut varier avec le mois ou la saison.

Données chimiques

Constantes cinétiques de réaction Les constantes cinétiques de réaction des mécanismes chimiques sont de deux natures. Il y a d'une part les réactions dont les constantes sont estimées à partir de quelques coefficients et quelques variables météorologiques (température T et pression), un exemple concerne les réactions dont les constantes suivent la loi d'Arrhenius.

$$k = Ae^{\frac{-E_a}{RT}} \tag{1.13}$$

où k est le constant cinétique, A le facteur pré-exponentiel, E_a l'énergie d'activation et R la constante des gaz parfaits. Ces données incluent les coefficients uni-, bi- et termoléculaire pour les réactions en phase gazeuse ou en phase aqueuse et aussi les données de coefficients d'équilibre pour les réactions réversibles. D'autre part, il faut estimer les constantes photolytiques. La section efficace d'absortion et le rendement quantique sont utilisés pour calculer les constantes photolytiques des gaz et liquides.

Coefficients d'activité Le coefficient d'activité est un facteur utilisé en thermodynamique pour rendre compte de l'activité d'une substance chimique dans un mélange de substances chimiques. Le coefficient d'activité est utilisé dans les CTM pour simuler la chimie particulaire pour la formation d'aérosol secondaire (voir Section 1.4).

Émissions

Les émissions biogéniques sont issues de la biomasse. On considère que les polluants sont émis à la surface. Les principaux polluants concernés sont l'isoprène, les terpènes et le monoxyde d'azote. Bien qu'une grosse partie des émissions en Europe proviennent des activités humaines, les émissions naturelles, y compris biogéniques, peuvent être importantes selon les saisons. Par exemple, les émissions de soufre en Italie sont dominées par des sources volcaniques, les émissions de COV dans la région méditerranéenne sont dominées par les émissions provenant de forêts pendant l'été, et les émissions de méthane en Scandinavie par les zones humides (Simpson et al., 1999). Le traitement des émissions anthropiques diffère selon les données disponibles. A l'échelle européenne, ces émissions sont fournies par l'organisme européen, European Monitoring and Evaluation Programme (EMEP) sur un maillage de 50 km par 50 km sous forme de taux annuels pour les catégories de polluants NO_x, COV, PM, NH_3, SO_2 et CO, et pour dix types d'émetteurs (dont le trafic et diverses industries) réparties en classes SNAP (Selected Nomenclature for Air Pollution). Les émissions sont réparties temporellement par mois, par type de jour, et puis par heure. Les facteurs appliqués dépendent du pays et de la classe SNAP. Une répartition verticale peut aussi être appliquée, surtout pour les émissions des cheminées d'usine, les émissions volcaniques et les feux de végétation.

Données météorologiques

Pour mener à bien une simulation, il faut disposer d'une vingtaine ou d'une trentaine de variables météorologiques. Parmi les plus importantes, on trouve bien sûr le vent, la température, les flux de surface, la hauteur de couche limite ou encore l'intensité du rayonnement solaire. Les modèles météorologiques ne proposent pas toujours les variables nécessaires à la simulation. En conséquence, quelques paramétrisations sont proposées pour diagnostiquer les variables indisponibles (diffusion verticale, atténuation du rayonnement, longueur de Monin-Obukhov, etc.).

Concentrations de polluants

Les concentrations de polluants sont nécessaires pour initialiser les simulations et surtout pour fournir des conditions aux limites du domaine de modélisation. Par exemple, les simulations à l'échelle régionale utilisent généralement des concentrations issues d'un modèle de chimie transport global.

1.2.3 Incertitudes du modèle

L'incertitude correspond aux variations des concentrations en sortie du CTM. Elle est estimée indépendamment des observations. L'origine de l'incertitude est triple (Mallet and Sportisse, 2006):

+ les données d'entrées (occupation des sols, inventaires d'émissions, champs de forage météorologiques, constantes cinétiques de réaction, etc).
+ les paramétrisations physiques ou chimiques (vitesse de dépôt, émissions biogéniques, fermeture turbulente, etc).
+ les approximations numériques (maillage, pas de temps, mécanisme chimique réduit, etc).

Selon des études précédentes, la fermeture turbulente, le mécanisme chimique et la formulation de la vitesse de dépôt introduisent la plus grande incertitude pour l'ozone (Mallet and Sportisse, 2006; Tang et al., 2011). Par ailleurs, le mélange vertical par la fermeture turbulente et le choix des niveaux verticaux a un grand impact sur les concentrations de nombreux polluants (O_3, NO_2, SO_2, NH_3 et PM) (Roustan et al., 2010a).

Incertitudes liées aux mécanismes chimiques

Les mécanismes chimiques utilisés dans les CTM sont simplifiés, ils ne prennent pas en compte toutes les espèces chimiques. Les mécanismes chimiques peuvent être conçus dans des buts différents. Par exemple, un mécanisme est conçu pour être utilisé uniquement dans la couche limite atmosphérique, tandis qu'un autre est développé pour simuler la chimie dans toute la troposphère et la basse stratosphère. De plus, les mécanismes simplifiés utilisent des hypothèses différentes pour l'agrégation des COV (voir Section 1.4). La formation des espèces intermédiaires, e.g., des radicaux péroxyles, est fortement influencée par ces hypothèses ainsi que la formation des polluants secondaires (O_3 et PM). En revanche, les différences entre les mécanismes sont très limitées dans les zones rurales, où la chimie est principalement contrôlée par les espèces minérales dont la chimie varie peu d'un mécanisme à l'autre (Gross and Stockwell, 2003). Les mécanismes sont évalués par des études en chambre atmosphérique pour les cinétiques et les coefficients stochiométriques. Mais ces évaluations ont un degré important d'incertitude. Par exemple, les parois de la chambre peuvent servir de source et de puits pour O_3, NO_x, aldéhydes, cétones et OH. Un autre problème est que la plupart des chambres atmosphériques fonctionnent avec des concentrations initiales plus élevées de COV et de NO_x que dans l'atmosphère réelle. Cette incertitude d'évaluation induit une incertitude sur les produits formés pendant les réactions.

Incertitudes liées au mélange vertical

L'incertitude liée au mélange vertical est due à la paramétrisation de la diffusion verticale et de la vitesse de dépôt (Tang et al., 2011). Il existe différentes paramétrisations pour la diffusion verticale. Elles sont classifiées en fonction de l'hypothèse de fermeture (locale ou non-locale), de la stabilité dans la couche limite (stable, neutre, instable et adiabatique), de l'ordre de la fermeture (premier, second, troisième, etc.) et de la dépendance de la discrétisation verticale (Stull, 1988). La diversité des paramétrisations de diffusion verticale induit une grande incertitude sur le coefficient et ainsi une grande incertitude sur le mélange vertical des polluants dans la couche limite.

1.3 Le bassin méditerranéen

Cette section introduit brièvement la zone d'étude de cette thèse ; ses spécificités démographiques, économiques, géographiques et climatiques avec une attention plus particulière pour la Corse où est concentré l'essentiel de mon travail de modélisation numérique.

1.3.1 Présentation du bassin méditerranéen

Le bassin méditerranéen est une région carrefour entre le Sud de l'Europe, le Nord de l'Afrique et le Proche-Orient (Figure 1.3). La pression anthropique est particulièrement importante (∼200 millions d'habitants sur les zones littorales). Elle se concentre sur plus de 20 pays très disparates, que ce soit au niveau taille, développement économique, relief ou occupation des sols, climat. Il s'agit également de la zone d'affluence touristique la plus importante au niveau mondial, avec près de 250 millions de touristes par an sur ses 46 000 km de littoral, soit près d'un tiers du tourisme mondial. La Mer Méditerranée représente aussi une superficie d'environ 2.5 millions de km^2, sur laquelle transite environ 30 % du trafic maritime mondial.

Figure 1.3: Carte du bassin méditerranéen (Source Google Maps)

Une distinction peut être faite entre la rive nord du bassin (l'Europe continentale) et la rive sud, qui englobe les pays nord africains, et, par extension, ceux du Proche-Orient. Ce contraste est d'abord économique. Il implique dans un futur proche une mutation majeure et rapide des économies sur la rive sud, induisant un accroissement de la pression anthropique et notamment dans les zones urbanisées du littoral. Une vingtaine de pays constitue le pourtour du bassin méditerranéen. Distinguons les pays de la Communauté européenne, soumis à la réglementation européenne, la plus restrictive sur la qualité de l'air : Espagne, France, Italie, Malte, Slovénie, Croatie, Grèce, Chypre ; des autres pays du bassin : Bosnie-Herzégovine, Monténégro, Albanie, Turquie, Syrie, Liban, Palestine, Israel, Egypte, Libye, Tunisie, Algérie et Maroc. Bien entendu, d'autres pays influent sur l'atmosphère du bassin méditerranéen : les pays européens avec un export de pollution anthropique ou encore les pays subsahariens pour les poussières désertiques. Le clivage nord/sud du bassin méditerranéen est donc ici une donnée importante à considérer avec un accroissement de la pression démographique et des mutations économiques sur la rive sud.

1.3.2 Le bassin ouest méditerranéen

A méso-échelle, la présence de nombreux reliefs (Alpes, Pyrénées, Monts Ibériques, Apennins, etc.) a une influence notable sur la circulation des masses d'air. Signalons par exemple les vents Mistral et Tramontane en provenance du continent européen, créés par une différence de pression nord-sud, et canalisés, pour le premier, par la vallée du Rhône, et, pour le second, par les Pyrénées et l'ouest du Massif Central. Ils vont impacter, d'autant plus en hiver, le bassin Ouest de la Méditerranée, par des vents violents, secs et froids. L'arc alpin favorise l'évacuation de la pollution intense de la vallée du Pô vers l'Adriatique et le bassin méditerranéen.

1.3.3 Les aérosols en Corse

En dehors des études pionnières réalisées par (Bergametti et al., 1989a,b), mais sans analyse du carbone, aucune observation long-terme des concentrations totales des aérosols en Corse, ni de leur variabilité temporelle, n'est aujourd'hui disponible dans la littérature, ce qui a motivé la présente étude. Le bilan présenté dans la figure 1.4 s'appuie avant tout sur des mesures réglementaires $PM_{2.5}$ et PM_{10} obtenues par l'association locale de la qualité de l'air Qualitair Corse.

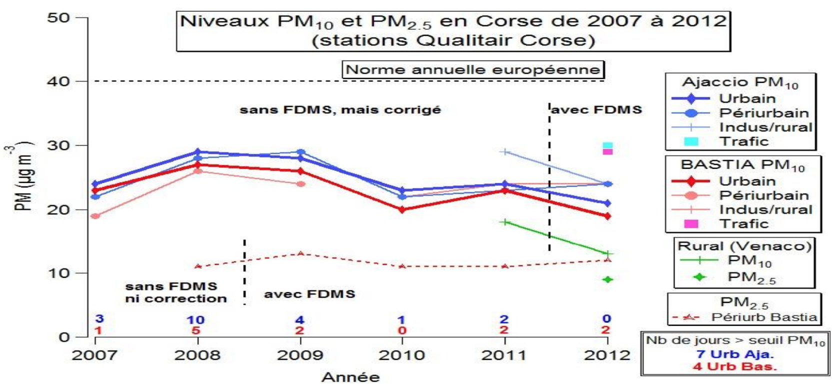

Figure 1.4: Evolution de la moyenne annuelle PM_{10} et $PM_{2.5}$ en Corse dans les différentes stations de mesures de Qualitair corse, avec le nombre de jours de dépassement du seuil journalier de 50 $\mu g.m^{-3}$ (Source: Rapport d'activités de Qualitair Corse, http://www.qualitaircorse.org/air-corse/qualite-air.php?menu=35)

L'Association Agréée de Surveillance de la Qualité de l'Air (AASQA) de Corse, Qualitair Corse, créée en 2003 (http://www.qualitaircorse.org), a la responsabilité depuis l'été 2006 de mesurer les aérosols en continu sur le territoire corse. Le réseau était initialement focalisé sur les PM_{10} dans les zones urbaines d'Ajaccio et de Bastia, et sur les $PM_{2.5}$ depuis fin 2007. Le réseau s'appuie depuis mai 2011 sur une station d'étude de la composition atmosphérique de fond rural, à Venaco, en PM_{10} tout d'abord, puis en $PM_{2.5}$ depuis mars 2012. Elle est située au centre de la Corse, à proximité de la ville de Corte et à environ 650 m d'altitude (figure 1.5).

Les concentrations annuelles en PM_{10} en Corse depuis 2007 sont nettement inférieures à la valeur limite européenne de 40 $\mu g.m^{-3}$ (moyenne annuelle) pour toutes les stations de Corse: rurale, péri-urbaines, urbaines, industrielles, et de trafic. Elles sont également en deça de l'objectif de qualité de la France de 30 $\mu g.m^{-3}$, bien que ce soit tout juste pour les deux stations trafics d'Ajaccio et de Bastia (30 et 29 $\mu g.m^{-3}$, respectivement, en 2012). Une légère amélioration des niveaux PM_{10} est observée entre 2007 et 2012, avec une valeur annuelle moyenne qui a sensiblement diminué d'environ 3 et 4 $\mu g.m^{-3}$ pour Ajaccio et Bastia, soit de 13 et 17 %, respectivement. Concernant les $PM_{2.5}$, uniquement la station périurbaine de Bastia, et récemment la station rurale de Venaco, effectuent cette mesure. Une moyenne annuelle bien inférieure à la valeur limite européenne pour 2013 (26.4 $\mu g.m^{-3}$) est observée, avec 11.6 $\mu g.m^{-3}$ de 2009 à 2012 pour Bastia et 9 $\mu g.m^{-3}$, pour Venaco en 2012 (une valeur à prendre avec précaution, car avec un taux de fonctionnement de seulement 35 %, de mars à juin). La valeur cible européenne de 20 $\mu g.m^{-3}$ pour 2020 est ainsi déjà respectée, et l'air en Corse est très proche de l'objectif de qualité de la France de 10 $\mu g.m^{-3}$ pour les $PM_{2.5}$, valeur également préconisée par l'Organisation Mondiale de la Santé.
De façon intéressante, en prenant les jeux de données PM_{10} depuis 2007 de tous les sites (urbains, péri-urbains, trafics, rural), une même variabilité des PM_{10} est observée entre la Haute-Corse et la Corse-du-Sud, indiquant un niveau de fond important qui est sans doute responsable d'une part majeure du PM, et de ses variabilités. En prenant en compte les résultats de 2011 et 2012 pour les stations rurales, urbaines et trafics, nous pouvons estimer grâce aux comparaisons des

Figure 1.5: Localisation des stations de Qualitair Corse de Venaco (rurale), de Giraud (urbaine, Bastia) et de Canetto (urbaine, Ajaccio)

concentrations annuelles des PM_{10} mesurées (Figure 1.4) en zones de trafic, les plus sujettes aux dépassements des normes: un fond régional d'environ 16 μg.m^{-3} (environ 55 %), auquel s'ajoute un niveau urbain de 6 μg.m^{-3} (environ 20 %), que complète un niveau lié au trafic de 8 μg.m^{-3} (environ 25 %).

Bien que les concentrations annuelles en PM_{10} et $PM_{2.5}$ respectent les réglementations européennes, de fortes concentrations d'aérosols organiques peuvent être observés (Lelieveld et al., 2002; Michoud et al., 2017), notamment en été, à cause de l'ensoleillement intense de la Méditerranée en été, ainsi que des nombreuses zones d'émissions biogéniques, qui peuvent former des aérosols organiques par interaction avec des sources anthropiques, comme détaillé dans la section sur la modélisation des aérosols secondaires.

1.3.4 Le projet ChArMEx

Le projet ChArMEx vise à comprendre l'état présent et futur de la composition de l'atmosphère et les impacts associés dans le bassin méditerranéen. Les cibles de ce projet sont les espèces gazeuses et particulaires de faible durée de vie (inférieure ou égale à un mois) qui sont la cause de la pollution atmosphérique et qui interagissent avec le climat. Les questions scientifiques auxquelles le programme ChArMEx tente de répondre peuvent se classer en trois catégories.

La première catégorie vise à caractériser l'état présent de la composition de l'atmosphère dans le bassin Méditerranéen et regroupe:
1. la connaissance du bilan régional de l'ozone qui implique de connaître la dynamique, les processus chimiques et d'import/export au niveau régional
2. la connaissance du bilan régional des aérosols secondaires
3. l'acquisition de connaissances concernant la part soluble des polluants, de métaux en particulier,

et la contamination de la chaine trophique maritime
4. la détermination des proportions des contributions naturelles et anthropiques des différents points évoqués précédemment.

Deux autres objectifs concernent les tendances passées et présentes et les projections pour le futur:
5. l'analyse des tendances des composés chimiques à moyen et long terme à partir de longues séries de données
6. la simulation de l'évolution future de la chimie troposphérique sur le bassin Méditerranéen.

La dernière catégorie correspond aux impacts présents et futurs et sont:
7. l'impact du forçage radiatif des aérosols et des composés gazeux
8. l'impact du transport à longue distance et des échanges verticaux sur les concentrations en aérosols et en gaz, et plus particulièrement sur la qualité de l'air
9. l'impact des dépôts et des perturbations des flux radiatifs sur la biogéochimie marine.

Pour ce faire, trois catégories de mesures ont été mises en place afin d'avoir les bases nécessaires pour répondre à ces différentes questions. Les LOP (Long Observation Period) correspondent à de longues séries (10 ans) de mesures satellites et de mesures in situ à partir de stations au sol. Les EOP (Enhanced Observation Period) correspondent à un renforcement temporaire (2-3 ans) des mesures afin de pouvoir documenter les phénomènes journaliers à saisonniers. Enfin, les SOP (Short Observation Period) correspondent à des périodes d'observations intenses impliquant des mesures par avions et par ballons ciblant la période estivale. Les SOP sont au nombre de quatre, TRAQA (Transport and Air Quality above the Mediterranean Sea, juin/juillet 2012), ADRIMED (Aerosol Direct Radiative Impact on the regional climate in the MEDiterranean region, juin/juillet 2013, Mallet et al. (2012)), SAFMED (Secondary Aerosol Formation in the MEDiterranean, juillet/août 2013, Di Biagio et al. (2015))et SAFMED+ (juin/juillet 2014).

Le travail réalisé durant cette thèse s'intègre directement dans l'objectif 2 grâce à la simulation avec un modèle chimie-transport (Polyphemus) de la formation des aérosols durant quatre différentes périodes: étés 2012, 2013, 2014 et l'hiver 2014, ce qui permet de réaliser un bilan à l'échelle régionale.

Ce travail répond également, en partie, à l'objectif 4 en étudiant l'impact des émissions anthropiques maritimes et côtières du bassin Méditerranéen sur la formation des aérosols dans cette région. Beaucoup de recherches sont actuellement réalisées dans le cadre de ChArMEx sur les aérosols et leurs contributions durant la période estivale (par exemple : Menut et al. (2015) et Rea et al. (2015)). Rea et al. (2015) réalisent une étude, sur l'été 2012, où sont étudiées les contributions des différents types de sources sur les concentrations de $PM_{2.5}$ et PM_{10}. Les sources considérées sont les émissions anthropiques, les poussières désertique, les sels marins, les émissions d'origine biogénique et les feux de biomasse. Menut et al. (2015) décrivent la variabilité des concentrations en aérosols et en ozone durant la campagne ADRIMED.

1.4 Modélisation des aérosols secondaires

1.4.1 Modélisation de la chimie des aérosols organiques

La formation de matière organique particulaire dans l'atmosphère est due à la présence de composés organiques suffisamment peu volatils pour former des particules. On parle alors de composés semi-volatils si ces composés sont à la fois présents dans la phase gazeuse et la phase particulaire et de composés non-volatils s'ils sont entièrement dans la phase particulaire. Ces composés peu volatils peuvent être formés par l'oxydation des composés organiques volatils (COV) par les différents oxydants de l'atmosphère (l'ozone, les radicaux hydroxyle et nitrate) dans l'air ou dans la phase aqueuse des nuages. Les précurseurs peuvent être d'origine anthropique comme les alcénes, les alcanes, les composés aromatiques, les hydrocarbures aromatiques polycycliques ou d'origine biogénique comme l'isoprène (le composé biogénique émis en plus grande quantité à l'échelle globale après le méthane), les monoterpènes, molécules constituées de deux blocs d'isoprène (comme l' α-pinène, le β-pinène ou le limonène), et les sesquiterpènes, molécules composées de trois blocs d'isoprène (comme l'humulène). Les COV biogéniques sont généralement issus de la photosynthèse. Les émissions de ces composés sont donc importantes quand celle-ci est favorisée, c'est-à-dire lorsque les températures et le rayonnement solaire sont élevés. Les émissions de COV biogéniques sont donc plus importantes en été. La formation d'aérosols organiques secondaires (AOS) biogéniques est donc favorisée en été. L'oxydation des précurseurs peut être très complexe et dépend généralement du régime d'oxydation: oxydation par l'ozone, par les radicaux hydroxyles (HO) ou par les radicaux nitrates. De plus, selon que les concentrations d'oxydes d'azote NO_x sont faibles (on parle alors de régime bas-NO_x) ou élevées (régime haut-NO_x), les quantités d'aérosols formés peuvent être très différentes. La structure moléculaire des composés formés, d'où découlent certaines propriétés physico-chimiques à prendre en compte, peut, elle aussi, être différente selon les concentrations de NO_x. Les composés organiques semi-volatils présents en phase gazeuse peuvent aussi être oxydés pour former d'autres composés plus ou moins volatils, on parle alors de vieillissement. Une partie des composés formés peut être plus volatile, on parle alors de composés formés par fragmentation (le composé semi-volatil s'est séparé en plusieurs molécules de plus petites tailles). L'autre partie, moins volatile, est formée par fonctionalisation (de nouveaux groupes fonctionnels se sont ajoutés à la molécule d'origine). Prendre en compte le vieillissement des composés semi-volatils peut être important, car cela influe sur la volatilité des composés (soit la capacité à former des aérosols) et leur degré d'oxydation (et donc la masse totale de l'aérosol).

Approche "Volatilité": Volatility-Basis-Set (VBS)

Dans l'approche de Donahue et al. (2006), la myriade de composés présents dans l'atmosphère est décrite en regroupant les espèces aux volatilités similaires dans une dizaine de classes de volatilités différentes établies en fonction de la concentration saturante C^*. Ces classes s'étendent sur un intervalle allant de 10^{-2} à 10^6 μg. m^{-3} et sont espacées d'un ordre de grandeur et permettent de définir des groupes de composés aux volatilités proches:

+ les composés peu volatils (Low Volatil Organic Compounds, LVOC) ayant une valeur de C^* comprise entre 0,01 et 1 μg. m^{-3} qui résident majoritairement en phase particulaire;
+ les composés organiques semi-volatils (Semi Volatil Organic Compounds, SVOC) ayant une valeur de C^* comprise entre 10 et 1000 μg. m^{-3} qui peuvent se trouver en phase gazeuse comme en phase condensée;
+ les composés modérément volatils (Intermediate Volatil Organic Compounds, IVOC) ayant une valeur de C^* comprise entre 10^4 et 10^6 μg. m^{-3} qui se trouvent quasiment entièrement dans la phase gazeuse.

Deux autres groupes sont également définis et correspondent à des composés soient uniquement volatils, soient uniquement en phase particulaire et qui n'apparaissent pas dans l'intervalle défini par l'approche VBS:

+ les composés non volatils (Non-Volatil Organic Compounds, NVOC) avec une valeur de C^* inférieure à 0,01 μg. m^{-3} qui se situent exclusivement en phase particulaire. Certains études suggèrent de les associer à la première classe de volatilité (Tsimpidi et al., 2010);

+ les composés volatils (Volatil Organic Compounds, VOC) avec une valeur de C^* supérieure à 10^6 μg. m^{-3}.

Les réactions d'oxydation ayant lieu dans l'atmosphère font évoluer la composition chimique des aérosols organiques. Ces réactions aboutissent à des modifications de la volatilité des composés que le modèle VBS classique vu précédemment (VBS-1D) vise à représenter. Cependant, parallèlement aux changements de volatilité (C^*), le contenu en atomes d'oxygène des espèces organiques est altéré. Ainsi, pour une classe de volatilité fixée, la composition chimique de la matière organique est fortement influencée par le rapport de la masse d'oxygène sur la masse de carbone des composés (rapport O/C). Le modèle VBS-1D a été amélioré afin de prendre en compte ce paramètre aboutissant ainsi au modèle VBS-2D (Jimenez et al., 2009; Donahue et al., 2011, 2012). Récemment, le développement des techniques de mesure des aérosols organiques et notamment de la spectrométrie de masse, ont permis de mettre en lumière la forte contribution des aérosols organiques oxygénés (OOA) à la masse totale d'aérosols organiques (Zhang et al., 2007). Ces espèces, caractérisées par un fort contenu en atomes d'oxygène, sont principalement d'origine secondaire et disposent d'un rapport O/C compris entre 0,25 et 1 pour les aérosols organiques les plus âgés (Aiken et al., 2008). Les OOA sont classiquement décomposés en deux sous-ensembles : les OOA faiblement volatils (LV-OOA), caractérisées par un fort rapport O/C (0,6 à 1) et donc représentatifs d'aérosols organiques particulièrement âgés et les OOA semi-volatils (SV-OOA), au rapport O/C amoindri (0,25 à 0,6) et représentatifs d'aérosols organiques plus récents.

L'approche VBS-2D permet donc de prendre en compte de manière plus réaliste (i.e. volatilité et composition chimique) la transformation de la matière organique dans l'atmosphère. Les produits d'oxydation de première génération modérément volatils partitionnant entre la phase gazeuse et la phase particulaire sont impliqués dans des réactions d'oxydation entraînant la formation de composés plus oxygénés et moins volatils, augmentant ainsi la masse d'AOS formée. En raison de son caractère récent et complexe, ce modèle demeure peu implémenté dans les modèles et fait principalement l'objet d'évaluations (Murphy et al., 2011, 2012; Donahue et al., 2011, 2012, 2013). Murphy et al. (2012) ont par exemple évaluer les capacités de ce modèle à restituer les concentrations en aérosols organiques en l'implémentant dans un modèle de transport Lagrangien à une dimension et en comparant ses résultats à des observations d'aérosols organiques réalisée via un Aerosol Mass Spectrometer (AMS) durant la campagne de mesure EUCAARI. Les auteurs rapportent que lorsque seul le processus de fonctionnalisation est paramétré, le modèle VBS-2D à tendance à surestimer, plus particulièrement en été, les concentrations massiques en aérosols organiques et sous-estimer les rapports O/C d'un facteur 2. En revanche, lorsque l'impact du processus de fragmentation sur la volatilité et le taux d'oxygénation est également paramétré (Donahue et al., 2012), les résultats sont en accord avec les concentrations bien que le rapport O/C demeure sous-estimé. Une étude plus récente, avec le modèle VBS-2D implémenté dans un modèle 0D, conduite par Chacon-Madrid and Donahue (2011) sur plusieurs molécules oxygénées (n-tridécanal, 2- et 7-tridécanone, 2- et 7-tridécanol et n-pentadécane) fait quant à elle état d'une surestimation systématique des rendements massiques en AOS par la méthode VBS-2D tenant compte des processus à la fois de fonctionnalisation et de fragmentation.

Approche "Odum"

Sur la base de résultats d'expériences réalisées en chambres de simulation atmosphérique, la première méthode empirique visant à développer des paramétrisations de formation d'aérosols organiques secondaires à partir de précurseurs gazeux fut proposée par Odum et al. (1996). Ils introduisent la notion de rendement massique Y. En faisant l'hypothèse que la condensation des aérosols secondaires sur les particules préexistantes se fait majoritairement par un processus d'absorption, la paramétrisation du rendement de formation Y dépendante de la masse d'aérosols organiques C_{OM} présente dans le système, s'écrit de la façon suivante:

$$Y = \frac{C_{OM}}{\Delta COV} \tag{1.14}$$

où C_{OM} représente la masse d'aérosols organiques formée et Δ COV la masse de précurseur ayant été consommée. La formation d'AOS à partir de l'oxydation d'un précurseur gazeux peut être schématisée de la manière suivante :

$$COV + Ox \longrightarrow \sum_{i=1}^{n} \alpha_i COV_i \tag{1.15}$$

où COV est le composé précurseur, O_x un des oxydants atmosphériques et α_i la fraction molaire (coefficient stoechiométrique) du COV impliqué dans la formation du composé organique semi-volatil i ($COSV_i$).

La contribution Y_i de chaque espèce s'exprime en fonction de la constante de partage entre les différentes phases $K_{OM,i}$ définie selon le modèle de Pankow (1994), de la fraction massique α_i et de la concentration massique en aérosols organiques C_{OM}.

$$Y = \frac{\alpha_i K_{OM,i} C_{OM}}{1 + K_{OM,i} C_{OM}} \tag{1.16}$$

Pour déterminer les paramètres de cette équation (α_i ,$K_{OM,i}$), Odum et al. (1996) utilisent les résultats d'expériences réalisées en chambre de simulation avec différentes espèces chimiques organiques (m-xylène, 1,2,4-triméthylbenzène et α-pinène). Pour chaque précurseur gazeux, une série d'expériences est menée en faisant varier sa concentration initiale (COV_0). A la fin de chaque expérience, lorsque la masse d'aérosols n'évolue plus, la quantité de précurseur ayant été consommée (Δ COV) et la masse totale d'aérosols organiques produite (C_{OM}) sont relevées. Le rendement global est déduit de ces données.

Ces résultats permettent de déterminer de manière empirique les paramètres de l'équation 1.16 à savoir les constantes de partage $K_{OM,i}$ et les fractions massiques α_i. Odum et al. (1996) supposent alors que l'oxydation de chaque précurseur peut former deux composés modèles (i=2). Les paramètres α_1, α_2, $K_{OM,1}$ et $K_{OM,2}$ sont déterminés afin de reproduire les données expérimentales.

Les premiers modules de formation d'AOS sont basés sur cette paramétrisation à deux-produits qui se trouve désormais largement utilisée dans les modèles de chimie-transport. Parmi ces modules figure principalement le module Secondary Organic Aerosol Model (SORGAM ; Schell et al. (2001)), implémenté dans des modèles européens tels que EURAD (Memmesheimer et al., 2004), LOTOS-EUROS (Schaap et al., 2008), REM-CALGRID (Stern et al., 2007), LM-MUSCAT (Wolke et al., 2004a,b) et américains comme WRF-Chem (Grell et al., 2005). Ce module est développé d'après l'approche à deux produits afin de paramétrer le rendement massique en AOS résultant de l'oxydation de précurseurs anthropiques (toluène, xylène) et biogéniques (α-pinène et limonène).

Bien que la capacité du modèle à deux produits à reproduire les rendements massiques obtenus en laboratoire soit avérée pour de nombreuses espèces (Odum et al., 1996), l'extrapolation de résultats issus d'expériences en chambre de simulation aux conditions atmosphériques soulève quelques problèmes. Tout d'abord, cette approche limite l'oxydation d'un COV à la formation de deux produits alors qu'il est désormais bien établi que dans l'atmosphère l'oxydation de certaines espèces peut conduire à la formation d'un grand nombre de composés. Par ailleurs, les rendements massiques sont déterminés sur la base d'expériences conduites dans des conditions particulières et donc entachée de nombreuses incertitudes dont la réduction nécessite de réaliser une multitude d'expériences sous diverses conditions pour chaque précurseur. Ainsi, l'impact de la concentration initiale en COV (Presto and Donahue, 2006; Shilling et al., 2009), du niveau de NO_x (Ng et al., 2007; Zhang et al., 2012), du type d'oxydant (Cai and Griffin, 2006; Fry et al., 2009), de la température (von Hessberg et al., 2009; Saathoff et al., 2009), de l'humidité relative (Seinfeld et al., 2001; von Hessberg et al., 2009), de l'intensité lumineuse (Hildebrandt et al., 2009), sur les rendements en AOS ont fait l'objet de nombreuses études scientifiques.

Approche moléculaire

Dans l'approche moléculaire, la formation d'aérosols est représentée par des composés suppléants (composés choisis judicieusement pour représenter la formation d'aérosol) auxquels sont attachés des structures moléculaires et des propriétés physico-chimiques connues. Les rendements en aérosols organiques secondaires sont basés sur des expériences en chambre, comme pour l'approche d'Odum. Cela permet de prendre en compte divers processus chimique et moléculaire comme la non-idéalité de l'aérosol, l'absorption dans la phase aqueuse des aérosols, la dissociation des acides en phase aqueuse et l'hygroscopicité (absorption d'eau par l'aérosol).

AEC (AER/EPRI/Caltech), H^2O (Hydrophylic Hydrophobic Organics, un modèle basé sur AEC qui a été développé par Couvidat and Seigneur (2011); Couvidat et al. (2012) sont des modèles qui utilisent l'approche moléculaire pour distinguer composés hydrophiles (c'est-à-dire composés qui se condensent principalement sur la phase aqueuse des particules) et composés hydrophobes (c'est-à-dire composés qui se condensent principalement sur la phase organique des particules). Les modèles MPMPO (Griffin et al., 2003) et SOAP (Couvidat and Sartelet, 2015) utilise une approche similaire, mais selon l'option utilisateur choisie, les composés peuvent se condenser à la fois sur la phase aqueuse et sur la phase organique.

Cette approche sera utilisée au cours de cette thèse, avec l'utilisation du modèle SOAP. Cependant, pour des raisons de temps de calcul, nous supposerons que chacune des espèces suppléantes se condense soit sur la phase aqueuse (espèce hydrophile), soit sur la phase organique (espèce hydrophobe).

1.4.2 Modélisation de la chimie des aérosols inorganiques

Les aérosols inorganiques secondaires (AIS) sont formés à partir de précurseurs gazeux. Ainsi, l'acide sulfurique gazeux (H_2SO_4) peut condenser sur les particules. Similairement, les équivalents en phase aérosol de l'acide nitrique gazeux sont les nitrates. L'acide nitrique et l'acide sulfurique, de par leur nature chimique, ont des comportements similaires contrairement à l'ammoniac qui a un caractère basique et qui va permettre de neutraliser l'acidité des acides sulfurique et nitrique. Les AIS sont principalement constitués de nitrate d'ammonium (acide nitrique et ammoniac) et de sulfate d'ammonium (acide sulfurique et ammoniac), ainsi que de chlorure de sodium et de nitrate de sodium. Du fait de sa faible pression de vapeur saturante, l'acide sulfurique a tendance à rapidement condenser pour se retrouver sous forme d'aérosol. En l'absence d'acide nitrique, l'ammoniac gazeux va permettre, de par son caractère basique, de neutraliser les aérosols en formant de l'hydrogénosulfate d'ammonium (NH_4HSO_4), du sulfate d'ammonium ($(NH_4)_2SO_4$) ou encore du bisulfate de triammonium ($(NH_4)_3H(SO_4)_2$) (Ansari and Pandis, 1998). Si l'on considère cette fois non plus une atmosphère contenant uniquement de l'acide sulfurique et de l'ammoniac, mais également de l'acide nitrique, la réponse du système est plus compliquée. Si les concentrations d'ammoniac sont faibles, la formation de nitrate d'ammonium ne sera pas favorisée car c'est la neutralisation de l'acide sulfurique qui aura lieu (Squizzato et al., 2013). Dans un deuxième temps, si la quantité d'ammoniac est suffisante, il va y avoir formation de nitrate d'ammonium (NH_4NO_3) à partir de l'ammoniac (NH_3) et de l'acide nitrique (HNO_3). La formation de nitrate d'ammonium est favorisée par des concentrations d'acide nitrique importantes, mais également une forte humidité et de faibles températures (Stockwell et al., 2000). La formation des aérosols inorganiques secondaires est contrôlée par la thermodynamique. Cependant, la solution décrite par la thermodynamique est la solution à l'équilibre. Dans l'atmosphère réelle, les transferts entre la phase gazeuse et la phase aérosol ne sont pas immédiats et l'équilibre thermodynamique peut ne pas être atteint. Wexler and Seinfeld (1990) montrent que le temps caractéristique de mise à l'équilibre des aérosols inorganiques secondaires peut varier de quelques secondes pour une grande quantité de petites particules à plus d'un jour pour les grosses particules en petites quantités. Par exemple, pour des particules faisant plus de quelques microns, le temps de mise à l'équilibre est de l'ordre d'une heure. Dans l'atmosphère, avec des variations rapides des concentrations gazeuses, les aérosols ayant une taille de quelques microns ou plus n'ont pas le temps d'atteindre l'équilibre thermodynamique.

1.5 Objectifs et plan de la thèse

D'après l'état de l'art et ce qui a été mentionné ci-dessus, l'étude de la formation des aérosols en région ouest-méditerranéenne reste donc une question ouverte et complexe. Cette région est un carrefour de nombreuses sources d'aérosols, où les interactions entre les différents aérosols naturels et anthropiques, l'atmosphère et la mer Méditerranée pourraient être importantes.

Le premier objectif est d'évaluer le modèle de chimie transport Polyphemus pendant trois campagnes de mesures dans le cadre du projet ChArMEx. Le deuxième objectif est d'améliorer les processus de formation des aérosols dans cette région afin d'améliorer la représentation des particules par les modèles et pouvoir établir des études d'impact fiables. Le troisième but est d'étudier l'origine des composés particulaires. Pour cela, nous étudierons la sensibilité des concentrations des PM_{10}, PM_1, AOS ainsi que les AIS aux émissions anthropiques, marines et aux conditions météorologiques. Enfin, le quatrième objectif est l'étude de la variabilité et la saisonnalité des AOS en termes de concentrations, compositions, propriétés et processus de formation. Nous présentons ci-dessous l'ensemble des questions scientifiques qui seront ainsi abordées dans cette thèse.

1.5.1 Quels sont les processus chimiques qui influent la formation des AOS en Méditerrannée pendant l'été? Est-ce-que le modèle est capable de rendre compte de l'état d'oxydation et d'oxygenation des AOS pendant l'été?

Le chapitre 2 discute les processus de formation des AOS pendant les étés 2012 et 2013. Des paramétrisations sont implémentées dans le modèle afin d'améliorer les performances du modèle en termes de concentrations, mais aussi en termes de propriété d'oxydation des AOS. Les concentrations mesurées et simulées des AOS , leurs compositions chimiques ainsi que la comparasion modèle-mesure des propriétés d'oxydation et d'oxygenation des AOS sont discutées.

La formation des AOS pendant l'été 2014 au dessus de forêts du Sud de la France est également étudiée. Les comparaisons des concentrations et propriétés modélisées par rapport à des mesures effectuées lors de vols avion sont discutées. La performance des paramétrisations implémentées (chapitre 2) en terme de concentration, composition chimique et état d'oxygenation des AOS est évaluée.

1.5.2 Quels sont les origines des aérosols secondaires en Méditerranée? Notamment, comment les émissions anthropiques, les sels marins, la météorologie influent la formation des particules PM_{10}, PM_1, les AOS et les AIS pendant l'été?

Le chapitre 3 est une étude de sensibilité des concentrations des PM_{10}, PM_1, les AOS et les AIS aux émissions anthropiques, aux sels marins, à la météorologie pendant les étés 2012 et 2013. Une comparaison des concentrations des AIS à des mesures en vol avion au dessus de la Méditérranée (sud de la France) est aussi établie avec différentes configurations afin d'affiner notre modélisation et tester la sensibilité aux modèles de formation des AIS.

1.5.3 Comment les aérosols organiques sont-ils formés pendant l'hiver? Est-ce-que le modèle est capable de reproduire la saisonnalité des concentrations, de la composition chimique ainsi que de l'état d'oxidation des AOS?

Le chapitre 4 présente une modélisation numérique des AOS pendant l'hiver 2014. Différents schémas de vieillissement des COSV sont impléméntés dans le modèle. L'importance du vieillissement des COSV issus de la combustion de la biomasse est discutée. Les concentrations, les compositions chimiques ainsi que les indices d'oxydation sont comparés.

Un résumé des résultats de cette thèse et des perspectives pour de futurs travaux sont présentés dans le chapitre 5.

Chapitre 2

Modélisation des concentrations et des propriétés des aérosols organiques pendant les campagnes ChArMEx étés 2012 et 2013 au dessus du bassin ouest Méditerranéen

Sommaire

Le bassin Méditerranéen est considéré comme l'une des régions les plus influencées par le changement climatique et la composition de l'air au nord de l'Afrique et au sud de l'Europe. Les aérosols organiques (AO) représentent 20-50% des aérosols fins au dessus des régions de moyennes latitudes et jusqu'à 90% au dessus les forêts tropicales (Kanakidou et al., 2005; Jimenez et al., 2009). Pendant l'été, une grande fraction des composés organiques au dessus de la Méditerranée est d'origine biogénique. Par exemple, El Haddad et al. (2013b, 2011) estiment qu'en été, la majeure partie de la masse organique des aérosols en zone urbaine au sud de Marseille est d'origine biogénique. De même,Minguillón et al. (2016, 2011) ont estimé grâce à une campagne de mesures en région de Barcelone (Espagne) que les aérosols organiques sont aussi majoritairement d'origine biogénique en été.

Les mesures en surface effectuées à Ersa au Cap-Corse (île de la Corse, sud-est de la France) ont montré, en accord avec Minguillón et al. (2016); El Haddad et al. (2013b); Minguillón et al. (2011); El Haddad et al. (2011), que les AO sont majoritairement d'origine biogénique, et sont produits d'oxydation des précurseurs gazeux (isoprène, monoterpènes et sesquiterpènes).

Des études basées sur des expériences en chambres (chambre de combustion pour étudier l'oxydation des composés volatils dans des conditions expérimentales aussi proches que possible des conditions atmosphériques) ont récemment amélioré la caractérisation de la formation d'aérosols organiques secondaires (AOS) via l'oxydation des monoterpènes. Par conséquent, pour bien modéliser la formation des AO dans les modèles de chimie transport (CTM), il est important d'utiliser ces donnés récentes pour améliorer les paramétrisations existantes.

Dans ce contexte, en plus des produits d'oxydation des monoterpènes déjà implantés dans le modèle (pinonaldehyde, acide pinonique et acide pinique), des mécanismes de formation d'AOS, l'uns de première génération et d'autres de deuxième génération à partir de l'oxydation des monoterpènes (α-pinène, β-pinene et limonène) ont été ajoutés à la chimie modélisée dans le modèle de chimie-transport (CTM).

Le premier mécanisme ajouté décrit le processus d'autoxidation des monoterpènes. Ce processus induit la formation d'espèces hydrophobes, hautement oxygénées, hautement oxidées et ayant d'importantes masses moleculaires et des concentrations de saturations suffisamment faibles pour être considérés comme des composés organiques volatils d'extrêmement faibles volatilités (ELVOCs) comme détaillé dans Ehn et al. (2014). Ce processus repose sur la formation de radicaux peroxydes via l'ozonolyse des monoterpènes. Ces radicaux subissent un enrichissement en oxygène grâce à l'abstraction de l'atome d'hydrogène et l'addition d'un atome d'oxygène dans la structure moléculaire de ces radicaux. Les réactions des radicaux peroxydes enrichis en oxygène forment les ELVOCs (monomères et dimères). Un modèle 0D a été établi pour décrire la formation des ELVOCs et les résultats de ce modèle 0D sont comparés aux résultats d'expériences en chambres de Ehn et al. (2014) dans les deux régimes bas et haut-NO_x. Les résultats du modèle 0D sont en accord avec les résultats d'expériences et de modèle de Ehn et al. (2014).

Le deuxième AOS ajouté est le nitrate organique. Ce dernier est formé quand un composé organique volatil (COV) biogénique et les émissions anthropiques, notamment d'oxydes d'azote (NO_x), interagissent. Le mécanisme responsable de la formation du nitrate organique a été développé par Pye et al. (2015). Ce mécanisme se base sur l'oxydation par OH des monoterpènes avec un rendement de 20.1% à travers la formation des radicaux peroxydes. Le nitrate organique est par ailleurs formé plus abondamment la nuit à travers la réaction des monoterpènes avec NO_3.

Le troisième SOA ajouté est un produit de deuxième géneration de α-pinene appelé MBTCA (3-methyl-1,2,3-butanetricarboxylic acid). Ce produit est un acide carboxylique produit par l'oxydation de l'acide pinonique (avec un rendement faible de 0.61%) qui lui-même est produit d'oxydation de l'α-pinene.

Une fois les trois paramétrisations intégrées dans le CTM Polair3d de la plateforme de modélisation de la qualité de l'air Polyphemus, les performances du modèle sont évaluées pendant les campagnes de mesures ChArMEx des été 2012 (du 6 Juin au 8 Juillet) et 2013 (du 6 Juin au 10 Août) sur un domaine du bassin Méditerranéeen centré sur la Corse. Les conditions limites et initiales de la simulation sont déduites d'une simulation sur un domaine plus grand (sur l'Europe). Les émissions biogéniques (émissions des monoterpènes, sesquiterpènes et isoprène) sont estimées avec le modèle MEGAN (Guenther et al., 2006). L'inventaire EDGAR_HTAP_V2 de 2010 est utilisé pour estimer les émissions anthropiques. Les émissions des composés organiques semi-volatils (COSVs) sont estimées en multipliant les émissions des aérosols organiques primaires (AOP) données par l'inventaire par 2.5. Les émissions des sels de mer sont générées à l'aide de la paramétrisation de Jaeglé et al. (2011). Les champs météorologiques sont modélisés grâce au modèle ECMWF (European Centre for Medium-Range Weather Forecasts). La dynamique des aérosols (coagulation et condensation/évaporation) est modélisée avec le modèle SIREAM (SIze REsolved Aerosol Model, Debry et al. (2007c)) avec une approche sectionnelle à 20 sections. La condensation/évaporation des inorganiques est décrite avec le modèle thermodynamique ISORROPIA (Nenes et al., 1998). Le partitionnement des aérosols organiques est calculé avec le modèle SOAP (Couvidat and Sartelet, 2015).

D'après les comparaisons aux mesures à la station Ersa, le modèle réussit à reproduire les concentrations des aérosols organiques et les concentrations simulées respectent les critères de but de Boylan et Russel (Boylan and Russell, 2006) (le biais (resp. erreur) fractionnel moyen est de -13% (resp. 39%) pour l'été 2012 et de -15% (resp. 49%) pour l'été 2013). Le modèle prédit que 75% de la masse organique est d'origine non-fossile, ce qui est en accord avec les mesures du carbone 14 (85%) entre le 16 et le 30 Juillet 2013. La composition chimique des AO est similaire pendant les deux étés. Avant ceux de l'isoprène, les produits d'oxydation des monoterpenes (ELVOCs, nitrate organique, MBTCA, pinonaldéhyde, acide pinonique, acide pinique) sont les espèces majoritaires et représentent aux alentours de 48% de la masse d'AO pendant les étés 2012 et 2013. Les ELVOCs et le nitrate organique representent presque 12% et 20% de la masse des AO respectivement. Par contre, le MBTCA contribue très faiblement aux concentrations d'AO. La partie anthropique des organiques est majoritairement originaire des AOP et AOS formés à partir des COSVs (19%) en comparaison avec les produits d'oxydation des aromatiques (3 à 5%).

Dans cette étude, on s'interesse aussi aux propriétés des AO (oxydation/oxygenation et hydrophilicité). Les indices d'oxydation et d'oxygenation communément utilisés sont le ratio matière organique sur le carbone organique OM:OC et le ratio oxygène sur carbone O:C respectivement. Ces indices sont importants car ils donnent des indications sur le degré d'hygroscopicité, les propriétés radiatives et l'abilité de l'aérosol à être un noyau de condensation (CCN). A la station Ersa, les indices mesurés sont très élevés (OM:OC = 2.43 et O:C= 0.99) indiquant que les AOS sont très agés et ont probablement subit plusieurs étapes d'oxydation. Sans prendre en compte la formations des ELVOCs et du nitrate organique, les ratios OM:OC et O:C sont sous-estimés par le modèle (1.57 et 0.65 respectivement). Avec les ELVOCs et le nitrate organique, les ratios OM:OC et O:C ont augmenté de 1.57 et 0.65 à 2.18 et 0.73 respectivement. Par conséquent, les espèces ajoutées (ELVOCs et nitrate organique en l'occurence) qui sont hautement oxygénées et oxidées ont amélioré les indices d'oxydation/oxygenation simulés. L'hypothèse de la formation d'organosulfate hautement oxydé et oxygéné comme produit de deuxième génération de l'isoprène via la formation d'IEPOX (radicaux époxidioles) (Nguyen et al., 2014; Couvidat et al., 2013b; Liggio et al., 2005) est prise en compte pour améliorerla simulation des indices d'oxydation/oxygénation. Cette hypothèse est motivée par l'importante corrélation entre les concentrations des organiques et celles du sulfate (71%). Les propriétés des AOS produits par l'isoprène en régime bas-NO_x ont été indentifiées à celles de l'organosulfate $C_6H_{11}O_3SO_4$. Ainsi, les ratios OM:OC et O:C ont augmenté de 2.18 et 0.73 à 2.37 et 0.84 respectivement. La propriété de l'hydrophilicité des organiques est aussi investiguée en comparant les concentrations du carbone organique hydrophile (WSOC) à celles mesurées entre le 15 et le 31 Juillet 2013. Le modèle réussit relativement bien à simuler les concentrations des WSOCs. Par contre, la fraction hydrophile simulée à Ersa (46%) est inférieure à celle mesurée (64%). Les différences de concentrations journalières des WSOCs sont reliées à la composition de la masse organique (par exemple le nitrate organique est supposé hydrophobe mais il peut subir une pseudo-hydrolyse (Pye et al., 2015)), ainsi que l'origine des masses d'air arrivant à Ersa.

L'activité biologique marine peut contribuer aux émissions d'aérosols (ODowd et al., 2004; Schwier et al., 2015). La fraction organique des sels de mer émise est fortement dépendente de la concentration de la chlorophylle-a. Deux paramétrisations sont testées: la paramétrisation de Schwier et al. (2015) dans laquelle la fraction organique des émissions des sels de mer dans le mode Aïtken dépend linéairement de la concentration de la chlorophylle-a et la paramétrisation de Gantt et al. (2012) dans laquelle la fraction organique des sels de mer dépend en plus de la concentration de la cholorophylle-a, de la vitesse de frottement de l'air sur la surface de la mer et du diamètre des particules émises. Les concentrations de la chlorophyll-a (extraites d'observations satellitaires MODIS) sont faibles, typiques des milieux marins stratifiés de la Méditerranée. La fraction organique des sels de mer est égale à 30% dans le mode Aïtken, 22% dans le mode d'accumulation et 1% dans le mode grossier. Ces fractions sont en accord avec la fraction moyenne mesurée par Schwier et al. (2015) de 24% dans le mode Aïtken en utilisant les mésocosmes pélagiques dans la baie de Calvi en Corse (France) pendant l'été 2012. Intégrées dans le modèle comme espèce inerte hydrophobe et faiblement volatile, les aérosols organiques marins contribuent faiblement (2%) aux concentrations d'aérosols organiques dans les zones très actives biologiquement (importantes concentrations de chlorophylle-a) pendant l'été 2013 en Méditérranée.

Ce chapitre est constitué de l'article:

Modelling organic aerosol concentrations and properties during ChArMEx summer campaigns of 2012 and 2013 in the western Mediterranean region (2017a), Mounir Chrit, Karine Sartelet, Jean Sciare, Jorge Pey, Nicolas Marchand, Florian Couvidat, Karine Sellegri, and Matthias Beekmann, Atmos. Chem. Phys., 17, 12509-12531, doi:10.5194/acp-2017-312.

Modelling organic aerosol concentrations and properties during ChArMEx summer campaigns of 2012 and 2013 in the western Mediterranean region

MounirChrit[1], KarineSartelet[1], JeanSciare[2,7], JorgePey[3*], NicolasMarchand[3], FlorianCouvidat[4], KarineSellegri[5], MatthiasBeekmann[6]

[1] CEREA, joint laboratory Ecole des Ponts ParisTech - EDF R&D, Université Paris-Est, 77455 Champs sur Marne, France.
[2] LSCE, CNRS-CEA-UVSQ, IPSL, Univ. Paris-Saclay, Gif-sur-Yvette, France
[3] Aix Marseille University, CNRS, LCE UMR 7376, Marseille, France
[4] INERIS, Verneuil en Halatte, France
[5] LAMP, Aubière, France
[6] LISA, UMR CNRS 7583, IPSL, Université Paris Est Créteil and Université Paris Diderot, France
[7] EEWRC, The Cyprus Institute, Nicosia, Cyprus
[*] Now at the Geological Survey of Spain, IGME, 50006 Zaragoza, Spain

Abstract In the framework of the Chemistry-Aerosol Mediterranean Experiment, a measurement site was set up at a remote site (Ersa) on Corsica Island in the northwestern Mediterranean Sea. Measurement campaigns performed during the summers of 2012 and 2013 showed high organic aerosol concentrations, mostly from biogenic origin. This work aims at representing the organic aerosol concentrations and properties (oxidation state and hydrophilicity) using the air-quality model Polyphemus with a surrogate approach for secondary organic aerosol (SOA) formation. Biogenic precursors are isoprene, monoterpenes and sesquiterpenes. In this work, the following model oxidation products of monoterpenes are added: (i) a carboxylic acid (MBTCA) to represent multi-generation oxidation products in the low-NOx regime, (ii) organic nitrate chemistry, (iii) extremely low volatility organic compounds (ELVOCs) formed by ozonolysis. The model shows good agreement to measurements of organic concentrations for both 2012 and 2013 summer campaigns. The modeled oxidation property and hydrophilic organic carbon properties of the organic aerosols also agree reasonably well with the measurements. The influence of the different chemical processes added to the model on the oxidation level of organics is studied. Measured and simulated water-soluble organic concentrations (WSOC) show that even at a remote site next to the sea, about 64% of the organic carbon is soluble. The concentrations of WSOC vary with the origins of the air masses and the composition of organic aerosols. The marine organic emissions only contribute to a few percent of the organic mass in PM_1, with maxima above the sea.

2.1 Introduction

The Mediterranean region is considered as one of the prominent regions that could be detrimentally impacted by climate and air composition changes over both southern Europe and northern Africa. Organic aerosols (OA) account for about 20-50% of the fine aerosol mass at continental mid latitudes (Saxena and Hildemann, 1996) and as high as 90% in tropical forest areas (Kanakidou et al., 2005; Jimenez et al., 2009). They contribute to more than 50% of EU-regulated $PM_{2.5}$ concentrations in Europe (Putaud et al., 2004). OA affect both climate and human health. They influence the radiation budget by mostly scattering sunlight resulting in negative direct radiative forcing (Fuzzi et al., 2006; Lin et al., 2014). Moreover, hydrophilic OA can act as a cloud condensation nuclei and hence modify cloud microphysical properties and lifetime. In terms of health effects, OA toxicity is linked to the oxidative stress which is induced by the ROS (Reactive Oxygen

Species). The oxidative potential may differ for the different organic precursors (Rattanavaraha et al., 2011; Jiang et al., 2016; Tuet et al., 2017).

OA are usually classified either as primary (POA) or as secondary aerosols (SOA). POA are directly emitted in the atmosphere, often as intermediate/semi-volatile organic compounds (I/S-VOCs), which partition between the gas and the particle phases (Robinson et al., 2007a). The gas-phase of I/S-VOC is missing from emission inventories (Couvidat et al., 2012; Kim et al., 2016). SOA are produced through chemical oxidation of volatile organic compounds (VOCs) and I/S-VOCs, and condensation of I/S-VOCs.

A large fraction of emitted VOCs is biogenic, especially in the western Mediterranean in summer, when solar radiation is high. Biogenic emissions may age and form SOA as they are transported through different environments (Hayes et al., 2015). Using aerosol mass spectrometer (AMS) measurements performed in an urban area in South France (Marseille) and positive matrix factorisation (PMF) techniques, El Haddad et al. (2011, 2013b) attributed 80% of the organic aerosol mass to biogenic secondary organic aerosols (BSOA), and they attributed near 40% of the BSOA to monoterpene oxidation products. These high biogenic concentrations in an urban area may be partly explained by the influence of anthropogenic emissions on biogenic SOA formation (Carlton et al., 2010; Hoyle et al., 2011; Sartelet et al., 2012).

Similar results were obtained through measurement campaigns in the Barcelona region (Spain), where Minguillón et al. (2011, 2016) have found a prevalence of non-fossil organic aerosol sources in remote and urban environments, and a clear evidence of biogenic VOC oxidation products and biogenic SOA formation under anthropogenic stressors.

The ChArMEx (Chemistry-Aerosol Mediterranean Experiment: http:// charmex.lsce.ipsl.fr) project has organized several summer campaigns to study atmospheric chemistry and its impacts in the western Mediterranean region. The TRAQA (Transport et Qualité de l'Air) campaign was set up in summer 2012 to study the transport and impact of continental air on atmospheric pollution over the basin (Sic et al., 2016). The ADRIMED (Aerosol Direct Radiative Impact in the Mediterranean; Mallet et al. (2016)) campaign was set up in June-July 2013 to assess the radiative impact of aerosols, while the SAF-MED (Secondary Aerosol Formation in the MEDiterranean) campaign was set up July-early August 2013 to understand and characterize the concentrations and properties of organic aerosols in the western Mediterranean and to figure out the origins of the high concentrations observed outside urban areas. Intensive ground-based in-situ measurements were performed during the summer 2013, while airborne measurements were performed during the summers 2013 and 2014 (Di Biagio et al., 2015; Freney et al., 2017). In agreement with the observations of El Haddad et al. (2013b) in Marseille on the French Mediterranean coast, the ground-based in-situ measurements performed at the remote site of Ersa on Cape Corsica, the northern tip of Corsica Island (South-East of continental France) showed that OA are mostly from biogenic origin. However, as over urban areas, anthropogenic emissions, from shipping or pollution plumes from European big cities, may influence biogenic SOA formation (Sartelet et al., 2012).

The VOC biogenic precursors of SOA are isoprene, monoterpenes and sesquiterpenes. Although sesquiterpenes emission factors are lower than those of isoprene and monoterpenes over Europe, their SOA yields are high because of their low saturation vapour pressures (Jaoui et al., 2013). For monoterpenes, first-generation oxidation products, such as pinonaldehyde, pinic and pinonic acids contribute to the formation of SOA, although their contributions may be low (Praplan et al., 2015). For α-pinene, further-generation oxidation steps may lead to the formation of very low volatile products, such as the tricarboxylic acid 3-methyl-1,2,3-butanetricarboxylic acid (MBTCA, Mller et al. (2012); Kristensen et al. (2014)) and oligomeric compounds. Ehn et al. (2014) and Kristensen et al. (2014) showed that highly-oxidised organic compounds are formed in the early stages of the oxidation of monoterpenes. Rissanen et al. (2015) proposed a mechanistic description of these extremely low volatile organic compounds (ELVOCs) formation from the most atmospherically abundant biogenic monoterpenes, such as α-pinene and limonene. These ELVOCs have been observed both during chamber and in-situ measurements in Germany (Mutzel et al., 2015). Several studies showed the importance of nighttime SOA formation from monoterpenes via nitrate radical oxidation, resulting in the formation of organic nitrates (Pye et al., 2015; Bean and Ruiz, 2016; Xu et al., 2015; Nah et al., 2016). Pye et al. (2010) showed the importance of reactive nitrogen and pointed out the fact that organic nitrate accounts for more than a half of the monoterpene oxidation products in the particle phase over the U.S..

For isoprene, in low-NOx environments, recent studies have focused on the formation of isoprene epoxydiols (IEPOX) in acidic aerosols (Surratt et al., 2010; Couvidat et al., 2013b). However, using aerosol mass spectrometer measurements, particle-phase IEPOX was not observed during the ChArMEx campaign over an isoprene-emitting forest in the South of France, suggesting it might have formed organo-sulfates (Freney et al., 2017). Several studies also showed the importance of non-IEPOX pathway for isoprene oxidation in low-NOx environment (Krechmer et al., 2015; Liu et al., 2016). Although ELVOCs may also form from isoprene oxidation, the yields may be low (Jokinen et al., 2015).

OA can also be emitted from the sea, because of phytoplankton activity: according to ODowd et al. (2004), OA from marine origin can contribute considerably to OA concentrations especially near the biologically productive waters. Recently derived parameterisations (Gantt et al., 2012; Schwier et al., 2015) relate the organic fraction of sea-salt emissions to the seawater chlorophyll-a concentrations. However, the contribution of these species to the organic budget over the Mediterranean Sea is not clear.

SOA modeling has undergone significant progress over the past few years due to the rapid increase of experimental data on SOA yields and molecular chemical composition resulting from the oxidation of a variety of VOC and I/S-VOC. SOA models used in meso-scale models can be grouped into two major categories: (1) models based on an empirical representation of SOA formation and (2) models based on a mechanistic representation of SOA formation. Models of the first category include the widely used two-compound Odum approach (Odum et al., 1996) and the more recent volatility basis set (VBS) approach (Donahue et al., 2006, 2011), or the multi-generational oxidation model (Jathar et al., 2015). Models of the second category use experimental data on the molecular composition of SOA and represent the formation of SOA using surrogate molecules with representative physico-chemical properties (Pun et al., 2006; Bessagnet et al., 2008; Carlton et al., 2010; Couvidat et al., 2012). The surrogate approach differentiates low-NOx and high-NOx regimes. The gas/particle partitioning may include both absorption into hydrophobic organic particles and dissolution into aqueous particles, and take into account some of the complexity involved in OA partitioning (such as non-ideality, multi-phase partitioning). Although these two categories of models are fundamentally different in their initial design (empirical vs. mechanistic), they aim at describing the same processes. Furthermore, they tend to converge as they continue to be developed and refined. For example, I/S-VOCs from anthropogenic emissions, which are usually specified by volatility classes, can be included in a mechanistic model (Albriet et al., 2010; Couvidat et al., 2013a), the VBS scheme can take into account the oxidative state of SOA (Jimenez et al., 2009), in particular its elemental O:C ratio (Donahue et al., 2011; Jathar et al., 2015). The recently developed 1.5-VBS (Koo et al., 2014) assigned a molecular structure to VBS products. Both the mechanistic and empirical approaches are scientifically valid and complementary; as shown by Kim et al. (2011a), the most important aspect of an SOA model is its comprehensiveness in terms of the precursors and processes being treated (completeness of the precursor VOC list, importance of low-NOx vs. high-NOx regimes, treatment of hydrophilic properties of the surrogates) rather than its fundamental design. Cholakian et al. (2017) study how the VBS approach can be used to represent the formation of SOA over the western Mediterranean and point out the importance of taking into account fragmentation and formation of non-volatile SOA in this framework.

This paper aims at investigating the chemical processes and surrogates that need to be taken into account in the mechanistic representation of SOA to reproduce the concentrations and properties of the observed biogenic SOA at the Ersa super-site in Corsica. The mechanistic representation included in the air-quality model Polyphemus (Couvidat et al., 2012) is modified by including recent research progress on monoterpenes SOA formation (ELVOC, MBTCA, organic nitrate). The influence of primary marine organic emissions is also studied. A further evaluation of the model by comparison to airborne measurements is presented in Freney et al. (2017).

The paper is structured as follows. Section 2 presents the air-quality model used as well as the improvements made in the mechanistic representation. Section 3 details the model input datasets and the measurement data. Section 4 compares the concentrations and the properties of OA to measurements, and the influence of the different chemical processes added to the model. Finally, section 5 studies the impact of the biological activity of the Mediterranean Sea on OA concentrations.

2.2 Model description

2.2.1 General features

In order to simulate aerosol formation over the western Mediterranean, the Polair3d/Polyphemus air-quality model is used (Mallet and Sportisse, 2005). The numerical algorithms used for transport, and the parameterisations used for dry and wet depositions are detailed in Sartelet et al. (2007). Gas-phase chemistry is modeled with the Carbon Bond 05 mechanism (CB05) (Yarwood et al., 2005). Different reactions are added to CB05 to model the formation of semi-volatile organic compounds from five classes of SOA precursors (intermediate and semi-volatile organic compounds of anthropogenic emissions, aromatic compounds, isoprene, monoterpenes and sesquiterpenes) (Kim et al., 2011b; Couvidat et al., 2012). For these classes of precursors, which include a great number of species, only a few surrogates are used to represent all the species.

As detailed in Couvidat and Seigneur (2011), isoprene may tetrols and methyl dihydroxy dihydroperoxide under low NOx, and methyl glyceric acids and organic nitrates under high NOx. Oxidation of isoprene by the nitrate radical NO_3 is also modeled.

For monoterpenes and sesquiterpenes, the oxidation scheme is based on Pun et al. (2006). Humulene is used to represent all sesquiterpenes. For monoterpenes, three precursors are used: API (for α-pinene and sabinene), BPI (for β-pinene and δ^3-carene) and LIM (for limonene and other monoterpenes and terpenoids). Depending on the NOx regimes, three surrogates are formed: pinonaldehyde, norpinic acid and pinic acid. Although a simple parameterisation was developed to represent the oligomerization of pinonaldehyde as a function of pH in Couvidat et al. (2012), it is not used here because its influence on SOA formation is not clear. As detailed in Couvidat et al. (2012), I/S-VOC emissions are emitted as three primary surrogates of different volatilities (characterized by their saturation concentrations C*: $\log(C^*)$ = -0.04, 1.93, 3.5). The ageing of each primary surrogate is represented through a single oxidation step, without NO_x-dependance, to produce a secondary surrogate of lower volatility ($\log(C^*)$ = -2.4, -0.064, 1.5 respectively) but higher molecular weight. For aromatic compounds, toluene and xylene are used as surrogate precursors. The precursors react with OH to form radicals that may then react differently under low-NO_x and high-NO_x conditions. Under low-NO_x conditions, the surrogate is not identified, but it is supposed to be hydrophobic. Under high-NO_x conditions, the surrogate formed are two benzoic acids (methyl nitro benzoic acid and methyl hydroxy benzoic acid). Table 2.1 describes the five classes of precursors used to represent the SOA formation and the surrogates used.

Precursors	Surrogate species
I/S-VOCs	3 volatility bins: log(C^*) = -0.04, 1.93, 3.5 with C^* the saturation concentration
Aromatics	Toluene, xylene
Isoprene	Isoprene
Monoterpenes	α-pinene, β-pinene, limonene
Sesquiterpenes	Humulene

Table 2.1: Precursors classes and the surrogate species used for SOA formation.

The SIze REsolved Aerosol Model (SIREAM) (Debry et al., 2007c) is used for simulating the dynamics of the aerosol size distribution by coagulation and condensation/evaporation. SIREAM uses a sectional approach and the aerosol distribution is described here using 20 sections of bound diameters: 0.01, 0.0141, 0.0199, 0.0281, 0.0398, 0.0562, 0.0794, 0.1121, 0.1585, 0.2512, 0.3981, 0.6310, 1.0, 1.2589, 1.5849, 1.9953, 2.5119, 3.5481, 5.0119, 7.0795 and 10.0 μm. The condensation/evaporation of inorganic aerosols is determined using the thermodynamic model ISORROPIA (Nenes et al., 1998) with a bulk equilibrium approach in order to compute partitioning between the gaseous and condensed phases of particles.

For organic aerosols, the gas-particle partitioning of the surrogates is computed using SOAP (Couvidat and Sartelet, 2015), and bulk equilibrium is also assumed for SOA partitioning. The gas-particle partitioning of hydrophobic surrogates is modelled following Pankow (1994), with absorption by the organic phase (hydrophobic surrogates). The pas-particle partitioning of hydrophilic surrogates is computed using the Henry's law modified to extrapolate infinite dilution conditions to all conditions using an aqueous-phase partitioning coefficient, with absorption by the aqueous phase (hydrophilic organics, inorganics and water). Activity coefficients are computed with the thermodynamic model UNIFAC (UNIversal Functional group, Fredenslund et al. (1975)). After condensation/evaporation, the moving diameter algorithm is used for mass redistribution among size bins.

2.2.2 ELVOCs

Ehn et al. (2014) and Kristensen et al. (2014) showed that hydrophobic high-molecular weight molecules of extremely low volatility form at the early stage of oxidation of the monoterpenes α-pinene and limonene by ozone. In the model, a unique gaseous precursor representing α-pinene and limonene is used for ELVOC formation. The ELVOC yield is assumed to be 11%, i.e. close to the average of the yields of α-pinene and limonene according to Ehn et al. (2014). Jokinen et al. (2015) suggested lower yields (Table 2.2). In this paper, sensitivity simulations with a lower bound of 3% and a upper bound of 18% are also conducted.

Relying on known chemistry and experimental findings, Ehn et al. (2014) and Rissanen et al. (2015) provided a formation pathway from monoterpenes to ELVOCs through the autoxidation process (Crounse et al., 2013).

The ozonolysis reaction leads to the formation of peroxy radicals (RO_2), which are the starting point of ELVOCs formation. These radicals undergo a fairly rapid ($\sim 1\ s^{-1}$) sequential intramolecular H-atom shift followed by O_2 addition leading to the formation of highly-oxygenated peroxy radicals ($R_{ELVOC}O_2$). This O_2 addition leads not only to an increase in molecular weight, but also

VOC	Ehn et al. (2014)	Jokinen et al. (2015)
α-pinene	7% ± 3.5%	3.4% ± 1.7%
limonene	17% ± 8.5%	5.3% ± 2.6%

Table 2.2: ELVOC yields and uncertainties.

Species	Molecular formula	Molar weight [g.mol^{-1}]	Saturation vapour pressure at 298 K [torr]	Enthalpy of vapourisation [KJ.mol^{-1}]	OM/OC	O/C
Monomer ELVOC	$C_{10}H_{14}O_9$	278	1.0 10^{-14}	50.0	2.3	1.2
Dimer ELVOC	$C_{19}H_{28}O_{11}$	432	1.0 10^{-14}	50.0	1.9	0.8
org_{NIT}	$C_{10}H_{17}NO_5$	231	5.0 10^{-6}	40.0	1.9	0.7
MBTCA	$C_8H_{12}O_6$	204	3.25 10^{-7}	109	2.1	1.0
SSorg		136	6.60 10^{-8}	50.0		

Table 2.3: Species introduced in the ELVOC, organic nitrate and MBTCA kinetic models.

to a decrease in the radical volatilities. Rissanen et al. (2015) investigated these reactions including the different steps, possible isomerizations as well as the most likely chemical pathways leading to an enrichment of peroxy radicals by oxygen. The oxygen-centered peroxy radical intermediates are internally rearranged by intramolecular hydrogen shift reactions, enabling more oxygen molecules to attach to the carbon backbone. Simultaneously, the sequential H-shift mechanism competes with reactions between peroxy radicals, NO and HO_2. Subsequently, the termination reactions lead to the formation of ELVOCs. ELVOC monomers and dimers are formed through reactions of $R_{ELVOC}O_2$ with RO_2 and HO_2. Following Ehn et al. (2014), the reactions for the ozonolysis of α-pinene and limonene (monoterpenes, MT) are included in the model as detailed in Appendix 2.7, as well as the kinetic constants used in the model (Table[2.A1] in Appendix 2.7). The formation of organic nitrate from $R_{ELVOC}O_2$ peroxy radicals is not considered in the model, as the reactions proposed by Ehn et al. (2014) led to negligible concentrations.

The aerosol species introduced in the model for ELVOC formation and their properties are detailed in Table [2.3]. The enthalpy of vapourisation of the monomer and dimer is set to 50 KJ.mol^{-1} (Svendby et al., 2008), and the saturation vapour pressure is assumed to be very low and is taken equal to 10^{-14} torr at 298 K.

2.2.3 Organic nitrates formation mechanism

Organic nitrates are formed where biogenic VOCs and anthropogenic NO_x sources interact (Pye et al., 2015; Xu et al., 2015; Bean and Ruiz, 2016; Nah et al., 2016). We used here the parameterisation of Pye et al. (2015) to account for the formation of organic nitrate compounds from the oxidation by OH and NO_3 of monoterpenes (MT). The oxidation of MT by OH leads to the formation of a peroxy radical $TERPRO_2$, and the oxidation by NO_3 leads to the formation of $TERPNRO_2$ (night-time chemistry). The peroxy radicals $TERPRO_2$ may react with NO to form organic nitrate with a molar yield of 20.1%, while the oxidation of $TERPNRO_2$ leads to higher yields. The reactions are described in Appendix 2.7, as well as the kinetic constants (Table [2.B1] in Appendix[2.7]).

Following Pye et al. (2015), the estimated vapour pressure of the condensing organic nitrate species is assumed to be 5.10^{-6} torr (Fry et al., 2009), and the enthalpy of vapourisation is taken as 40 KJ.mol^{-1}. The aerosol species (orgNIT) introduced in the model and its properties are summarized in Table[2.3]. The organic nitrate is assumed to be hydrophobic (Liu et al., 2012).

2.2.4 MBTCA: an aging product of the pinonic acid

It was shown in a set of studies that ozonolysis and OH-initiated reactions of terpenes produce organic acids (Hatakeyama et al., 1991; Hoffmann et al., 1997; Warnke et al., 2006). Szmigielski et al. (2007) identified MBTCA (3-methyl-1,2,3-butanetricarboxylic acid) as the most relevant organic acid for atmospheric SOA. It is produced by the OH-oxidation of pinonic acid, which is itself produced by the OH-oxidation of α-pinene. The OH-oxidation of pinonic acid to form MBTCA is added to the model with a kinetic constant k = 9.0 × 10^{-12} $cm^3.s^{-1}$ (Jaoui and Kamens, 2001) and a yield of 0.0061 (Mller et al., 2012). Following Couvidat et al. (2012), MBTCA is supposed to be hydrophilic, with a OM/OC ratio of 2.125 (Table 2.3).

2.3 Model and measurement setup

The simulation domain and the input data are now detailed, as well as the measurements used in this study.

2.3.1 Model setup

Domains

Two nested simulations are performed: one over Europe and one over a Mediterranean domain centered around the Ersa super-site surroundings in Corsica (Figure 2.1).

The coordinates of the European southwestern-most point are (15°W , 35°N) in longitude/latitude. The domain of simulation covers an area of 50° × 35° with a uniform spatial step of 0.5° along both longitude and latitude. For the nested Mediterranean domain, the southwestern-most point is (4°W , 39°N) in longitude/latitude. The domain of simulation covers an area of 11° × 8° with a uniform spatial step of 0.125° (∼13 km) along both longitude and latitude. 14 vertical levels are considered from the ground to 12 km. The heights of the cell interfaces are 0, 30, 60, 100, 150, 200, 300, 500, 750, 1000, 1500, 2400, 3500, 6000, 12000 m.

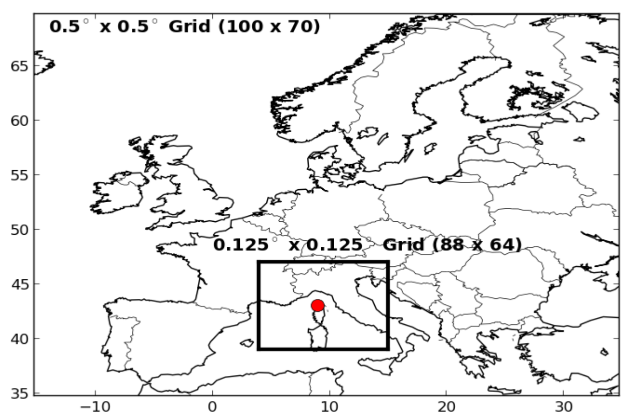

Figure 2.1: The nested modeling domains: the nesting domain over Europe and a nested domain over the north-western Mediterranean, as delimited by a black rectangular contour in the figure. The red point indicates the Ersa station in Corsica Island.

The dates of simulation are chosen such as matching those of the measurements. For 2012, the simulations are run between 2 June and 8 July 2012 (6 June and 8 July 2012 respectively) for the nesting (nested respectively) domains. For 2013, the simulations are run between 2 June and 10 August 2013 (6 June and 10 August 2013 respectively) for the nesting (nested respectively) domains.

Boundary conditions for the European domain are obtained from the global chemistry-transport model MOZART v4 (Horowitz et al., 2003) (https://www.acom.ucar.edu/wrf-chem/mozart.shtml).

The European simulation provides initial and boundary conditions to the Mediterranean simulation.

Meteorological data

Meteorological data are provided by the European Center for Medium-Range Weather Forecasts (ECMWF) model. The vertical diffusion is computed using the Troen and Mahrt parameterisation (Troen and Mahrt, 1986). The Global Land Cover 2000 (GLC-2000; http://www.gvm.jrc.it/glc2000/) data set is used for land cover.

Emissions

Anthropogenic emissions are generated using the EDGAR-HTAP_V2 inventory for 2010 (http://edgar.jrc.ec.europa.eu/htap_v2/). The monthly and daily temporal distribution for the different activity sectors are obtained from GENEMIS (1994), and the hourly temporal distribution from Sartelet et al. (2012). Following Sartelet et al. (2007), NO_x emissions are split in mass into 90% of NO, 9.2% of NO_2 and 0.8% of HONO. SO_x emissions are split into 98% of SO_2 and 2% of H_2SO_4 (in molar concentrations). For emissions of non methane volatile organic compounds, the speciation of Passant (2002) is used. $PM_{2.5}$ primary particle emissions are speciated into dust, primary organic aerosols (POA) and black carbon (BC). POA are assumed to be the particle phase of I/S-VOC. Total I/S-VOC emissions (gas and particle phases) are estimated as detailed in Couvidat et al. (2012), by multiplying POA by a fixed value, and by assigning them to species of different volatilities. The volatility distribution is kept the same for all emission sectors, although more detailed volatility distributions could be defined following the work of May et al. (2013b,c); Jathar et al. (2014). In this study, the ratio I/S-VOC/POA is set to 2.5 (Kim et al., 2016; Zhu et al., 2016). Setting the ratio SVOC/POA to 1, i.e. ignoring I/S-VOC, has little impact on the organic concentrations, as shown in Figure 2.2. Particles of diameters higher than 2.5 μm are all speciated into dust. Biogenic emissions are estimated with the Model of Emissions of Gases and Aerosols from Nature (MEGAN, Guenther et al. (2006)). Over the Mediterranean domain, during the period of the 2013 summer simulation, the average emissions of sesquiterpenes, monoterpenes and isoprene are 0.001, 0.019 and 0.024 $\mu g.m^{-2}.s^{-1}$ respectively. Hence, comparing to isoprene and monoterpene emissions, the sesquiterpene emissions are lower by a factor of 95.8% and 94.7% respectively.

Sea-salt emissions are parameterised following Jaeglé et al. (2011), which models the generation of sea salt by the evaporation of sea spray produced by bursting bubbles during whitecap formations due to the friction with surface wind. The emitted sea-salt mass is assumed to be made of 30.61% sodium (Seinfeld and Pandis, 2006b), 25.40% chloride and 4.22% sulfate following results from measurements in mesocosms made in Corsica in July 2012 (Schwier et al., 2015). The organic fraction of sea-salt emissions is not taken into account in the simulation presented here. However, it is estimated in section 2.5, where the contribution of organic sea-salt emissions to organic concentrations is assessed.

2.3.2 Measured data

The model results are compared to observational data from ChArMEx campaigns during the summers of 2012 and 2013. The station is located at the red point in Figure [2.1]. The measurement site is located at Ersa (42°58'N, 9°21.8'E), it is located on a ridge at an altitude of about 530 m above the sea level and has an unimpeded view of the sea over ~300° from the SSW to SSE (Mallet et al., 2016). The ground-based comparisons are performed by comparing the measured concentrations to the simulated ones using the concentrations of the model cell the closest to the

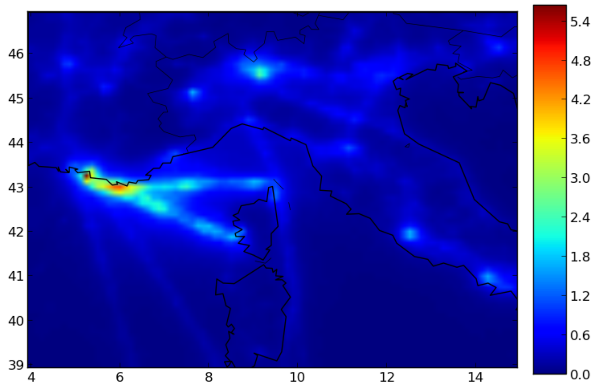

Figure 2.2: Relative difference (%) of OM_1 concentrations simulated using the emission ratio I/S-VOC/POA = 2.5 and 1.

station. The central coordinate of this cell at which concentrations are computed is (42°52N, 9°22'30"E), which is very close to the station and with a similar altitude above sea level (494 m). Cholakian et al. (2017) studied the difficulty to correctly represent in a model the orography of Ersa site, which is a cape at the northern edge of Corsica. They concluded that the representativeness error is about 10% for organic aerosols.

To evaluate the organic concentrations and oxidation properties, an ACSM (Aerosol Chemical Speciation Monitor) was used to measure the real-time chemical composition and mass loading of aerosols with aerodynamic diameters between 70 and 1000 nm (sulfate, nitrate, ammonium, chloride and organic compounds), between 8 June and 2 July 2012, and between 6 June and 3 August 2013. The ratio OM/OC and the oxidation state of organics are estimated using the ACSM measurements following Kroll et al. (2011).

Other instruments were deployed in 2013 to evaluate the organic properties: a PILS-TOC-UV to estimate the water-soluble fraction of organics (Sciare et al., 2011) between 14 July and 5 August 2013, and a Hi-Vol quartz filter sampling DIGITEL for ^{14}C measurements in organics between 16 July and 30 July 2013.

A direct evaluation of the simulated concentrations of ELVOCs or organic nitrates cannot be done because they were not measured during the campaigns.

2.3.3 Model/measurements comparison method

To evaluate a model, several approaches and performance scores can be used. Here, we compare model simulation results to measurements using a set of performance statistical indicators: the simulated mean ($\overline{s}$), the root mean square error (RMSE), the correlation coefficient, the mean fractional bias (MFB), the mean fractional error (MFE). They are defined in Table [4.A1] of Appendix 2.7. Based on the MFB and the MFE, Boylan and Russell (2006) proposed a performance and a goal evaluation criteria as detailed in Table [4.A2] of Appendix 2.7.

2.4 Comparison to measurements

The concentrations of organic aerosols are compared to measurements for the summers 2012 and 2013. The origins of organic aerosols (fossil vs non fossil), and their properties (oxidation state, hydrophylic properties) are compared to the measurements performed during the intensive measurement period of the summer 2013. In the simulation presented here, the ELVOC yield is assumed to be 11%, as detailed in section 2.2.2. Two sensitivity simulations are performed using a lower bound yield (3%) and an upper bound yield (18%). In Appendix 2.7, similarly to what is presented in this section for the reference simulation, the sensitivity simulations are compared to each other and to the measurements in terms of the mass of OM_1, the organic aerosol composition, the OM:OC and O:C ratios.

2.4.1 Organic concentrations

The comparisons of the measured and modeled temporal profiles of the concentration of the submicron organic mass (OM_1) at Ersa are shown in Figure [2.3] for the two summer campaigns of 2012 and 2013.

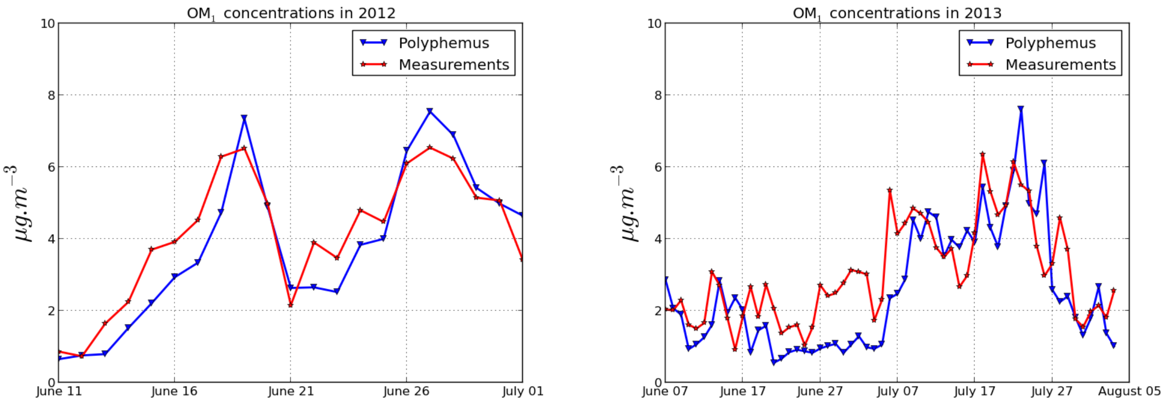

Figure 2.3: Comparison of measured and simulated daily OM_1 concentration at Ersa during the summer campaigns of 2012 (left panel) and 2013 (right panel).

The model shows satisfactory results at Ersa station, as shown by the statistics in Table [2.4]. Both the goal and the performance criteria of Boylan and Russell (2006) are verified for both years (MFB $\leq$ 30% and MFE $\leq$ 50%). The overall concentration of OM_1 is reasonably well modeled, although it is slightly underestimated 2.58 (respectively 3.71) μg.m^{-3} against 2.89 (respectively 4.14) μg.m^{-3} in the measurements for 2013 (respectively 2012). Overall, the model reproduces very well the peaks and troughs of OM_1 concentrations in both 2012 and 2013 with the exception of a few days in late June-early July 2013. This period is a period with air trajectories passing over France (Arndt et al., 2017), during which aging processes of biogenic compounds may be particularly important with formation of aged hydrophilic SOA. In the model, this process would lead to the formation of aged carboxylic acids, with MBTCA used as surrogate. However, the simulated concentration is low because the yield used is very low (it corresponds to the yield of MBTCA only).

Year	$\bar{o}$ [μg.m^{-3}]	$\bar{s}$ [μg.m^{-3}]	RMSE [μg.m^{-3}]	Correlation [%]	MFB	MFE
2012	4.14	3.71	2.00	61.7	-0.13	0.39
2013	2.89	2.58	1.53	67.3	-0.15	0.49

Table 2.4: Statistics of model to measurements comparisons for hourly organic concentrations in particles of diameters lower than 1 μm during the summer campaigns of 2012 and 2013. $\bar{o}$ and $\bar{s}$ are the observed and simulated means, respectively. RMSE is the root mean square error, MFB and MFE are the mean fractional bias and error, respectively (see Appendix2.7).

2.4.2 Sources of OA

In both 2012 (6 June to 8 July) and 2013 (6 June to 10 August), the modeled organic mass is dominated essentially by biogenic particles (figure[2.4]). They represent 77% and 75% of the organic mass. In the model, for comparisons to the ^{14}C measurements, the biogenic-origin organic compounds are assumed to be non fossil, and the anthropogenic-origin organic compounds are assumed to be fossil. Although in winter, some of the anthropogenic-origin organic compounds may originate from wood combustion (residential heating) and be non fossil, we assume that the fraction of anthropogenic-origin organic compounds from residential heating is low in summer. The simulated OC is computed by dividing the modeled organic mass of each model surrogate by the OM/OC ratio of the surrogate.

During the period when ^{14}C measurements were performed (16 to 30 July), 75% of the modeled organic mass is biogenic, in agreement with the ^{14}C measurements, which estimated that 85% is non fossil. The measured and simulated means are 2.5 μgC.m^{-3} and 1.9 μgC.m^{-3} respectively for non-fossil OC, and 0.5 μgC.m^{-3} and 0.6 μgC.m^{-3} respectively for fossil OC. Although fossil OC is well modeled, non-fossil OC is slightly under-estimated between 16 and 30 July.

The modeled average chemical compositions of OM_1 at Ersa during the summers 2012 and 2013 are presented in Figure [2.4]. The chemical composition is very similar between the years 2012 and 2013.

Monoterpene oxidation products including ELVOCs and organic nitrate represent a large part of biogenic aerosols (about 48% in 2012 and 2013). ELVOCs and organic nitrate are abundant. ELVOCs represent 10% of OM_1 in 2012 and 15% in 2013. Organic nitrate represent 24% of the organic mass in 2012 and 20% in 2013. The route to organic particulate nitrate may essentially (but not exclusively) be active during the night as NO_3 efficiently photolyzes during the day and the production yields are more important during the night, and higher organic-nitrate concentrations are observed at night (Figure 2.5).

MBTCA, an oxidation product of monoterpenes, represents a tiny portion of OM_1, following the very low molar yield used. After monoterpenes, the most important biogenic precursor is isoprene; its oxidation products represent about 20% of OM_1 in 2012 and 16% in 2013. Although sesquiterpenes emissions are lower than isoprene and monoterpenes emissions, their oxidation products represent about 10% of OM_1. Anthropogenic oxidation products represent about 22% and 25% of OM_1 in 2012 and 2013 respectively. Most of anthropogenic oxidation products originate from intermediate and semi-volatile organic emissions (about 19% of OM_1, they are referred as anthropogenic SOA and POA in Figure [2.4]), and from aromatic oxidation products (3 to 5% of OM_1).

2.4.3 Oxidation state of organics

The level of oxidation of ambient organic aerosols is assessed by the organic matter to organic carbon ratio (OM/OC) and the oxygen-to-carbon ratio (O:C). OM is made up of many different molecular structures and it may include not only particulate organic carbon but also oxygen, hydrogen, nitrogen and/or sulphate. Hence, a high OM/OC ratio indicates a high degree of oxidation of the organic aerosols, and probably a high degree of hygroscopicity (Jimenez et al., 2009). There is a variety of methods that have been used to calculate OM/OC ratio as reported by Xing et al. (2013). In our case, the ambient OM/OC ratio is calculated by weighting the ratio $(OM/OC)_i$ of each surrogate species i by the relative mass of the surrogate: $OM/OC = \sum_{i=1}^{N_{esp}} (OM/OC)_i \times OM_i/OM$, where $Nesp$ is the number of surrogate species. The ratio $(OM/OC)_i$ of the surrogate species i depends only on the molecular structure of the species and the number of carbons in the molecule. The O:C oxygen to carbon ratio allows for the degree of oxygenation of the organics to also be

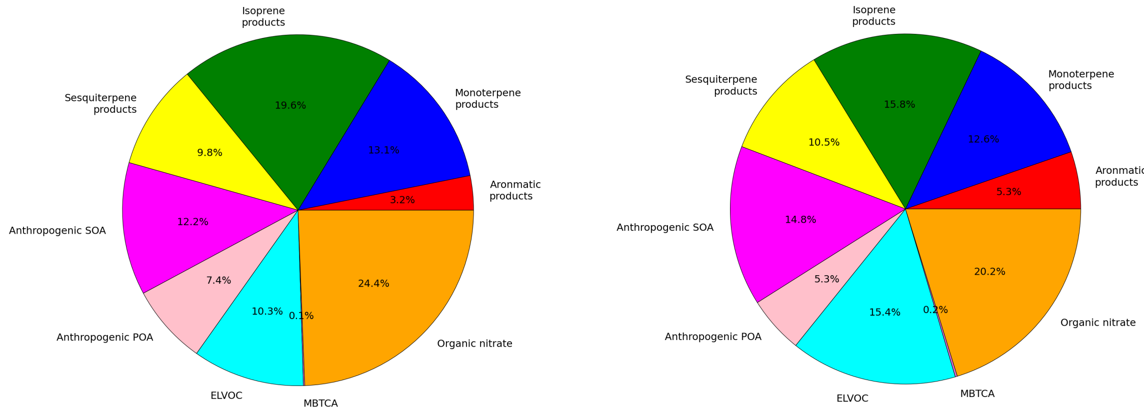

Figure 2.4: Simulated composition of OM_1 during the summer campaigns of 2012 (left panel) and 2013 (right panel).

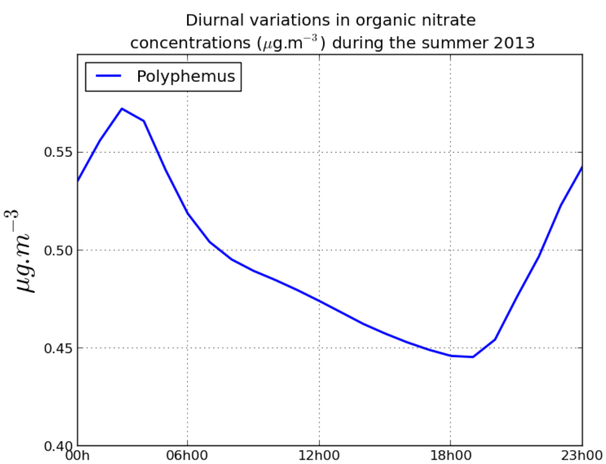

Figure 2.5: Diurnal variations in simulated organic nitrate concentrations during the summer 2013 at ERSA.

considered.

The measured and simulated temporal evolutions of both OM/OC and O:C ratios for submicron organic aerosols are shown in Figure [2.6] during the whole summer 2013 campaign period. The contributions from ELVOCs, organic nitrate and MBTCA are highlighted.

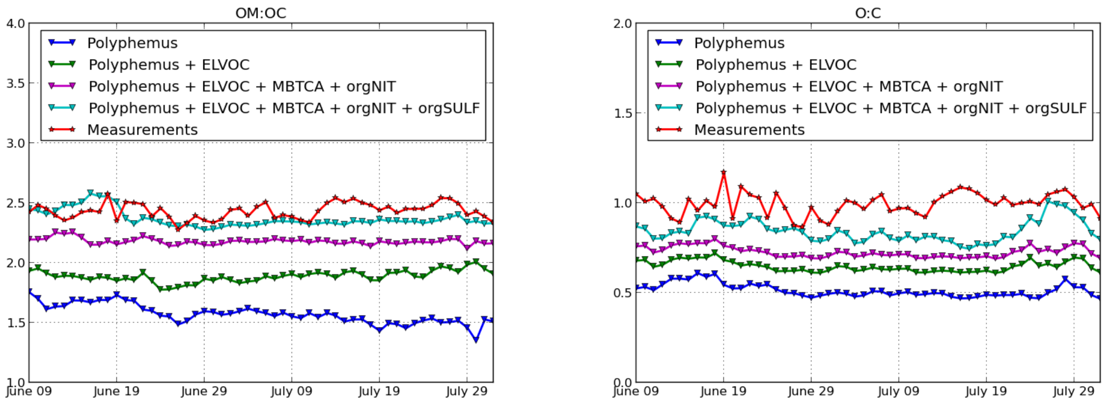

Figure 2.6: Daily variations of the ratios OM/OC (left panel) and O:C (right panel) during the 2013 campaign. The red line represents the measurements. The blue line represents model results without taking into account the concentrations of ELVOCs, MBTCA and organic nitrate. The green and magenta lines represent the model results by also taking into account ELVOCs (green) and MBTCA and organic nitrate (magenta). The cyan line represents the model results when assuming that a surrogate from isoprene oxidation is an organo-sulfate.

Relying on the measured values, the organic species over Ersa are highly oxidised and oxygenated. In fact, the measured value of the OM/OC ratio (2.43) is higher than the value of 2.1 suggested by Turpin and Lim (2001) for a rural site like Kern Refuge (U.S.). The measured O:C ratio is 0.99. In agreement with the measurements, all simulations show a relatively stable OM/OC ratio and O:C ratio during the simulated period.

Without taking into account the ELVOCs, MBTCA and organic nitrate species, the model strongly under-estimates both the OM/OC ratio and the O:C ratio. This is because of the absence of highly oxidized species in the model, as all the other modeled organic compounds with non-negligible mass tend to have low OM/OC and O:C ratios.

Taking into account the formation of ELVOCs leads to improvements in the predicted oxidation state of aerosols: the OM/OC ratio (respectively O:C) changes from 1.57 to 1.89 (respectively 0.51 to 0.65), although the monomer and dimer ELVOCs only represent 15.7% of the OM_1 mass.

MBTCA has a low impact on the organics oxidation level, despite its high OM/OC ratio, because it constitutes only a tiny part of the OM_1 mass (0.2%).

Taking into account organic nitrate leads to an improvement of both ratios. The OM/OC increases from 1.89 to 2.18 and the O:C ratio increases from 0.65 to 0.73.

A possible way to explain the under-estimation of the OM/OC ratio (2.17 simulated against 2.43 measured) and the O:C ratio (0.73 simulated and 0.99 measured) is to take into account the formation of organo-sulfate. As both organic and sulfate are the major components of aerosols at Ersa (Nicolas, 2013), there may be formation of organo-sulfate, as suggested by the transmission electron microscopy measurements of Freney et al. (2017) in the South of France.

The measurements performed at Ersa show a good correlation between sulfate and organic OM_1 concentrations, with a linear regression coefficient of 0.64. In agreement with the measurements, the simulated concentrations of sulfate and organics are also well correlated with a linear regression coefficient of 0.71. Although the formation of organo-sulfate is not modeled here, the modeled correlation is high because both sulfate and organics are formed by oxidation of precursors, and oxidant concentrations largely depend on meteorological variables, such as temperature and dilution within a variable mixing layer. Furthermore, a large part of biogenic SOA is hydrophilic and therefore higher condensation of sulfate enhances their partitioning into the particulate phase, as the mass of the aqueous phase increases through the condensation of sulfate (Couvidat and Sartelet, 2015).

In laboratory, the formation of organosulfate was observed from the uptake of monoterpene oxidation products (pinonaldehyde) on acidic sulfate aerosols (Liggio and Li, 2006; Surratt et al., 2008), from the uptake of ELVOC (Mutzel et al., 2015), and from the uptake of isoprene oxidation products (Liggio et al., 2005; Nguyen et al., 2014). Isoprene SOA may be formed via the reactive uptake of isoprene-epoxydiol (IEPOX), a second generation oxidation product of isoprene, in the presence of hydrated sulfate (Surratt et al., 2010; Couvidat et al., 2013b; Nguyen et al., 2014). Using aerosol mass spectrometer measurements, Hu et al. (2015) estimated that IEPOX-OA makes a large fraction of the OA (between 17 to 36% in the U.S.) outside urban areas, in agreement with Budisulistiorini et al. (2015). In regions where aerosols are acidic, IEPOX-derived OA may be strongly dependent on the sulfate concentration, which acts as nucleophile and facilitates the ring-opening reaction of IEPOX and organosulfate formation (Nguyen et al., 2014; Xu et al., 2015).

In order to take into account the influence of the formation of organo-sulfates on OA properties, the surrogate products of the model are modified. As Mediterranean aerosol composition displays large concentrations of sulfate, isoprene oxidation products may lead to the formation of organo-sulfate. In the model, the components formed from the low-NOx oxidation of isoprene are BiPER and BiDER. The surrogate BiPER is supposed to be a methyl dihydroxy dihydroperoxide. Although BiDER is not identified, it is assumed to have the properties of a methyl tetrol (Couvidat and Seigneur, 2011). If we assumed that this compound has the same properties as a sulfate ester of formula $C_6H_{11}O_3SO_4$, the ratios OM/OC and O:C increase to get closer to measurements (Figure 2.6). In fact, the average OM/OC ratio (respectively O:C) increases from 2.18 (respectively 0.73) to 2.37 (respectively 0.84), which compares very well with the average measured ratios (2.43 for OM/OC and 0.99 for O:C). Even though the ratio O:C still seems to be slightly under-estimated, the discrepancies may be explained by uncertainties in the measurements. Measurements performed at the same place between 10 July and 6 August with an HR-toF-AMS (aerosol mass spectrometer) shown an average OM/OC ratio of 2.34 ($\pm$0.14) and an average O:C ratio 0.92 ($\pm$0.11).

2.4.4 Water-soluble organics

Water-soluble organics constitue a major fraction of organic compounds. On average between 15 and 31 July 2013, submicron water-soluble organic carbon (WSOC) represents 64% of the organic carbon in the measurements and 46% in the model. WSOC concentrations are well modeled on average (the measured mean is 1.0 μgC.m^{-3} and the modeled mean is 0.9 μgC.m^{-3}). Figure [2.7] shows the daily concentrations of WSOC in the model and according to the measurements. Although the WSOC concentrations are well modeled between 21 and 31 July, they are under-estimated between 15 and 20 July. These differences between the periods in the ability of the model to represent WSOC concentrations may be linked to differences in the organic aerosol composition and in the origins of air masses. This is illustrated by the comparison of 16 and 30 July. WSOC concentrations are under-estimated on 16 July, but are well modeled on 30 July. 16 July is characterised by low/calm winds in a time when 30 July is characterised by winds from south-east France. Figure [2.8] shows the chemical composition of modeled OM_1 for both days. On 30 July, hydrophilic oxidation products of isoprene constitute most of the mass: they represent 26% of the concentrations against 9% on 16 July. However, organic nitrate (from monoterpene oxidation) represents as much as 35% of OM_1 concentrations on 16 July, against only about 10% on 30 July, because the low winds of 16 July probably enhance the influence of NO_x emissions from ships on pollutant concentrations.

Although this organic nitrate is assumed to be hydrophobic, it may have undergone hydrolysis resulting in nitric acid and nonvolatile secondary organic aerosol that may change the hydrophylicity of organics and the organic composition, as detailed in Pye et al. (2015).

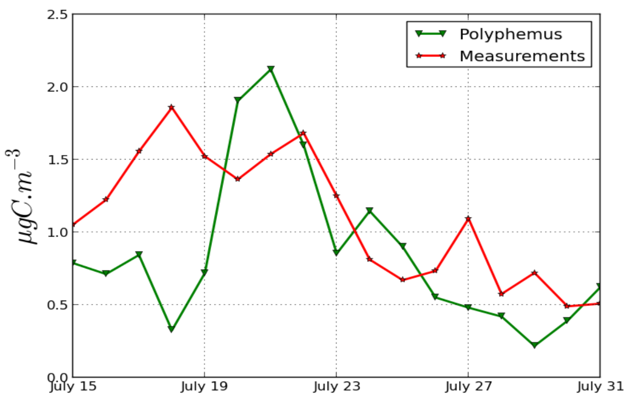

Figure 2.7: Measured and simulated submicron water soluble organic carbon (μgC.m^{-3}) at Ersa

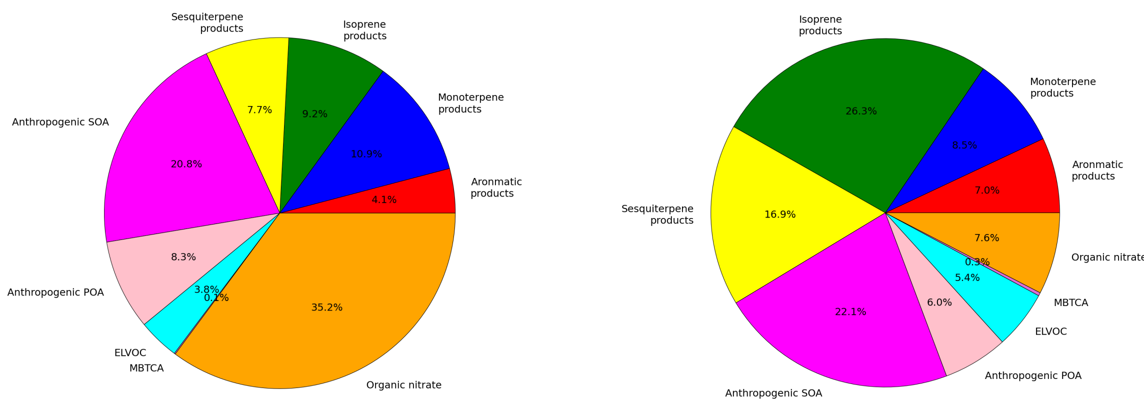

Figure 2.8: Simulated chemical composition of OM$_1$ on 16 July (left panel) and on 30 July 2013 (right panel)

2.5 Impact of the biological activity of the Mediterranean Sea

According to ODowd et al. (2004), organic aerosols of marine origin can contribute to organic OM$_1$ concentrations especially near biologically productive waters. Particles of diameters larger than 1 μm tend to contain mostly inorganic compounds, and the fraction of organic increases with decreasing diameter for particles of diameters smaller than 1 μm (ODowd et al., 2004; Schwier et al., 2015).

Several studies found a correlation between the organic mass fraction of sea-spray aerosol (OM$_{SSA}$) and the concentrations of oceanic parameters like chlorophyll-a [chl-a], which is used as a proxy for biological activity and related ocean chemistry (ODowd et al., 2008; Gantt et al., 2011; Schwier et al., 2015). Several parameterisations exist to estimate the fraction of organics in primary marine aerosols. Whereas in the parameterisation of Schwier et al. (2015), which is designed for Aitken mode aerosols, the organic fraction only depends on chl-a, it depends also on the 10 m wind speed and the particle diameter in Gantt et al. (2012). OM$_{SSA}$ decreases with increasing 10 m wind speed, because for strong wind speeds, bubbles are not enough enriched by organic matter due to the wave breaking. Concerning the size-dependence, Gantt et al. (2012) showed that the maximum organic fraction in the Aitken and accumulation modes is about 80 to 90%, while the fraction is less than 2% in the coarse mode.

The concentrations of the chlorophyll-a are obtained from monthly averaged MODIS/AQUA satellite data (http://oceandata.-
sci.gsfc.nasa.gov/MODIS-Aqua/L3SMI, Hu et al. (2012)), with a spatial resolution of 4km×4km. They are shown in the left panel of Figure [2.9].

Values are low, typical of oligotrophic conditions that characterize stratified surface Mediterranean waters in summer. The highest chl-a concentrations are recorded around the coastal zones meaning shallow water, places where sea currents bring cold waters with plants and nutrients from sea floor or brought from the rivers to the surface due to the rising slope of the sea floor.

Far from the coasts, the chl-a is more or less uniform (less than 0.2 mg.m^{-3}). The chl-a temporal average near Ersa is 0.14 mg.m^{-3}.

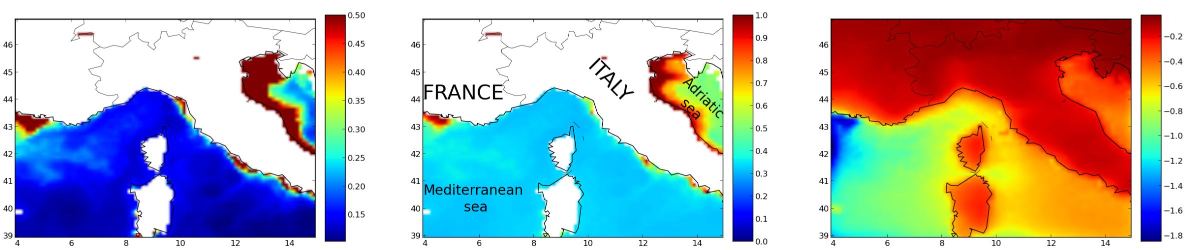

Figure 2.9: Left panel: Temporal average of chl-a in sea surface in units of $mg.m^{-3}$ during the summer of 2013 (from 6 June to 3 August). Middle panel: Organic mass fraction of emitted sea-spray aerosols of diameters between 0.01 and 0.1585 μm. Right panel: Relative difference (%) in the concentrations of OM_1 between the base simulation and the simulation including organic sea-salt emissions.

The emitted organic mass fraction of sea salt is shown in the middle panel of Figure [2.9] using the parameterisation of Gantt et al. (2012) for aerosols of diameters between 0.01 and 0.1585 μm. The organic fraction map has almost the same spatial distribution as the chl-a map. The fraction of marine organic emissions is higher near the shores of the continent. The temporal average of emitted OM_{SSA} near Ersa is detailed in Table [2.5] for aerosols of different sizes. As expected, the organic fraction is higher for aerosols in the Aitken mode (~ 0.31) than in the accumulation mode (~ 0.22) than in the coarse one (~ 0.01). These simulated organic fractions are consistent with the fraction obtained by the Schwier et al. (2015) parameterisation for the Aitken mode (0.23). They are also consistent with the average fraction of 0.24 found experimentally by Schwier et al. (2015) using pelagic mesocosms in the bay of Calvi (Corsica, France) during the summer of 2012 (an average fraction of 0.24).

Diameter range [μm]	[0.01,0.1585]	[0.1585,1.0]	[1.0,2.5119]	[2.5119,10.0]
Temporal average of OM_{SSA} in Ersa	0.31	0.22	0.02	0.01

Table 2.5: Temporal averages of OM_{SSA} near Ersa using the parameterisation of Gantt et al. (2012) as a function of aerosol particle diameter, over the summer of 2013 (from 6 June to 3 August).

A simulation was performed using the organic fraction of primary marine emissions computed with the Gantt et al. (2012) parameterisation, in order to assess the impact of the marine organics on the concentrations of organics OM_1. The organic emissions are affected to a new species called "SSorg", which is assumed to be hydrophobic and not very volatile. The properties are detailed in Table [2.3]. The values are assumed to be the same as those taken for methyl nitro benzoic acid in the model, following the lack of data characterising the properties of these species. Secondary marine OM formation is not taken into account.

The right panel of Figure [2.9] shows the relative difference of organic OM_1 concentrations between the base simulation and the simulation including organic sea-salt. The contribution of the organic sea-salt emissions to organic OM_1 is small (a few percent at the maximum) and localised above the sea. On average over the marine domain, the organic sea-salt emissions contribute to about 1.8% of the organic OM_1 concentrations. Despite the larger chl-a and organic fraction over the Adriatic Sea, the contribution of SSorg to OM_1 concentrations is not as high as the one over the Mediterranean Sea in the South of France. This is due to the fact that the surface wind-driven flux of sea salts over the Adriatic Sea is not as important as over the Mediterranean Sea in the South of France.

2.6 Conclusion

This paper presents comparisons of modeled organic concentrations and properties to surface measurements performed at Ersa (Cap Corsica, France) during the summers 2012 and 2013. The air-quality model of the Polyphemus platform is used with a surrogate approach to model secondary organic aerosols (SOA). The previously-published surrogate approach is modified to better represent observed organic aerosol (OA) properties, by taking into account the formation of extremely low volatility organic compounds (ELVOCs) and organic nitrate from monoterpene oxidation. The concentrations of organic matter compare well to the measurements performed with an ACSM (Aerosol Chemical Speciation Monitor).

During the summer 2013, the added surrogates led to a significant increase of mass concentrations: they contributed to 15% of the OM_1 mass for ELVOC, 20% for organic nitrate from monoterpene oxydation and 0.2% for MBTCA. In agreement with ^{14}C measurements, most of the organic aerosol is from non-fossil (biogenic) origin. The inclusion in the model of ELVOC and organic nitrate formation greatly improves the modeled oxidation state of particles, as assessed by the OM/OC and O:C ratios. Despite the model improvements, these ratios remain underestimated compared to measurements (2.18 simulated against 2.43 measured for OM/OC and 0.73 simulated against 0.99 measured for O:C). However, the ratios are better modeled by assuming that a surrogate species from isoprene oxidation is an organo-sulfate (2.37 simulated for OM/OC and 0.84 for O:C), suggesting that further work should focus on a better description of organo-sulfate formation. Although an organic acid, MBTCA, was introduced as a second generation product of monoterpenes, its yield should be revisited to include the formation of several carboxylic acids, rather than a single species. Concerning the hydrophilic properties of aerosols, as much as 64% of organic carbon is soluble. Therefore, taking into account the hydrophylic properties of aerosols is crucial to model the partitioning of aerosols between the gas and particle phases. The average concentration of water soluble organic carbon is relatively well modeled by comparison to measurements performed using a PILS-TOC-UV (with a mean value of 1.0 $\mu gC.m^{-3}$ in the measurements and 0.9 $\mu gC.m^{-3}$ in the model) over the second half of July 2013. Daily comparisons to measurements show that although organic nitrate is assumed hydrophobic here, its hydrolysis should be modeled to better represent the hydrophylic properties of organics. There are other pathways and mechanisms that are not considered in the model, but that may change the concentrations and hydrophylicity of organics (Shrivastava et al., 2017). For example, salting effects (via activity coefficients) are not considered, although inorganics provide a mass onto which hydrophilic organic surrogates may condense. Furthermore, pathways such as the aging chemistry of VOCs and I/S-VOCs from biomass burning (wildfires) and organic cloud processing are not considered. However, these pathways may be relatively low during the studied periods. Marine organic aerosols were added to the model, with a parameterisation depending on chlorophyll-a, 10 m wind speed and particle diameters. Although the emitted organic fraction is high for particles of small diameters (Aitken and accumulation modes), its contribution to the total organic mass OM_1 is only a few percents at the maximum. Its contribution over the continent is always lower than 1 to 2%.

acknowledgements This research has received funding from the French National Research Agency (ANR) projects SAF-MED (grant ANR-12-BS06-0013). This work is part of the ChArMEx project supported by ADEME, CEA, CNRS-INSU and Météo-France through the multidisciplinary programme MISTRALS (Mediterranean Integrated Studies aT Regional And Local Scales). The station at Ersa was partly supported by the CORSiCA project funded by the Collectivité Territoriale de Corse through the Fonds Européen de Développement Régional of the European Operational Program 2007-2013 and the Contrat de Plan Etat-Région. Eric Hamounou and François Dulac are acknowledged for their great help in organizing the campaigns at Ersa. CEREA is a member of Institut Pierre-Simon Laplace (IPSL).

2.7 Appendix

Formation of ELVOC

The reactions involved in the formation of ELVOCs are

$$MT + O_3 \xrightarrow[k_1]{} \gamma_{RO_2}.RO_2 + (1-\lambda-\gamma_{RO_2}).R'O_2 + OH + 0.001\,HO_2 \quad (2.1)$$

$$R'O_2 \xrightarrow[k_{H/O2}]{} \alpha.R''O_2 \quad (2.2)$$

$$R''O_2 \xrightarrow[k_{H/O2}]{} \alpha.R'''O_2 \quad (2.3)$$

$$R'''O_2 \xrightarrow[k_{H/O2}]{} \alpha.R_{elvoc}O_2 \quad (2.4)$$

$$RO_2 + R'O_2 \xrightarrow[k_2]{} Products \quad (2.5)$$

$$RO_2 + NO \xrightarrow[k_3]{} \delta.RO_2 \quad (2.6)$$

$$RO_2 + HO_2 \xrightarrow[k_4]{} Products \quad (2.7)$$

$$R_{elvoc}O_2 + RO_2(or HO_2) \xrightarrow[k_5]{} \beta.Monomer + (1-\beta).Dimer \quad (2.8)$$

$$R_{elvoc}O_2 + NO \xrightarrow[k_6]{} \chi.nitrate_{org} + \phi.Monomer \quad (2.9)$$

Kinetic constant	Value (cm^3s^{-1} or s^{-1})
k_1	$8.4\ 10^{-17}$
k_2	$1.0\ 10^{-12}$
k_3	$4.7\ 10^{-12}$
k_4	$2.7\ 10^{-11}$
k_5	$5.0\ 10^{-11}$
k_6	$4.7\ 10^{-12}$
k_{H/O_2}	0.5

Table 2.A1: Kinetic constants used in the ELVOC kinetic model

After numerous combinations, the stoichiometric coefficients of equations [2.1] were determined, such as reproducing the observations of Ehn et al. (2014) for both the low-NOx and high-NOx regimes (Table 2.A2).

Stoichiometric coefficient	γ_{RO_2}	λ	α	δ	β	χ	ϕ
Value	0.0002	0.0998	1.0	0.995	0.6	0.00012	0.00001

Table 2.A2: Stoichiometric coefficients used in the model

For model validation, comparisons are made to the experiments of Ehn et al. (2014). In the low-NOx regime, the experiments of Ehn et al. (2014) lasted 45 min and the initial ozone concentration was 80 ppb. In the model, we modified the initial concentration of α-pinene from 0 ppb to 11 ppb to reproduce the observations. Figure [2.A1], which shows one-fifth of the ELVOC concentrations as a function of the α-pinene reaction rate, reproduces successfully the extended data Figure 10 of Ehn et al. (2014). According to Figure [2.A1], the increase of peroxy radicals has a square root dependence while ELVOC monomers and dimers evolve nearly linearly. Therefore, the total ELVOC concentration has a near-linear dependence on the amount of α-pinene reacting with O_3 indicative of first-generation oxidation products. These findings are consistent qualitatively and quantitatively with Ehn et al. (2014) measured and modeled results.

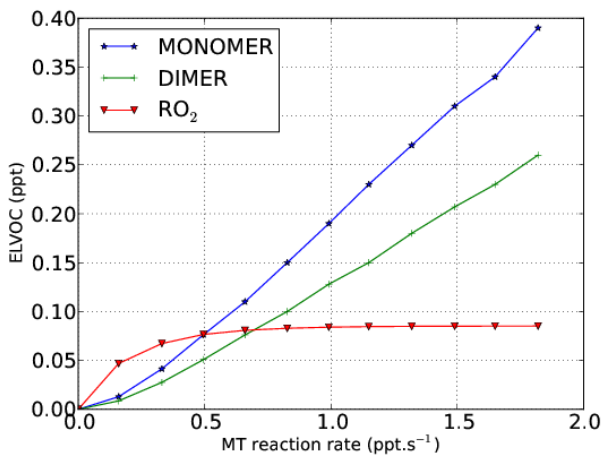

Figure 2.A1: ELVOC concentrations as a function of the α-pinene reaction rate for the low-NO_x experiment

In the high NO_x regime, the experiments of Ehn et al. (2014) also lasted 45 min and the initial ozone and α-pinene concentrations were 80 ppb and 5 ppb respectively. The initial NO concentration was changed gradually from 0.3 ppb to 5 ppb. Figure [2.A2], which shows one-fifth of the ELVOC as a function of the RO_2 concentration, reproduces successfully the Extended Data Figure 10 of Ehn et al. (2014). While increasing NO concentration, both monomer and dimer concentrations decrease rapidly as expected because a fraction of peroxy radicals is consumed by the NO reaction. Moreover, the dimer concentration decreases rapidly while the monomer concentration decreases more slowly. Simultaneously, the organic nitrate concentration increases with increasing NO.

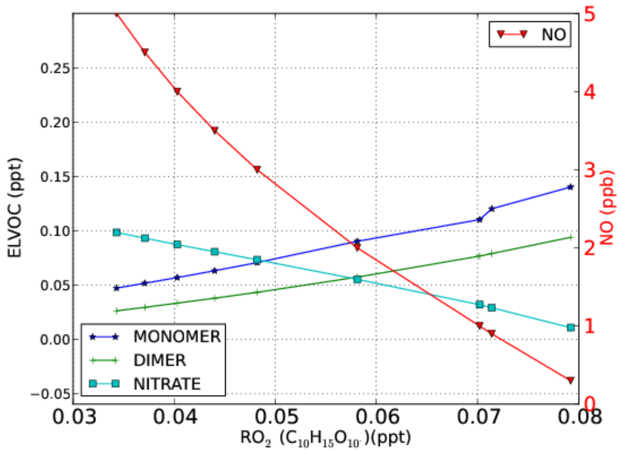

Figure 2.A2: ELVOC concentration as a function of the RO_2 concentration in the high-NO_x regime.

Formation of organic nitrate

The formation of organic nitrate (orgNIT) from monoterpenes (MT) is modeled with the following reactions:

$$Terpene + OH \xrightarrow[k'_1]{} TERPRO_2 \tag{2.10}$$

$$TERPRO_2 + NO \xrightarrow[k'_2]{} 0.201 orgNIT \tag{2.11}$$

$$MT + NO_3 \xrightarrow[k'_3]{} TERPNRO_2 \tag{2.12}$$

$$TERPNRO_2 + NO \xrightarrow[k'_4]{} 0.688 orgNIT + Products \tag{2.13}$$

$$TERPNRO_2 + HO_2 \xrightarrow[k'_5]{} orgNIT + Products \tag{2.14}$$

$$TERPNRO_2 + NO_3 \xrightarrow[k'_6]{} 0.422 orgNIT + Products \tag{2.15}$$

$$TERPNRO_2 + RO_2 \xrightarrow[k'_7]{} (1 - 0.578\delta) orgNIT + Products \quad \text{where } \delta = 50\% \tag{2.16}$$

Kinetic constant	Value (cm^3s^{-1} or s^{-1})
k'$_1$	α-pinene (1.21 10^{-11} exp(444/T))
	Limonene (4.20 10^{-11} exp(401/T))
	β-pinene (2.38 10^{-11} exp(357/T))
	Humulene (2.93 10^{-10})
k'$_2$	2.27 10^{-11} exp(435/T)
k'$_3$	α-pinene (1.19 10^{-12} exp(490/T))
	Limonene (1.22 10^{-11})
	β-pinene (2.51 10^{-12})
	Humulene (1.33 10^{-12} exp(490/T))
k'$_4$	2.6 10^{-12} exp(380/T)
k'$_5$	2.65 10^{-13} exp(1300/T)
k'$_6$	2.3 10^{-12}
k'$_7$	3.5 10^{-14}

Table 2.B1: Kinetic constants used in the organic nitrate formation mechanism

Statistic indicators and criteria

The statistic indicators used in this paper are described in Table 4.A1. The performance and goal criteria used in this paper are described in Table 4.A2.

Statistic indicator	Definition
Root mean square error (RMSE)	$\sqrt{\frac{1}{n}\sum_{i=1}^{n}(c_i - o_i)^2}$
Correlation (Corr)	$\frac{\sum_{i=1}^{n}(c_i - \bar{c})(o_i - \bar{o})}{\sqrt{\sum_{i=1}^{n}(c_i - \bar{c})^2}\sqrt{\sum_{i=1}^{n}(o_i - \bar{o})^2}}$
Mean fractional bias (MFB)	$\frac{1}{n}\sum_{i=1}^{n}\frac{c_i - o_i}{(c_i + o_i)/2}$
Mean fractional error (MFE)	$\frac{1}{n}\sum_{i=1}^{n}\frac{\mid c_i - o_i \mid}{(c_i + o_i)/2}$

Table 2.C1: Definitions of the statistics used in this work. $(o_i)_i$ and $(c_i)_i$ are the observed and the simulated concentrations at time and location i, respectively. n is the number of data

Criteria	Performance criterion	Goal criterion
$\mid$ MFB $\mid$	$\leq 60\%$	$\leq 30\%$
MFE	$\leq 75\%$	$\leq 50\%$

Table 2.C2: Boylan and Russel criteria

Sensitivity to ELVOC yield

The ELVOC yield in the reference simulation is 11%. Two sensitivity simulations are performed, using a lower bound (3%, Jokinen et al. (2015)) and a higher bound (18%, Ehn et al. (2014)).

The comparison of OM_1 concentrations is shown in Figure 2.D1 and the statistical evaluation is shown in Table 2.D1. The correlation between the measurements and the simulation is not modified by the ELVOC yield. However, the higher the yield, the closer to zero the bias is (it decreases from -26% to -7%) and the lower the error MFE. However, the lower RMSE is obtained with a yield of 11% (1.53 μg.m^{-3} with a yield of 11% against 1.54 μg.m^{-3} with a yield of 3% and 1.59 μg.m^{-3} with a yield of 18%).

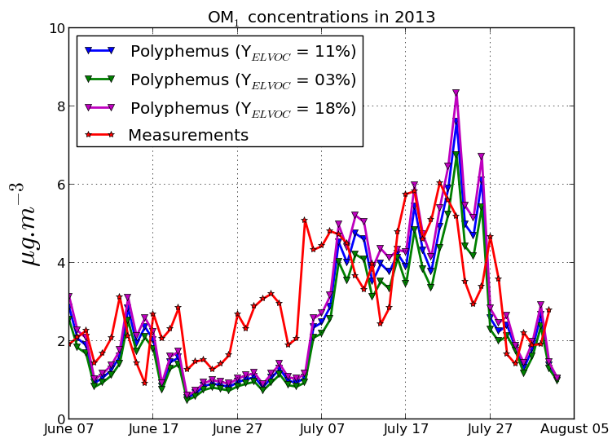

Figure 2.D1: Simulated daily concentrations of OM_1 using a molar ELVOC yield of 11% (blue plot, reference simulation), 18% (magenta plot) and 3% (green plot).

ELVOC yield (%)	$\overline{s}$ [μg.m^{-3}]	RMSE [μg.m^{-3}]	Correlation [%]	MFB	MFE
03	2.30	1.54	67.2	-0.26	0.52
11	2.58	1.53	67.3	-0.15	0.49
18	2.82	1.59	67.2	-0.07	0.47

Table 2.D1: Statistics of model to measurements comparisons for organic concentrations in particles of diameters lower than 1 μm during the summer campaign of 2013 using an ELVOC molar yield of 3%, 11% (reference) and 18%. $\overline{s}$ represents the simulated mean concentrations. The observed mean concentration is $\overline{o} = 2.89$ μg.m^{-3}.

The simulated composition of OM_1 using ELVOC yields of 3% and 18% are shown in Figure 2.D2. Using an ELVOC yield of 3% (respectively 18%), the ELVOCs represent 4.7% (respectively 22.9%) of the OM_1 mass.

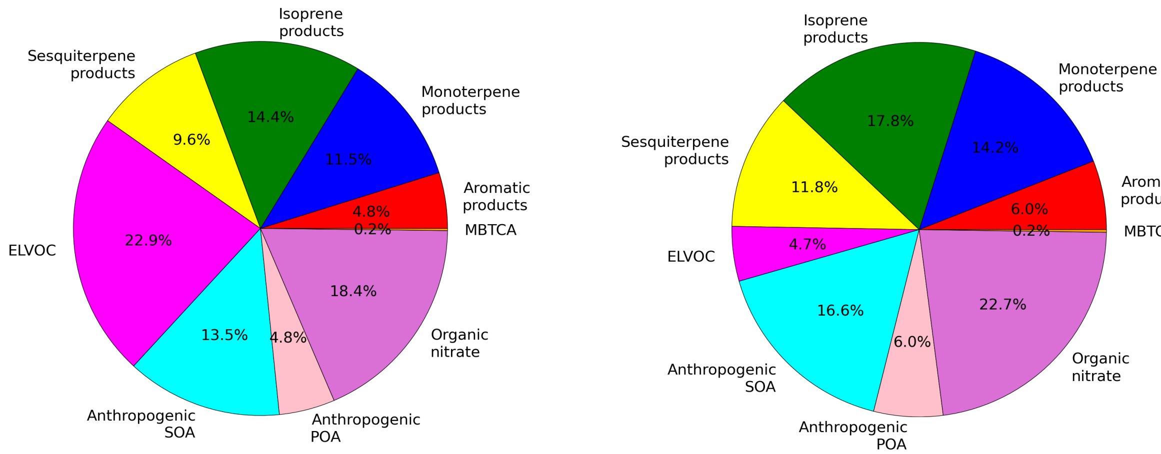

Figure 2.D2: Simulated composition of OM_1 using the upper (left panel) and lower (right panel) bounds of ELVOCs molar yields

The OM:OC and O:C ratios are plotted using the three yields (3%, 11% and 18%) in Figure 2.D3. The simulated means of the two ratios using the three ELVOC yields (3%, 11% and 18%) are shown in table 2.D2. The ratios using the upper bound of ELVOC yields are the closest to the measurements. The OM:OC and O:C ratios may be higher if organo-sulfate are considered (section 2.4.3).

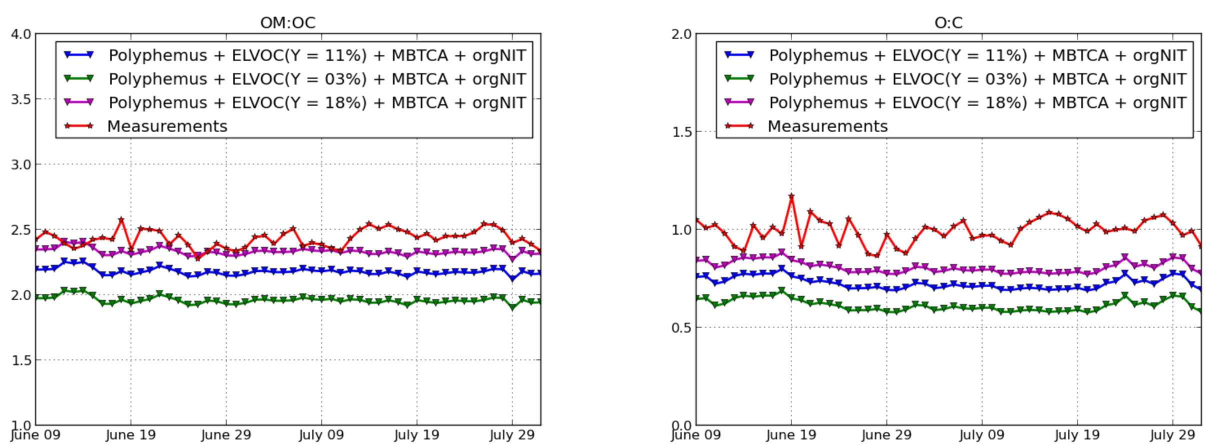

Figure 2.D3: Comparisons of the OM:OC ratio (left panel) and the O:C ratio (right panel) for simulations using an ELVOC molar yield of 3%, 11% and 18%.

ELVOC yield (%)	OM:OC	O:C
3	1.96	0.61
11	2.18	0.73
18	2.33	0.81

Table 2.D2: Simulated means of the OM:OC and O:C ratios during the summer campaign of 2013 using an ELVOC molar yield of 3%, 11% and 18%. The measured means of OM:OC and O:C are 2.43 and 0.99 respectively.

Chapitre 3

Sources des aérosols au dessus du bassin ouest Méditerranéen pendant l'été

Sommaire

Nous nous intéressons dans ce chapitre à la compréhension des sources des aérosols organiques et inorganiques au dessus du bassin ouest de la Méditerranée et évaluer la sensibilité des concentrations des aérosols à différents paramètres d'entrée du modèle (les champs météorologiques, les émissions anthropiques, les émissions des sels de mer ainsi que le modèle de représentation de la condensation/évaporation). Toutes ces données d'entrée sont d'importantes sources d'incertitudes. Par exemple, en ce qui concerne les champs météorologiques, le mélange vertical turbulent affecte la dilution des polluants et leur transport vertical, la formation des nuages affecte la photochimie et la distribution en taille des particules, les précipitations ont une incidence sur les dépôts humides. Comme la pollution au dessus de la Méditerranée (MED) est en grande partie transportée (par exemple des poussières viennent du Sahara au Sud et des composés biogéniques et anthropiques du continent européen), les champs météorologiques peuvent grandement influencer les concentrations. Les incertitudes sur les émissions concernent les taux d'émissions, les espèces émises (composés organiques semi-volatiles et de volatilité intermédiaire (I/S-VOCs)), leur distribution spatiale et temporelle (surtout pour les émissions des bateaux). En effet, les émissions de bateaux contribuent de manière importante à la masse des particules de diamètre inférieur à 10 μm (11% à l'le Lampedusa et 8% au Cap Granitola en Sicilie (Becagli et al., 2017))..De plus, Aksoyoglu et al. (2016) ont montré que les émissions des bateaux en MED contribuent jusqu'à 60% aux concentrations du sulfate, car le dioxyde de souffre (SO_2) est un polluant majeur émis par le transport maritime. En ce qui concerne les sels marins, leurs émissions influencent la formation des particules et des noyaux de condensation (CCN). Or, d'après Grythe et al. (2014), les émissions des sels de mer sont les plus incertaines parmi toutes les émissions. La modélisation de ces émissions est basée sur des paramétrisations empiriques qui dépend de la vitesse de friction entre l'air et la surface de la mer, la salinité, et la temperature de la surface de mer.

Dans le cadre du projet ChArMEx, des études de sensibilité à ces paramèrtes du modèle sont conduites pendant les étés 2012 (6 juin au 8 juillet), 2013 (6 juin au 10 août) et 2014 (10 juillet 2014). Les concentrations simulées sont comparées à celles mesurées à la station Ersa (Cap Corse, France) pendant les étés 2012 et 2013, et au dessus du domaine MED durant le vol d'avion de 2014 (selon l'altitude, la longitude et la latitude de l'avion).

Avant l'étude de la sensibilité à la météorologie, une évaluation des champs météorologiques a été effectuée en utilisant les sorties de quatre modèles: ECMWF, WRF avec une projection longitude/latitude (WRF-lon/lat), WRF avec une projection Lambert (WRF-Lambert) et WRF avec projection lambert avec analyse (WRF-Lambert-OBSGRID: analyse du modèle WRF-Lambert avec des observations de température, humidité relative et vent à partir des mesures en surface et en radiosonde). La température, l'humidité relative, la vitesse et la direction du vent sont comparées à Ersa pendant les étés 2012 et 2013. Les quatre simulations de la météorologie donnent des températures simulées en accord avec les mesures à Ersa et des biais presque nulles.

ECMWF simule la vitesse du vent la plus proche aux mesures avec des corrélations entre 69% et 87%. WRF lon-lat est aussi en accord avec les mesures avec des corrélations entre 60% et 65%. WRF-lambert et WRF-Lambert-OBSGRID simulent moins bien les vitesses de vent avec des corrélations négatives.

Quant à l'humidité relative, tous les modèles simulent bien l'humidité relative à Ersa pendant les étés 2012 et 2013 avec des biais fractionnels moyens inférieurs à 32% et des erreurs fractionnelles moyennes inférieures à 18%. La direction du vent simulée est similaire pendant les étés 2012 et 2013 surtout avec les modèles ECMWF et WRF-lon/lat. Les champs simulés par ECMWF et WRF-lon/lat se comparant le mieux aux données d'observation, ils sont utilisés pour l'étude de sensibilité à la météorologie.

La simulation de référence utilise les champs ECMWF comme champs météorologiques, EDGAR _HATP_V2 comme inventaire d'émissions anthropiques, la paramétrisation de Jaeglé et al. (2011)

pour générer les émissions de sels marins. Par comparaisons des concentrations simulées aux observations à ERSA, les concentrations de PM_{10}, PM_1, OM_1 sont bien modélisés pendant les deux campagnes de mesures de 2012 et 2013 et le critère de but de Boylan and Russell (2006) est vérifié. Les concentrations de PM_{10} pendant l'été 2012 sont plus élevées que celles pendant l'été 2013 à cause des épisodes de poussières désértiques plus importants pendant l'été 2012.

Les études de sensibilité montrent que les concentrations de PM_{10} et PM_1 sont sensibles aux émissions de sels de mer (avec une erreur RMSE normalisée de 65% et 40% respectivement). Elles sont aussi sensibles à la météorologie (avec une RMSE normalisée de 33% et 21% respectivement) et moins sensibles aux émissions anthropiques (avec une RMSE normalisée de 17% et 10% respectivement). La composition chimique des PM_{10} et des PM_1 permet d'identifier les sources des aérosols et de comprendre les sensibilités observées pour les PM_{10} et PM_1. Les aérsols organiques contribuent largement à la masse des PM_{10} (30% en 2012 et 33% en 2013). La fraction des aérosols inorganiques dans les PM_{10} est également très importante (31% en 2012 et 39% en 2013). Parmi les aérosols inorganiques, le sulfate principalement originaire des sources anthropiques représente presque 18% de la masse de PM_{10} en 2012 et 19% en 2013. Le carbone suie, originaire des émissions du traffic (notamment maritime) et des activités inductrielles dans les grandes villes au sud de la France et le nord de l'Italie, contribue faiblement aux concentrations des PM_{10} à Ersa (5% en 2012 et 7% en 2013). Les poussières tranportées du Sahara au sud de la MED représentent 34% et 21% de la masse des PM_{10} pendant les étés 2012 et 2013 respectivement. Les PM_1 sont composés principalement d'aérosols organiques (41% en 2012 et 38% en 2013) et du sulfate (30% en 2012 et 24% en 2013).

L'étude de sensibilité des concentrations des aérosols organiques dans les PM_1 montre que ces dernières sont dépendantes des champs météorologiques (avec une erreur RMSE normalisée de 49%), aux émissions anthropiques (avec une erreur RMSE normalisée de 32%), aux émissions des sels de mer (avec une erreur RMSE normalisée de 29%) sur lesquelles peut condenser les aérosols organiques secondaires hydrophiles. La sensibilité aux émissions des composés organiques semi-volatils et de volatilité intermédiaire est très faible (avec une erreur RMSE normalisée de 1%).

Quant aux aérosols inorganiques secondaires (AIS), le sulfate s'avère très sensible aux émissions anthropiques et à celles du traffic des bateaux en particulier (avec une erreur RMSE normalisée de 44% pour les AIS dans les PM_{10}). La météorologie et les émissions des sels marins induisent une erreur normalisée de 22% pour les concentrations des AIS dans les PM_{10}. Le nitrate, le chloride, le sodium et l'ammonium sont très sensibles à la paramétrisation des sels de mer et sont mieux modélisés en utilisant la paramétrisation de Jaeglé et al. (2011) que celle communément utilisée de Monahan et al. (1986), car la paramétrisation de Jaeglé et al. (2011) a une dépendance moins forte à la vitesse de frottement de l'air sur la surface de la mer. La météorologie influence les AIS car elle influence le partage gaz/particules, mais également car elle influence la formation des aérosols organiques (à cause de son influence sur les émissions biogéniques) et la formation de nitrate organique. Les AIS sont par ailleurs sensibles aux émissions anthropiques à cause de l'influence de ces dernières sur les concentrations de NO_x et d'oxydants.

Les concentrations de sulfate, d'ammonium et de nitrate ont été évaluées par comparaisons aux observations faites durant le vol avion du 10 juillet 2014 au dessus de la MED. Le but est d'étudier la formation des aérosols au dessus de la mer sous un régime de Mistral (vent fort nord et nord ouest provenant de la vallée du Rhône (France)). Les comparaisons sont faites quand l'avion vole à basses altitudes (altitudes de vol en dessous de 800 m par rapport au niveau de la mer) et quand l'avion vole dans la couche limite (en pratique, les comparaisons mesures/modèle sont effectuées quand la hauteur de couche limite est supérieure à 1200 m). La comparaison du profil vertical des concentrations mesurées et simulées (simulation de réference) du sulfate montre que le sulfate est légèrement surestimé par le modèle. Une simulation sans émission de sulfate marin montre que le sulfate est majoritairement d'origine anthropique et que l'influence du sulfate marin est négligeable. Cette conclusion est appuyée par l'étude de sensibilité suivante: En addition, quand les émissions anthropiques des oxydes sulphuriques sont toutes spéciées en SO_2 au lieu d'être spéciées en 98% de SO_2 et 2% de H_2SO_4 comme dans la simulation de référence, les concentrations simulées du sulfate sont plus basses en raison de la diminution des émissions de H_2SO_4 qui se condense très rapidement pour former du sulfate en phase particulaire. A cause du caractère semi-volatile du chloride, de l'ammonium et du nitrate, les concentrations simulées dépendent des hypothèses utilisées pour la modélisation de la condensation/évaporation. Dans le modèle de réference, on suppose que toutes les espèces inorganiques dans les particules sont en équilibre thermodynamique avec les gaz. Deux études de sensibilité sont conduites: la première concerne l'hypothèse de l'équilibre thermodynamique (équilibre thermodynamique vs modèle de condensation/évaporation dynamique) et la deuxième concerne l'état du mélange, c-à-d on fait l'hypothèse que le sodium et le chloride ne sont pas mélangés avec les autres inorganiques (mélange interne vs mélange externe). La comparaison des profils verticaux des concentrations mesurées et simulées avec l'hypotèse de l'équilibre thermodynamique montre la sous-estimation des concentrations du nitrate ce qui est probablement dû à la surestimation du sulfate mais aussi au fait que l'hypothèse de l'équilibre thermodynamique n'est pas vérifiée. Quand la condensation/évaporation est calculée dynamiquement, les concentrations simulées de nitrate sont plus proches de celles observées. En plus, quand l'hypothèse du mélange externe est faite pour les sels marins, les concentrations simulées d'ammonium sont plus proches de celles observées, montrant que le mélange des aérosols inorganiques ainsi que la modélisation de l'échange gaz/particules par un modèle dynamique influencent fortement les concentrations simulées.

Une étude des cartes de concentrations au dessus du bassin ouest de la MED montre que les concentrations des aérosols organiques sont élevées au dessus des zones où les émissions biogéniques sont importantes (l'Italie et la Corse). Les concentrations de sulfate sont importantes au dessus des routes des bateaux reliant Marseille à Bastia et Ajaccio. D'importantes concentrations d'aérosols inorganiques secondaires (AIS) sont simulées au dessus des zones où les émissions anthropiques sont importantes (au dessus du nord de l'Italie et des grandes villes).

Au dessus du domaine MED, les AIS et les aérosols organiques sont très sensibles à la météorologie surtout au dessus de l'Italie et des zones où les concentrations des aérosols organiques sont importantes à cause de l'influence de la température sur le partitionnement des AIS semi-volatile et de l'influence de la météorologie sur les émissions biogéniques. Les aérosols organiques sont aussi sensibles aux émissions des sels de mer au dessus des zones où les concentations d'AIS sont importantes parce que les aérosols organiques hydrophiles sont absorbés par les AIS. Par ailleurs, la sensibilité du sulfate et des AIS aux émissions anthropiques est importante. Les différences des concentrations de sulfate sont surtout localisées au dessus des routes des bateaux parce que les émissions relatives au traffic maritime sont spatiallement mieux représentées avec l'inventaire EDGAR_HTAP_V2 qu'avec EMEP.

Ce chapitre est constitué de l'article:
Aerosol sources in the western Mediterranean during summertime: A model-based approach (2017b), Mounir Chrit, Karine Sartelet, Jean Sciare, Jorge Pey, José B. Nicolas, Nicolas Marchand, Evelyn Freney, , Karine Sellegri, Matthias Beekmann, and François Dulac, Atmos. Chem. Phys.Discuss., submitted.

Aerosol sources in the western Mediterranean during summertime: A model-based approach

MounirChrit[1], KarineSartelet[1], JeanSciare[2,6], JorgePey[3*], José B.Nicolas[4], NicolasMarchand [3], EvelynFreney[4], KarineSellegri[4], MatthiasBeekmann[5] and FrançoisDulac[2]

[1] CEREA, joint laboratory Ecole des Ponts ParisTech - EDF R&D, Université Paris-Est, 77455 Champs sur Marne, France.
[2] LSCE, CNRS-CEA-UVSQ,IPSL,Université Paris Saclay, Gif-sur-Yvette, France
[3] Aix Marseille University-CNRS, LCE, Marseille, France
[4] LAMP, UMR CNRS-Université Blaise Pascal, OPGC, Aubière, France
[5] LISA, UMR 7583, Université Paris Diderot-Université Paris-Est Créteil, IPSL, Créteil, France
[6] EEWRC, The Cyprus Institute, Nicosia, Cyprus
[*] Now at the Spanish Geological Survey, IGME, 50006 Zaragoza, Spain

Abstract In the framework of ChArMEx (the Chemistry-Aerosol Mediterranean Experiment), the air-quality model Polyphemus is used to understand the sources of inorganic and organic particles in the western Mediterranean and to evaluate the uncertainties linked to the model parameters (meteorological fields, anthropogenic and sea-salt emissions, hypotheses related to the model representation of condensation/evaporation). The model is evaluated by comparisons to in-situ aerosol measurements performed during three consecutive summers (2012, 2013 and 2014). The model-to-measurement comparisons concern the concentrations of PM_{10}, PM_1, Organic Matter in PM_1 (OM_{PM_1}) and inorganic aerosol concentrations monitored at a remote site (Ersa) in Corsica Island, as well as during airborne measurements performed above the western Mediterranean Sea. Organic particles are mostly from biogenic origin. The model parameterization of sea-salt emissions has shown to strongly influence the concentrations of all particulate species (PM_{10}, PM_1, OM_{PM_1} and inorganic concentrations). Although the emission of organic matter by the sea has shown to be low, organic concentrations are influenced by sea-salt emissions, because they provide a mass onto which gaseous hydrophilic organic compound can condense. PM_{10}, PM_1, OM_{PM_1} are also very sensitive to meteorology, because it affects not only the transport of pollutants, but also natural emissions (biogenic and sea salt). To avoid large and unrealistic sea-salt concentrations, a parameterization with an adequate wind-speed power law is chosen. Sulfate is shown to be strongly influenced by anthropogenic (ship) emissions. PM_{10}, PM_1, OM_1 and sulfate concentrations are better described using the emission inventory with the best spatial description of ships emissions (EDGAR-HTAP). However, this is not true for nitrate, ammonium and chloride concentrations, which are very dependent on the hypotheses used in the model for condensation/evaporation. Model simulations show that sea-salt aerosols above the sea are not mixed with background transported aerosols. Taking into account the mixing state of particles with a dynamic approach of condensation/evaporation may be necessary to accurately represent inorganic aerosol concentrations.

3.1 Introduction

Fine particulate matter (PM) in the atmosphere are of concern due to their effects on health, climate, ecosystems and biological cycles, and visibility. These effects are especially important in the Mediterranean region. The western Mediterranean basin experiences high gaseous pollution levels originating from Europe (Millán et al., 1997) in particular during summer, when photochemical activity is at its maximum. Furthermore, the western Mediterranean basin is impacted by various natural sources: Saharan dust, intense biogenic emissions in summer, oceanic emissions, and biomass burning, all of them being emitters of gases (e.g. volatile organic compounds (VOC), nitrogen oxides (NO_x)) and/or primary particles (Bossioli et al., 2016; Tyrlis and Lelieveld, 2012; Monks et al., 2009; Gerasopoulos et al., 2006). During the TRAQA 2012 and SAFMED 2013 measurement campaigns, (Di Biagio et al., 2015) observed that aerosols in the western Mediterranean basin are strongly impacted by dust outflows and continental pollution. A large part of this continental pollution is secondary, i.e. it is formed in the atmosphere by chemical reactions (e.g. Sartelet et al., 2012). These reactions involve compounds, which may be emitted from different sources (e.g. biogenic and anthropogenic). Using measurements and/or modelling, several studies showed that as much as 70% to 80% of organic aerosol in summer in the western Mediterranean region is secondary and from contemporary origins (El Haddad et al., 2011; Chrit et al., 2017).

Air-quality models are powerful tools to simulate and predict the atmospheric chemical composition and the properties of aerosols at regional scales. In spite of the tremendous efforts deployed recently, the sources and the transformation mechanisms of atmospheric aerosols are not fully characterized nor fully understood. For organic aerosols, difficulties in the modeling partly lie in the representation of volatile and semi-volatile organic precursors in the models, which can only take into account a limited number of compounds or classes of compounds (Kim et al., 2011a; Chrit et al., 2017). Difficulties in modeling aerosol concentrations are strongly linked to uncertainties in meteorology and in emissions (Roustan et al., 2010b). For example, the turbulent vertical mixing affects the dilution and chemical processing of aerosols and their precursors (Nilsson et al., 2001; Aan de Brugh et al., 2012), clouds affect aerosol chemistry and size distribution (Fahey and Pandis, 2001; Ervens et al., 2011), and photochemistry (Tang et al., 2003; Feng et al., 2004), and precipitation controls wet deposition processes (Barth et al., 2007; Yang et al., 2012; Wang et al., 2013). Over the Mediterranean region, uncertainties due to meteorology and transport may strongly impact pollutant concentrations, because the basin is influenced by pollution transported from different regions, such as dust from Algeria, Tunisia and Morocco as well as both biogenic and anthropogenic species from Europe (Chrit et al., 2017; Denjean et al., 2016). Chrit et al. (2017) and Cholakian et al. (2017) showed that although organic aerosol concentrations at a remote marine site of the western Mediterranean are mostly of biogenic origin, they are strongly influenced by air-masses transported from the continent and by maritime shipping emissions.

In addition to the meteorological uncertainties, uncertainties in emission inventories are also important. There are uncertainties in biogenic emissions (Sartelet et al., 2012), as well as in anthropogenic emission inventories. For anthropogenic emissions, uncertainties concern not only the emissions themselves, but also the pollutants that are to be considered in the inventory and the spatial and temporal distributions of the emissions. For example, intermediate and semi volatile organic compounds are missing from emission inventories, even though they may strongly affect the formation of organic aerosols (Couvidat et al., 2012; Denier van der Gon et al., 2015). The spatial distribution of ships and harbor traffic differs depending on emission inventories. However, over the Mediterranean Sea, ships and harbor traffic emissions may strongly affect the formation of particles. Becagli et al. (2017) found experimentally that the minimum ship emission contributions to PM_{10} is 11% at Lampedusa Island, and 8% at Capo Granitola on the southern coast of Sicily. Aksoyoglu et al. (2016) showed that ship emissions in the Mediterranean may contribute up to 60% of sulfate concentrations, as SO_2 is a major pollutant emitted from maritime transport. However, by comparison to on-road vehicles, ships emissions are still poorly characterized (Berg et al., 2012). Besides, the multiplicity of the Mediterranean sources of pollution and their interactions makes it difficult to quantify the ship contribution to aerosol concentrations.

Seas and oceans are a significant source of sea-spray aerosols (SSA). They strongly affect the formation of cloud condensation nuclei and particle concentrations. However, according to Grythe et al. (2014), sea-spray aerosols (SSA) have one of the largest uncertainties among all emissions.

The modeling of sea-salt emissions is based on empiric or semi-empiric formulas. There is a tremendous amount of parameterization of the SSA emission fluxes (Grythe et al., 2014). The SSA emission parameterization of Monahan et al. (1986) is commonly used to model sea-salt emissions of coarse particles (e.g. Sartelet et al., 2012; Solazzo et al., 2017; Kim et al., 2017). However, the strong non-linearity of the source function versus wind speed (power law with an exponent of 3.41) may lead to an overestimation of emissions at high-speed regimes, as suggested by Guelle et al. (2001) and Witek et al. (2007). Many studies showed that wind speed has the dominant influence on the sea-salt emissions (Hoppel et al., 1989; Grythe et al., 2014). However, other parameterizations use different power laws with different exponents for the wind speed (e.g. 2.07 for Jaeglé et al. (2011)), and have introduced other parameters like sea-surface temperature (Schwier et al., 2017; Jaeglé et al., 2011; Sofiev et al., 2011) and the water salinity (Grythe et al., 2014). Although the influence of marine emissions on primary organic aerosols is low for the Mediterranean (Chrit et al., 2017), their influence on inorganic aerosols is not (Claeys et al., 2017).

The aim of this work is to evaluate some of the processes that strongly affect inorganic and organic aerosol concentrations in the western Mediterranean in summer (transport and emissions), how do the data/parameterizations commonly used in air-quality models affect the concentrations. To that end, sensitivity studies relative to transport (meteorology) and emissions (anthropogenic and sea salt) are performed with the air-quality model Polyphemus and are compared to measurements performed at the marine remote Ersa super-site (Cap Corsica, France) during the summer campaigns of 2012 and 2013, and to flight measurements performed above the Western Mediterranean Sea in summer (July) 2014.

This paper is structured as follows. The air-quality model Polyphemus set-up is first described for the different input data-sets/parameterizations used, as well as the measurements. Second, the meteorological fields used as input to the air-quality model are evaluated. Third, the model is evaluated by comparisons to the measurements and sensitivities studies to meteorology, sea-salt emission parameterizations and anthropogenic emissions are performed to determine the main aerosol sources and sensitivities.

3.2 Simulations set-up and measured data

In order to simulate aerosol formation over the western Mediterranean, the Polair3d/Polyphemus air quality model is used, with the set-up described in Chrit et al. (2017) and summarized here.

3.2.1 Simulations set-up

Simulations are performed over the same domains and using the same input data as in Chrit et al. (2017). Two nested simulations are performed: one over Europe (nesting domain, horizontal resolution: $0.5°\times0.5°$) and one over a Mediterranean domain centered around Corsica (nested domain, horizontal resolution: $0.125°\times0.125°$), centered around the Ersa surface super-site (red point in Figure [3.1]).

Simulations are performed during the summers of 2012, 2013 and 2014. The dates of simulations are chosen to match the periods of observations performed during ChArMEx (Chemistry-Aerosol Mediterranean Experiment). The Mediterranean simulations (nested domain) are performed from 6 June to 8 July 2012, from 6 June to 10 August 2013; and from 9 to 10 July 2014.

In the reference simulation, meteorological data are provided by the European Center for Medium-Range Weather Forecasts (ECMWF) model (horizontal resolution: $0.25° \times 0.25°$). The vertical diffusion is computed using the Troen and Mahrt (1986) parameterization. In the sensitiv-

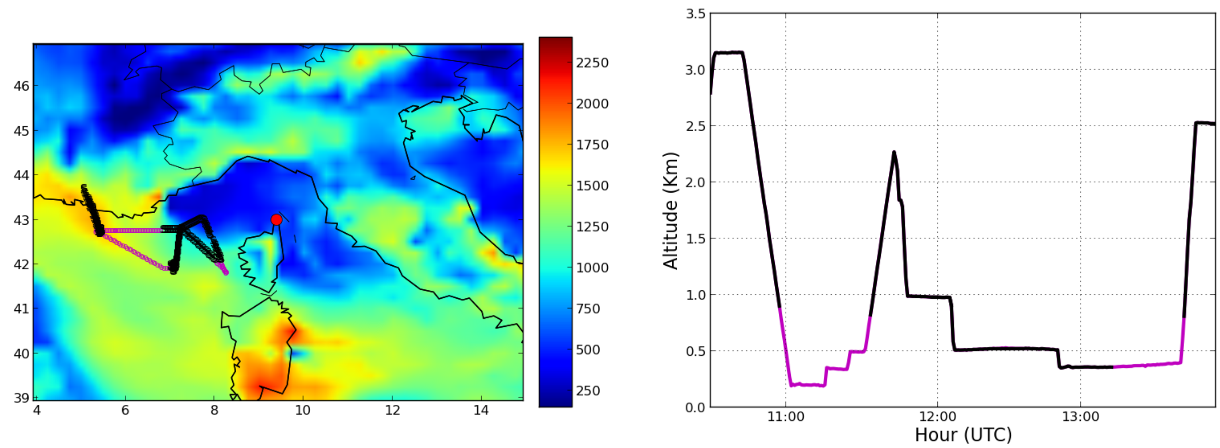

Figure 3.1: Mediterranean domain used for the simulations and planetary boundary layer (PBL) height on 10 July 2014 at noon, as obtained from the ECMWF meteorological fields (left panel). Ersa is located at the red point on northern tip of Corsica Island. The (black and purple) crosses indicate the trajectory of the flight of 10 July 2014 over the Mediterranean Sea. Altitudes during the flight (right panel). The portions conducted above the continent at the beginning and at the end of the flight from/to Avignon airport have been removed. For the model to measurement comparisons, only the transects indicated by purple crosses/lines are considered.

ity study relative to meteorology, meteorological fields from the Weather Research and Forecasting model (WRF, Skamarock et al. (2008)) are used in the Mediterranean simulation. To simulate WRF meteorological fields over the Mediterranean domain, WRF simulations are conducted on two nested domains: one over Europe and one over the Mediterranean. Before conducting the sensitivity study relative to meteorology (section 3.3) by using two different meteorological datasets, WRF is run with a number of different configurations, which are compared to measurements in section 3.3.

In the first configuration (WRF-Lon-Lat), horizontal resolutions of $0.5° \times 0.5°$ and $0.125° \times 0.125°$ are used for the nesting and nested domains respectively with a longitude-latitude projection. In the second configuration (WRF-Lambert), a Lambert (conic conform) projection is used with horizontal resolutions of 55.65 km $\times$ 55.65 km and 13.9 km $\times$ 13.9 km for the nesting and nested domains respectively. The third configuration (WRF-Lambert-OBSGRID) also uses a Lambert projection, but the meteorological fields are improved by nudging global observations of temperature, humidity and wind from surface and radiosonde measurements (NCEP (National Centers for Environmental Prediction) operational global surface and upper-air observation subsets, as archived by the Data Support Section (DSS) at NCAR (National Center for Atmospheric Research)).

Biogenic emissions are estimated using Model of Emissions of Gases and Aerosols from Nature (MEGAN) (Guenther et al., 2006). In the reference simulation, yearly anthropogenic emissions are generated using the EDGAR-HTAP_V2 inventory for 2010 (http://edgar.jrc.ec.europa.eu/htap_v2/). EDGAR-HTAP_V2 inventory uses total national emissions from the European Monitoring and Evaluation Program (EMEP) emission inventory that are re-allocated spatially using EDGAR4.1 proxy subset (Janssens-Maenhout et al., 2012). The differences between the two inventories do not lie only in the spatial allocation of emissions, but also in the spatial resolution. EMEP provides a resolution of 0.5° x 0.5° while the resolution of EDGAR-HTAP_V2 is 0.1° x 0.1°. To illustrate the differences between the two inventories, NO_x emissions from the EMEP emission inventory, as well as absolute differences of NO_x emissions between the HTAP and EMEP inventories are shown in Figure 3.2. The highest discrepencies between the two inventories mostly concern the shipping emissions (very low in EMEP emission inventory (≤ 0.2 μg m^{-2} s^{-1}) whereas they can be as high as 2.8 μg m^{-2} s^{-1} over the sea in HTAP emission inventory), as well as emissions over large cities, mostly Genoa, Marseille and Rome (with emissions as high as 2.5 μg.m^{-2}.s^{-1} higher in HTAP emission inventory).

Gaseous anthropogenic intermediate/semi-volatile organic compounds (I/S-VOC) emissions are missing from emission inventories, they are estimated here as detailed in Zhu et al. (2016) by multiplying the primary organic emissions (POA) by 1.5, and by assigning them to species of different volatilities. A sensitivity study where I-S/VOC emissions are not taken into account is also performed.

Sea-salt emissions are parameterized using Jaeglé et al. (2011) in the reference simulation and using the commonly-used Monahan et al. (1986) for a sensitivity study. These two parameterizations are different in terms of the source function, which is defined as the total mass of sea-salt aerosol (SSA) released by area and time units. In fact, the source functions of these two parameterizations have a different dependency on the wind speed. In terms of emitted sea-salt mass, the largest differences are located over the sea in the south of France (with differences as high as 1400%), where the shear stress exerted by the wind on the sea surface is the highest. Following Schwier et al. (2015), the emitted dry sea-salt mass is assumed to be made of 25.40% of chloride, 30.61% of sodium and 4.22% of sulfate.

The condensation/evaporation of inorganic aerosols is determined using the thermodynamic model ISORROPIA (Nenes et al., 1998) with a bulk equilibrium approach in order to compute the partitioning between the gaseous and particle phases of aerosols. Because the concentrations and the partitioning between gaseous and particle phases of inorganic aerosols (chloride, nitrate, ammonium) is strongly affected by condensation/evaporation and reactions with other pollutants, sensitivities of inorganic concentrations to hypothesis used in the modeling (thermodynamic equilibrium, mixed sea-salt and anthropogenic aerosols) are also performed (section 3.4.4).

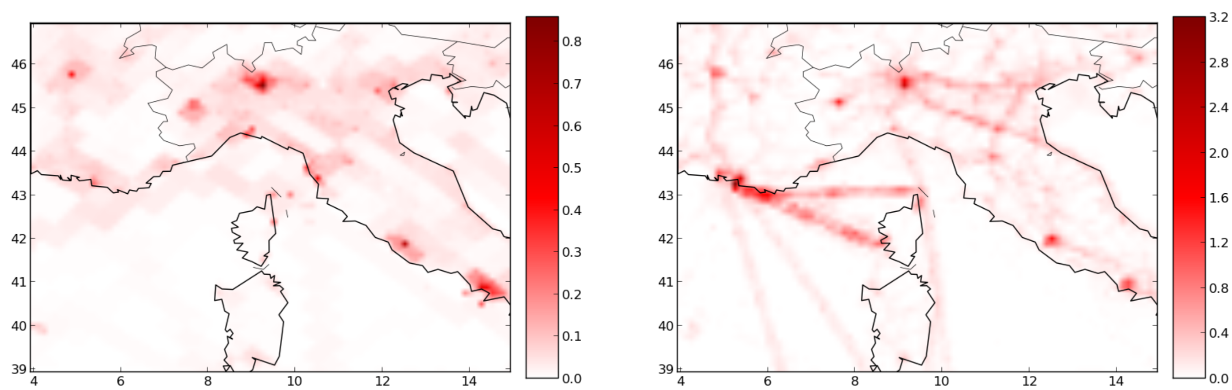

Figure 3.2: Average NO$_x$ emissions over the summer campaign 2013 from the EMEP emission inventory (left panel) and absolute differences (μg m^{-2} s^{-1}) of NO$_x$ emissions between HTAP and EMEP inventories. The horizontal and vertical axes show longitude and latitude in degrees respectively.

Sensitivity studies to meteorology fields, anthropogenic emission inventory, I/S-VOC emissions and sea-salt emissions are outlined in section 3.4. These studies are performed using two different inputs for the parameter of concern in the sensitivity test and fixing the others. Table 3.1 summarizes the performed simulations as well as the different input data used. Table 3.2 summarizes

Table 3.1: Summary of the different simulations and their input data. S1, S2, S3, S4 and S5 represent the simulation number.

Nomenclature	Anthropogenic emission inventory	Meteorological model	Sea-salt emission parameterization	I/S-VOC/POA
S1	HTAP	ECMWF	Jaeglé et al. (2011)	1.5
S2	HTAP	WRF Lon-Lat	Jaeglé et al. (2011)	1.5
S3	HTAP	ECMWF	Monahan et al. (1986)	1.5
S4	EMEP	ECMWF	Jaeglé et al. (2011)	1.5
S5	HTAP	ECMWF	Jaeglé et al. (2011)	0.0

the different simulation comparisons, as performed in the conducted sensitivity studies.

Table 3.2: Summary of the different sensitivity simulations for the ground-based evaluation.

Sensitivity study to	Compared simulations	Discussed concentrations	Period
Meteorology	S1 and S2	Inorganics - PM_{10} - PM_1 - OM_1	Summer 2013
Anthropogenic emission inventory	S1 and S4	Inorganics - PM_{10} - PM_1 - OM_1	Summers 2012 and 2013
Marine emissions	S1 and S3	Inorganics - PM_{10} - PM_1 - OM_1	Summer 2013
I/S-VOC/POA	S1 and S5	OM_1	Summer 2013

3.2.2 Measured data

The model results are compared against observational data performed in the framework of several ChArMEx campaigns. Simulated concentrations are compared to ground-based measurements performed at Ersa (43°00'N, 9°21.5'E), which is located at the northern edge of Corsica Island, at a height of about 530 m above sea level (Figure 3.1). A Campbell meteorological station was used to measure air temperature and wind velocity. Continuous measurements of PM_{10} and PM_1 were performed using TEOM (THERMO, model 1400) and TEOM-FDMS (THERMO, model 1405) instruments respectively. For the composition of particles, nitrate, sulfate, ammonium and organic concentrations in PM_1 were characterized using an ACSM (Aerosol Chemical Speciation Monitor), and in PM_{10} they were characterized using a PILS-IC (Particle Into Liquid Sampler coupled with Ion Chromatography), which also allows an estimation of chloride and sodium concentrations (see Michoud et al. (2017) for more details). The inorganic precursors HNO_3, HCl and SO_2 were measured using a WAD-IC (Wet-Annular Denuder coupled with Ion Chromatography).

Airborne measurements based in Avignon, France were preformed aboard the ATR-42, run by SAFIRE (French aircraft service for environmental research, http://safire.fr). Full details of the aerosol measurements aboard the aircraft as well as the fligt details are provided in Freney et al. (2017). On 10 July 2014, a flight was dedicated to measure concentrations above the sea under Mistral regime (northern and northwestern high-speed winds). This flight was approximately 3 hours in duration and the aircraft flew over the south of France and the Mediterranean Sea at altitudes varying from 100 to 3000 m above sea level (m.a.s.l). Comparisons between model and measurements are not performed during transit, but only above sea, at altitudes below 800 m.a.s.l. and in the boundary layer. A horizontal projection of the aircraft path during this flight is presented in Figure 3.1. The purple crosses indicate the locations where model and measurement comparisons are performed. Measurements of the non-refractory submicron aerosol chemical properties were performed using a compact aerosol time of flight mass spectrometer (C-ToF-AMS) providing mass concentrations on organic sulfate, ammonia and chloride particles with a time resolution of less than 5 minutes.

3.3 Meteorological evaluation

Aerosol phenomenology in Cape-Corsica is influenced by diverse meteorological situations as well as transport of pollution from a number of sources. It is therefore crucial to estimate, as accurately as possible, the input meteorological data used in the air quality model. The four meteorological datasets (ECMWF, WRF-Lon-Lat, WRF-Lambert, WRF-Lambert-Obsgrid) are compared to observations of air temperature and wind at Ersa in Figure 3.B1 for the summer campaign periods of 2012 and Figure 3.B2 for the summer 2013 (Appendix 3.7).

The observed and simulated temperature, wind speed, wind direction and relative humidity at Ersa during these summers, and the statistical scores defined in Table [4.A1] of Appendix 4.7 of comparison of the four model results to measurements (hourly time series) are shown in Tables 3.1 to 3.4 respectively.

Table 3.1: Temperature (observed and simulated means) from the observations and the four meteorological models at Ersa during the summer campaigns 2012 and 2013 and statistics of comparison of model results to observations (correlation, mean fractional bias and mean fractional error). The temperature means and the RMSE are in Kelvin. $\bar{o}$ refers to the measured mean.

		Meteorological models	ECMWF	WRF-Lon-Lat	WRF-Lambert	WRF-Lambert-OBSGRID
2012	$\bar{o} = 294.66$	Simulated mean $\bar{s}$ ± RMSE	295.09 ± 1.50	294.05 ± 2.79	294.86 ±3.02	294.17 ± 3.45
		Correlation (%)	96.3	77.1	66.7	54.8
		MFB	0.00	0.00	0.00	0.00
		MFE	0.00	0.01	0.01	0.01
2013	$\bar{o} = 294.04$	Simulated mean $\bar{s}$ ± RMSE	295.82 ± 3.23	294.42 ± 2.42	295.31 ± 2.66	295.10 ± 2.60
		Correlation (%)	70.0	78.2	79.0	78.3
		MFB	0.01	0.00	0.00	0.00
		MFE	0.01	0.01	0.01	0.01

The four meteorological simulations reproduce well the ground temperature measured at Ersa. Statistically, the correlation to temperature measurements is high: between about 54% and 96% for all models, and the root-mean-square-error (RMSE) is low (below 3.4 K). The best model differs depending on the year: the correlation of ECMWF to measurements is the highest (96%) and the RMSE the lowest (1.5 K) in 2012, but in 2013, the correlation of ECMWF is the lowest (70%) and its RMSE the highest (3.2 K). The mean fractional biases and errors (MFB and MBE) of the simulated temperatures are almost null.

For wind speed, ECMWF systematically leads to better statistics than WRF, despite the fine horizontal resolution of WRF (0.125° x 0.125°). ECMWF agrees best with the measurements, with the highest correlation (between 69% and 87%) and the lowest errors (MFE is between 33% and 47%). WRF-Lon-Lat also performs well with correlations between 60% and 65% and MFE between 47% and 64%. WRF-Lambert and WRF-Lambert-Obsgrid have poorer statistics with negative correlations and MFE between 71% and 74%.

The averaged wind direction is quite similar for summers 2012 and 2013 (202° and 186° respectively). The mean wind direction is well represented by ECMWF for the summers 2012 and 2013, and WRF-Lon-Lat for the summer 2012. Errors are higher with the two models using Lambert projection which tend to under-estimate the wind direction angle. For relative humidity, the observed mean relative humidity is 0.65 in 2012 and 0.70 in 2013. It is relatively well reproduced by the models (between 0.70 and 0.77 in 2012 and between 0.69 and 0.78 in 2013). All models perform well with MFE below 32% and MFB below 18%. WRF-Lon-Lat leads to the best statistics in 2012 and WRF-Lambert-Obsgrid leads to the best statistics in 2013.

As ECMWF and WRF-Lon-Lat are shown to perform overall better than the two other models (Tables 3.3), they will be used for the meteorological sensitivity study.

Table 3.2: Wind velocity statistics for the four meteorological models at Ersa during the summer campaigns of 2012 and 2013. The wind velocity means and the RMSE are in m.s^{-1}. $\bar{o}$ refers to the measured mean.

		Meteorological models	ECMWF	WRF-Lon-Lat	WRF-Lambert	WRF-Lambert-OBSGRID
2012	$\bar{o} = 4.53$	Simulated mean $\bar{s}$ ± RMSE	4.86 ± 2.36	6.96 ± 3.93	5.60 ± 3.94	5.06 ± 3.89
		Correlation (%)	69.3	60.3	-26.0	-34.3
		MFB	0.14	0.46	0.34	0.26
		MFE	0.47	0.64	0.74	0.74
2013	$\bar{o} = 3.21$	Simulated mean $\bar{s}$ ± RMSE	3.44 ± 1.32	3.98 ± 2.12	5.14 ± 3.64	4.86 ± 3.44
		Correlation (%)	87.3	65.5	-6.6	-2.1
		MFB	0.01	0.10	0.38	0.30
		MFE	0.33	0.47	0.73	0.71

Table 3.3: Wind direction statistics for the four meteorological models at Ersa during the summer campaigns 2012 and 2013. The wind direction means and the RMSE are in degrees. $\bar{o}$ refers to the measured mean.

		Meteorological models	ECMWF	WRF-Lon-Lat	WRF-Lambert	WRF-Lambert-OBSGRID
2012	$\bar{o}$ = 201.89	Simulated mean $\bar{s}$ ± RMSE	195.73 ± 91.64	200.48 ± 58.94	107.07 ± 120.47	101.30 ± 119.53
		Correlation (%)	27.6	54.1	7.2	12.0
		MFB	-0.14	-0.02	-0.62	-0.66
		MFE	0.40	0.22	0.68	0.69
2013	$\bar{o}$ = 186.28	Simulated mean $\bar{s}$ ± RMSE	206.67 ± 107.84	231.03 ±117.91	101.57 ± 120.47	111.46 ± 122.76
		Correlation (%)	33.2	21.6	3.6	1.7
		MFB	-0.02	0.13	-0.50	-0.48
		MFE	0.48	0.46	0.67	0.68

Table 3.4: Relative humidity statistics for the four meteorological models at Ersa during the summers 2012 and 2013. The relative humidity means and the RMSE are dimensionless. $\bar{o}$ refers to the measured mean.

		Meteorological models	ECMWF	WRF-Lon-Lat	WRF-Lambert	WRF-Lambert-OBSGRID
2012	$\bar{o}$ = 0.65	Simulated mean $\bar{s}$ ± RMSE	0.74 ± 0.24	0.72 ± 0.22	0.70 ± 0.25	0.77 ± 0.25
		Correlation (%)	14.3	34.5	7.9	14.0
		MFB	18	15	11	31
		MFE	32	28	32	31
2013	$\bar{o}$ = 0.70	Simulated mean $\bar{s}$ ± RMSE	0.73 ± 0.20	0.78 ± 0.21	0.70 ± 0.20	0.69 ± 0.21
		Correlation (%)	9.7	23.3	23.0	21.8
		MFB	8	14	3	1
		MFE	26	25	25	25

The model performances presented above compare well to other studies (Kim et al., 2013; Cholakian et al., 2017). In this study, for ECMWF and WRF-Lon-Lat during the summers of 2012 and 2013, RMSE ranges between 1.5 K and 3.2 K for temperature, between 1.3 m s^{-1} and 3.9 m s^{-1} for wind speed, and between 58° and 118° for wind direction. At Ersa, for the summer 2013 (not exacly the same period), Cholakian et al. (2017) found RMSE between 1.5 K and 2.3 K for temperature, between 1.6 m s^{-1} and 1.9 m s^{-1} for wind speed, and between 92° and 117° for wind direction at ERSA from 10 July to 5 August 2013 using the mesoscale WRF model. Moreover, Kim et al. (2013) reported RMSE ranging between 1 K and 4 K for temperature, and 0.6 m s^{-1} to 3.0 m s^{-1} for wind speed over Greater Paris during May 2005 using WRF model with a longitude-latitude map projection.

3.4 Evaluation and sensitivities

This section focuses on the evaluation of the reference simulation (S1) against aerosol measurements (PM_{10}, PM_1, OM_{PM_1} and inorganic aerosols (IA) species), and on the factors controlling simulated aerosol concentrations (meteorology, sea-salt and anthropogenic emissions). This evaluation is performed against ground-based measurements during the summers 2012 and 2013, and against airborne measurements during the flight of 10 July 2014. The criteria of Boylan and Russell (2006) are used to evaluate the model-to-measurement comparisons. The performance criterion is verified if —MFB— ≤ 60% and MFE ≤ 75% (MFB and MFE stand respectively for the mean fractional bias and the mean fractional error and are defined in Table [4.A1] of Appendix 4.7), while the goal criterion is verified if —MFB— ≤ 30% and MFE ≤ 50%. To evaluate the sensitivity of the modelled concentrations to input data, the different simulations summarized in Table 3.1 are compared to the reference simulation S1 by computing the normalized root-mean-square-error (RMSE of the concentration differences between a simulation and S1, divided by the mean concentration of S1).

Table 3.1: Comparisons of simulated PM_{10}, PM_1 and OM_1 daily concentrations to observations (concentrations and RMSE are in μg m^{-3}) during the summer campaign periods of 2012 and 2013. $\bar{s}$ stands for simulated mean, and $\bar{o}$ for observed mean. Simulation details are given in table 3.1

		PM_{10} (2012)	PM_1 (2012)	OM_1 (2012)	PM_{10} (2013)	PM_1 (2013)	OM_1 (2013)
Measured mean $\bar{o}$		22.38	7.57	3.89	11.46	7.02	2.88
S1	$\bar{s}$ ± RMSE	16.44 ± 7.55	9.40 ± 2.72	3.39 ± 0.78	9.69 ± 3.17	6.98 ± 1.77	2.56 ±1.07
	Correlation (%)	76.8	78.9	95.2	70.9	67.5	81
	MFB	-30	18	-20	-19	-1	-17
	MFE	30	27	23	26	20	35
S2	$\bar{s}$ ± RMSE	—	—	—	7.49 ± 4.75	6.42 ± 1.91	1.61 ± 1.62
	Diff. with S1 (%)	—	—	—	-23	-8	-37
	Norm. RMSE (%)	—	—	—	33	21	49
S3	$\bar{s}$ ± RMSE	—	—	—	14.94 ± 5.02	9.45 ± 2.95	3.26 ± 1.03
	Diff. with S1 (%)	—	—	—	54	35	27
	Norm. RMSE (%)	—	—	—	65	40	29
S4	$\bar{s}$ ± RMSE	13.87 ± 10.95	7.66 ± 1.56	2.37 ± 1.64	8.48 ± 4.02	6.86 ± 2.03	1.98 ± 1.29
	Diff. with S1 (%)	-16	-19	-30	-12	-2	-23
	Norm. RMSE (%)	23	2	43	17	10	32
S5	$\bar{s}$ ± RMSE	—	—	—	—	—	2.54 ± 1.07
	Diff. with S1 (%)	—	—	—	—	—	-1
	Norm. RMSE (%)	—	—	—	—	—	1

3.4.1 PM_{10} and PM_1

The statistical scores of the simulated PM_1 and PM_{10} are shown in Table 3.1 for the summer campaigns of 2012 and 2013. The time series of measured and simulated PM_{10} and PM_1 during the summer 2013 are presented in Figure 3.C1 of Appendix 3.7.

PM_{10} and PM_1 are well modeled during both the summer campaigns of 2012 and 2013, and the performance and goal criteria are always met. The measured mean concentration of PM_1 is very similar in 2012 and 2013 (7.6 and 7.0 μg m^{-3} respectively). However, the mean PM_{10} concentration is double in 2012 compared to 2013 (22.4 and 11.5 μg m^{-3} respectively), probably because of higher occurrence of transported desert dust in 2012.

Although the mean PM_1 and PM_{10} concentrations are well modeled in 2013, the mean PM_1 concentration is slightly over-estimated during summer 2013 and the mean PM_{10} concentration is slightly under-estimated in 2012. This under-estimation of PM_{10} may be due to difficulties in accurately representing the transported dust episodes, which are frequent in summer in the western Mediterranean (Moulin et al., 1998) and are represented in the Mediterranean simulation by dust boundary conditions from the global model MOZART4.

The comparisons of the different simulations at Ersa in Table 3.1 shows that both PM_{10} and PM_1 concentrations are strongly influenced by sea-salt emissions (S3, with a normalized RMSE of 65% and 40% respectively), especially as the emissions of the two parameterizations differ by as much as 1400% over the sea in Southern France (section 4.2.1). PM_{10} and PM_1 concentrations are also very sensitive to meteorology (S2, with a normalized RMSE of 33% and 21% respectively) and anthropogenic emissions (S4, with a normalized RMSE of 17% and 10% respectively).

Knowing the chemical composition of PM_{10} and PM_1 provides important information to understand the different sources of aerosol particles arriving at Ersa, and to understand the sensitivities presented above. Figure 3.1 shows the composition of PM_{10} and PM_1 and the percentage contribution of each compound to PM in 2012 and the associated variability.

Inorganic aerosols account for a large part of the PM_{10} mass: during the summer campaign periods of 2012 and 2013, the inorganic fraction in PM_{10} is 31% and 39% respectively. Among inorganics, sulfate, largely originating from anthropogenic sources, occupies a large portion of

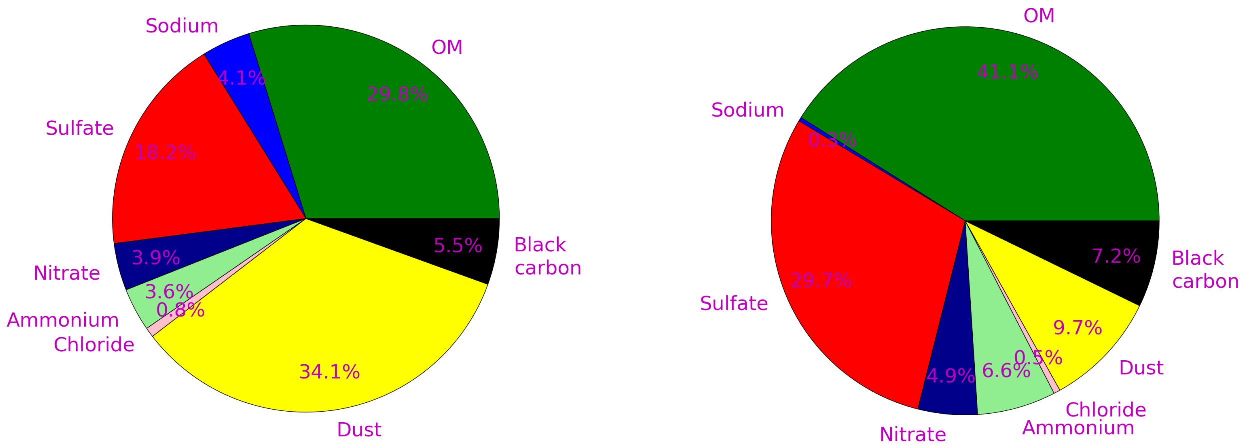

Figure 3.1: PM_{10} (left panel) and PM_1 (right panel) average relative composition during the summer 2012 campaign period

PM_{10} (18% in 2012 and 19% in 2013). The organic mass (OM) also largely contributes to PM_{10} (30% in 2012 and 33% in 2013). Black carbon (originating from traffic, shipping emissions and industrial activities in big cities in the south of France and the north of Italy) contributes to a small portion of PM_{10} (5% in 2012 and 7% in 2013). Saharan dust can be transported by air-masses to the Mediterranean atmosphere via medium-range transport and is an important component of the PM_{10} with contributions of 34% and 21% during the summer campaigns of 2012 and 2013, respectively.

The PM_1 mass is dominated by organic matter (41% in 2012 and 38% in 2013) and sulfate (30% in 2012 and 24% in 2013). The percentage of sodium (from sea salt) is significant in PM_{10} (4% in 2012 and 10% in 2013), but it is negligible in the PM_1 mass (less than 1%).

3.4.2 OM_{PM_1}

The statistical evaluation of OM_{PM_1} during the summer campaigns of 2012 and 2013 is available in Table 3.1. As discussed in Chrit et al. (2017), the performance and goal criteria are both satisfied, due to the addition in the model of highly oxidized species (extremely low volatility organic compounds, organic nitrate and the carboxylic acid MBTCA (3-methyl-1,2,3-butanetricarboxylic acid) as a second generation oxidation product of α-pinene). Adding these species to the model was also required to correctly model OM properties (oxidation state and affinity to water). The time series of measured and simulated OM_{PM_1} concentrations during the summer 2013 campaign are presented in Figure 3.C1 of Appendix 3.7. The comparison of the different simulations at Ersa in Table 3.1 shows that OM_{PM_1} is particularly influenced by meteorology (S2 with a normalized RMSE of 49%), because meteorology influences biogenic emissions, but also by inorganic sea-salt emissions (S3 with a normalized RMSE of 29%), which provides mass onto which hydrophilic SOA can condense especially sulfate, and anthropogenic emissions (S4 with a normalized RMSE of 32%), as they affect the formation of oxidants through photochemistry and emit anthropogenic precursors. The sensitivity to anthropogenic I/S-VOC emissions is low (S5, with a normalized RMSE of only 1%).

3.4.3 Inorganic species

Ground-based evaluation

The statistical scores of the simulated inorganic concentrations are shown in Table 3.2 for PM_1 concentrations during the summer 2012 campaign and in Table 3.3 and Table 3.4 for PM_{10} and PM_1 inorganic concentrations respectively during the summer 2013 campaign. The time series of measured and simulated inorganic concentrations during the summer 2013 campaign are presented in Figures 3.C2 and 3.C3 of Appendix 3.7.

Inorganic concentrations of PM_1 aerosol were measured in 2012, and in both PM_1 and PM_{10} in 2013. Some of the inorganic gaseous precursors (SO_2, HNO_3 and HCl) were also measured only for a few days in 2013 (between 21 July and 26 July 2013).

For the 2012 reference simulation (S1), for the PM_1, sulfate and nitrate concentrations satisfy both the performance and goal criteria. Ammonium concentrations are however under-estimated, despite the performance criterion being satisfied in terms of MFE. This under-estimation of ammonium increases if EMEP emission inventory with lower ship emissions over the Mediterranean Sea is used, suggesting that ammonium nitrate formation is strongly dependent on the ship NO_x emissions (because they lead to the formation of the gaseous precursors HNO_3 of ammonium nitrate).

For the 2013 reference simulation (S1), in PM_{10}, sulfate and ammonium satisfy the performance and goal criteria, while sodium satisfies only the performance criterion. The mean concentrations of modelled chloride and nitrate are both under-estimated. This under-estimation is probably due to uncertainties on the measurements. In fact, nitrate and chloride are difficult to measure, there can be some negative artefacts (volatilization of the aerosol phase during sampling) or positive artefacts (condensation of gaseous phase onto the particles or filters during sampling), depending on the sampling conditions. Moreover, this underestimation may be also due to difficulties in representing the partitioning between the gas and the particle phases. For chloride, as shown in Figure 3.C2 of Appendix 3.7, although the mean concentration is under-estimated, the peaks are over-estimated. For example, between 21 and 26 July 2013, the particle-phase chloride concentration is 0.34 $\mu g\ m^{-3}$ in the simulation, but only 0.05 $\mu g\ m^{-3}$ in the measurements. The total chloride (gas + particle phase) is well modeled (1.2 $\mu g\ m^{-3}$ in the measurements and 1 $\mu g\ m^{-3}$ simulated), but the gas/particle ratio is much higher in the measurements (18.4) than in the model (2.4). For nitrate, the total nitrate (gas + particle phase) is under-estimated between 21 and 26 July 2013 (2.7 $\mu g\ m^{-3}$ in the measurements and 6.6 $\mu g\ m^{-3}$ simulated), and most of it is in the gas phase (only 0.4 $\mu g\ m^{-3}$ in the particle phase in the measurements and 0.2 simulated). Contrary to chloride, the gas/particle ratio is much higher in the model (28.2) than in the measurements (5.4). The reason for these difficulties to represent the gas/particle ratios of chloride is that the measured PILS chloride concentrations include only non-refractory chloride. The reason of the difference of nitrate ratio is likely related to the internal-mixing hypothesis and the bulk-equilibrium assumption in the modeling of condensation/evaporation. They are investigated in the following section, during the comparison to airborne measurements.

For the 2013 reference simulation (S1), in PM_1, as in PM_{10}, sulfate and ammonium satisfy the performance criterion, which is also almost satisfied for nitrate. The measured and simulated PM_1 and PM_{10} concentrations are relatively similar for sulfate and ammonium, suggesting that most of the mass is in PM_1.

The comparisons of the different simulations at Ersa in Tables 3.3 and 3.4 show that inorganics in PM_{10} and PM_1 have similar sensitivities, because of the bulk equilibrium assumption made in the modeling of condensation/evaporation. Sulfate is more sensitive to anthropogenic (ship) emissions (with a normalized RMSE of 44% in PM_{10}) than meteorology (with a normalized RMSE of

Table 3.2: Comparisons of simulated PM_1 inorganic daily concentrations to observations (concentrations are in μg m^{-3}) using S1 and S4 during the summer 2012.

	Inorganics	Nitrate	Sulfate	Ammonium
	Measured mean $\bar{o}$	0.41	2.06	1.39
S1	Simulated mean $\bar{s}$ ± RMSE	0.51 ±0.28	2.53 ± 1.13	0.68 ±0.85
	Correlation (%)	20.1	71.4	47.8
	MFB	15	31	-72
	MFE	50	39	72
S4	Simulated mean $\bar{s}$ ± RMSE	0.53 ± 0.36	1.71± 1.28	0.50 ± 1.04
	Diff. with S1 (%)	+4%	-32%	-26%
	Norm. RMSE (%)	45	46	32

22%) and sea-salt emissions (with a normalized RMSE of 22%). Nitrate, chloride and sodium, and ammonium to a lower extent, are highly sensitive to sea-salt emissions with normalized RMSEs between 62% and 933% (Jaeglé et al. (2011) parameterization has a lower dependance to wind speed than Monahan et al. (1986) parameterization). They are also strongly affected by meteorology (with normalized RMSEs between 43% and 130%), because meteorology affects the natural emissions (sea salt and biogenic), as discussed in section 3.5. By influencing biogenic emissions, meteorology affects the formation of organics and hence the formation of inorganics (because of the formation of organic nitrate). Inorganic concentrations are also strongly affected by anthropogenic emissions (with normalized RMSEs between 48% and 267%), because anthropogenic emissions affect the NO_x emissions, and hence the oxidants and the nitrate formation. Because nitrate, ammonium and chloride partition between the gas and the particle phases, their uncertainties are linked and they are strongly affected by assumptions in the modeling of condensation/evaporation, as detailed in the section 3.4.4.

3.4.4 Airborne evaluation

The considered flight (10 July 2014, 10:21-14:09 UTC) was conducted by the French aircraft ATR42 deployed by SAFIRE in the south of France above the Mediterranean Sea. The purpose was to study aerosol formation, evolution and properties in marine conditions, under Mistral regime (north/north-west winds coming from the Rhône Valley characterized by high wind speeds). Altitudes and a horizontal projection of the trajectory of the aircraft during this flight are presented in Figure 3.1. The aircraft flew at low altitudes (under 800 m.a.s.l.) over the Mediterranean Sea for about 2 hours, allowing us to evaluate the modeling of sea-salt aerosols. As shown in Figure 3.1, the planetary boundary layer height, as modelled by ECMWF meteorological fields, exhibit strong spatial variations. For the comparisons of inorganic concentrations to airborne measurements, the reference simulation S1 is run a few days during the summer 2014 and it is compared to the observed concentrations when the flight is below 800 m.a.s.l. and where the boundary layer is spatially uniform (above 1200 m). The transects where model to measurements are performed are indicated by purple crosses/lines in Figure 3.1.

Figure 3.2 shows the comparison of sulfate to the airborne measurements using different model configurations, and Figure 3.3 shows the comparison of nitrate and ammonium concentrations in PM_1. Sulfate is the inorganic compound with the highest PM_1 concentrations (about 0.54 μg m^{-3}), followed by ammonium (about 0.32 μg m^{-3}), and nitrate (about 0.14 μg m^{-3}).

Sulfate

As shown in Figure 3.2, the PM_1 sulfate concentration is over-estimated in the simulation with a mean concentration of about 0.55 μg m^{-3} against 0.47 μg m^{-3} in the measurements. To un-

Table 3.3: Comparisons of simulated PM_{10} inorganic daily concentrations to observations (concentrations are in μg m^{-3}) using S1, S2, S3 and S4 during the summer 2013.

	Inorganics	Nitrate	Sulfate	Ammonium	Chloride	Sodium
	Measured mean $\overline{o}$	0.42	1.52	0.76	0.18	0.53
S1	Simulated mean $\overline{s}$ ± RMSE	0.33 ± 0.42	2.05 ± 0.84	0.58 ± 0.39	0.12 ± 0.45	0.70 ± 0.54
	Correlation (%)	5.7	69.7	47.6	-11.4	55.5
	MFB	-43	32	-20	-67	30
	MFE	86	40	43	105	70
S2	Simulated mean $\overline{s}$ ± RMSE	0.19 ±0.46	2.10 ± 0.82	0.49 ± 0.44	0.13 ± 0.44	0.77 ±0.57
	Diff. with S1 (%)	-42%	+2 %	-16%	+8%	+10%
	Norm. RMSE (%)	130	22	52	100	43
S3	Simulated mean $\overline{s}$ ± RMSE	0.88 ± 1.27	2.14 ±0.97	0.31 ± 0.60	0.59 ± 1.14	1.77 ± 2.34
	Diff with S1 (%)	+167%	+4%	-47%	+392%	+153%
	Norm. RMSE (%)	376	22	62	933	291
S4	Simulated mean $\overline{s}$ ± RMSE	0.24 ±0.41	1.33 ±0.67	0.34 ± 0.56	0.27 ± 0.64	0.98 ± 0.77
	Diff. with S1 (%)	-27%	-35%	-41%	+125%	+40%
	Norm. RMSE (%)	66	44	48	267	50

Table 3.4: Comparisons of simulated PM_1 inorganic daily concentrations to observations (concentrations are in μg m^{-3}) using S1, S2, S3 and S4 during the summer 2013.

	Inorganics	Nitrate	Sulfate	Ammonium
	Measured mean $\overline{o}$	0.30	1.47	0.65
S1	Simulated mean $\overline{s}$ ± RMSE	0.32 ± 0.31	1.86 ±0.94	0.58 ± 0.38
	Correlation (%)	22.9	28.9	32
	MFB	-24	27	-6
	MFE	77	55	55
S2	Simulated mean $\overline{s}$ ± RMSE	0.18 ± 0.28	1.72 ± 0.66	0.50 ± 0.52
	Diff. with S1 (%)	-44%	-8%	-14%
	Norm. RMSE (%)	134	19	44
S3	Simulated mean $\overline{s}$ ± RMSE	0.87 ± 1.20	1.89 ± 0.81	0.31 ± 0.50
	Diff. with S1 (%)	+172%	+2%	-47%
	Norm. RMSE (%)	384	29	62
S4	Simulated mean $\overline{s}$ ± RMSE	0.23 ± 0.25	1.08 ± 0.71	0.34 ±0.48
	Diff. with S1 (%)	-28%	-42%	-41%
	Norm. RMSE (%)	69	34	47

derstand the reasons of this over-estimation, different sensitivity simulations are performed. The first sensitivity simulation (referred to as "S1-without-SO_4 in SSE", where SSE stands for sea-salt emissions) differs from S1 simulation by the fact that sulfate is only emitted from anthropogenic sources and marine sulfate is not taken into account. The second sensitivity simulation (referred to as "S1-H_2SO_4-0%") differs from S1 by the fact that SO_x emissions are split into 100% of SO_2 and 0% of H_2SO_4, instead of 98% of SO_2 and 2% of H_2SO_4 in S1. The measurement-to-model comparison of the vertical profile of the PM_1 sulfate concentrations using the three simulations is shown in Figure 3.2. The influence of marine sulfate is negligible: the simulated means using S1 with and without the emissions of marine sulfate are nearly equal ($\approx 0.55\ \mu g.m^{-3}$) indicating that the PM_1 sulfate concentration is almost totally from anthropogenic sources. A comparison of PM_{10} sulfate concentrations for the two simulations show that this is also the case for PM_{10} sulfate concentrations. However, PM_1 sulfate concentrations are strongly influenced by anthropogenic emissions. For example, PM_1 sulfate concentrations are lower if the fraction of H_2SO_4 in the SO_x emissions is lower than in the reference simulation (the simulated mean concentrations with and without H_2SO_4 in SO_x emissions are 0.55 and 0.52 $\mu g.m^{-3}$ respectively), because of the rapid condensation of H_2SO_4 (which saturation vapor pressure is almost zero) onto particles.

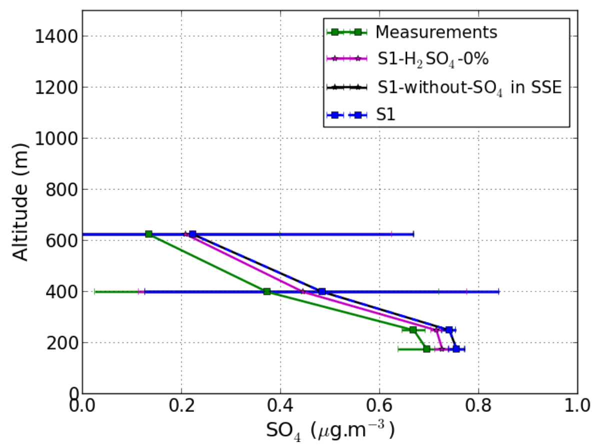

Figure 3.2: Measurements are averaged at four model levels from airborne observations below 800 m.a.g.l along the flight path shown in Figure 3.1 on July 10, 2014. The concentrations of the S1 simulations (standard and with options, see text for details) are also averaged in time along the flight path. Results from S1 and from S1-without-SO4 in SSE (sea-salt emissions) are quite similar.

Ammonium and nitrate

In the reference simulation S1, ammonium and nitrate are under-estimated compared to the measurements.

Figure 3.3 shows the comparison of nitrate and ammonium concentrations in PM_1 to the airborne measurements using different model configurations. Because ammonium and nitrate and chloride are semi-volatile inorganic species, their concentrations may depend on the assumptions made in the modeling of condensation/evaporation. In the reference simulation, bulk thermodynamic equilibrium is assumed between the gas and particle phases for all inorganic species. In the first sensitivity simulation (referred to as "S1-Dynamic"), the condensation/evaporation is computed dynamically rather than assuming thermodynamic equilibrium. In the second sensitivity simulation (referred to as "S1-IA-externally-mixed"), sea-salt (chloride and sodium) emissions are assumed not to be mixed with the other aerosols. In S1-IA-externally-mixed, bulk equilibrium is assumed for ammonium, nitrate and sulfate, while chloride and sodium do not interact with the other inorganic species.

Under the thermodynamic equilibrium approach (S1), nitrate is underestimated (the measured and simulated means are 0.10 and 0.05 $\mu g.m^{-3}$ respectively), probably because the sulfate is overestimated as detailed in section 3.4.4, but also because the assumption of thermodynamic equilibrium between the gas and particle phases is not verified. Nitrate concentrations are closer to measurements if condensation/evaporation is computed dynamically, especially between 400 m and 600 m altitude, where the mean concentrations are 0.07 $\mu g.m^{-3}$ in the measurements, 0.02 $\mu g.m^{-3}$ with S1 and 0.07 $\mu g.m^{-3}$ with S1-Dynamic). If sea-salt aerosols are externally mixed, than nitrate is even more under-estimated than in S1. This is because nitrate tends to replace chloride in sea salt if thermodynamic consideration is taken into account.

For ammonium, the comparisons to the measurements are best if sea-salt particles are assumed not to be mixed (the measured and simulated means are 0.27 and 0.26 $\mu g.m^{-3}$ respectively). The differences of the vertical profiles between the dynamic and the equilibrium approaches indicates that the assumption of the thermodynamic equilibrium is not verified (the condensation/evaporation process is not instantaneous). For instance, the simulated mean of ammonium using the equilibrium and dynamic approaches is 0.20 and 0.13 $\mu g.m^{-3}$ respectively.

Because both the mixing-state of particles and the dynamic of condensation/evaporation strongly influence PM_1 inorganic concentrations over the Mediterranean Sea, a model capable of representing the mixing state of particles with the dynamic of condensation/evaporation (e.g. Zhu et al., 2015) may allow a better representation of inorganic concentrations.

3.5 Sensitivity studies over the western Mediterranean region

Section 3.4 was dedicated to explain how the simulated concentrations of particles at Ersa are influenced by the different input data used (meteorology, sea salt, anthropogenic emissions) and modeling hypotheses. This section generalizes the sensitivity study of section 3.4 by investigating over the Mediterranean domain how the concentrations are influenced by the input data.

Figure 3.D1 of Appendix 3.7 shows maps over the Mediterranean domain of the concentrations of PM_{10}, OM_1, sulfate and other secondary inorganic aerosols (SIA: nitrate, ammonium and chloride) from the simulation S1 during the summer 2013. The highest PM_{10} concentrations correspond to high OM_1, sulfate or SIA concentrations. OM_1 concentrations are high nearby locations of high biogenic emissions (such as over Italy and Corsica). Sulfate concentrations are particularly high over the Mediterranean Sea, nearby the main ship routes (Figure 3.2). SIA concentrations are high in places of high anthropogenic emissions, such as North of Italy, as well as in main cities.

Figure 3.D2 of Appendix 3.7 shows maps of the relative difference of the concentrations of PM_{10}, OM_1, sulfate and SIA between S2 and S1 (sensitivity to meteorology). SIA concentrations show the highest sensitivity to meteorology, with relative concentration differences between S2 and S1 reaching between -90% and -60% locally over Italy. Sulfate shows the lowest sensitivity with relative concentration differences mostly between -20% and 20%. The larger influence of meteorology on SIA than on sulfate concentrations is partly explained by the influence of the temperature on the partitioning of SIA between the gas and particle phases, as SIA is highly semi volatile. OM_1 concentrations are quite sensitive to meteorology over the whole Mediterranean domain, with relative concentration differences mostly between -60% and -20%, especially nearby regions where the biogenic emissions are the highest. The places of the highest OM_1 concentrations also correspond to the places where SIA concentrations are the most sensitive to meteorology. By influencing biogenic emissions, meteorology influences the formation of organics (OM_1) and hence the formation of SIA by the formation of organic nitrate for example. The influence of meteorology

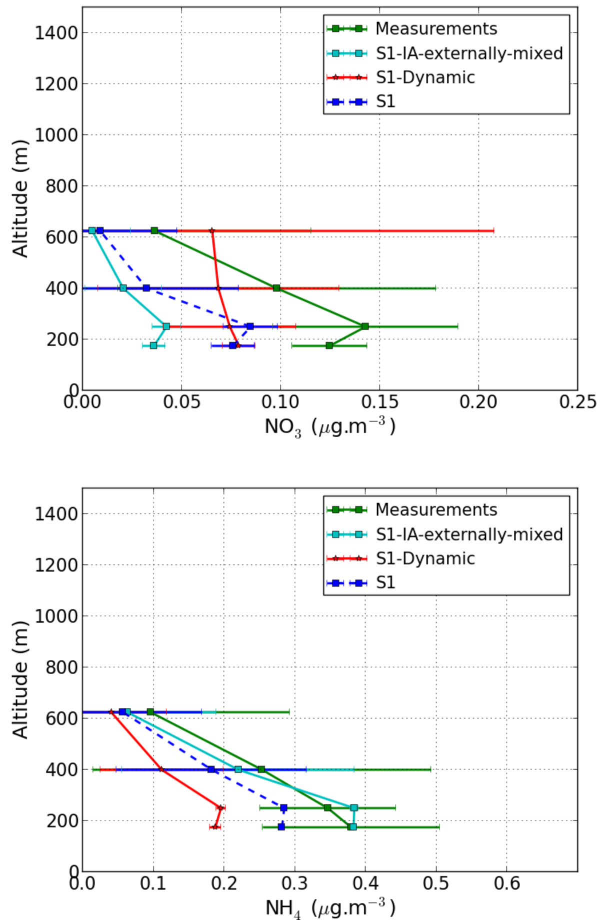

Figure 3.3: Vertical profile averaged at four model levels of NO_3 (left panel) and NH_4 (right panel). Measurements are averaged at the same four model levels from airborne observations below 800 m.a.g.l along the flight shown in Figure 3.1 on July 10, 2014 (around noon)

on sulfate concentrations is limited in this study, because the formation of organo-sulfate is not modeled in our simulations.

Figure 3.D3 of Appendix 3.7 shows maps of the relative difference of the concentrations of PM_{10}, OM_1, sulfate and SIA between S3 and S1 (sensitivity to sea-salt emissions). Although sulfate is little influenced by sea-salt emissions at Ersa (the relative concentration difference is between 0% and 20%), the effect is stronger over the western part of the Mediterranean domain (with relative concentration differences between S3 and S1 between 20% and 60%), where SIA concentrations are also strongly influenced by sea-salt emissions. The influence of sea-salt emissions on OM_1 concentrations is also important, but it is less important than SIA (the relative concentration differences of SIA are between 90% and 180%) over the western Mediterranean part of the domain, compared to between 20% and 60% for OM_1 and between 40% and 60% for sulfate. The increase of OM_1 concentrations when sea-salt emissions are high is due to the hydrophilic organic compounds in OM_1, which are absorbed onto inorganic concentrations. The organic concentrations originating from sea-salt emissions are very low, as discussed in Chrit et al. (2017), and they are not taken into account here.

Figure 3.D4 of Appendix 3.7 shows maps of the relative difference of the concentrations of PM_{10}, OM_1, sulfate and SIA between S4 and S1 (sensitivity to anthropogenic emissions). Sensi-

tivities to sulfate and SIA concentrations are more spatially localized than sensitivities to OM_1 concentrations, and they are higher, with relative concentration differences between S4 and S1 between -40% and 20% for OM_1 and between -40% and 60% for SIA. Sulfate concentrations are strongly sensitive to anthropogenic emissions nearby the main ship routes, with negative (S4-S1) concentrations between -60% and -40%, as ship routes are not well represented in the EMEP emission inventory (simulation S4). For SIA concentrations, the influence of anthropogenic emissions can either be negative or positive (increase or decrease of concentrations), because of the different spatial distributions of the two emission inventories, which affect directly the nitrate formation.

3.6 Conclusions

This paper presents the evaluation of the air-quality model Polyphemus at Ersa and over the Mediterranean Sea, as well as a sensitivity study of the simulated concentrations to input data and model parameters (meteorological fields, anthropogenic and marine emissions, intermediate/semi-volatile organic compounds (I/S-VOC) emissions, different options in condensation/evaporation modeling). For most pollutants, the best model performance is obtained when the meteorological fields that represent the best wind direction are used together with the emission inventory with the most accurate spatial description of ships emissions (EDGAR-HTAP). Using ECMWF and WRF to model the meteorological fields, there is a high sensitivity of secondary pollutants (inorganics and organics) to meteorology, stressing the importance of accurate meteorological modeling. This influence of meteorology on concentrations is due to the impact on sea salt and biogenic emissions, influencing directly the formation of SIA and OM, as well as the impact on temperatures, influencing the secondary aerosol formation. Sulfate is less sensitive to meteorology than SIA, because it is not volatile. However, this low sensitivity may change if the formation of organo-sulfate is modeled (not done here). Both inorganic and organic concentrations are highly sensitive to sea-salt emissions, as great discrepancies exist between different published parameterizations. The commonly used Monahan parameterization of sea-salt emissions leads to an over-estimation of all particulate concentrations, especially of sodium concentrations. A parameterization with a lower exponent in the wind-speed power law is chosen to model sea-salt emissions (Jaeglé et al., 2011) and leads to better model performance. The overestimation of the modeled sea-salt concentrations using Monahan parameterization has an incidence on the overestimation of the modeled concentrations of inorganic compounds, such as nitrate, which replaces chloride in the particles when the thermodynamic equilibrium approach is used to model condensation/evaporation. This assumption (the thermodynamic equilibrium approach) was shown not to be accurate both at Ersa and over the Mediterranean Sea. At Ersa, the gas/particle ratio is too high for nitrate and too low for chloride if the thermodynamic equilibrium approach is used, as the exchange between the gas and particle phases is not instantaneous, but it is dynamic. This dynamic exchange is strongly influenced by the particle composition, and comparisons to measurements over the Mediterranean Sea suggest that sea-salt particles are not mixed with background (transported) particles. The modeling of sea-salt emissions influences not only inorganic concentrations, but also organics (OM_1), as hydrophylic organic species condense onto the inorganic mass. Sulfate concentrations are strongly influenced by ship emissions and show distinct maxima over the Mediterranean sea. The emissions of I/S-VOC play a limited role in the OM_1 concentrations during the summer 2013, suggesting that the influence of ship emissions on OM_1 is mostly due to anthropogenic VOC precursors (aromatics) and NO_x emissions, which lead to the formation of oxidants that may oxidize biogenic aerosol precursors (and form organic nitrate for example).

acknowledgements This research has received funding from the French National Research Agency (ANR) projects SAF-MED (grant ANR-12-BS06-0013). This work is part of the ChArMEx project supported by ADEME, CEA, CNRS-INSU and Météo-France through the multidisciplinary programme MISTRALS (Mediterranean Integrated Studies aT Regional And Local Scales). The station at Ersa was partly supported by the CORSiCA project funded by the Collectivité Territoriale de Corse through the Fonds Européen de Développement Régional of the European Operational Program 2007-2013 and the Contrat de Plan Etat-Région. Eric Hamounou is acknowledged for his great help in organizing the campaigns at Ersa. CEREA is a member of Institut Pierre-Simon Laplace (IPSL).

3.7 Appendix

Statistical indicators

Table 3.A1: Definitions of the statistics used in this work. $(o_i)_i$ and $(c_i)_i$ are the observed and the simulated concentrations at time and location i, respectively. n is the number of data

Statistic indicator	Definition
Root mean square error (RMSE)	$\sqrt{\frac{1}{n}\sum_{i=1}^{n}(c_i - o_i)^2}$
Correlation (Corr)	$\frac{\sum_{i=1}^{n}(c_i - \bar{c})(o_i - \bar{o})}{\sqrt{\sum_{i=1}^{n}(c_i - \bar{c})^2}\sqrt{\sum_{i=1}^{n}(o_i - \bar{o})^2}}$
Mean fractional bias (MFB)	$\frac{1}{n}\sum_{i=1}^{n}\frac{c_i - o_i}{(c_i + o_i)/2}$
Mean fractional error (MFE)	$\frac{1}{n}\sum_{i=1}^{n}\frac{\mid c_i - o_i \mid}{(c_i + o_i)/2}$

Meteorological evaluation

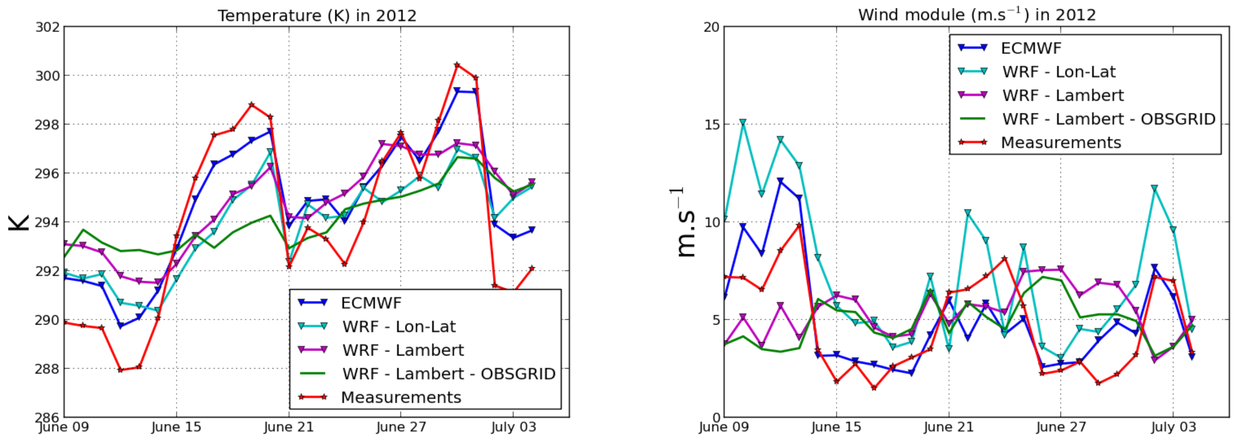

Figure 3.B1: Ground Temperature (left panel) and wind velocity (right panel) at Ersa during the summer 2012.

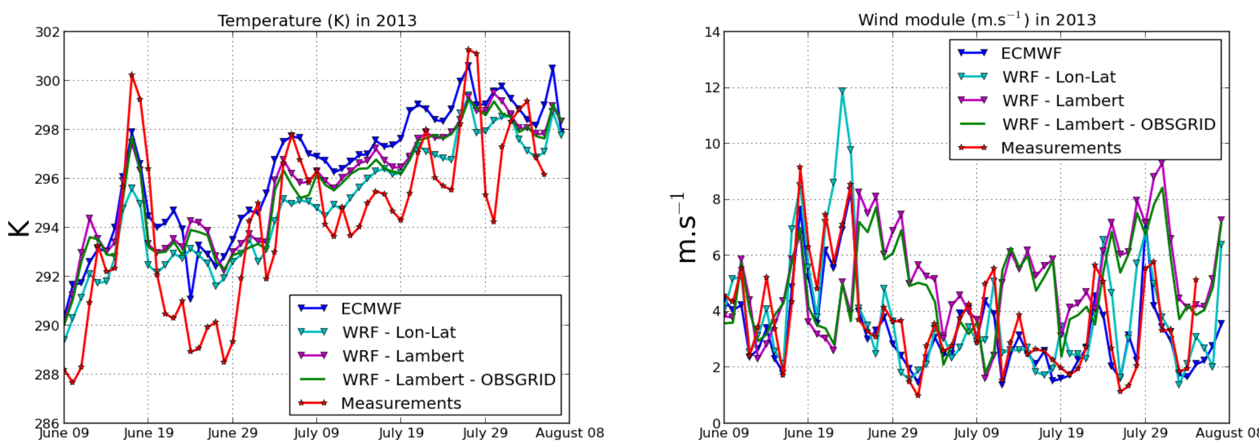

Figure 3.B2: Ground Temperature (left panel) and wind velocity (right panel) at Ersa during the summer 2013.

Model to measurement comparisons in 2013

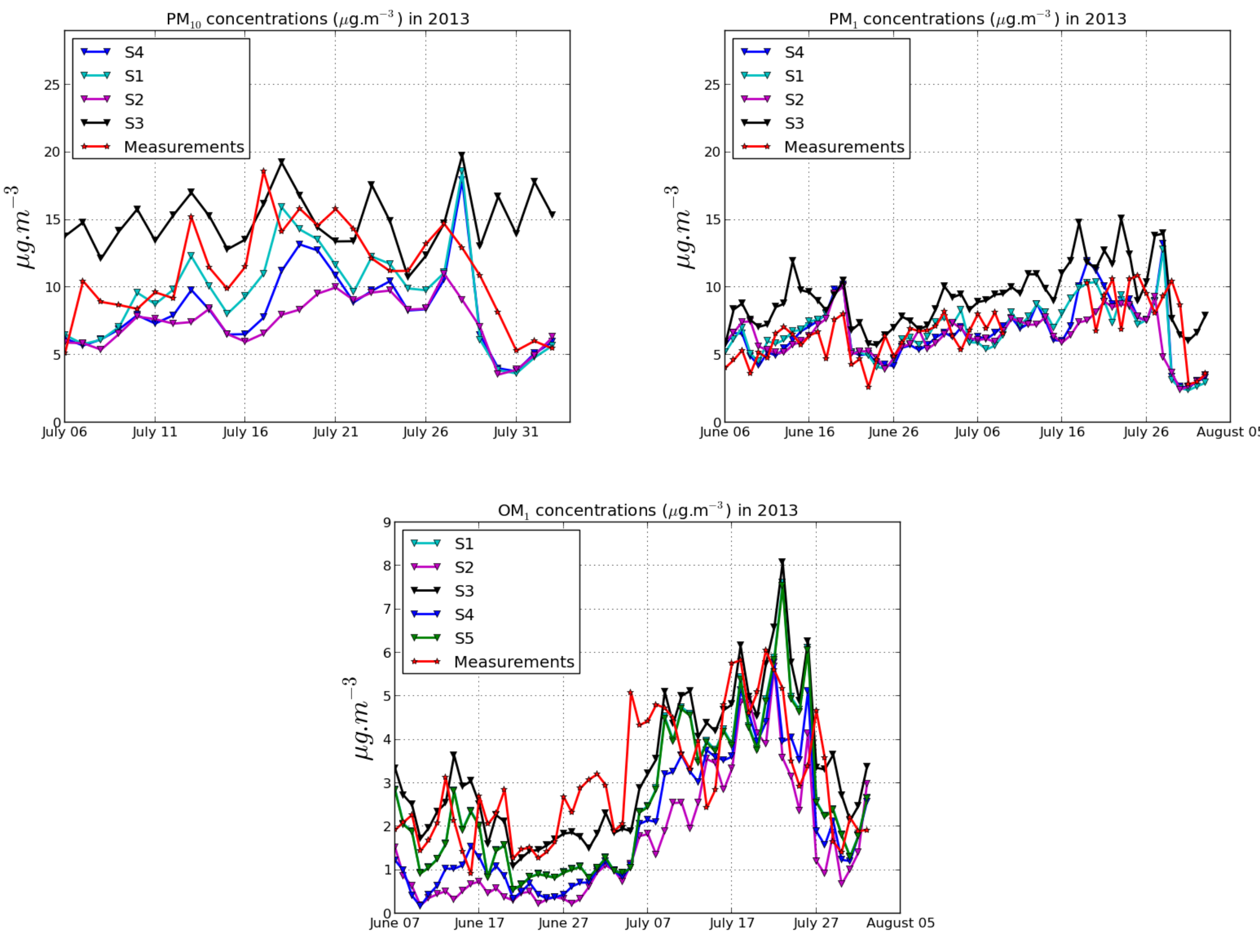

Figure 3.C1: Comparisons of PM_{10} (upper left panel), PM_1 (upper right panel), OM_{PM_1} (lower panel) concentrations simulated and observed at Ersa during the summer 2013.

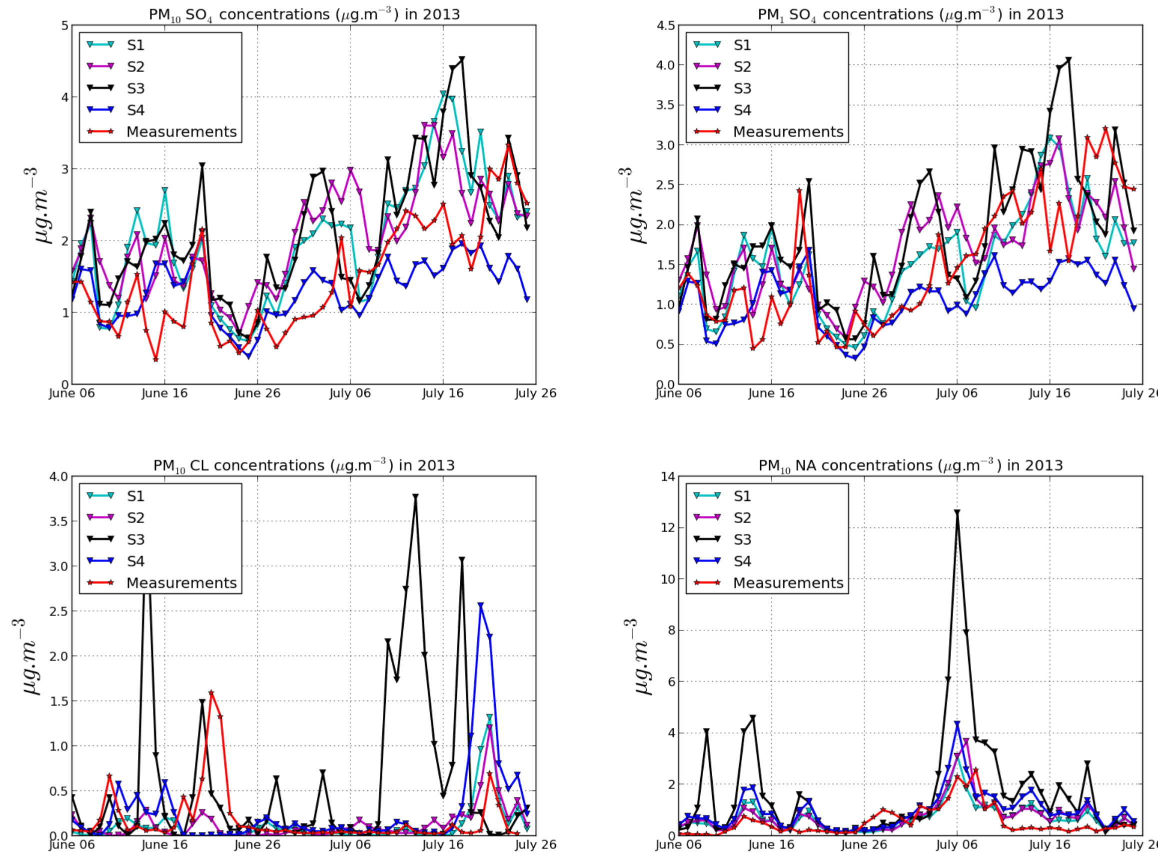

Figure 3.C2: Comparisons of simulated and observed PM_{10} sulfate (upper left panel), PM_1 sulfate (upper right panel), PM_{10} chloride (lower left panel) and PM_{10} sodium (lower right panel) concentrations at Ersa during the summer 2013.

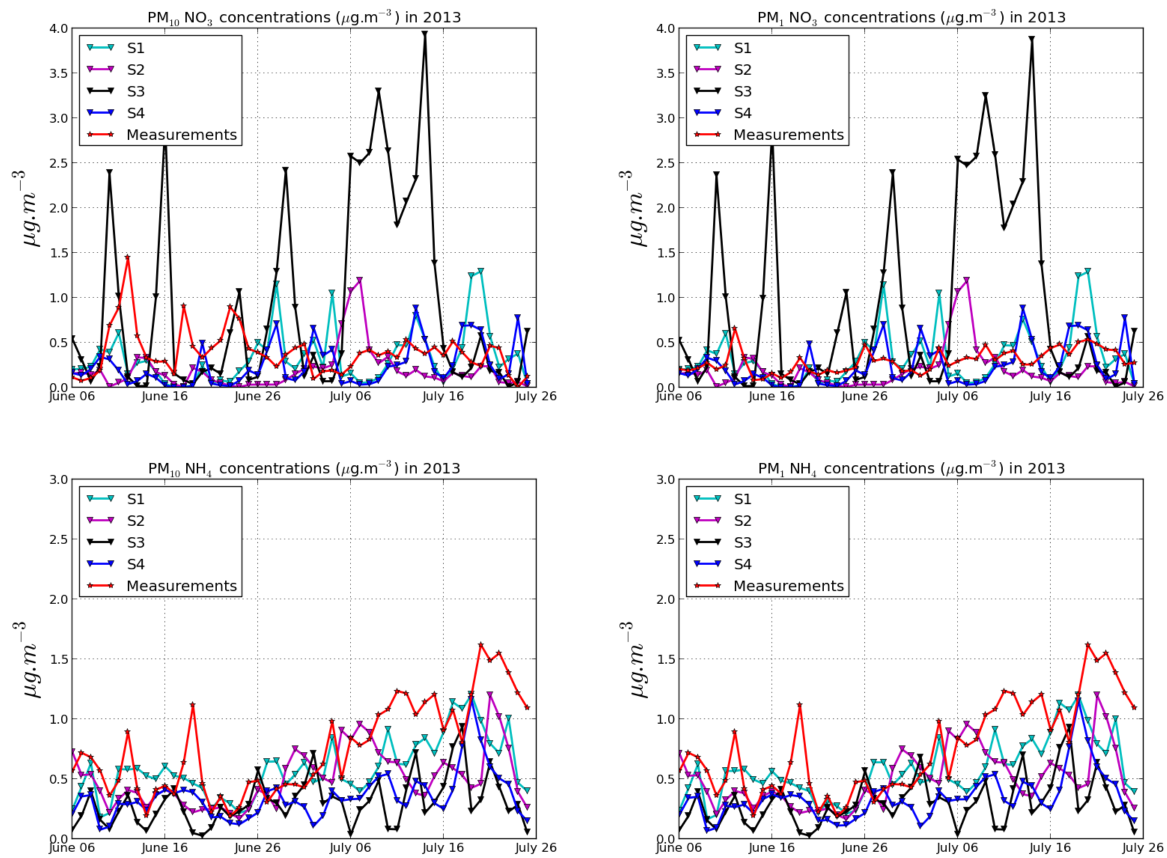

Figure 3.C3: Comparisons of simulated and observed PM_{10} nitrate (upper left panel), PM_1 nitrate (upper right panel), PM_{10} ammonium (lower left panel) and PM_1 ammonium (lower right panel) concentrations at Ersa during the summer 2013.

Concentration sensitivities in the summer 2013

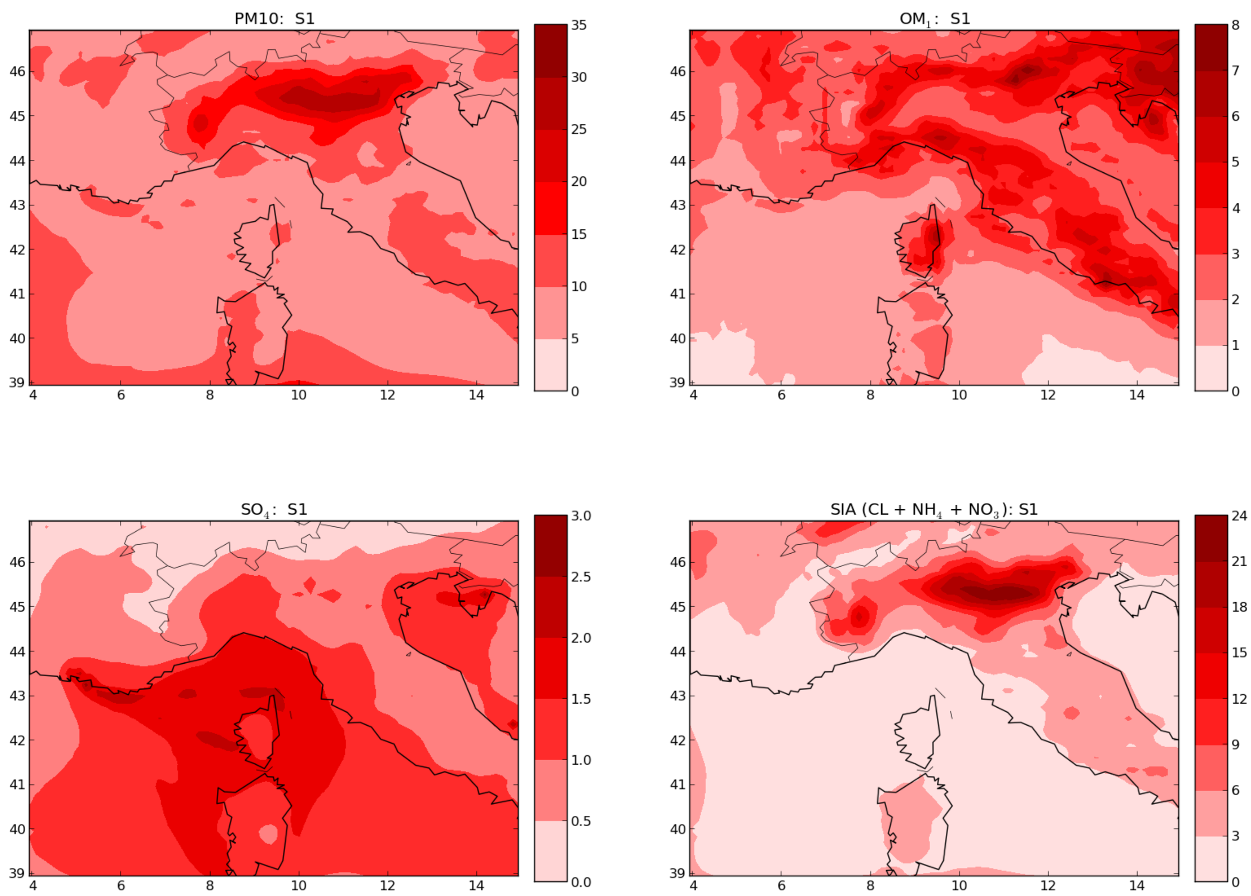

Figure 3.D1: Maps of the concentrations of PM_{10} (upper left panel), OM_1 (upper right panel), sulfate (lower left panel) and other inorganics (nitrate, ammonium and chloride) (lower right panel) during the summer 2013 in μg m^{-3}.

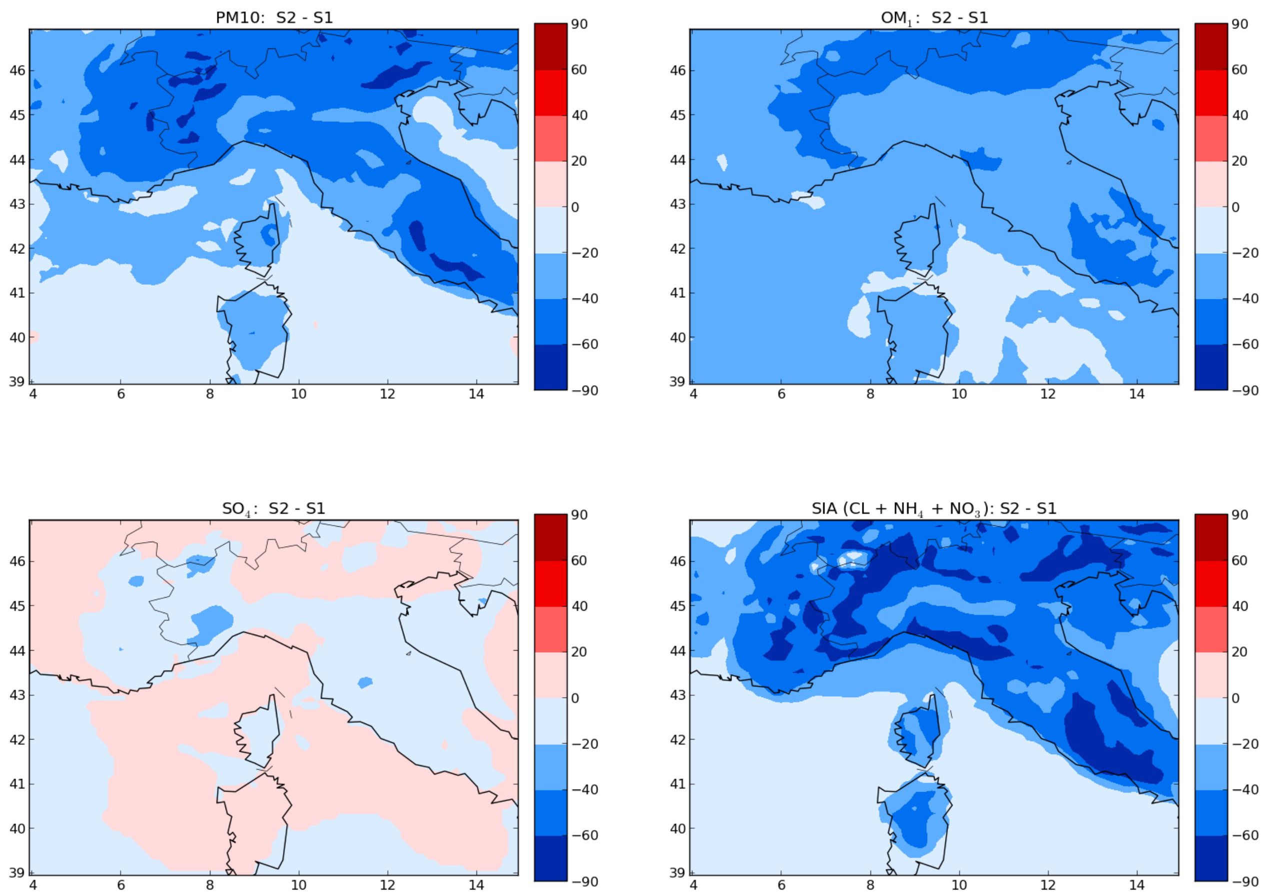

Figure 3.D2: Maps of the relative differences of the concentrations of PM_{10} (upper left panel), OM_1 (upper right panel), sulfate (lower left panel) and other inorganics (nitrate, ammonium and chloride) (lower right panel) in % between S1 and S2 (right panel) during the summer 2013.

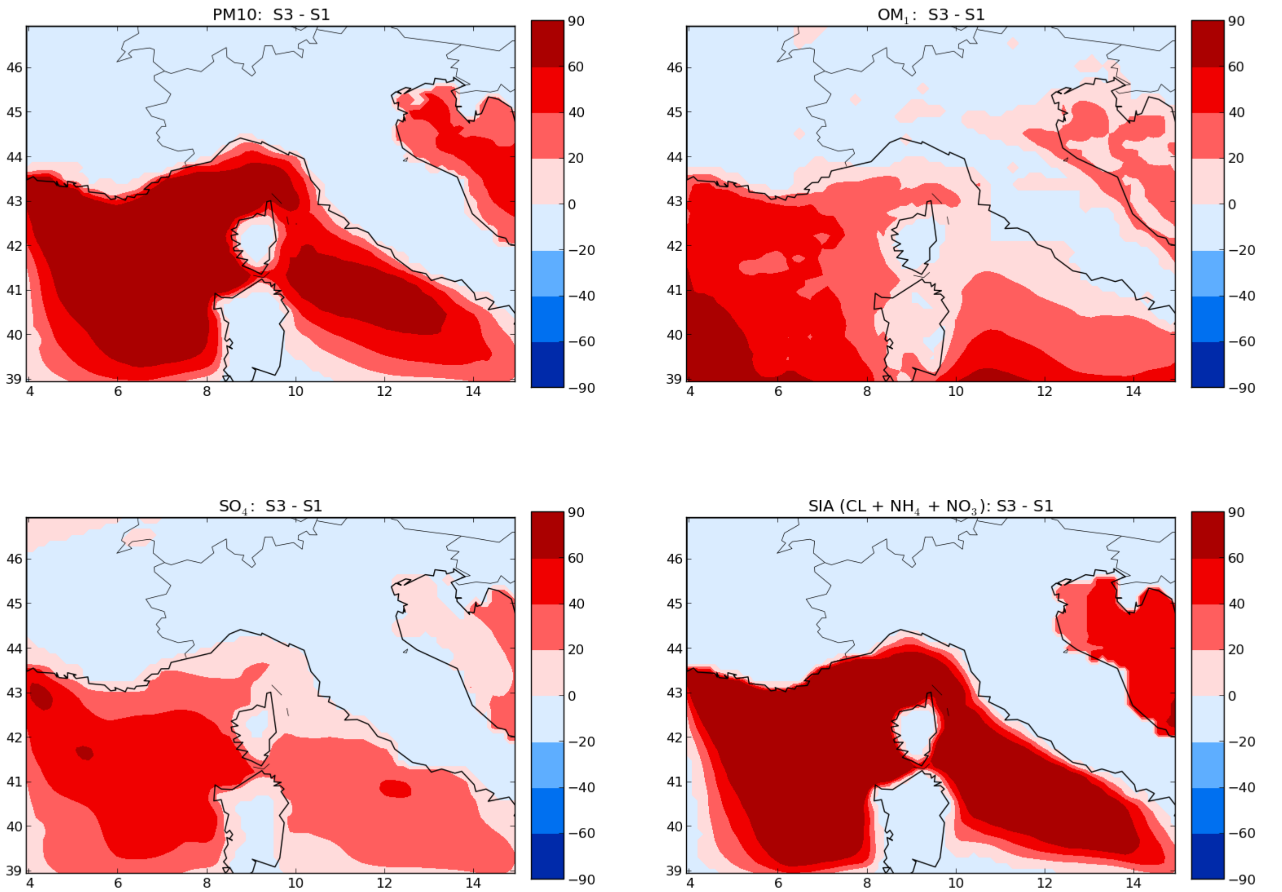

Figure 3.D3: Maps of the relative differences of the concentrations of PM_{10} (upper left panel), OM_1 (upper right panel), sulfate (lower left panel) and other inorganics (nitrate, ammonium and chloride) (lower right panel) in % between S1 and S3 (right panel) during the summer 2013.

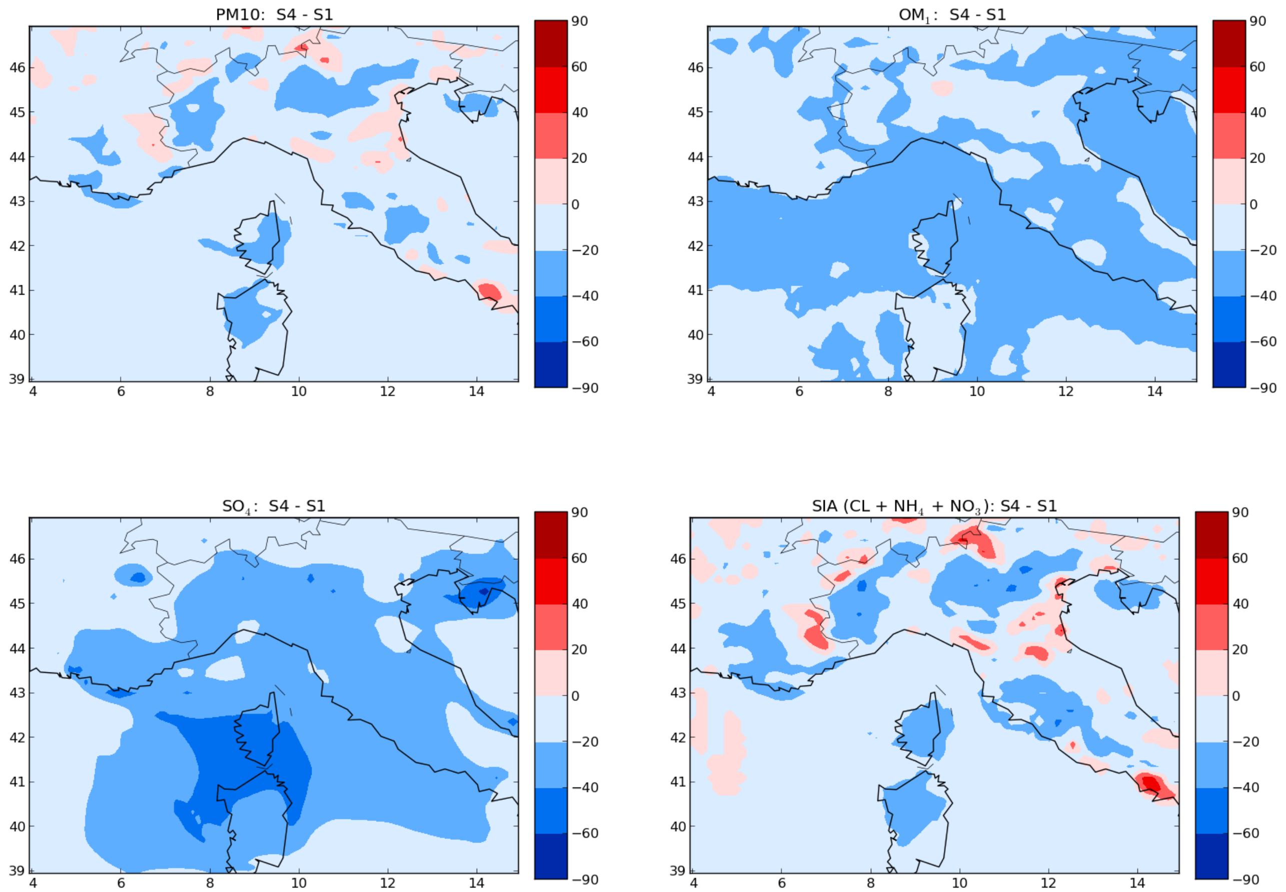

Figure 3.D4: Maps of the relative differences of the concentrations of PM_{10} (upper left panel), OM_1 (upper right panel), sulfate (lower left panel) and other inorganics (nitrate, ammonium and chloride) (lower right panel) in % between S1 and S4 (right panel) during the summer 2013.

Chapitre 4

Modélisation des concentrations et des propriétés des aérosols organiques au dessus du bassin ouest Méditerranéen pendant l'hiver 2014

Sommaire

Les aérosols organiques secondaires (AOS) sont principalement formés par le partitionnement des produits d'oxydation des composés organiques volatils (COVs) et des composés organiques semi-volatils et de volatilité intermédiaire (COVIS). Ces derniers ne sont généralement pas renseignés dans les inventaires d'émissions, et ils ne sont pris en compte dans les modèles de chimie-transport que depuis quelques années.

Les COVIS sont souvent classés selon leur volatilité: composés organiques volatils de volatilité intermédiaires (COVI) de concentration de saturation entre 10^4 et 10^6 μg.m^{-3} , les composés organiques semi-volatils (COSV) de concentrations de saturation entre 0.1 et 10^4 μg.m^{-3} ainsi que les composés orgainques volatils de faible volatilité (COVF) de volatilité entre 10^{-4} et 0.1 μg.m^{-3}, ...

Plusieurs études éxpérimentales et numériques ont été conduites (El Haddad et al., 2013a; Minguillón et al., 2016; Chrit et al., 2017) dans le but de comprendre l'origine et la composition des aérosols organiques (AO) pendant différentes saisons en Méditérranée. Pendant l'été, ces études ont montré que les AO sont essentiellement produits d'oxydation de COV biogéniques, tels que les monoterpènes. En hiver, les précurseurs de l'AO ne sont plus majoritairement biogéniques, mais plutôt anthropiques. Par exemple, Canonaco et al. (2015) ont montré grâce à des mesures au dessus de Zürich, que l'origine des AO est différente selon les saisons et que le secteur résidentiel pendant l'hiver est le secteur d'émission le plus important en termes de contribution aux concentrations des AO. Ciarelli et al. (2017a) ont aussi souligné l'importance du secteur résidentiel qui contribue entre 60 et 70% à la formation des AOS, majoritairement formés à partir de l'oxidation des COVIS.

Donc, la modélisation des AO pendant l'hiver nécessite la caractérisation des COVIS en termes d'émissions et de vieillissement. Les émissions des COVIS sont souvent calculées à partir des émissions d'aérosols organiques primaires (AOP) multipliées par un ratio COVIS/AOP. Ce ratio dépend du secteur d'émissions. Pour le trafic automobile, Kim et al. (2016) ont estimé que ce ratio est de 1.5 en se basant sur des mesures à l'échappement d'un échantillon de véhicules représentatifs de la flotte automobile française. Couvidat et al. (2012) ont utilisé un ratio de 4 et 6 et ont trouvé que le ratio de 6 est mieux adapté pour la modélisation des AO en hiver en Europe.

L'approche la plus utilisée pour décrire l'évolution et le vieillissement des COVIS est l'aproche Volatility Basis Set (VBS) qui consite à diviser les COVIS en différentes classes de volatilité. Cette approche met en compétition deux processus: la fragmentation et la fonctionalisation, et plusieurs étapes d'oxydation sont utilisées pour représenter le vieillissement des COVIS. Couvidat et al. (2012) a aussi developpé un simple schéma d'oxydation des COVIS basé sur une seule étape d'oxidation. L'état d'oxydation des AO est un paramètre important pour évaluer ces différentes paramétrisations. Ce chapitre a pour but de quantifier l'effet des émissions des COVIS sur la formation d'AO ainsi que leur état d'oxidation/oxygénation pendant l'hiver au dessus du bassin ouest Méditerranéen. Ce chapitre discute par ailleurs la sensibilité des AO aux différents paramètres représentant les émissions et le vieillissement des COVIS notamment la distribution de volatilité, schéma à une ou à plusieurs étapes d'oxydation, présence de COV non traditionnels (COVNT) qui sont un ensemble de composés émis par le secteur résidentiel notamment. Ces COVNT ne sont pas pris en compte généralement dans les modèles, mais une paramétrisation a été définie par Ciarelli et al. (2017b) pour les prendre en compte. Différentes simulations de sensibilité ont été conduites pour comprendre les paramètres les plus influants sur les concentrations des AO et leur état d'oxydation au dessus de la station de mesures Ersa située au Cap Corse (France) et plus généralement en Méditerranée de l'Ouest pendant l'hiver.

Les données d'entrée du modèle sont décrites dans le chapitre précédent. La paramétrisation décrivant le vieillissement des COVIS est décrite dans Couvidat et al. (2012), deux autres paramétrisations basées sur l'approche VBS sont décrites dans Koo et al. (2014) et Ciarelli et al. (2017b). Les distributions de volatilité des émissions des COVIS mises en jeu sont celles décrites dans Couvidat et al. (2012), May et al. (2013b,c) et May et al. (2013a). La sensibilité à la distribution de volatilité des émissions est discutée en comparant 2 simulations: la première dans laquelle une distribution de volatilité spécifique au secteur résidentiel est appliquée aux émissions de COVIS pour toutes les sources anthropiques et la deuxième dans laquelle une distribution de volatilité spécifique aux émissions de voitures (diesel et essence) est appliquée pour les COVIS émis par les sources autres que le secteur résidentiel.

La sensibilité au schéma de vieillissement des COVIS anthropiques est étudiée en comparant deux simulations avec des schémas différents: un schéma simple à une étape d'oxydation et un schéma où le vieillissement multigénérationnel est pris en compte. Le rôle de COVNT est étudié en prenant en compte les émissions de ces derniers et leur schéma de vieillissement proposé par Ciarelli et al. (2017b). La sensibilité aux émissions des COVIS émis par le secteur résidentiel est discutée en augmentant ces émissions, c-à-d en choisissant un rapport COVIS/AOP égal à 4.

La majorité des simulations réussissent à reproduire les fortes concentrations d'AO et montrent que les concentrations sont élevées au dessus des grandes villes telles que Marseille, Turin, Rome, Milan, confirmant l'origine anthropique de la majorité des AO. La modélisation montre que les AOP et les AOS formés à partir des COVIS sont les espèces majoritaires dans la masse des AO (entre 60 et 84%). Le secteur résidentiel contribue aux alentours de 32% aux concentrations des AO. Les AOS produits d'oxydation des COVs aromatiques habituellement pris en compte dans les modèles contribuent très faiblement aux concentrations des AO (3%). Par contre, les AOS provenant des COVNT repésentent entre 18 et 21% de la masse organique. La contribution des AO d'origine biogénique est faible (15-18%), car les émissions biogéniques sont faibles en hiver. La simulation dans laquelle les COVNT sont pris en compte avec un ratio d'émissions de 4.75 par rapport aux COVIS, ainsi celle dans laquelle la même distribution de volatilité à l'émission est adoptée pour les émissions de COVIS de toutes sources anthropiques, sur-estime et sous-estime respectivement de manière importante les concentrations d'AO. Ceci suggère que les émissions de COVNT sont surestimées avec un ratio de 4.75, et qu'une meilleure caractérisation de la distribution de volatilité des émissions de COVIS qui dépend du secteur d'émission est importante.

Sur l'ensemble du domaine de simulation, la distribution de volatilité des émissions a une influence plus importante que l'influence du schéma d'oxydation. L'effet du rapport d'émissions COVIS/AOP est le plus important paramètre impactant les concentrations des AO au dessus des grandes villes.

Deux configurations donnent les concentrations les plus proches des mesures. La première est celle du schéma à une étape d'oxydation avec un rapport COVIS/AOP de 4 pour le secteur résidentiel (1.5 pour les autres secteurs). La deuxième configuration utilise un schéma d'oxydation multigénérationel avec un rapport COVIS/AOP de 1.5 pour tous les secteurs. Dans ces deux simulations, une distribution de volatilité spécifique aux émissions des voitures est utilisée pour les émissions des COVIS des sources anthropiques autres que le secteur résidentiel, pour lequel une distribution de volatilité spécifique est utilisée.

L'état d'oxydation et d'oxygénation des AO est aussi étudié grâçe à deux indices: OM:OC et O:C. Les mesures de ces derniers montrent que les OA sont hautement oxidés et oxygénés au dessus d'Ersa. Le modèle sous-estime ces deux indices pour toutes les simulations. Le schéma à plusieurs étapes d'oxydation a un effet peu remarquable sur ces deux indices. Par contre, les AOS issus des COVNT, hautement oxidés et oxygénés, contribuent à une petite amélioration de l'état d'oxidation/oxygénation modélisé. Pour améliorer la modélisation de ce dernier, il semble nécessaire d'ajouter au modèle des paramétrisations donnant naissance à des molécules hautement oxygénées (MHO) comme décrit par Molteni et al. (2018) et du nitrate organique.

Ce chapitre est constitué de l'article:
Modeling organic aerosol concentrations and properties during ChArMEx winter cam-

paign of 2014 in the western Mediterranean region (2018b), Mounir Chrit, Karine Sartelet, Jean Sciare, Marwa Majdi, François Dulac, J. B. Nicolas and J.-E. Petit, Atmos. Chem. Phys. Discuss., submitted.

Modeling organic aerosol concentrations and properties during winter 2014 in the northwestern Mediterranean region

MounirChrit[1], KarineSartelet[1], JeanSciare[2,3], MarwaMajdi[1,5], JoséNicolas[2], Jean-EudesPetit[2,4], FrançoisDulac[2].

[1] CEREA, joint laboratory Ecole des Ponts ParisTech - EDF R&D, Université Paris-Est, 77455 Champs sur Marne, France.
[2] LSCE, CNRS-CEA-UVSQ, IPSL, Université Paris-Saclay, Gif-sur-Yvette, France
[3] EEWRC, The Cyprus Institute, Nicosia, Cyprus
[4] INERIS, Parc Technologique ALATA, 60550 Verneuil-en-Halatte, France
[5] Laboratoire de Métérologie Dynamique (LMD)-IPSL, Sorbonne Université, CNRS UMR 8539, Ecole Polytechnique, Paris, France

Abstract In the framework of the Chemistry-Aerosol Mediterranean Experiment, measurements of organic aerosols are performed at a remote site (Ersa) on Corsica Island in the northwestern Mediterranean Sea during the winter 2014, when high organic concentrations from anthropogenic origin are observed. This work aims at representing the observed organic aerosol concentrations and properties (oxidation state) using the air-quality model Polyphemus with a surrogate approach for secondary organic aerosol (SOA) formation. Because intermediate/semi-volatile organic compounds (I/S-VOC) are the main precursors of SOA at Ersa during the winter 2014, different parameterizations to represent the emission and ageing of I/S-VOC were implemented in the chemistry-transport model of the air-quality platform Polyphemus (different volatility distribution emissions, single-step oxidation vs multi-step oxidation within a Volatility Basis Set framework, inclusion of non-traditional volatile organic compounds NTVOC). Simulations using the different parameterizations are compared to each other and to the measurements (concentration and oxidation state). The high observed organic concentrations are well reproduced whatever the parameterizations. They are slightly under-estimated with most parameterizations, but they are slightly over-estimated when the ageing of NTVOC is taken into account. The volatility distribution at emissions influences more strongly the concentrations than the choice of the parameterization that may be used for ageing (single-step oxidation vs multi-step oxidation), stressing the importance of an accurate characterization of emissions. Assuming the volatility distribution of sectors other than residential heating to be the same as residential heating may lead to a strong under-estimation of organic concentrations. The observed organic oxidation and oxygenation states are strongly under-estimated in all simulations, even when a recently developed parameterization for modeling the ageing of I/S-VOC from residential heating is used. This suggests that uncertainties in the ageing of I/S-VOC emissions remain to be elucidated, with a potential role of organic nitrate from anthropogenic precursors and highly oxygenated organic molecules.

4.1 Introduction

Organic aerosols (OA) are the main fraction of submicron particulate matter (PM_1) (Jimenez et al., 2009). Even though the sources of its primary fraction (POA) are nominally known (e.g. traffic, residential heating), large uncertainties remain regarding their emissions (Gentner et al., 2017; Shrivastava et al., 2017). POA has been considered as non-volatile in emissions inventories and chemistry-transport models (CTMs); however, recent studies have provided clear evidences that a large portion of POA emissions partition between the gas and the particle phases (Robinson et al., 2007b). Organic species that compose OA are often classified depending on their volatility:

intermediate volatility organic compounds (IVOC) (with saturation concentration C^* in the range 10^4-10^6 $\mu g\, m^{-3}$), semi-volatile organic compounds (SVOC) (with saturation concentration C^* in the range 0.1-10^4 $\mu g\, m^{-3}$), or low-volatility organic compounds (LVOC) (with saturation concentration C^* lower than 0.1 $\mu g\, m^{-3}$) (Lipsky and Robinson, 2006; Grieshop et al., 2009; Huffman et al., 2009; Cappa and Jimenez, 2010; Fountoukis et al., 2014; Tsimpidi et al., 2010; Woody et al., 2016; Ciarelli et al., 2017b,a).

OA originates not only from the partitioning of POA between the gas and the particle phases, but also from secondary aerosol formation (SOA) through the gas-to-particle partitioning of the oxidation products of biogenic and anthropogenic volatile organic compounds (VOC) and intermediate and semi volatile organic compounds (I/S-VOC). The main biogenic VOC precursors are terpenes (α-pinene, β-pinene, limonene, humulene) and isoprene (Shrivastava et al., 2017), while the main anthropogenic ones are aromatics (e.g. toluene, xylenes) (Dawson et al., 2016; Gentner et al., 2017).

Available measurements and modeling studies are useful to elucidate the composition and origin of OA in different seasons (Couvidat et al., 2012; Hayes et al., 2015; Canonaco et al., 2015; Chrit et al., 2017; Ciarelli et al., 2017b). Indeed, over the Mediterranean region, the oxidation of biogenic VOC may dominate the formation of OA during the summer (El Haddad et al., 2013a; Minguillón et al., 2016; Chrit et al., 2017). Chrit et al. (2017) found that I/S-VOC emissions do not influence much the concentrations of OA in summer over the Mediterranean region, but biogenic SOA prevail. Because biogenic emissions are low in winter, Canonaco et al. (2015) demonstrated a clear shift in the SOA origin between summer and winter during a measurement campaign from February 2012 to February 2013 conducted in Zürich using the Aerosol Chemical Speciation Monitor (ACSM, Ng et al. (2011)) measurements. This last study notably highlights the importance of biogenic VOC emissions and biogenic SOA production in summer, and the importance of residential heating in winter. Ciarelli et al. (2017a) performed a source apportionment study at the European scale and revealed that residential combustion (mainly related to wood burning) contributed around 60-70% to SOA formation during the winter whereas non-residential combustion and road-transportation sector contributed about 30-40% to SOA formation. Moreover, residential heating can also be a source of POA, which may make up a large fraction (20% to 90%) of the submicron particulate matter in winter (Murphy et al., 2006; May et al., 2013d; Shrivastava et al., 2017).

Modeling OA concentrations in winter is challenging, because it involves mostly the characterization of I/S-VOC emissions and ageing. Standard gridded emission inventories, such as those of the European Monitoring and Evaluation Programme (EMEP, www.emep.int) over Europe, do not yet include I/S-VOC emissions, and their emissions are still highly uncertain. For example, Denier van der Gon et al. (2015) estimated that emissions from residential wood combustion were under-estimated by a factor 2-3 in the 2005 EUCAARI inventory. As an indirect method to account for the missing organic emissions in the absence of precise emission inventories, numerous modeling studies estimate the I/S-VOC emissions from POA emissions (Couvidat et al., 2012; Bergström et al., 2012; Koo et al., 2014; Zhu et al., 2016; Ciarelli et al., 2017a) or more recently from VOC emissions (Zhao et al., 2015, 2016; Ots et al., 2016; Murphy et al., 2017). A ratio of I/S-VOC/POA of 1.5 has been used in several air quality studies (Bergström et al., 2012; Koo et al., 2014; Zhu et al., 2016; Ciarelli et al., 2017a). For example, Zhu et al. (2016) simulated the particle composition over Greater Paris during the winter MEGAPOLI campaign and they found that simulated OA agreed well with observed OA when gas-phase I/S-VOC emissions are estimated using a ratio I/S-VOC/POA of 1.5, as derived following the measurements at the tailpipe of vehicles representative of the french fleet (Kim et al., 2016). However, various ratios are used to better fit the measurements. For example, over Europe, Couvidat et al. (2012) used a ratio I/S-VOC/POA of 4 but also of 6 in a sensitivity simulation to better fit the observed OA concentrations in winter. Koo et al. (2014) used a ratio IVOC/POA of 1.5 but also of 3 in their high IVOC emission scenario.

The atmospheric evolution (also known as ageing) of I/S-VOC as well as their impacts on atmospheric OA concentrations remain poorly characterized (Murphy et al., 2006) and deserve a better understanding. A widely used approach to model the ageing of I/S-VOC in CTMs is the volatility basis set (VBS) approach (Donahue et al., 2006). I/S-VOC are divided into several classes of volatility where each class is represented by a surrogate. When oxidized by the hydroxyl radical, it leads to the formation of surrogates of lower volatility classes. This approach tends to lead to an overestimation of simulated organic concentrations (Cholakian et al., 2017) if fragmentation is not considered (formation of high volatility surrogates during the oxidation). Although the one-dimensional basis set 1-D VBS accounts for the volatility of the surrogates, it does not allow the representation of varying oxidation levels of OA. The more powerful prognostic tool to date, bi-dimensional VBS approach (2D-VBS), although it is computationally burdensome, describes the ageing of I/S-VOC using not only the volatility property (C^*) but also the oxidation level (the oxygen-to-carbon ratio O:C), taking into account two competing processes: functionalization and fragmentation (Donahue et al., 2012). Koo et al. (2014) developed a 1.5-D ageing VBS-type scheme that accounts for fragmentation, functionalization and multigenerational ageing, and that represents both the volatility and the oxidation properties of the surrogates. When oxidized by a hydroxyl radical, each surrogate leads to the formation of more oxidized and less volatile surrogates with a reduced carbon number. Functionalization and fragmentation are implicitly taken into account in this approach, because of the increase of the oxygen number and the decrease of the carbon number of the surrogates formed. The 1.5-D VBS module is implemented within two widely used CTMs namely CAMx(ENVIRON, 2011) and CMAQ (Byun and Ching, 1999). Couvidat et al. (2012, 2013b, 2017) and Zhu et al. (2016) used a simplified ageing scheme with 3 volatility bins. When oxidized by the hydroxyl radical, each surrogate forms a less volatile and more oxidized surrogate, that does not undergo multigenerational ageing. This simplified ageing scheme is implemented in the two widely used CTMs Polyphemus (Chrit et al., 2017) and Chimere (Couvidat et al., 2017). In winter, when anthropogenic emissions impact the most air quality, anthropogenic emissions such as toluene and xylenes may also form SOA, although they may be less efficient than I/S-VOC (Couvidat et al., 2013a). To take into account emissions and ageing of anthropogenic VOC that are usually not considered in CTMs (phenol, naphtalene, m-,o-,p- cresol, etc.), Ciarelli et al. (2017b) modified the approach of Koo et al. (2014) by adding non traditional VOC (NTVOC) that have a limit saturation concentration between VOC and IVOC.

The oxidation level of OA is important, because it is indicative of the degree of hygroscopicity, surface tension (Jimenez et al., 2009), and radiative property of the OA in addition to its ability to act as cloud condensation nuclei (CCN) over the Mediterranean (Jimenez et al., 2009; Duplissy et al., 2011; Wong et al., 2011). Chrit et al. (2017) showed that, in summer in the western Mediterranean region, OA is highly oxidized and oxygenated. The CTM Polyphemus/Polair3d used in their study does represent this high oxidation level of OA after adding to the model formation processes of highly oxidized species (autoxidation) and organic nitrate formation.

Although the organic matter to organic carbon ratio (OM:OC) was first believed to lie between 1.2 and 1.4 (Grosjean and Friedlander, 1975), recent studies (Turpin and Lim, 2001; El-Zanan et al., 2005) show that OM:OC is rather close to 1.6 for urban aerosols and 2.1 for non urban aerosols. Zhang et al. (2005a) developed an algorithm to deconvolve the mass spectra of OA obtained with an Aerodyne^{TM} Aerosol Mass Spectrometer (AMS) in order to estimate the mass concentrations of hydrocarbon-like and oxygenated organic aerosols (HOA and OOA). The mass of HOA represents primary sources, with a OM:OC ratio close to 1.2 and O:C ratio close to 0.1, while the mass of OOA represents secondary sources (aged and oxygenated) with a OM:OC ratio close to 2.2 and O:C ratio close to 1 (Aiken et al., 2008). Using this technique, Zhang et al. (2005b) found an average OM:OC ratio of 1.8 in Pittsburgh in September. Over Europe, Crippa et al. (2014) found that secondary OA is dominant in the OA fraction, with primary sources contributing to less than 30% to the total mass fraction. Xing et al. (2013) measured a ratio OM:OC ratio over 14 cities throughout China and found that in summer, OM:OC is nearly 1.75 $\pm$ 0.13, while the ratio is lower in winter (1.59 $\pm$ 0.18). The OM:OC ratio is lower during winter due to the slow oxidation process owing to the low temperatures in addition the low biogenic contribution to OA mass during winter. At Ersa, over the Mediterranean during the summer, Chrit et al. (2017) found high OM:OC and O:C ratios (2.5 and 1 respectively). They are due to aged biogenic OA, which Chrit et al. (2017) were able to represent by adding the formation of extremely low-volatility species and organic nitrate to the model and by considering the formation of organosulfate.

Quantifying the effect of I/S-VOC emissions and their impact on the atmospheric organic budget as well as the OA oxidation/oxygenation levels during different seasons is challenging in spite of the recent advances concerning the description of I/S-VOC (Stockwell et al., 2015; Ciarelli et al., 2017b). This work aims at evaluating how commonly used parameterizations and assumptions of I/S-VOC emissions and ageing perform to model the OA concentrations and properties in the western Mediterranean region in winter. To that end, the CTM from the air quality platform Polyphemus is used with different parameterizations of I/S-VOC emissions and ageing.

This paper is structured as follow: section 2 presents the setup of the air-quality model used and reference measurements. Section 3 presents the different emissions and ageing mechanisms used to describe the evolution of I/S-VOC as well as the comparison method. Section 4 compares the simulated concentrations, compositions of OA for the simulations using the different parameterizations. Finally, section 5 compares the measured and simulated OM:OC and O:C ratios.

4.2 Model and measurement set-up

The period of interest of this study is January-March 2014, hereafter referred to as the winter 2014 campaign.

4.2.1 General model setup

The Polyphemus/Polair3d air-quality model is used, with a similar setup as Chrit et al. (2017). The numerical algorithms used for transport, and the parameterizations used for dry and wet depositions are detailed in Sartelet et al. (2007). Gas-phase chemistry is modeled with the Carbon Bond 05 mechanism (CB05) (Yarwood et al., 2005). Different reactions are added to CB05 to model the formation of semi-volatile organic compounds from five classes of SOA precursors (intermediate and semi-volatile organic compounds of anthropogenic emissions, aromatic compounds, isoprene, monoterpenes and sesquiterpenes) (Kim et al., 2011b; Couvidat et al., 2012). For these classes of precursors, which include a great number of species, only a few surrogates are used to represent all the species.

The SIze REsolved Aerosol Model (SIREAM) (Debry et al., 2007b) is used for simulating the dynamics of the aerosol size distribution by coagulation and condensation/evaporation. SIREAM uses a sectional approach and the aerosol distribution is described here using 24 sections of bound diameters: 0.01, 0.0141, 0.0199, 0.0281, 0.0398, 0.0562, 0.0794, 0.1121, 0.1585, 0.199, 0.25, 0.316, 0.4, 0.5, 0.63, 0.79, 1.0, 1.2589, 1.5849, 1.9953, 2.5119, 3.5481, 5.0119, 7.0795 and 10.0 μm. The condensation/evaporation of inorganic aerosols is determined using the thermodynamic model ISORROPIA (Nenes et al., 1998) with a bulk equilibrium approach in order to compute partitioning between the gaseous and condensed phases of particles. For organic aerosols, the partitioning is computed using SOAP (Couvidat and Sartelet, 2015), and bulk equilibrium is also assumed for SOA partitioning. After condensation/evaporation, the moving diameter algorithm is used for mass redistribution among size bins. The simulations are run between 01 January and 01 April 2014 for both the nesting (Europe) and the nested (Mediterranean) domains. The simulation domains (Europe and Mediterranean) and the spatial resolution used in the present study are the same as the ones used in Chrit et al. (2017). Boundary conditions for the European domain are obtained from the global chemistry-transport model MOZART v4.0 (Horowitz et al., 2003) (https://www.acom.ucar.edu/wrf-chem/mozart.shtml). The European simulation provides initial and boundary conditions to the Mediterranean one.

Meteorological data are provided by the European Center for Medium-Range Weather Forecasts (ECMWF) model. The vertical diffusion is computed using the Troen and Mahrt parameterization (Troen and Mahrt, 1986). The Global Land Cover 2000 (GLC-2000; http://www.gvm.jrc.it/glc2000/) data set is used for land cover. Sea-salt emissions are parameterized following Jaegle et al. (2011) and are composed of f 30.61% sodium, 25.40% chloride and 4.22% sulfate following Schwier et al. (2015). Biogenic emissions are estimated with the Model of Emissions of Gases and Aerosols from Nature (MEGAN, Guenther et al. (2006)). Anthropogenic emissions are generated using the EDGAR-HTAP_V2 inventory for 2010 (http://edgar.jrc.ec.europa.eu/htap_v2/). The monthly and daily temporal distribution for the different activity sectors are obtained from GENEMIS (1994), and the hourly temporal distribution from Sartelet et al. (2012). NO_x, SO_x and $PM_{2.5}$ emissions are speciated as described in Chrit et al. (2017). I/S-VOC gas-phase emissions are estimated from the POA emissions from residential heating by multiplying them by a constant factor assumed to be 1.5 in the default simulation. As described in section 4.3.5, different values will be used and compared for I/S-VOC gas-phase emissions from residential heating and from other sectors. The I/S-VOC emissions from residential heating are assumed to be those of the sector "htap_6_residential" of the EDGAR-HTAP_V2 inventory. The emissions from this sector (shown in Figure 4.1) concern the emissions from heating/cooling and equipment/lightening of buildings as well as waste treatment. The I/S-VOC emissions from residential heating are obtained from the POA emissions of sector 6 by multiplying them by a constant factor noted R_{RH} = I/S-VOC/POA. These emissions over the Mediterranean domain are located over big cities (Marseille, Milan, Rome, etc). I/S-VOC emissions from the six other anthropogenic sources (shown in Figure 4.1) are estimated from the POA emissions by multiplying them by a constant factor noted R = I/S-VOC/POA. These emissions are located over big cities and along the main traffic routes, as well as the shipping routes linking Marseille to Ajaccio and Bastia. Different approaches will also be used to represent the ageing of I/S-VOC, as described in section 4.3.

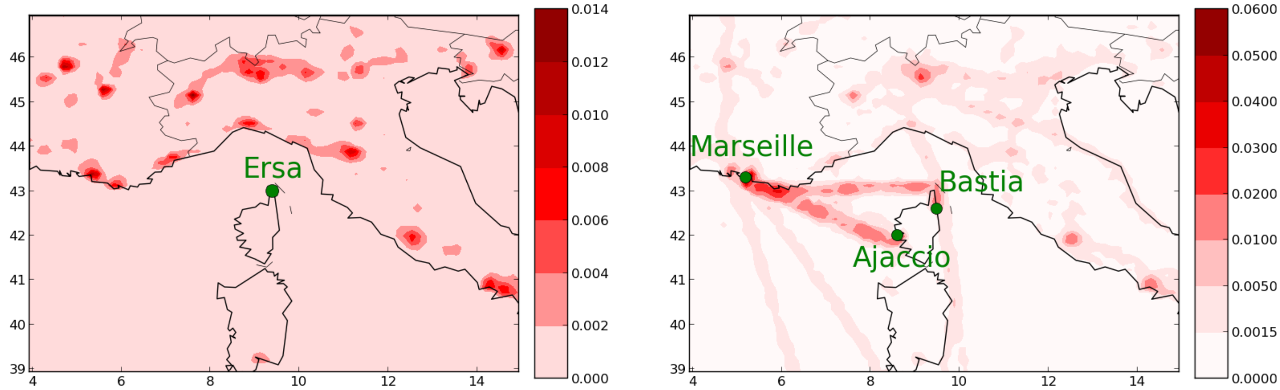

Figure 4.1: Surface emissions of POA from the residential heating sector (left panel) and from the other six anthropogenic sectors (right panel) during the winter 2014. The emissions are in μg.m^{-2}.s^{-1}

4.2.2 Measurement setup

The ground-based measurements were performed in the framework of ChArMEx (The Chemistry-Aerosol Mediterranean Experiment) at Ersa (42°58'N, 9°21.8'E) on the northern tip of Corsica Island. It is located on a ridge at an altitude of about 530 m above the sea level and has an unimpeded view of the sea over ∼300° from the SSW to SSE (Mallet et al., 2016). The ground-based comparisons are performed by comparing the measured concentrations to the simulated ones using the concentrations of the model cell the closest to the station. The central coordinate of this cell at which concentrations are computed is (42°52N, 9°22'30"E), which is very close to the station and with a similar altitude above sea level (494 m), as detailed in Chrit et al. (2017).

To evaluate organic concentrations and oxidation properties, an Aerodyne^{TM} ACSM was used to measure the near real-time chemical composition and mass loading of aerosols with aerodynamic diameters between 70 and 1000 nm with a 30-min time resolution (Ng et al., 2011) . This instrument has been continuously running at Ersa between June 2012 and July 2014 (Nicolas, 2013), with an on-site set-up similar to the one presented in Michoud et al. (2017). A recent intercomparison exercise, which he ACSM used in this study has successfully taken part in, report an expanded uncertainty of 19% for OM (Crenn et al., 2015). OM:OC and O:C ratios are estimated using these measurements following the methodology provided in Kroll et al. (2011). Although Crenn et al. (2015) and Fröhlich et al. (2015) have shown consistent results (eg satisfactorily Z-scores) in terms of fragmentation pattern, higher discrepancies were observed for f_{44} (mass fraction of m/z44), which is an essential variable in the calculation of these elemental ratios. In this respect, results are presented with an uncertainty which can be estimated as being twice the one of PM (i.e. around 40%).

4.2.3 Model/measurements comparison method

To evaluate the model, we compare model simulation results to measurements at the Ersa site using a set of performance statistical indicators. These indicators are: the simulated mean ($\overline{s}$), the root mean square error (RMSE), the correlation coefficient (corr), the mean fractional bias (MFB), the mean fractional error (MFE). Table 4.A1 of Appendix 4.7 lists the key statistical indicators definitions used in the model-to-data intercomparison. Furthermore, the criteria of Boylan and Russell (2006) (detailed in Table 4.A2 of Appendix 4.7) is used to assess the performance of the simulations.

4.3 Modeling of I/S-VOC emissions and ageing

In order to understand the behavior of the different parameterizations commonly used in CTMs to represent emissions and ageing of I/S-VOC in the western Mediterranean region, several simulations using different parameterizations are compared. These parameterizations are those described in Couvidat et al. (2012), Koo et al. (2014) and Ciarelli et al. (2017b). The differences concern the emission ratios used to estimate I/S-VOC from POA (R and R_{RH}), the ageing scheme (one step or multi-generational), the modeling of NTVOC, as well as the ratio OM:OC and volatility distribution at emissions.

4.3.1 One-step oxidation scheme

The one-step oxidation mechanism of Couvidat et al. (2012) is based on the fitting of the curve of dilution of POA from diesel exhaust of Robinson et al. (2007b). I/S-VOC are modeled with three surrogate species POAlP, POAmP and POAhP of different volatilities characterized by their saturation concentrations (0.91, 86.21 and 3225.80 μg m^{-3} respectively). The properties of the primary and aged I/S-VOC are shown in Table 4.1 of Appendix 4.7. The ageing of each of these primary surrogates is modeled by a one-step OH-oxidation reaction in the gas phase (Appendix 4.7), leading to the formation of secondary surrogates SOAlP, SOAmP and SOAhP. Once formed, these secondary surrogates do not undergo further oxidations. Compared to the primary surrogates, the volatility of the secondary surrogates is reduced by a factor of 100 and their molecular weight is increased by 40% (Grieshop et al., 2009; Couvidat et al., 2012) to represent functionalization and fragmentation.

4.3.2 Multi-generational step oxidation scheme

In sensitivity simulations, for anthropogenic I/S-VOC emissions, the oxidation mechanism is based on the hybrid (1.5-D) volatility basis set (VBS) approach of Koo et al. (2014). This mechanism combines the simplicity of the 1-dimensional (1-D) VBS with the ability to describe evolution of OA in the 2-dimensional space of oxidation state and volatility. This basis set uses five volatility surrogates, characterized by saturation concentrations ranging from 0.1 to 1000 μg m^{-3}. The surrogates VAP0, VAP1, VAP2, VAP3 and VAP4 refer to the primary surrogates and VAS0, VAS1, VAS2, VAS3 and VAS4 refer to the secondary ones. Table 4.C1 of Appendix 4.7 lists their properties.

In the scheme developed by Koo et al. (2014), the OH-oxidation reaction of the primary surrogates leads to a mixture of primary and secondary surrogates of lower volatility. Reduction in the carbon number and increase in the oxygen number of the lower volatility surrogate indicates that functionalization and fragmentation are implicitly accounted for. This mechanism is detailed in Appendix 4.7.

4.3.3 Multi-generational step oxidation scheme for residential heating

In sensitivity simulations, for anthropogenic I/S-VOC emissions from residential heating, the VBS model developed by Ciarelli et al. (2017b) is also used. As in the previously detailed multi-step oxidation scheme, five surrogates with volatilities characterized by saturation concentrations ranging from 0.1 to 1000 μg m^{-3} are used. The primary surrogates (BBPOA1, BBPOA2, BBPOA3, BBPOA4, BBPOA5) react with OH to form secondary surrogates (BBSOA0, BBSOA1, BBSOA2,

Profil N°		1	2
Reference		May et al. (2013b,c)	Couvidat et al. (2012)
Sat. Conc.	0.9	0.35	0.25
	86.2	0.51	0.32
	3225.8	0.14	0.43

		1	2
		May et al. (2013b,c)	May et al. (2013a)
Sat. Conc.	0.1	0.15	0.20
	1	0.20	0.10
	10	0.31	0.10
	100	0.20	0.20
	1000	0.14	0.4

Table 4.1: Summary of the volatility distributions of the primary I/S-VOC surrogates. Saturation concentrations (Sat. Conc.) are expresssed in μg m^{-3}.

BBSOA3, BBSOA4), whose volatility is one order of magnitude lower than the primary surrogate. In opposition to the one-step and multi-step oxidation schemes detailed above, here the secondary surrogates may also undergo OH-oxidation forming the secondary surrogate of lower volatility. As in the other schemes, reduction in the carbon number and increase in the oxygen number of the secondary surrogates indicates that functionalization and fragmentation are taken into account. The properties of the VBS surrogates are shown in Table 4.D1 of Appendix 4.7, where reactions are also detailed.

Data from recent wood combustion and ageing experiments performed in smog chamber by Ciarelli et al. (2017b) show significant contribution of SOA from non-traditional volatile organic compounds (NTVOC: phenol, m-, o-, p-cresol, m-, o-, p-benzenediol/2-methylfuraldehyde, dimethylphenols, guaiacol/methylbenzenediols, naphthalene, 2-methylnaphthalene/1-methylnaphthalene, acenaphthylene, syringol, biphenyl/acenaphthene, dimethylnaphthalene) to OA mass. These NTVOC are usually not accounted as SOA precursors in CTMs. The NTVOC mixture saturation concentration is estimated to be $\sim 10^6$ μg m^{-3} falling with the IVOC saturation concentrations range limit (Koo et al., 2014; Donahue et al., 2012). NTVOC emissions are estimated using a ratio of NTVOC/SVOC of 4.75 (Ciarelli et al., 2017b) and their OH-oxidation produces four secondary surrogates of different volatilities. These four surrogates may undergo OH-oxidation leading to the less volatile and more oxidized secondary surrogate, similarly to the multi-step oxidation described in section 4.3.3. This mechanism is detailed in Appendix 4.7 and the surrogates properties are listed in Table 4.D2 of Appendix 4.7.

4.3.4 Volatility distribution and properties of primary emissions

In the one-step oxidation scheme of Couvidat et al. (2012), the emission distribution is based on the fitting of the curve of dilution of diesel exhaust from Robinson et al. (2007b) and is shown in Table 4.1. This emission distribution is approximately similar to the one measured by May et al. (2013a) for biomass burning, and used in the multi-step oxidation scheme for residential heating of Ciarelli et al. (2017b). In the multi-step oxidation scheme of Koo et al. (2014) for anthropogenic emissions, the emission distribution is obtained from averaging the emission distributions from gasoline and diesel vehicles measured by May et al. (2013b,c). As shown in Table 4.1, the emitted I/S-VOC are less volatile than in the biomass-burning volatility distribution of May et al. (2013b). Here, the volatility distributions are assigned to a profile number (equal to 1 or 2), depending on whether the volatility profile is similar to the profile from biomass burning emissions of May et al. (2013b) (profile number 2) or whether it is similar to the profile from vehicle emissions of May et al. (2013c) and May et al. (2013a) (profile number 1).

The one-step and multi-step oxidation schemes also differ in the OM:OC and O:C ratios of the emitted surrogates. In the one-step oxidation scheme of Couvidat et al. (2012), the OM:OC and O:C ratios are assumed to be constant (1.3) and close to the average OM:OC and O:C ratios of Koo et al. (2014). However, for residential heating, the multi-oxidation scheme of Ciarelli et al.

Profil N°		1	2			1	2
Reference		Couvidat et al. (2012)				Koo et al. (2014)	Ciarelli et al. (2017b)
Sat. Conc.	0.9	1.3 (0.15)	1.7 (0.55)	Sat. Conc.	0.1	1.36 (0.16)	1.64 (0.37)
					1	1.31 (0.12)	1.53 (0.29)
	86.2	1.3 (0.15)	1.7 (0.55)		10	1.26 (0.07)	1.44 (0.22)
					100	1.21 (0.03)	1.36 (0.15)
	3225.8	1.3 (0.15)	1.7 (0.55)		1000	1.17 (0)	1.28 (0.09)

Table 4.2: Summary of the OM:OC (and O:C) ratio of the primary I/S-VOC surrogates. Saturation concentrations (Sat. Conc.) are expresssed in μg m^{-3}.

(2017b) assumes higher OM:OC and O:C rations, as described in Table 4.2. Here, the OM:OC and O:C ratios are assigned to a profile number (equal to 1 or 2), depending on whether the ratios are similar to the profile from biomass burning emissions of Ciarelli et al. (2017b) (profile number 2) or whether they are lower (profile number 1).

4.3.5 Sensitivity simulations

The setup of the different simulations is summarized in Table 4.3. The simulation S1 uses the setup commonly used in air-quality simulations with the Polyphemus platform: the one-step ageing scheme of Couvidat et al. (2012) is used for both residential heating and other anthropogenic sectors.

The simulation S2 is conducted to evaluate the impact of the volatility distribution of emissions. Instead of using a volatility distribution specific of biomass burning for all sectors as in S1, the volatility distribution specific of car emissions is used for anthropogenic sectors other than residential heating.

The simulation S3 is conducted to evaluate the impact of the ageing scheme. The volatility distributions are similar as S2, but multi-generational schemes are used rather than a single-oxidation strep for all anthropogenic sectors.

The simulation S4 is evaluated to estimate the impact of NTVOC. It has the same setup as S2 with multi-generational ageing, but NTVOC are taken into account.

The simulations S5 and S6 are conducted to assess the impact of the I/S-VOC/POA ratio used for residential heating (R_{RH}). The simulation S5 has the same setup as the simulation S2 (single-step oxidation), but it differs in the ratio R_{RH}, which is assumed to be equal to 4 rather than 1.5. The simulation S6 has the same setup as the simulation S4 (multi-step oxidation and NTVOC), but it differs in the ratio R_{RH}, which is assumed to be equal to 4 rather than 1.5.

In terms of the OM:OC ratio, the ratio specific of car emissions is used for emissions from anthropogenic sectors other than residential heating. For residential heating, higher OM:OC ratios are used in all simulations, except in S1, where the ratio specific of car emissions is used for all sectors.

4.4 Organic concentrations

The spatial distribution of OM_1 concentrations averaged over the first 3 months of 2014 (Figure 4.E1 of Appendix 4.7) shows that high OM_1 concentrations are mostly located over big cities like Marseille, Genoa, Turin, Milan, Rome and Naples and along maritime traffic routes, stressing that organics during wintertime are likely to be mostly of anthropogenic origins.

The simulated composition of OM_1 at Ersa is shown in Figure 4.1 for the simulations S4 and S5. In all simulations, primary and secondary organic aerosols (POA and SOA) from anthropogenic

Simulation	Residential heating					Other anthropogenic sectors			
	Ageing	Volatility profile	R_{RH}	OM:OC profile	NTVOC	Ageing	Volatility profile	R	OM:OC profile
S1	one-step (Couvidat)	2	1.5	1	No	one-step (Couvidat)	2	1.5	1
S2	one-step (Couvidat)	2	1.5	2	No	one-step (Couvidat)	1	1.5	1
S3	multi-step (Ciarelli)	2	1.5	2	No	multi-step (Koo)	1	1.5	1
S4	multi-step (Ciarelli)	2	1.5	2	Yes	multi-step (Koo)	1	1.5	1
S5	one-step (Couvidat)	2	4.0	2	No	one-step (Couvidat)	1	1.5	1
S6	multi-step (Ciarelli)	2	4.0	2	Yes	multi-step (Koo)	1	1.5	1

Table 4.3: Summary of the parameters used in the different simulations performed.

I/S-VOC are the main components of the organic mass (between 60% and 84%). POA tends to account for almost the same fraction of the organic mass than SOA (between 46% and 62%). Similarly, in the U.S., Koo et al. (2014) found that the SOA account for less than half of the modeled OA mass in winter 2005 due to the slow chemical ageing during the cold season. Over Europe, in March 2009, Ciarelli et al. (2017a) simulated that POA accounts between 12 and 68% of the OA, with an average value of 38%. The emission sector 6 (residential heating) has a large contribution to OA (between 31% and 33%). This is also in line with Ciarelli et al. (2017a) who found that over Europe in March 2009, the contribution of the residential sector to OA varies between 20% and 45% with an average value of 38%. Furthermore, this sector contributes more to SOA (between 42% and 52% of SOA from I/S-VOC) than to POA (between 17% and 31% of SOA from I/S-VOC), because their I/S-VOC emissions are more volatile. The contribution from aromatic VOC is low (lower than 3%), and when NTVOC are considered, they represent between 18% and 21% of the organic mass. The model simulations performed revealed that, for the winter of 2014, biogenic SOA contribute only to a small extent to the organic mass SOA (15-18%). Ciarelli et al. (2017a) also estimated the biogenic contribution to the organic budget to be between 5 and 20% over Europe.

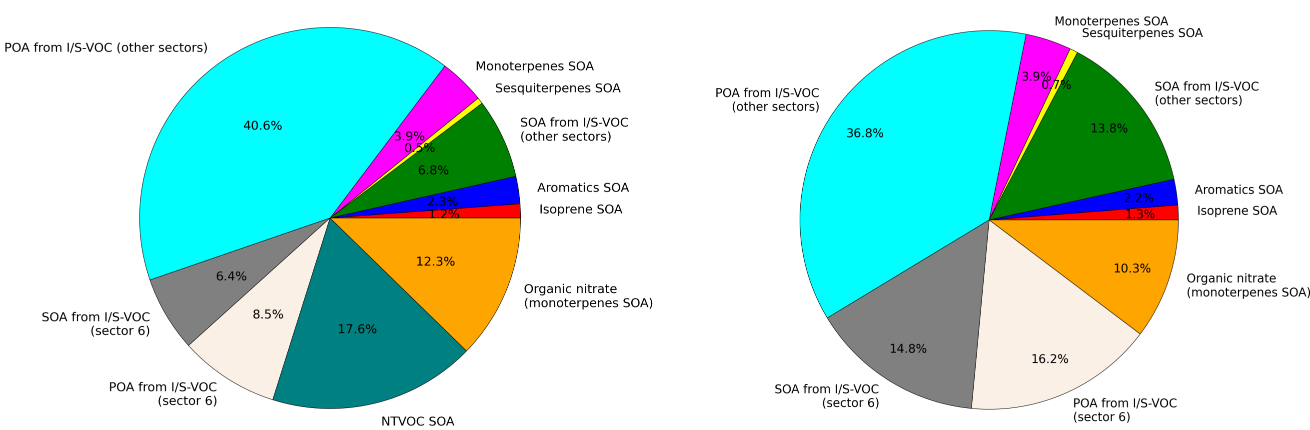

Figure 4.1: Simulated composition of OM_1 during the winter campaign of 2014 for two simulations: S4 (left panel) and S5 (right panel).

The statistical evaluation of the simulations is shown in Table 4.1. The performance criterion is satisfied for all simulations and the goal criterion is satisfied for S2, S3, S4 and S5. The goal criterion is not satisfied for the simulation S1, which uses single-step oxidation with a biomass-burning type volatility distribution for all anthropogenic sectors, and for the simulation S6, which uses multi-step oxidation with NTVOC and a high R_{RH} ratio. The simulation S1 strongly under-estimates the OM_1 concentration at Ersa, whereas the simulation S6 strongly over-estimates it.

All the simulations tend to under-estimate the OM_1 concentrations at Ersa, except for the two simulations where NTVOC are taken into account (S4 and S6), which over-estimate the OM_1 concentrations at Ersa.

The model-to-measurement correlation is high for all simulations (between 76 and 83%).

Other CTMs showed the same under-estimation of OM_1 concentrations during winter over Europe, even when I/S-VOC emissions are taken into account (Couvidat et al., 2012; Denier van der Gon et al., 2015). The CTM CAMX (Comprehensive Air Quality Model with extensions) also under-estimated the organic concentrations over Europe during February and March 2009 (Ciarelli et al., 2017a), but considerable improvement was found for the modeled organic aerosol (OA) mass with the mean fractional bias (MFB) reduced from -61 to -29 %, when the parameterization of (Ciarelli et al., 2017b) with NTVOC was added.

	Simulations	S1	S2	S3	S4	S5	S6
$\bar{o}$ = 1.45	$\bar{s}$ ± RMSE	0.75 ± 1.14	1.06 ± 0.91	1.20 ± 0.85	1.65 ± 0.79	1.25 ± 0.80	2.06 ± 1.08
	Correlation (%)	78.3	76.7	76.2	82.4	78.8	82.7
	MFB (%)	-55	-23	-11	17	-7	38
	MFE (%)	59	40	37	39	35	48

Table 4.1: Statistics of model to measurements comparisons for daily OM_1 concentrations during the winter campaign of 2014 at Ersa. $\bar{o}$ and $\bar{s}$ are the observed and simulated means, respectively. RMSE is the root mean square error, MFB and MFE are the mean fractional bias and error respectively.

The model-to-measurement comparison during the first 3-months of 2014 in terms of the daily concentrations of OM_1 at Ersa is shown in Figure 4.2.

Globally, the temporal variations of the simulated concentrations are well reproduced by the model. The simulation S1, which uses single-step oxidation with a biomass-burning type volatility distribution for all anthropogenic sectors, under-estimates the peaks. However, the peaks are well reproduced by the simulations S2, S3 and S5. The simulations S4 and S6, which take into account NTVOC over-estimate the peaks. All simulations under-estimate the beginning of the peak between 9 and 15 March, probably due to uncertainties in meteorology especially rain episodes, and changes in the origin of air masses.

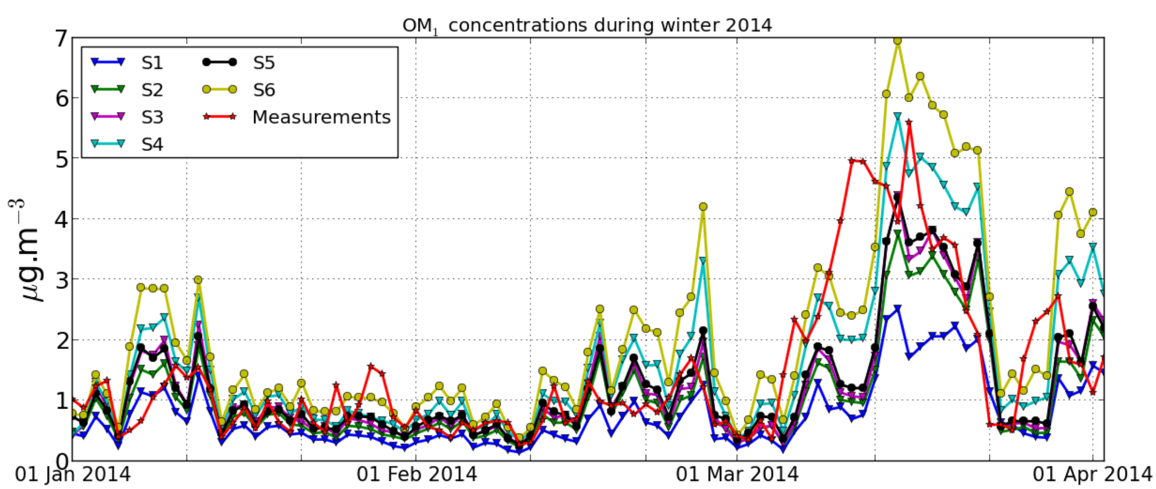

Figure 4.2: Comparison of measured and simulated daily OM_1concentrations at Ersa from 1 Jnury to 2 April.

As detailed in section 4.3.5, the difference between the simulations S2 and S1 originates in differences in the volatility distribution of emissions from anthropogenic sectors other than residential heating. In the simulation S2, a less volatile distribution is used than in the simulation S1, leading to larger OA concentrations in the particle phase. This difference in the volatility distribution makes a large difference in the OA concentrations, removing the strong under-estimation simulated in simulation S1 (the MFB is -55% in S1 and only -23% in S2).

Considering multi-step ageing for all anthropogenic sectors also leads to an increase of OA concentrations (the MBF of the simulation S3 is -11%, which is lower in absolute value than the simulation S2). However, the influence of the multi-step ageing (difference between S2 and S3 shown in Figure 4.E1 of Appendix 4.7) is lower than the influence of the volatility distribution (difference between S1 and S2 shown in Figure 4.E1 of Appendix 4.7). This larger influence of the volatility distribution than the multi-step ageing is true not only at Ersa, but also over the whole Mediterranean domain, where the average RMSE between the simulations S1 and S2 is 0.01 μg m^{-3} (impact of volatility), against 0.005 μg m^{-3} for the RMSE between the simulations S2 and S3 (impact of multi-step ageing).

At Ersa, increasing the ratio R_{RH} from 1.5 to 4 (difference between simulation S3 and S2 shown in Figure 4.E1 of Appendix 4.7) has almost the same impact as considering the multi-step ageing (difference between simulations S5 and S2 shown in Figure 4.E1 of Appendix 4.7), although the statistics are slightly better when the ratio R_{RH} is increased from 1.5 to 4 than when multi-step ageing is considered. However, this is not true over the whole Mediterranean domain, where the impact of increasing the ratio R_{RH} from 1.5 to 4 is large over cities, whereas the impact of multi-step ageing stays low (see Figure 4.E1 of Appendix 4.7). Over the whole Mediterranean domain, the average RMSE between the simulations S2 and S5 is 0.014 μg m^{-3} (impact of increasing the ratio R_{RH} from 1.5 to 4), against 0.005 μg m^{-3} for the RMSE between the simulations S2 and S3 (impact of multi-step ageing).

Although considering NTVOC leads to a slight increase in correlation, it also leads to an over-estimation of OA concentrations at Ersa. Over the whole Mediterranean domain, the impact of NTVOC is high with an average RMSE between the simulations S4 and S3 of 0.0211 μg m^{-3}.

Finally, the best statistics, in terms of MFE and MFB are obtained for the simulation S5, with a one-step ageing scheme, a volatility distribution typical of biomass burning for the residential sector with a ratio R_{RH} of 4, and a volatility distribution typical of car emissions for other sectors with a ratio R of 1.5.

4.5 Oxidation and oxygenation of organics

The oxidation state is quantified using two metrics: OM:OC and O:C calculated as detailed in Chrit et al. (2017). Figure 4.1 shows the daily variations of the measured and simulated ratios for the different simulations.

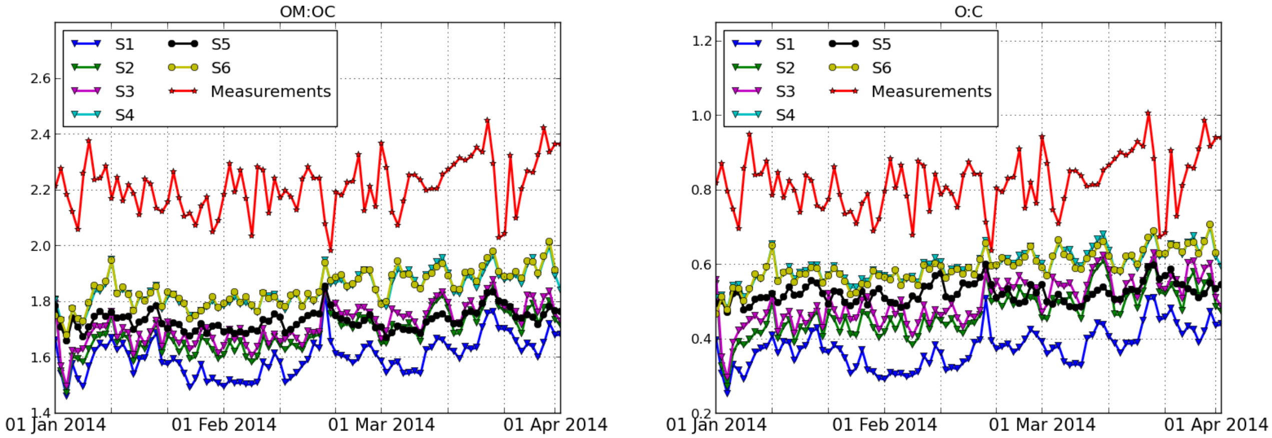

Figure 4.1: Daily variations of the ratios OM:OC (left panel) and O:C (right panel) from 01 January to 02 April 2014 at Ersa.

Organics at Ersa are highly oxidized and oxygenated: the measured OM:OC and O:C ratios at Ersa are respectively 2.21 ± 0.09 and 0.82 ± 0.07. These values are lower than the index measured during the summer 2013 by Chrit et al. (2017) (2.43 ± 0.07 and 0.99 ± 0.06 for the measured OM:OC and O:C ratios at Ersa respectively), due to the slower oxidation process owing to the lower temperatures during winter. The average simulated OM:OC and O:C ratios are shown in Table 4.1. Both index are strongly underestimated by all simulations, due to the high contribution of POA to the OM_1 concentrations (POA is less volatile and oxygenated than SOA). The simulations using multi-step ageing schemes for I/S-VOC emissions have higher OM:OC and O:C ratios, although the differences are very low (the OM:OC ratio is 1.69 ± 0.53 in S2 (single-step) and 1.72 ± 0.50 in S3 (multi-step). Organics in the simulations where the strength of I/S-VOC emission from residential heating was increased (simulations S5 and S6) have higher OM:OC and O:C ratios because POA and SOA from I/S-VOC from residential heating are more oxidized and oxygenated than POA and SOA from other anthropogenic sources. Similarly, organics in the simulations where NTVOC are taken into account have higher OM:OC and O:C ratios, because in the model, NTVOC lead to very oxidized and oxygenated OA. However, the simulated ratios OM:OC and O:C stay under-estimated (1.85 ± 0.38 and 0.60 ± 0.24 at most, against 2.21 ± 0.09 and 0.82 ± 0.07 in the measurements).

Simulations	S1	S2	S3	S4	S5	S6	Measurements
OM:OC	1.60 ± 0.62	1.69 ± 0.53	1.72 ± 0.50	1.85 ± 0.38	1.74 ± 0.49	1.85 ± 0.38	2.21 ± 0.09
O:C	0.38 ± 0.45	0.47 ± 0.36	0.50 ± 0.33	0.60 ± 0.23	0.53 ± 0.31	0.59 ± 0.24	0.82 ± 0.07

Table 4.1: Daily averages of OM:OC and O:C ratios at Ersa during winter 2014 for different simulations. The average measured OM:OC ratio is 2.21 and the average measured O:C ratio is 0.82.

4.6 Conclusion

This paper presents comparisons of modeled organic concentrations and properties to surface measurements performed at Ersa (Cape Corsica, France) during the winter 2014. This work aims at evaluating how commonly used parameterizations and assumptions of intermediate/semi-volatile organic compound (I/S-VOC) emissions and ageing perform in modeling the organic aerosol (OA) concentrations and properties in the western Mediterranean region in winter. To that end, the chemistry-transport model from the air quality platform Polyphemus is used with different parameterizations of I/S-VOC emissions and ageing (different volatility distribution emissions, single-step oxidation vs multi-step oxidation within a Volatility Basis Set framework, including non-traditional volatile organic compounds NTVOC). Winter (JFM) 2014 simulations are performed and compared to measurements obtained with an ACSM at the background station of Ersa in the North of Corsica Island. In all simulations, OA at Ersa is mainly from anthropogenic sources (15 to 18% of OA is from biogenic sources). The emission sector 6 (residential heating) has a large contribution to OA (between 31 and 33%). The contribution from aromatic VOC is low (lower than 3%). NTVOC, as modeled with the parameterization of Ciarelli et al. (2017b) represent between 18% and 21% of the organic mass. For most simulations, the concentrations of OA compare well to the measurements. All the simulations tend to under-estimate the OA concentrations at Ersa, except for the two simulations where NTVOC are taken into account, which, however, over-estimate the OA concentrations. Over the whole western Mediterranean domain, the volatility distribution at the emission influences more strongly the concentrations than the choice of the parameterization that may be used for ageing (single-step oxidation vs multi-step oxidation). Modifying the volatility distribution of sectors other than residential heating leads to a decrease of 29% in OA concentrations at Ersa, while using the multi-step oxidation parameterization rather than the single-step one leads to an increase of 13%. The best statistics are obtained using two configurations: the first one is a one-step ageing scheme, a volatility distribution typical of biomass burning for the residential sector with a ratio I/S-VOC/POA at emission of 4, and the second one is a multi-generational ageing scheme, a volatility distribution typical of car emissions for other sectors with a ratio R I/S-VOC/POA at emission of 1.5.

Both the OM:OC and O:C ratios are underestimated at Ersa in all simulations. The largest simulated OM:OC ratio is equal to 1.85 ± 0.83, against 2.21 ± 0.09 in the measurements. For the winter campaign, Chrit et al. (2017) improved the simulated OM:OC ratio by taking into account the formation of extremely-low volatile organic compounds and organic nitrate from monoterpene oxidation. Similarly, the formation of organic nitrate and highly oxygenated organic molecules (Molteni et al., 2018) from aromatic precursors should be added to better represent the observed OA properties. However, adding these new OA formation pathways may lead to an increase in OA concentrations, suggesting that the actual parameterizations, particularly those with NTVOC may need to be revisited, for example by better characterizing their deposition.

Acknowledgements This research has received funding from the French National Research Agency (ANR) projects SAF-MED (grant ANR-12-BS06-0013). This work is part of the ChArMEx project supported by ADEME, CEA, CNRS-INSU and Météo-France through the multidisciplinary programme MISTRALS (Mediterranean Integrated Studies aT Regional And Local Scales). It contributes to ChArMEx work packages 1 and 2 on emissions and aerosol ageing, respectively. The ACSM at Ersa was funded by the CORSiCA project funded by the Collectivité Territoriale de Corse through the Fonds Européen de Développement Régional of the European Operational Program 2007-2013 and the Contrat de Plan Etat-Région. Eric Hamounou is acknowledged for his great help in setting up the Ersa station. CEREA is a member of the Institut Pierre-Simon

Laplace (IPSL).

4.7 Appendix

Statistical indicators and criteria

Statistic indicator	Definition
Root mean square error (RMSE)	$\sqrt{\frac{1}{n}\sum_{i=1}^{n}(c_i - o_i)^2}$
Correlation (Corr)	$\frac{\sum_{i=1}^{n}(c_i - \bar{c})(o_i - \bar{o})}{\sqrt{\sum_{i=1}^{n}(c_i - \bar{c})^2}\sqrt{\sum_{i=1}^{n}(o_i - \bar{o})^2}}$
Mean fractional bias (MFB)	$\frac{1}{n}\sum_{i=1}^{n}\frac{c_i - o_i}{(c_i + o_i)/2}$
Mean fractional error (MFE)	$\frac{1}{n}\sum_{i=1}^{n}\frac{\mid c_i - o_i \mid}{(c_i + o_i)/2}$

Table 4.A1: Definitions of the statistics used in this work. $(o_i)_i$ and $(c_i)_i$ are the observed and the simulated concentrations at time and location i, respectively. n is the number of data

Criteria	Performance criterion	Goal criterion
|MFB|	$\leq 60\%$	$\leq 30\%$
MFE	$\leq 75\%$	$\leq 50\%$

Table 4.A2: Boylan and Russel criteria

Single-step ageing of I/S-VOC (Couvidat et al., 2012)

$$POAlP + OH \xrightarrow[k]{} SOAlP \quad (4.1)$$
$$POAmP + OH \xrightarrow[k]{} SOAmP \quad (4.2)$$
$$POAhP + OH \xrightarrow[k]{} SOAhP \quad (4.3)$$
$$(4.4)$$

with k = 2.0×10^{-11} cm^3. $molecule^{-1}$. s^{-1}.

Surrogate	Emission fraction	Molecular weight	$\log_{10}(C^*)$ at 298K	ΔH_{vap}	OM/OC	O/C
POAlP	0.25	280	-0.04	106.0	1.3	0.15
POAmP	0.32	280	1.94	91.0	1.3	0.15
POAhP	0.43	280	3.51	79.0	1.3	0.15
SOAlP	—	392	-2.04	106.0	1.82	0.56
SOAmP	—	392	-0.06	91.0	1.82	0.56
SOAhP	—	392	1.51	79.0	1.82	0.56

Table 4.B1: Properties of the primary and secondary anthropogenic I/S-VOC. The molecular weights are in $g.mol^{-1}$. ΔH_{vap} is the enthalpy of vaporisation in $KJ.mol^{-1}$.

Multi-step ageing of I/S-VOC (Koo et al., 2014)

$$VAP1 + OH \xrightarrow[k]{} 0.864VAP0 + 0.142VAS0 \quad (4.5)$$
$$VAP2 + OH \xrightarrow[k]{} 0.877VAP1 + 0.129VAS1 \quad (4.6)$$
$$VAP3 + OH \xrightarrow[k]{} 0.889VAP2 + 0.116VAS2 \quad (4.7)$$
$$VAP4 + OH \xrightarrow[k]{} 0.869VAP3 + 0.137VAS3 \quad (4.8)$$
$$(4.9)$$

with k = 4.0×10^{-11} cm^3. $molecule^{-1}$. s^{-1}.

Surrogate	Emission fraction	Molecular weight	$\log_{10}(C^*)$ at 298K	ΔH_{vap}	OM/OC	O/C
VAP0	0.15	278	-1	96.0	1.36	0.16
VAP1	0.20	275	0	85.0	1.31	0.12
VAP2	0.31	272	1	74.0	1.26	0.07
VAP3	0.20	268	2	63.0	1.21	0.03
VAP4	0.14	266	3	55.0	1.17	0.00
VAS0	—	172	-1	35	2.05	0.70
VAS1	—	167	0	35	1.92	0.60
VAS2	—	163	1	35	1.81	0.51
VAS3	—	158	2	35	1.70	0.43
VAS4	—	153	3	35	1.59	0.34

Table 4.C1: Properties of the VBS species (the primary and secondary anthropogenic SVOC). The molecular weights are in $g.mol^{-1}$. ΔH_{vap} is the enthalpy of vaporisation in $KJ.mol^{-1}$.

Multi-step ageing of I/S-VOC from residential heating (Ciarelli et al., 2017b)

$$BBPOA4 + OH \xrightarrow[k]{} BBSOA3 \tag{4.10}$$

$$BBPOA3 + OH \xrightarrow[k]{} BBSOA2 \tag{4.11}$$

$$BBPOA2 + OH \xrightarrow[k]{} BBSOA1 \tag{4.12}$$

$$BBPOA1 + OH \xrightarrow[k]{} BBSOA0 \tag{4.13}$$

$$BBSOA3 + OH \xrightarrow[k]{} BBSOA2 \tag{4.14}$$

$$BBSOA2 + OH \xrightarrow[k]{} BBSOA1 \tag{4.15}$$

$$BBSOA1 + OH \xrightarrow[k]{} BBSOA0 \tag{4.16}$$

$$NTVOC + OH \xrightarrow[k]{} 0.143BB3SOA4 + 0.097BB3SOA3 + 0.069BB3SOA2 + 0.011BB3SOA1 \tag{4.17}$$

$$BB3SOA4 + OH \xrightarrow[k]{} BB3SOA3 \tag{4.18}$$

$$BB3SOA3 + OH \xrightarrow[k]{} BB3SOA2 \tag{4.19}$$

$$BB3SOA2 + OH \xrightarrow[k]{} BB3SOA1 \tag{4.20}$$

$$BB3SOA1 + OH \xrightarrow[k]{} BB3SOA0 \tag{4.21}$$

$$\tag{4.22}$$

with k = 4.0×10^{-11} cm^3. $molecule^{-1}$. s^{-1}.

Surrogate	Emission fraction	Molecular weight	$\log_{10}(C^*)$ at 298K	ΔH_{vap}	OM/OC	O/C
NTVOC	4.75	113	6	—	—	—
BBPOA0	0.20	216	-1	85.0	1.64	0.37
BBPOA1	0.10	216	0	77.5	1.53	0.29
BBPOA2	0.10	216	1	70.0	1.44	0.22
BBPOA3	0.20	216	2	62.5	1.36	0.15
BBPOA4	0.40	215	3	55.0	1.28	0.09
BBSOA0	—	194	-1	35.0	1.80	0.50
BBSOA1	—	189	0	35.0	1.70	0.43
BBSOA2	—	184	1	35.0	1.61	0.36
BBSOA3	—	179	2	35.0	1.53	0.29
BB3SOA0	—	149	-1	35.0	2.48	1.05
BB3SOA1	—	144	0	35.0	2.29	0.90
BB3SOA2	—	140	1	35.0	2.12	0.76
BB3SOA3	—	135	2	35.0	1.96	0.63
BB3SOA4	—	131	3	35.0	1.82	0.52

Table 4.D1: Properties of the VBS species (the NTVOC and primary and secondary RH-I/S-VOC). The molecular weights are in $g.mol^{-1}$. ΔH_{vap} is the enthalpy of vaporisation in $KJ.mol^{-1}$.

Surrogate	Emission fraction	Molecular weight	$\log_{10}(C^*)$ at 298K	ΔH_{vap}	OM/OC	O/C
NTVOC	4.75	113	6	—	—	—
BBPOA0	0.20	216	-1	85.0	1.64	0.37
BBPOA1	0.10	216	0	77.5	1.53	0.29
BBPOA2	0.10	216	1	70.0	1.44	0.22
BBPOA3	0.20	216	2	62.5	1.36	0.15
BBPOA4	0.40	215	3	55.0	1.28	0.09
BBSOA0	—	194	-1	35.0	1.80	0.50
BBSOA1	—	189	0	35.0	1.70	0.43
BBSOA2	—	184	1	35.0	1.61	0.36
BBSOA3	—	179	2	35.0	1.53	0.29
BB3SOA0	—	149	-1	35.0	2.48	1.05
BB3SOA1	—	144	0	35.0	2.29	0.90
BB3SOA2	—	140	1	35.0	2.12	0.76
BB3SOA3	—	135	2	35.0	1.96	0.63
BB3SOA4	—	131	3	35.0	1.82	0.52

Table 4.D2: Properties of the NTVOC and their oxidation products). The molecular weights are in $g.mol^{-1}$. ΔH_{vap} is the enthalpy of vaporisation in $KJ.mol^{-1}$.

Maps of OM_1 concentrations and differences between simulations.

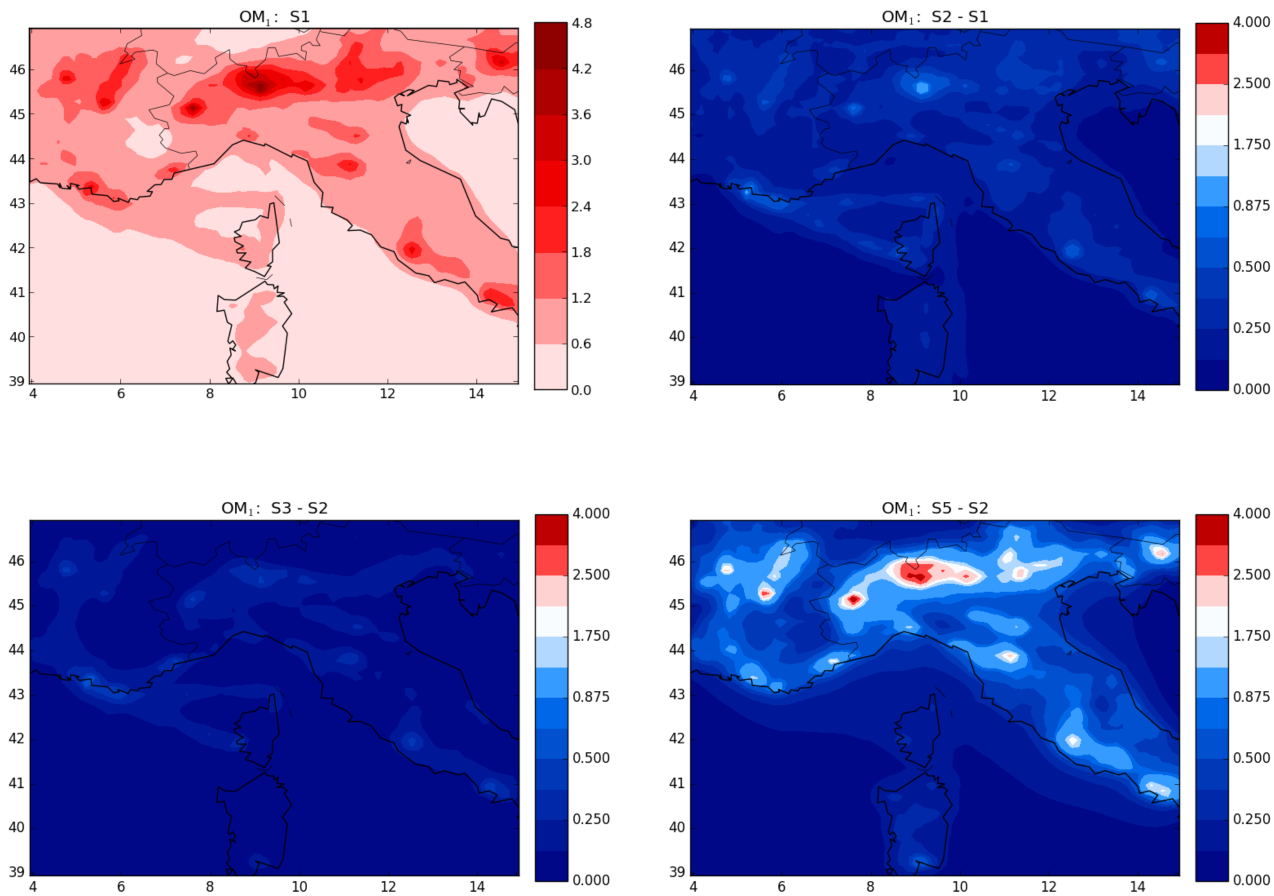

Figure 4.E1: Maps of the concentrations of OM_1 (μg m^{-3}) averaged over January to March 2014 using S1 (upper left panel) and the absolute difference of OM_1 concentrations between S2 and S1 (upper right panel, impact of volatility), S3 and S2 (lower left panel, impact of multi-step ageing), and S5 and S2 (lower right panel, impact of increasing R_{RH} from 1.5 to 4.

Chapitre 5

Conclusions et perspectives

Sommaire

5.1 Conclusions

Le premier but de cette thèse était d'évaluer le modèle de chimie-transport "POLYPHEMUS" pendant trois campagnes de mesures en Méditerranée, le bassin ouest en particulier, dans le cadre du projet "ChArMEx": étés 2012 et 2013 en plus de l'hiver 2014. Le deuxième but était d'améliorer la modélisation des aérosols dans cette région. Le troisième objectif était de comprendre l'origine des particules et les différents processus chimiques qui régient leur formation dans l'atmosphère méditerranéen. La quatrième était d'évaluer le modèle "POLYPHEMUS" pendant l'hiver 2014 et de comprendre les différences entre l'été et l'hiver en termes de composition, propriétés des composés organiques pour comprendre leur origine et les processus de leur formation et leur évolution pendant la saison froide.

Les mesures conduites à ERSA pendant les étés 2012 et 2013 enregistrent d'importantes concentrations d'aérosols organiques, principalement d'origine biogénique. Pour cela, de nouveaux mécanismes chimiques ont été ajoutés au modèle dans le but de reproduire non pas seulement les concentrations des composés organiques mais aussi leurs propriétés. Ces processus mènent à la formation de nouveaux aérosols organiques secondaires (AOS) à partir de la condensation des produits d'oxydation des monoterpenes: le premier produit ajouté est le MBTCA (acide carboxylique) comme produit d'oxydation des monoterpenes de deuxième génération en régime bas-NO_x (Mller et al., 2012). Le deuxième produit ajouté provenant des monoterpenes est le nitrate organique (Pye et al., 2015). Le mécanisme de formation de ce dernier est une claire évidence de la réaction des composés organiques volatils (COVs) biogéniques avec les NO_x d'origine anthropique (Pye et al., 2015) ainsi que l'importance de la chimie nocturne des COVs (monoterpenes). Le troisième produit correspond à des AOS (monomers et dimers) provenant de la condensation des produits d'ozonolyse des monoterpenes appelés composés organiques volatils d'extrêmement faible volatilité (COVELs). Ces produits ont une très faible volatilité, ils sont hydrophobes, hautement oxidés et hautement oxygenés. Ces espèces sont formées grâce à un processus appelé "autoxidation". Un modèle 0D "bote" a été développé pour détérminer les coefficients stoechiométriques du mécanisme chimique décrivant ce processus d'autoxidation développé par Ehn et al. (2014) en régimes bas-NO_x et haut-NO_x. Une étude de sensibilité au rendement des COVELs a été aussi établie pour quantifier l'incertitude aux différents rendements experimentaux proposés par Ehn et al. (2014) et Jokinen et al. (2015). Le modèle reproduit bien les concentrations mesurées durant les deux campagnes de mesures des étés 2012 et 2013. Le modèle a réussi aussi à reproduire l'origine des composés organiques (presque 75% des composés organiques sont biogéniques et sont formés en grande partie à partir de l'oxydation des monoterpenes). Par ailleurs, l'influence de chacun des processus sur le degré d'oxydation representé par le ratio matière organique sur carbone organique (OM:OC) ainsi que le degré d'oxygénation representé par le ratio oxygène sur carbone (O:C) a été étudiée. En effet, ces ratios se sont clairement améliorés grâce aux nouvelles espèces ajoutées. Néanmoins, les ratios simulés concordent mieux avec les mesures quand on ajoute l'hypothèse de la formation d'organosulfates à partir de l'oxydation de l'isoprene. Quant à l'hydrophylicité des aérosols organiques, le modèle prédit que 46% du carbone organique est hydrophile durant la deuxième moitié de Juillet sous-estimant ainsi ce même pourcentage mesuré (64%). Les concentrations de cette fraction d'organiques dépendent de l'origine des masses d'air et de la composition des organiques. Les émissions des aérosols organiques marins ont été quantifiées grâce à de récentes paramétrisations empiriques reliant la fraction organique des sels de mer (émise principalement dans le mode d'Aitken) à l'activité biologique des phytoplanktons représentée par la chlorophylle-a. Leur contribution aux concentrations d'organiques s'avère faible et ne dépasse pas 2%.

Dans une deuxième partie, des comparaisons des concentrations des PM_{10}, PM_1, OM_1 et des composés inorganiques secondaires ont été effectuées pendant les étés 2012 et 2013 et en basse altitude pendant un vol d'avion de l'été 2014. Le modèle réussit à reproduire les concentrations mesurées à la station de mesure Ersa (Cap-Corse, France). Par ailleurs, des études de sensibilité à la météorologie, aux émissions anthropogéniques, aux émissions anthropogéniques de composés organiques semi-volatils et de volatilité intermédiaire (COVIS) et aux émissions des sels de mers ont été établies et révèlent que les concentrations des aérosols organiques et inorganiques secondaires sont sensibles à la météorologie qui joue un rôle important dans les quantités des COVs émis ainsi que le transport à méso-échelle. Le sulfate, en raison de son caractère non-volatile est moins sensible à la météorologie. Les émissions marines ont une influence considérable sur les aérosols. La paramétrisation de Monahan et al. (1986) communément utilisée induit une sur-estimation des concentrations des particules. Une paramétrisation qui a une dépendance moins forte à la vitesse de frottement du vent sur la surface de la mer est plus adaptée, comme par exemple celle de Jaeglé et al. (2011). Les émissions marines influencent aussi la partie hydrophile des aérosols organiques parce que cette dernière peut condenser sur des composés inorganiques d'origine marine. Un autre volet de cette évaluation a consisté en la comparaison des concentrations du sulfate, nitrate et ammonium à basses altitudes (en dessous de 800 m.a.g.l) au dessus de la Méditerrannée (sud de la France) à des mesures effectuées lors d'un vol d'avion (le 10 Juillet 2014). Le sulfate, originaire en majeure partie du traffic maritime, represente une importante fraction des aérosols au dessus de la Méditerranée. Cette comparaison révéle que le partitionnement gaz-particule n'est pas instantannée pour le nitrate et l'ammonium et que l'hypothèse de l'équilibre thermodynamique n'est pas vérifiée. En plus, l'échange de la matière est influencé par la composition des particules: les comparaisons des profils verticaux du chloride, nitrate et ammonium durant ce vol d'avion montrent que les sels de mer ne sont pas mélangés avec les particules transportées.

Une troisième partie présente l'évaluation des concentrations modélisées des AO d'une part, et de l'état d'oxydation/oxygénation modélisé des AO Ersa pendant l'hiver 2014 ainsi que l'évaluation des différentes paramétrisations communément utilisées pour modéliser les émissions et le vieillissement des composés organiques semi-volatils et de volatilité intermédiaire (COVIS). Pour cela, le modèle de chimie-transport de la plateforme de modélisation de la qualité de l'air Polyphemus est utilisé avec différentes paramétrisations décrivant les émissions et le vieillissement des COVIS (distribution de volatilité, schéma une étape d'oxydation vs schéma multigénérationnel dont des schémas basés sur l'approche Volatility Basis Set (VBS), émissions des composés organiques volatils non-traditionnels COVNTs). La majorité des AO prédits par le modèle est d'origine anthropogénique (15 à 18% des AO est d'origine biogénique). Le secteur du chauffage résidentiel correspondant au secteur 6 de l'inventaire d'émissions EDGAR_HTAP_V2 a une large contribution aux concentrations d'AO au dessus d'Ersa et au dessus du domaine MED (31 à 33%). La contribution des composés organiques volatils aromatiques (toluène et xylène) est très faible (3%). Les AO secondaires issus du partitionnement des produits d'oxydation des COVNTs modélisés grâce à la paramétrisation de Ciarelli et al. (2017b) représentent entre 18 et 21% des AO. Les deux simulations dont les concentrations prédites ne respectent pas le critère de but de Boylan and Russell (2006) sont la simulation dans laquelle la paramétrisation et la distribution de Couvidat et al. (2012) sont appliquées aux COVIS de toutes les sources anthropogéniques ainsi que la simulation dans laquelle les COVNTs sont émis avec un rapport COVIS/AOP de 4. Au dessus du domaine MED centré sur la Corse (France), la distribution de volatilité influe plus les concentrations de AO que le type du schéma d'oxydation. Par ailleurs, cette étude a montré en se basant sur les comparaisons des concentrations des AO, qu'un schéma à une étape d'oxydation avec un rapport COVIS/AOP de 4 ainsi qu'un schéma à plusieurs étapes d'oxydation est utilisé avec un rapport de 1.5 sont les configurations les mieux adaptées. Les indices d'oxydation et d'oxygénation (OM:OC et O:C respectivement) restent sous-estimés par toutes les simulations bien qu'ils soient améliorés en incluant les AO secondaires hautement oxygénés, produits des COVNTs. La formation de molecules hautement oxygénées via le mécanisme proposé par Molteni et al. (2018) ainsi que celui du nitrate organique pendant l'hiver sont des processus à prendre en compte afin d'améliorer la modélisation de l'état d'oxydation/oxygénation des AO.

5.2 Perspectives

Les travaux futurs devraient porter sur les axes suivants: ajouter la formation des organosulfates au modèle, représenter l'état du mélange des aérosols, décrire plus finement les émissions et le vieillissement des COVIS et prendre en compte la formation des molécules hautement oxygénées d'origine anthropogénique.

5.2.1 Formation des organosulfates

Les organosulfates (OS) peuvent être formés à partir de différents COVs biogéniques dont l'isoprène ou les terpènes. Les mécanismes de formation des OS dans l'atmosphère sont bien loin d'être élucidés. Notamment, il a été observé la formation d'esters de sulfate à partir des composés dérivés de l'oxydation de l'isoprène (epoxidol, IEPOX) qui peut réagir avec l'ion sulfate (Eddingsaas et al., A 2010; Darer et al., 2011; Couvidat et al., 2013b).

5.2.2 Représenter le mélange des aérosols

L'influence de l'état du mélange sur la formation des aérosols a été observée pour les espèces inorganiques lors du vol d'avion du 10 Juillet 2017. Une simulation avec le modèle SCRAM (Zhu et al., 2015) qui prend en compte l'état du mélange des particules s'impose afin de prendre en compte le rôle de la composition des espèces inorganiques sur la condensation/évaporation. Dans cette modélisation, une approche dynamique est utilisée pour le partitionnement entre les phases gaz et particule, au lieu de considérer que le partitionnement est instantané.

5.2.3 Incertitudes sur le vieillissement des COVIS

Les modèles de chimie transport ont ajouté récemment les COVIS ainsi que leur vieillissement (Ciarelli et al., 2016; Shrivastava et al., 2015; Tsimpidi et al., 2014). Les émissions des COVIS sont très incertaines, les COVIS originaires du chauffage résidentiel en particulier. Par exemple, Shrivastava et al. (2015) ont trouvé que le ratio des émissions des COVIS originaires du chauffage résidentiel sur les $PM_{2.5}$ varie de 0.9 à 9. Dzepina et al. (2009) ont montré que le ratio des émissions d'COVIS gazeux sur les COVIS particulaires varie de 2 à 24 et dépend largement selon la source d'émission. Par exemple, les émissions des COVs de volatilité intermédiaire (COVI) sont aussi très incertaines et varient de 1 à 3 fois les émissions des composés organiques semi-volatils (COSV) (Couvidat et al., 2012).

La distribution de volatilité qui dépend du secteur d'émission est aussi une source d'incertitude (May et al., 2013b,c,a). Il est nécessaire d'inclure les émissions des COVIS gazeux dans les inventaires d'émissions. En outre, plus d'études éxpérimentales sont nécessaires pour modéliser les AOS à partir des COVIS de différentes sources ainsi que la structure moléculaires des éspèces à modéliser pour étudier l'effet de la non-idéalité du mélange sur les aérosols organiques.

Une autre source d'incertitude est le dépôt des COVIS en phase gazeuse. En effet, la solubilité de ces derniers dans l'eau est mal connue. Pye and Seinfeld (2010) ont considéré que les COVIS primaires sont hydrophobes et les secondaires sont hydrophiles.

La chimie des COVIS est aussi une autre source d'incertitude en termes des schémas d'oxydation, de la distribution de volatilité et sa résolution ainsi qu'en termes de la quantité d'oxygène ajoutée qui peut varier de 1, 2 et 3 avec des probabilités de 20, 40 and 40% (Zhao et al., 2015). Cette incertitude induit par suite une incertitude sur les propriétés d'oxidation de ces composés qui sont majoritairement présents dans l'atmosphère pendant l'hiver.

5.2.4 Formations des molécules hautement oxygénées

Similairement au processus d'autoxidation des terpènes, Molteni et al. (2018) ont identifié lors d'expériences d'oxydation de COVs aromatiques cycliques (benzène, toluène, o-/m-/p-xylène, mésitylène) et polycycliques (naphtalène et biphényle) des molécules hautement oxygénées (MHO). Les MHO sont produites partir des COVs aromatiques avec un rendement entre 0.3 et 4% suite à une série de processus d'autoxidation. Ces espèces sont des monomers et des dimers qui peuvent avoir une très faible volatilité formant ainsi des (COVEL). Ces derniers sont potentiellement des contributeurs à la nucléation et à la croissance des particules au dessus des zones urbaines.

Chapitre 6

Appendix: Aerosol composition and the contribution of SOA formation over Mediterranean forests

Evelyn Freney, Karine Sellegri, Mounir Chrit, Kouji Adachi, Joel Brito, Antoine Waked, Agnès Borbon, Aurélie Colomb, Régis Dupuy, Jean-Marc Pichon, Laetitia Bouvier, Claire Delon, Corine Jambert, Pierre Durand, Thierry Bourianne, Cécile Gaimoz, Sylvain Triquet, Anaïs Féron, Matthias Beekmann, François Dulac, and Karine Sartelet

Atmos. Chem. Phys. Discuss., doi: 10.5194/acp-2017-482

Atmos. Chem. Phys., 18, 7041–7056, 2018
https://doi.org/10.5194/acp-18-7041-2018

Atmospheric Chemistry and Physics
Open Access

Aerosol composition and the contribution of SOA formation over Mediterranean forests

Evelyn Freney[1], **Karine Sellegri**[1], **Mounir Chrit**[2], **Kouji Adachi**[3], **Joel Brito**[1], **Antoine Waked**[1,a], **Agnès Borbon**[1], **Aurélie Colomb**[1], **Régis Dupuy**[1], **Jean-Marc Pichon**[1], **Laetitia Bouvier**[1], **Claire Delon**[4], **Corinne Jambert**[4], **Pierre Durand**[4], **Thierry Bourianne**[5], **Cécile Gaimoz**[6], **Sylvain Triquet**[6], **Anaïs Féron**[6], **Matthias Beekmann**[6], **François Dulac**[7], **and Karine Sartelet**[2]

[1]Laboratoire de Météorologie Physique, CNRS-Université Clermont Auvergne, UMR6016, 63117, Clermont Ferrand, France
[2]CEREA, Joint Laboratoire École des Ponts ParisTech – EDF R & D, Université Paris-Est, 77455 Marne-la-Vallée, France
[3]Meteorological research institute, Atmospheric Environment and Applied Meteorology Research Department, 1-1 Nagamine, Tsukuba, Ibaraki 305-0052, Japan
[4]Laboratoire d'Aérologie, CNRS-Université de Toulouse, CNRS, UPS, Toulouse, France
[5]Centre National de Recherches Météorologiques, Météo-France-CNRS, Toulouse, URA1357, France
[6]Laboratoire Interuniversitaire des Systèmes Atmosphériques, LISA/IPSL, UMR CNRS 7583, Université Paris Est Créteil (UPEC), France
[7]Laboratoire des Sciences du Climat et de l'Environnement, LSCE/IPSL, UMR 8212 CEA-CNRS-UVSQ, Université Paris-Saclay, Gif-sur-Yvette, France
[a]now at: IMT Lille Douai, Sciences de l'Atmosphère et Génie de l'Environnement (SAGE), 59508 Douai CEDEX, France

Correspondence: Evelyn Freney (evelyn.freney@uca.fr)

Received: 19 May 2017 – Discussion started: 18 July 2017
Revised: 27 March 2018 – Accepted: 4 April 2018 – Published: 23 May 2018

Abstract. As part of the Chemistry-Aerosol Mediterranean Experiment (ChArMEx), a series of aerosol and gas-phase measurements were deployed aboard the SAFIRE ATR42 research aircraft in summer 2014. The present study focuses on the four flights performed in late June early July over two forested regions in the south of France. We combine in situ observations and model simulations to aid in the understanding of secondary organic aerosol (SOA) formation over these forested areas in the Mediterranean and to highlight the role of different gas-phase precursors. The non-refractory particulate species measured by a compact aerosol time-of-flight mass spectrometer (cToF-AMS) were dominated by organics (60 to 72 %) followed by a combined contribution of 25 % by ammonia and sulfate aerosols. The contribution from nitrate and black carbon (BC) particles was less than 5 % of the total PM_1 mass concentration. Measurements of non-refractory species from off-line transmission electron microscopy (TEM) showed that particles have different mixing states and that large fractions (35 %) of the measured particles were organic aerosol containing C, O, and S but without inclusions of crystalline sulfate particles. The organic aerosol measured using the cToF-AMS contained only evidence of oxidized organic aerosol (OOA), without a contribution of fresh primary organic aerosol. Positive matrix factorization (PMF) on the combined organic–inorganic matrices separated the oxidized organic aerosol into a more-oxidized organic aerosol (MOOA), and a less-oxidized organic aerosol (LOOA). The MOOA component is associated with inorganic species and had higher contributions of m/z 44 than the LOOA factor. The LOOA factor is not associated with inorganic species and correlates well with biogenic volatile organic species measured with a proton-transfer-reaction mass spectrometer, such as isoprene and its oxidation products (methyl vinyl ketone, MVK; methacroleine, MACR; and isoprene hydroxyhydroperoxides, ISOPOOH). Despite a significantly high mixing ratio of isoprene (0.4 to 1.2 ppbV) and its oxidation products (0.2 and 0.8 ppbV), the contribution of specific signatures for isoprene epoxydiols SOA (IEPOX-SOA) within the aerosol organic mass spectrum (m/z 53 and m/z 82) were very weak, suggesting that the presence of

isoprene-derived SOA was either too low to be detected by the cToF-AMS, or that SOA was not formed through IEPOX. This was corroborated through simulations performed with the Polyphemus model showing that although 60 to 80 % of SOA originated from biogenic precursors, only about 15 to 32 % was related to isoprene (non-IEPOX) SOA; the remainder was 10 % sesquiterpene SOA and 35 to 40 % monoterpene SOA. The model results show that despite the zone of sampling being far from industrial or urban sources, a total contribution of 20 to 34 % of the SOA was attributed to purely anthropogenic precursors (aromatics and intermediate or semi-volatile compounds).

The measurements obtained during this study allow us to evaluate how biogenic emissions contribute to increasing SOA concentrations over Mediterranean forested areas. Directly comparing these measurements with the Polyphemus model provides insight into the SOA formation pathways that are prevailing in these forested areas as well as processes that need to be implemented in future simulations.

1 Introduction

The contribution of anthropogenic aerosol particles is thought to be of the order of $10\,\mathrm{Tg\,C\,yr^{-1}}$; however, that of natural biogenic aerosols has been estimated to be as much as $90\,\mathrm{Tg\,C\,yr^{-1}}$, having an important effect on climate in both populated and remote areas of the world (IPCC, 2007; Hallquist et al., 2009). Our knowledge of how primary emissions from anthropogenic and natural sources contribute to the formation of secondary aerosols and their evolution in the atmosphere continues to improve with considerable advances in numerical simulations. However, discrepancies between simulations and measurements still exist and are more apparent over remote and forested environments than over anthropogenic environments (Ganzeveld et al., 2008; Lelieveld et al., 2008). The most commonly emitted biogenic volatile organic compounds (BVOCs) include isoprene and monoterpenes, with isoprene emissions accounting for approximately 44 % (Kesselmeier and Staudt, 1999; Arneth et al., 2008). These species can be difficult to characterize because of their high temporal and spatial variability. Studies have shown that the formation yields of secondary organic aerosol (SOA) from biogenic emissions alone are relatively low compared to those from anthropogenic sources, but when emissions from both biogenic and anthropogenic sources are combined, the resulting yield for SOA formation is much higher than either anthropogenic or biogenic emissions alone (Day et al., 2009; Bryan et al., 2012; Shilling et al., 2013; Hu et al., 2015).

The increasing improvement of instrumentation (namely aerosol mass spectrometry) available for the detection of different biogenic species has led to an increase in the characterization of biogenic SOA in rural (Schwartz et al., 2010; Slowik et al., 2010; Setyan et al., 2014), boreal (Kulmala et al., 2000; Allan et al., 2006), Amazonian (Martin et al., 2010), and some other tropical and subtropical forests (Capes et al., 2009; Robinson et al., 2011). Using aerosol mass spectrometry, a number of studies have identified specific signatures for isoprene-derived SOA (Allan et al., 2014; Budisulistiorini et al., 2015). Hu et al. (2015) showed, through comparison with model simulations, that the global distribution of a particular SOA formation route from isoprene to epoxydiols is largely focused in the Southern Hemisphere and over Siberian forests far from anthropogenic emissions. The occurrence of these species in the Northern Hemisphere has been documented in several studies (Budisulistiorini et al., 2015), but in general the contribution is less than that reported in the South Hemisphere.

The Mediterranean region is thought to be extremely sensitive to climate change and is influenced by air masses from the Atlantic, continental Europe, and northern Africa, as well as increasing emissions from biomass burning, intense shipping, and from the increasing population density in Mediterranean coastal cities (e.g. Sciare et al., 2003; Barnaba and Gobbi, 2004; Lyamani et al., 2006; Alados-Arboledas et al., 2011; Mallet et al., 2013). Several studies have shown that during the summer months the aerosol radiative effect within the Mediterranean is one of the most significant in the world (Markowitz et al., 2002; Papadimas et al., 2012). Sartelet et al. (2012) modelled aerosol loading in Europe and North America and retrieved high concentrations of ozone and SOA over the Mediterranean Sea. It was estimated that biogenic emissions contributed to the formation of up to 72–88 % of the SOA over Europe. In order to better characterize the sources of SOA and its precursors over the Mediterranean, the SAFMED (Secondary Aerosol Formation in the Mediterranean) experiment took place in the Mediterranean as part of the Chemistry-Aerosol Mediterranean Experiment (ChArMEx; http://charmex.lsce.ipsl.fr/, last access: 22 January 2017) during Summer 2014. In this work, we present observations from four research flights over the forested Mediterranean region. The objectives of these flights were to combine both aerosol and gas-phase measurements to investigate the origin of SOA over these forested areas.

2 Methodology

2.1 ATR42

All airborne measurements were performed aboard the ATR42 research aircraft, run by SAFIRE (French aircraft service for environmental research; http://www.safire.fr, last access: 12 July 2016). The ATR (Avion de Transport Régional) is a turbo propeller aircraft approximately 23 m long and 25 m wide, with a payload of about 4.6 t (www.atraircraft.com, last access: 22 October 2017). The aircraft was based in Avignon, France. Aircraft flight plans were decided depending on forecasts from meteorological and air quality models made available on a dedicated operational web server called the ChArMEx Operation Centre (ChOC; http://choc.sedoo.fr, last access: 22 April 2018). A series of different standard meteorological parameters were measured aboard the ATR42 including temperature, pressure, relative humidity, turbulence, wind speed, direction, and downward and upward radiances.

2.2 Online aerosol chemical and physical properties

In order to sample aerosol particle species, a forward facing aerosol inlet was fitted in place of a side window. This inlet is designed with an outer sleeve for channelling air and an inner tube with a large diameter and low curvature to limit particle losses due to deposition. This inlet is both isokinetic and isoaxial and has a 50 % sampling efficiency for aerosol particles with diameters of 4.5 µm (Crumeyrolle et al., 2013). From the aerosol inlet, the sampled aerosols are directed through a manifold to a number of different instruments. Aerosol particle number concentrations were measured using a condensation particle counter (CPC, cut-off diameter 5 nm) and scanning mobility particle sizer (SMPS) with 162 size channels for particle diameters ranging from 17 nm up to 400 nm, with a time resolution of 84 s. Measurements of aerosol chemical properties were performed using a compact aerosol time-of-flight mass spectrometer (cToF-AMS) (Drewnick et al., 2005). This instrument was operating with a time resolution of 40 s in order to ensure that the maximum amount of spatial information (aircraft covers approximately 5 km in 40 s) could be obtained while maintaining a high enough signal-to-noise ratio. Prior to being sampled into the cToF-AMS, aerosol particles passed through a pressure-controlled inlet. This inlet maintained a constant pressure of about 400 hPa throughout the duration of the flight (Bahreini et al., 2008). However, all reported concentrations are in standard temperature and pressure (used here 22 °C, 950 hPa). In order to provide quantitative information on aerosol mass concentrations, a collection efficiency (CE) must be applied to the aerosol mass concentrations. This is based on the principle that the cToF-AMS aerodynamic inlet is designed to sample dry spherical particles and that particles with non-spherical shapes will not be as efficiently sampled. In addition to this, sampled aerosol particles can sometimes be lost in the instrument as a result of particle bounce on the heating filament. This CE correction is chemical dependant (Middlebrook et al., 2012); however since the contribution of nitrate and sulfate remained lower than 25 % at all times, the CE remained at 50 % throughout the sampling period. The total mass measured by the cToF-AMS (added to that from the black carbon (BC) measurements) was compared to the total aerosol concentration measured by the SMPS set-up (Fig. S1 in the Supplement). BC concentrations were obtained using a single-particle soot photometer (SP2, Droplet Measurement Technologies). Full details of this instrument are available in Baumgardner et al. (2007).

2.3 Gas-phase measurements

Gas-phase species were sampled on-board through a rear-facing 1/4 inch Teflon tube. Ozone and CO were measured using ultraviolet and infrared analysers (Thermo Fisher environmental instruments) (Nedelec et al., 2003). The NO and NO_x measurements were performed using an ozone chemiluminescence instrument (Environment SA AC42S instrument). The quantification of NO_2 is obtained by converting NO_2 to NO using a molybdenum converter at 320 °C. As some NO_y is also converted into NO in the molybdenum oven, the NO_2 and NO_x concentrations can be overestimated. In this work, these measurements will be referred to as NO_w, and represent $NO + NO_2 +$ an unquantified NO_y. For measurements of volatile organic compounds (VOCs), a unit mass resolution proton-transfer-reaction mass spectrometer (PTR-MS) from Ionicon Analytik (Innsbruck, Austria) was used, with a time resolution of 19 s. Full details of the PTR-MS configuration on-board and operating conditions are provided in Borbon et al. (2013). During the so-called biogenic flights, 16 protonated masses were monitored. Compounds of interest are

- VOCs of biogenic origin (BVOCs) and their first generation oxidation products including m/z 69 (isoprene), m/z 71 (sum of methyl vinyl ketone, MVK; methacroleine, MACR; and isoprene hydroxyhydroperoxides, ISOPOOH), m/z 137 (sum of monoterpenes);
- anthropogenic volatile organic compounds including m/z 79 (benzene), m/z 93 (toluene), m/z 107 (C8 aromatics), and m/z 121 (C9 aromatics);
- oxygenated VOCs including m/z 33 (methanol), m/z 45 (acetaldehyde), and m/z 59 (acetone).

Detection limits, defined as 3σ of background mixing ratios ranged from 0.05 to 2.70 ppbV over a 1 s dwell time. Instrumental background signal was determined through periodic air sampling (triplicates) of ambient air scrubbed through a custom-built catalyst converter (platinum-coated steel wool) heated to 250 °C. Three complete calibrations over a 0.1–20 ppb range were performed before, during, and after the campaign. The standard gas used was provided by Ionimed (Innsbruck, Austria) and contained several VOCs including isoprene, α-pinene, benzene, toluene, and o-xylene at 1 ppmV certified at ±5 %. A second parts-per-billion-level gaseous standard from NPL (UK) was used to cross-check the quality of the calibration and to perform regular one-point calibration control for isoprene and C6–C9 aromatics (4 ± 0.8 ppbV). A relative difference of less than 10 % was measured. The calibration factor for all major VOCs (the slope of the mixing ratio with respect to product ion signal normalized to H_3O^+) ranged from 2.35 (m/z 137) to 18.9 (m/z 59) counts s^{-1}.

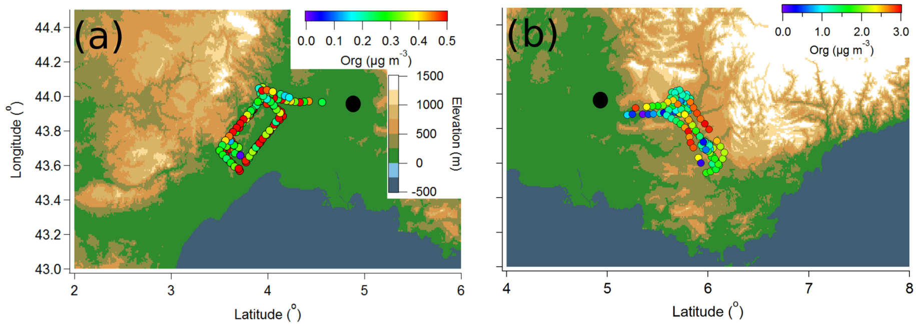

Figure 1. Typical flight track travelling **(a)** west (RF15 and RF21) and **(b)** east (RF20 and RF23) of Avignon (black circle). Points of the flight track are coloured by organic aerosol concentrations.

2.4 Statistical analysis

Detailed analysis of the organic aerosol mass spectra measured using the cToF-AMS was performed using positive matrix factorization (PMF) (Paatero and Tapper, 1994). The PMF2 software package was used in conjunction with the PMF evaluation tool (version 2.04; Ulbrich et al., 2009). Recommended procedures of down-weighting for certain m/z values were followed (Ulbrich et al., 2009) as well as removal of several m/z values due to low (m/z 19 and 20) or high signal (m/z 29). In this particular case, m/z values from inorganic ions (SO_4, NO_3) were equally combined with the organic matrices to better separate different factors. Error values for all m/z values were calculated in the same way using the SQUIRREL software (version 1.53). The number of factors was determined using correlations with external factors (temporal series of VOC measurements). The reported correlations used later on in the discussion were calculated using simple linear regression.

2.5 Electron microscopy analysis

Aerosol particles were collected on transmission electron microscope (TEM) grids using a sampler consisting of two impactor stages. The 50 % cut-off of each of these stages was calculated to be 1.6 and 0.2 µm, with a flow rate of approximately 1.0 L min^{-1}. The samples were collected only when the aircraft was travelling at a constant altitude, usually lasting between 15 and 20 min. The TEM grids on the submicron stage of the impactor were then analysed using a 120 kV TEM (JEM-1400, JEOL) to provide detailed information on individual aerosol compositions and shapes. The advantage of having TEM analysis is the ability to detect both refractory and non-refractory aerosol particles. Composition of each sample collected was analysed using energy-dispersive X-ray spectrometer (EDS) with scanning-TEM mode (Adachi et al., 2014). There were at least 230 particles analysed from each grid. Particles were classified into five aerosol categories based on their compositions: organic aerosol (C dominant), sulfate (S dominant), sulfate + organic (C and S dominant), sea salt (Na dominant), and other (e.g. mineral dust (Si is dominant, but also included traces of Ca and K)). Morphological differences between aerosol particles also allowed us to determine the extent of internal and external mixing. Organic aerosol generally had an amorphous morphology with no evidence of a crystal structure. EDS analysis of the homogeneously mixed amorphous particles showed that these particles contained C, O, and S without any evidence of crystalline structure. Sulfate particles (likely $(NH_4)_2SO_4$) had a crystalline structure and were sensitive to the electron beam (evaporation). Internal mixtures of organic and sulfate were mostly crystalline $(NH_4)_2SO_4$ surrounded by an amorphous carbon material.

2.6 Back trajectory analysis

In order to determine the history of air masses prior to being sampled by the aircraft, air mass trajectories were calculated for a 24 h period using the Lagrangian model HYSPLIT (http://ready.arl.noaa.gov/HYSPLIT.php, last access: 1 February 2018). These air mass trajectories were calculated for intervals of 5 min along the flight track and provide information on the dominant air mass sources during the flight. Back trajectories of 24 h provided enough information to determine whether air masses were slow moving and local or fast moving and arriving over larger distances (Fig. S2). For all flights, the air mass trajectory path was constant along the flight track at low altitudes, showing that air masses of the same origin were measured during each flight. 72 h back trajectories were also computed (although not shown) in order to determine possible aerosol sources over longer timescales.

2.7 Overview of flights

Four research flights (RF) dedicated to biogenic emissions were carried out: 30 June (RF15), 3 July (RF20), 5 July (RF21), and 7 July 2014 (RF23). Each flight was approximately 3.5 h in duration, and the aircraft flew over forested areas with elevations varying from 250 to 500 m above ground level (a.g.l.) during straight and level runs. The flight plan consisted of the aircraft leaving the city of Avi-

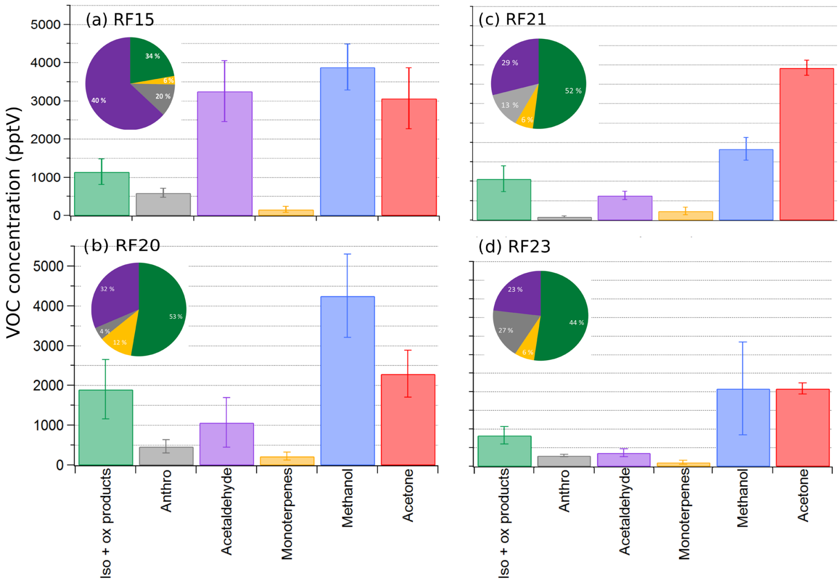

Figure 2. Contribution of the different measured gas-phase species aboard the ATR42: **(a)** RF15, **(b)** RF20, **(c)** RF21, **(d)** RF23. The pie charts illustrated in each figure represent the contribution of all VOC species except those of methanol and acetone.

gnon (southern France) and travelling east or west for about 50 km before starting a vertical sounding. Vertical soundings were performed from around 100 up to 3300 m above sea level (a.s.l.). Using the vertical profiles of VOC concentrations and relative humidity, the atmospheric boundary layer height was determined for each flight, and varied from 1300 m a.s.l. (RF20) up to 1900 m a.s.l. (RF15) (Fig. S3). Two of the flights (RF15, RF21) flew west over the Puéchabon Mediterranean national forest region (northwest of Montpellier, Fig. 1a), where the principle type of vegetation is evergreen oaks (*Quercus ilex*) and Alpine pines (*halepensis*). The evergreen oak is known to emit several different types of monoterpene species but mainly α-pinene (Loreto et al., 1996). The other two flights (RF20, RF23) flew east over the Oak Observatory field site at Observatoire de Haute-Provence (O3HP, https://o3hp.obs-hp.fr, last access: 14 July 2016, Fig. 1b). This area is dominated by downy oak trees (*Quercus pubescens*) but also contains Montpellier maple (*Acer monspessulanum*) and smokey bushes (*Cotinus coggygria*) in a lower canopy stage. Since *Quercus pubescens* is the dominant type of vegetation, it makes this region a strong isoprene-emitting region and an ideal area to study isoprene chemistry and its relation to aerosol particles (Zannoni et al., 2015).

For the flight RF20, temperatures were stable, varying from 18 to 19 °C in the boundary layer, and wind speeds were always less than $5 \pm 1\ \mathrm{m\,s^{-1}}$, originating from a southeasterly direction. HYSPLIT air mass back trajectories show that for a 24 h period prior to the measurements, air masses were slow moving and remained within a 200 km radius of the sampling site (Fig. S2b). This, together with the clear skies and relatively high temperatures, made ideal conditions to study local biogenic emissions. RF23 had similar temperatures to those recorded on RF20 (17 to 20 °C), but with some cloud cover. Wind speeds ranged between 2 and $4\ \mathrm{m\,s^{-1}}$; air masses arrived from a southerly direction passing over the coast line prior to being sampled along the flight track (Fig. S2d). For the two westerly flights, average temperatures were slightly higher, with average values of 23 ± 1 °C. Wind speeds were low ($3 \pm 1\ \mathrm{m\,s^{-1}}$). Air masses travelled much greater distances over the western (RF15) and northwestern (RF21) parts of France prior to being sampled (Fig. S2a, c).

3 Results

3.1 Gas-phase properties

The principal VOC species measured with the PTR-MS during all flights were acetone (m/z 59) and methanol (m/z 33), followed by isoprene (m/z 69) and its oxidation products (MVK + MACR + ISOPOOH) (m/z 71) and then VOC species representative of monoterpene emissions (m/z 137) (Fig. 2). Isoprene and its oxidation products showed a high temporal variation during flights, suggesting a more local influence of these VOC species. Monoterpene VOC, with a short atmospheric lifetime were measured in low concentration with little temporal evolution. Anthropogenic VOC species (m/z 93 (toluene), m/z 79 (benzene), and C8 and C9 aromatics) never contributed more than 5 % to the total VOCs measured (Table 1, Fig. 2). Despite this, we cannot ignore the presence of the anthropogenic VOC species measured during all flights. During westerly flights (RF15 and RF21), air masses arrived from the north (Fig. S2), possibly transporting accumulated anthropogenic emissions from over main-

Table 1. Mean concentrations of the different gas-phase species measured during low and constant altitude of each flight. The error represents $\pm 1\sigma$ on all the measurements.

Flight	Date (2014)	Isoprene (pptV)	MVK+ MACR + ISOPOOH (pptV)	Monoterpenes (pptV)	Toluene (pptV)	Benzene (pptV)	C8 + C9 aromatics (pptV)	O_3 (ppbV)	CO (ppbV)	NO_w (ppbV)	NO (ppbV)
RF15	30 Jun	583 ± 290	214 ± 91	117 ± 82	146 ± 59	93 ± 61	200 ± 85	40 ± 8.8	118 ± 27	4.2 ± 0.8	0.17 ± 0.3
RF20	3 Jul	1240 ± 527	756 ± 287	205 ± 107	149 ± 82	102 ± 42	196 ± 79	53 ± 4.0	136 ± 46	7.9 ± 2.3	0.31 ± 0.2
RF21	5 Jul	600 ± 262	365 ± 182	179 ± 128	147 ± 176	108 ± 53	135 ± 39	31 ± 8.0	79 ± 11	5.86 ± 0.7	0.29 ± 0.3
RF23	7 Jul	392 ± 197	230 ± 159	119 ± 87	74 ± 34	88 ± 18	125 ± 36	52 ± 3.0	88 ± 9	5.6 ± 2.1	0.29 ± 0.9

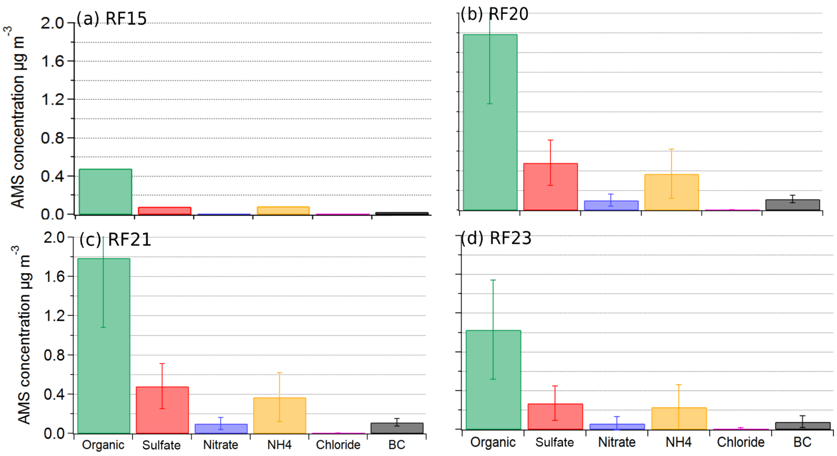

Figure 3. Contribution of the non-refractory aerosol chemical species aboard the ATR42: **(a)** RF15 3006 **(b)** RF20 0307, **(c)** RF21 0507, **(d)** RF23 0707.

land France. Easterly flights (RF20 and RF23), being principally influenced by local or southerly air masses, are likely impacted by anthropogenic activities over the Marseille and Fos sur Mer (Fos-Berre) industrial area.

3.2 Aerosol chemical properties

In the following section we will report average values for different chemical species measured during low and constant altitude parts of the flights (below the boundary layer height determined from the vertical profiles shown in Fig. S3). For all flights, the aerosol composition measured by the cToF-AMS instrument shows that the organic compounds contributed a significant fraction to the total aerosol concentration (with average values of 72 (±36) % for RF20 and 71 (±30) % for RF23) (Table 2, Fig. 3). The second most dominant species measured were sulfate and ammonium aerosol particles, with a combined contribution of up to 25 ± 10 %. The contribution from nitrate species was on average 3 (±1.5) %. BC measured using the SP2 never exceeded 5 % of the total PM_1 mass (Fig. 3). O : C values were 1.05 (±0.05) for the total organic aerosol, with high $f_{44} > 0.2$ and corresponding low $f_{43} < 0.6$. These mass spectral signatures suggested that the majority of the organic aerosol was secondary, with little influence from fresh primary organic aerosol.

As described in Sect. 2.5, the chemical composition of aerosol particles collected on TEM grids was determined using EDS. At least 230 particles were analysed during each flight providing information of particle size and composition. The absolute number of particles analysed using offline electron microscopy is small in comparison to what is measured by online particle counters; however this technique provides us with a qualitative snapshot into particle mixing state, morphology, and composition. Only filters from the submicron stages are discussed here and showed that at least 35 (±5) % of all aerosol particles measured were made up of homogeneously mixed amorphous (no evidence of a crystal structure) particles. EDS analysis showed that these amorphous particles were composed of homogeneously distributed C, O, and S (Fig. 4a.i, ii, iii). The molecular structure of these compounds is unknown. Externally mixed crystalline sulfate particles contributed 15 % (±5 %), and 10 % were internally mixed amorphous C and crystalline sulfate (likely ammonium sulfate) species (Figs. 4b, S4). The remaining fractions contained signals for sea salt (Na Cl) and dust (Si, Ca) particles.

3.3 Aerosol physical properties

Aerosol number concentrations and size distributions were measured using a CPC and SMPS (respectively) during the

Table 2. Concentrations ($\mu g\, m^{-3}$) of the different chemical species measured aboard each flight during low-altitude legs. Error values are standard deviations calculated on the mean values of the measurements.

Flight	Date (2014)	NR-PM1 $\mu g\, m^{-3}$	Org $\mu g\, m^{-3}$	SO_4 $\mu g\, m^{-3}$	NO_3 $\mu g\, m^{-3}$	BC $\mu g\, m^{-3}$
RF15	30 Jun	0.70 ± 0.08	0.48 ± 0.23	0.08 ± 0.07	0.013 ± 0.01	0.03 ± 0.02
RF20	3 Jul	2.70 ± 1.10	1.79 ± 0.70	0.48 ± 0.2	0.10 ± 0.06	0.11 ± 0.03
RF21	5 Jul	0.99 ± 0.50	0.72 ± 0.40	0.20 ± 0.09	0.03 ± 0.02	0.11 ± 0.04
RF23	7 Jul	1.64 ± 0.70	0.96 ± 0.60	0.30 ± 0.18	0.06 ± 0.07	0.08 ± 0.06

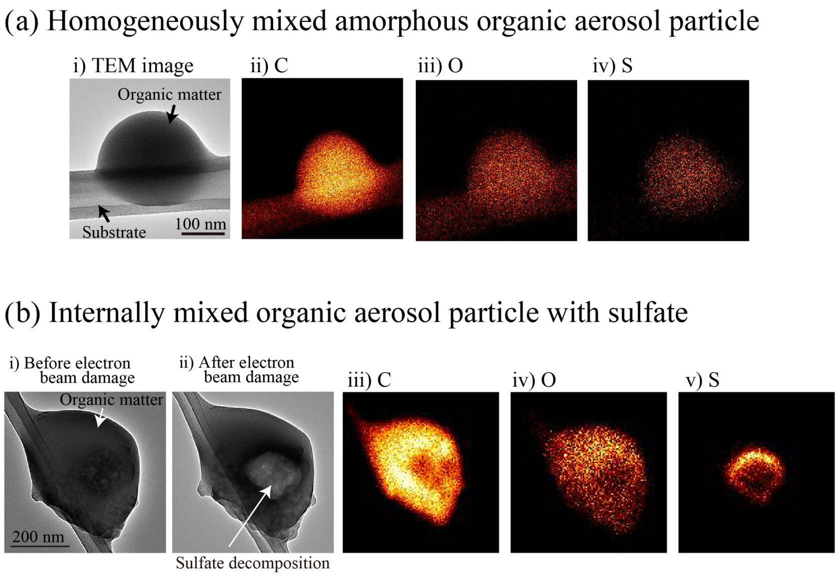

Figure 4. Panel **(a)** shows **(i)** an example of an amorphous particle deposited on a carbon substrate. EDS mapping analysis showing signals for **(ii)** carbon, **(iii)** oxygen, and **(iv)** sulfur. **(b)** Internally mixed amorphous particles with signals **(i)** before and **(ii)** after electron beam damage. EDS analysis showing signals for **(iii)** carbon, **(iv)** oxygen, and **(v)** sulfur.

four biogenic flights (Fig. 5). During the westerly flight RF15, when air masses were travelling from the north-west of France, particle concentrations were on average $1500 \pm 300\, cm^{-3}$ and the principle size mode was less than 90 nm at altitudes of around 500 m. At higher altitudes aerosol number concentration decreased to $600 \pm 200\, cm^{-3}$ with modal diameters of around 30 ± 20 nm (Fig. 5a). The measured particle concentrations during the other westerly flight, RF21, were on average $1895 \pm 1707\, cm^{-3}$. The fraction of fine particles, < 40 nm in diameter (F40), measured during these flights was high, explaining the lower aerosol mass measured using the cToF-AMS instrument (Table 2). During the two easterly flights, average aerosol number concentrations were considerably higher at $3332 \pm 1920\, cm^{-3}$ than the westerly flights (Fig. 5b and d). The size distribution of the aerosol had a single mode at around 100 nm. However, during periods with increased aerosol concentrations, the size distribution spectra showed an additional mode between 20 and 40 nm (nucleation-mode particles). Calculating the difference in aerosol particle concentrations measured by the CPC (cut-off 5 nm) from that measured by the SMPS, we were able to determine the contribution of nucleation-mode particles.

The increases in fine-mode particles measured at lower altitudes (~ 500 m a.g.l.) during all flights are likely linked to new particle formation. Observations of new particle formation from biogenic emissions have been reported over Boreal forests (Sihto et al., 2006), European coniferous forests (Held et al., 2004), and African savannah forests (Laakso et al., 2013), as well as during laboratory studies (Kiendler-Scharr et al., 2009). Monoterpene oxidation products were shown to produce new particles more efficiently by nucleation than the isoprene oxidation products (Spracklen et al., 2008; Bonn et al., 2014). Some of these studies have also shown that high concentrations of isoprene relative to monoterpenes can inhibit new particle formation (Kiendler-Scharr et al., 2009; Kanawade et al., 2011), although the underlying processes are not yet clear. Calculating the ratio of isopreneC / monoterpeneC (carbon associated with isoprene / monoterpene) and comparing it to the number con-

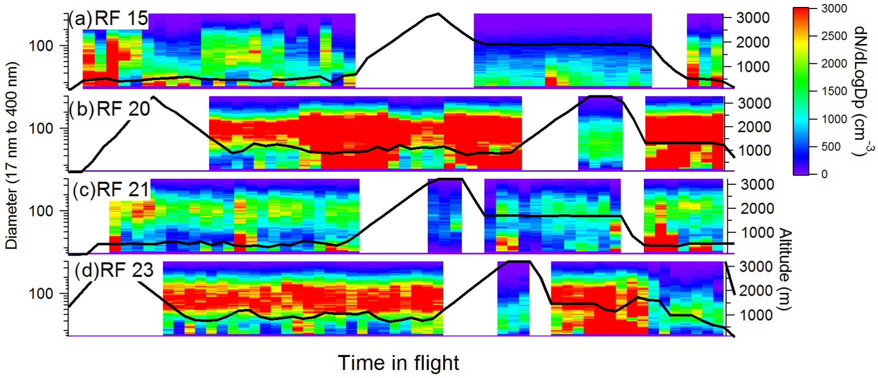

Figure 5. Aerosol size distribution measured with the SMPS for **(a)** RF15 **(b)** RF20, **(c)** RF21, and **(d)** RF23 from 17 up to 400 nm. The colour scale indicates aerosol concentration $dN/d\log D_p$. Altitude is illustrated as the black line and is represented on the right-hand axis.

centration of nucleation-mode particles (Fig. 6), this relationship between biogenic VOC species and nucleation-mode particles was investigated. As a result of the low time resolution of the SMPS, we were limited to a small number of points per flight. Data were combined for all flights, giving average ratios of isopreneC / monoterpeneC varying between 0.05 and 8 (average 3 ± 1), with the lowest values corresponding to the highest fractions of fine-particle concentrations. Although the variation among points is high, the general trend of these observations is in agreement with previous field studies over mixed deciduous forests (Kanawade et al., 2011) and with laboratory studies in controlled environments showing that high concentrations of monoterpenes relative to isoprene can favour new particle formation (Kiendler-Scharr et al., 2009). The average ratios of isopreneC / monoterpeneC measured during these Mediterranean flights were higher than those reported in Finnish forests (ratios of 0.18) and lower than the ones measured in Michigan (ratios of 26.4) and Amazonian forests (ratios of 15.2) (Kanawade et al., 2011). In general, high ratios are associated with a very low or a suppressed number of new particle formation events.

3.4 Secondary organic aerosol

From cToF-AMS measurements, average mass concentrations measured during the two easterly flights were approximately $2.0 \pm 0.5\,\mu g\,m^{-3}$, whereas those measured by the westerly flights were considerably less at approximately $1\,\mu g\,m^{-3}$, making more detailed analysis of aerosol chemical properties difficult. For this reason the remaining analysis is focused on the two easterly flights.

For both easterly flights, increases in organic aerosol concentrations were observed in the valley area between the two high-elevation zones (between 43.6 and 43.8° N) during horizontal transects of the flight. For RF20, these increases were accompanied by significant increases in the fine particulate matter between 20 and 40 nm, and also those at 90 nm. In addition, increases in the ratio of isoprene oxidation products to isoprene were observed in the same region, implying a more oxidized air mass. A time series plot of total organic aerosol (OA) with MACR + MVK + ISOPOOH shows a good relationship (Fig. S5a), and plotting the OA concentration against the ratio of MACR + MVK + ISOPOOH / isoprene provides us with a means to observe the evolution of the organic aerosol with the relative age of the air mass with respect to biogenic emissions (Fig. S5b). The ratios of MACR + MVK + ISOPOOH / isoprene measured during this flight are comparable to those measured over this forested area (0.4 to 0.8) during ground-based measurements (Zannoni et al., 2016). We observe a reasonable correlation ($r = 0.46$) and positive slope ($b = 1.1$) with increasing OA as the relative air mass age increases, suggesting that SOA formation is likely to have originated from biogenic precursors. Similar plots were prepared using anthropogenic precursor gases toluene and benzene (Fig. S6), showing a negative correlation with increasing organic mass concentration of $r = 0.35$ and a slope of -0.56. However, as the toluene and benzene concentrations are both close to the detection limit, care needs to be taken when interpreting these ratios. Generally, although anthropogenic precursor species are present, the VOC concentrations and trends measured suggest that the increases in OA concentrations are primarily related to biogenic emissions.

In order to extract additional information on the OA measured during the flights, we performed PMF analysis. Since the temporal evolution of both the organic and inorganic concentrations was similar, we chose to combine the mass spectral signatures for SO_4 and NO_3 into the PMF matrix alongside those of the organic species. Mass spectral signatures of NH_4 were not included since higher "noise" was associated with these m/z values. Adding the inorganic signals into the PMF matrix allows us to separate different aerosol sources and not only those related to organic compounds. For both flights a two-factor solution (f-peak 0) was chosen to best describe the sources of the aerosol particles and those two factors have maximum correlations with external

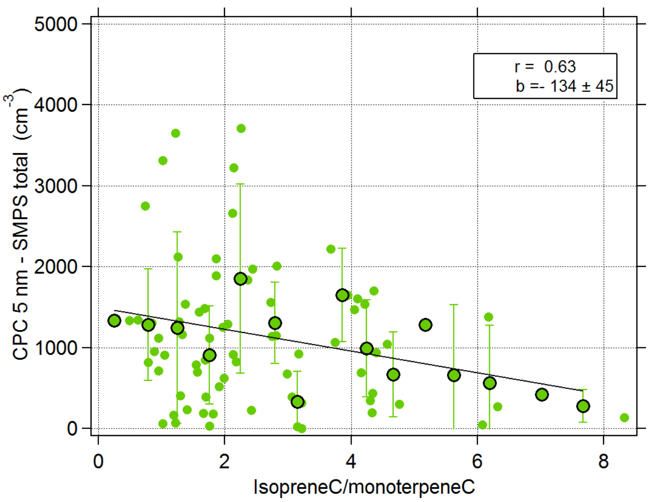

Figure 6. Ratios of isoprenec / monoterpeneC plotted as a function of the nucleation-mode particles (difference between the CPC (cut-off 5 nm) and the SMPS (cut-off 17 nm)). Values for the four biogenic flights, as well as average values calculated over a number of isoprenec / monoterpeneC ratios are included (size bins of 0.5). Error bars represent $\pm 1\sigma$ of the average CPC5nm – SMPS values. The black line represents the linear correlation fit.

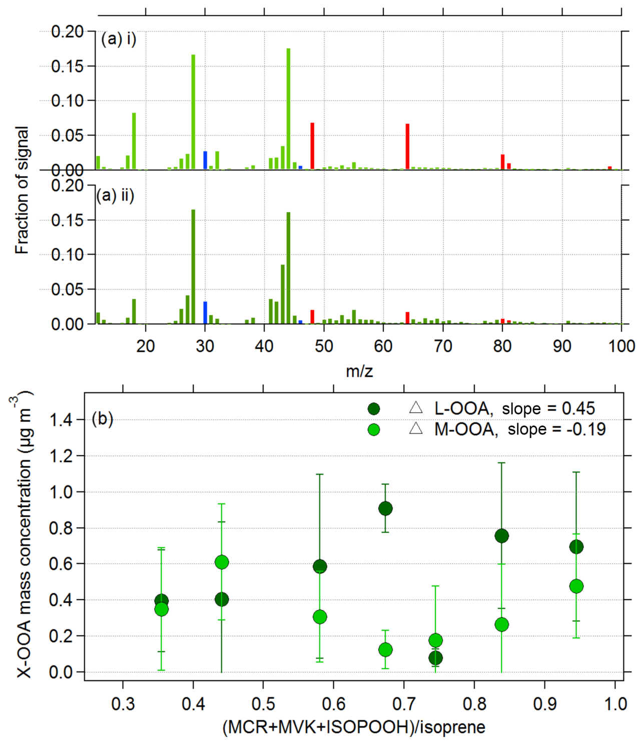

Figure 7. (a) A two-factor solution determined from PMF analysis of the biogenic research flights. **(i)** The more-oxidized organic aerosol (MOOA) associated with inorganic peaks for sulfate (red) and nitrate (blue); **(ii)** the less-oxidized organic aerosol (LOOA) with a lower contribution of inorganic peaks. **(b)** Variations of these two species with aging air mass (using MACR + MVK + ISOPOOH as a proxy for photochemical age of air mass). The delta values (Δ) are calculated based on background concentrations measured outside of the study region.

species (Table 3). Additional details of the PMF analysis are included in Figs. S7 to S9 as well as Table S1 in the Supplement. The two resolved factors include (i) a more-oxidized organic aerosol (MOOA, contributing 55 % to the resolved factors), containing high contributions from m/z 44 and associated with inorganic peaks (m/z 30, 46 (NO_3), and 48, 64, and 80 (SO_4)), and (ii) a less-oxidized organic aerosol species (LOOA, contributing 45 %) with little contribution from inorganic m/z (Fig. 7a). These two factors MOOA and LOOA are very similar to the OOA-1 and OOA-2 species identified from ground-based measurements during a biogenic event over a forested area in Canada (Slowik et al., 2010). Slowik et al. (2010) showed similar trends with the two identified oxidized organic aerosols, where one was associated with inorganic aerosols and the other was not correlated with inorganic aerosols, while the other was well correlated with biogenic VOC species.

During the flights, as the valley area is approached, we observe the sampled air masses becoming gradually more oxidized with respect to biogenic emissions, providing us with a well-defined sample area to evaluate the contribution of biogenic SOA on background and/or regional air masses. In order to isolate the formation of OA resulting from the oxidation of VOC species, the change in the OA concentrations above the background was calculated (ΔOrg). The background values were determined based on measurements during transects of the flight between the valley area and the airport. During this time, aerosol concentrations were low with little temporal variation. Particle size measurements display a single mode at 100 nm with average particle concentrations of 3000 cm^{-3}. Measurements of VOC species during this background period result in average concentrations of isoprene of 1544 ± 696 pptV and lower concentrations of longer-lived species MACR + MVK + ISOPOOH of 661 ± 239 pptV (Table S2).

For the resolved PMF factors, LOOA and MOOA, background values were determined to be 0.27 and 0.41 µg m^{-3}, respectively, (Table S2). Organic factors corrected for background concentrations are referred to as Δ-LOOA and Δ-MOOA. Plotting these two factors against the ratio of MACR + MVK + ISOPOOH / isoprene (relative air mass age) (Figs. 7 and S10), we observe a significant increase in the Δ-LOOA species with air mass age until a maximum is reached at ratios of 0.65. Given that MOOA does not change with the relative air mass age in the measured area, and that it is associated with SO_4 and NO_3 species, it is reasonable to suggest that the MOOA is associated with long-range-transported aerosol. A slower increase in concentrations of LOOA at higher ratios suggests that as the relative photochemical age of the air mass increases, LOOA becomes more oxidized and is converted to MOOA, as has recently been

Table 3. Pearson r (Pr) correlations for different time series during RF20 and RF23.

	MOOA		LOOA	
	RF20 Pr ($n=91$)	RF23 Pr ($n=144$)	RF20 Pr ($n=91$)	RF23 Pr ($n=169$)
PTR-MS m/z 69 (isoprene)	0.11	0.41	0.51	0.67
PTR-MS m/z 71 (MVK + MACR + ISOPOOH)	0	0.28	0.64	0.71
PTR-MS m/z 137	0.59	0.58	0.29	0.49
PTR-MS m/z 93	0.15	0.25	0.27	0.38
PTR-MS m/z 79	0.04	0.21	0	0.15
BC	0.52	0.48	0.61	0.48
CO	0.37	0.48	0.34	0.60
NO_w	0.56	0.44	0.51	0.60

illustrated in chamber experiments by Palm et al. (2018). Plotting these two factors as a function of air mass age using anthropogenic VOC species (ratio of toluene / benzene), we observe a relatively flat and decreasing trend (Fig. S10a). These observations would suggest the contribution of toluene and benzene, although not insignificant, plays a lesser role in the formation of the SOA measured during these flights.

Given the good correlation between the LOOA and isoprene and its oxidation products, we investigated the possibility of identifying isoprene-derived SOA. Several recent publications have identified signature peaks in aerosol mass spectrometry for isoprene-derived SOA using the m/z 53 and m/z 82 (ionization products of IEPOX) (Allan et al., 2014; Budisulistiorini et al., 2015; Zhang et al., 2017). In this study, the contribution of these peaks in both types of spectra was very low (fraction of signal < 0.004), although somewhat more pronounced for LOOA. These contributions are similar to background contributions of f_{82} (fraction of m/z 82 to the total organic signal) observed globally by Hu et al. (2015) and Lee et al. (2016), ranging from 0.0002 to 0.0035, and would lead us to believe that we have no significant contributions of f_{82} in our aerosol mass spectra. Factors influencing the formation of isoprene SOA include aerosol acidity and the presence of NO_x and sulfate (Nguyen et al., 2014), with the highest yields of isoprene SOA being measured under low-NO_x conditions (< 30 pptV) and in the presence of acidic aerosols (Gaston et al., 2014). Aerosol concentrations measured with the cToF-AMS appear to be fully neutralized with little evidence of acidity (Fig. S11), and the NO_w concentrations measured during these flights varied from 6 up to 10 ppbV; however the average concentrations of NO were 0.30 ± 0.2 ppbV, suggesting that the real contribution of NO_x (see Sect. 2.3) is also likely to be low, but still higher than parts-per-trillion-level concentrations measured in truly remote forested areas. There have been some reports of isoprene-derived SOA formation (hereafter isoprene SOA) in high-NO regions but the contribution of this pathway is considered to be much smaller (Jacobs et al., 2014).

Other sources of biogenic SOA can originate from the oxidation of monoterpene and sequesterpene VOC species, or additionally from isoprene SOA, that do not follow the IEPOX route. In both cases, the contribution of m/z 91 in the cToF-AMS mass spectra, often identified as being the $C_7H_7^+$ fragment (Lee et al., 2016; Riva et al., 2016), would be enhanced. This m/z 91 was present in all OA mass spectra and was higher for the LOOA ($f_{91} = 0.007$). However, in previous studies these f_{91} values are considered background (Hu et al., 2015; Lee et al., 2016), hence making it difficult to associate the measured SOA with these formation routes. It should be noted that m/z 91 can also be associated with fragments of primary anthropogenic OA, and the contribution of anthropogenic aerosols from the industrial zone (Fos-sur-Mer) south of the flight area cannot be ruled out.

In general, the yield of formation of SOA from the isoprene VOC precursor is relatively low compared to other biogenic species such as monoterpenes, and also compared with aromatic precursors (Ait-Helal et al., 2014). Since the measured aerosol particles are neutralized (Fig. S11) and the measured NO concentrations are still reasonably high (0.30 ppbV), we assume that isoprene-derived SOAs, following the IEPOX formation route, do not contribute significant amounts to the OA measured during these flights. Given the increase in OA with the relative biogenic air mass age, we could suspect that additional sources of SOA could originate from other isoprene SOA formation routes and/or terpene precursors. This is also coherent with the increase in the number concentrations of fine particles at the lower isopreneC / monoterpeneC ratios discussed in Sect. 3.3.

3.5 Model evaluation of secondary organic aerosol formation

In order to evaluate the relative contribution of the different gaseous precursors to SOA formation over these forested regions, two simulations were performed using the Polyphemus model. Full details of the model set-up are available in Chrit et al. (2017). The domain of the air quality simulation has a horizontal resolution of $0.125° \times 0.125°$, while

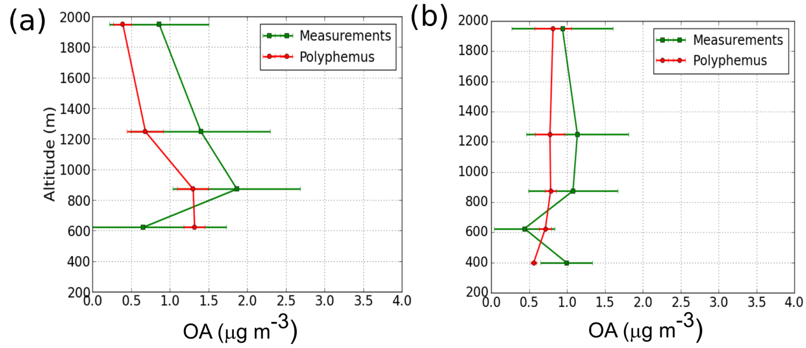

Figure 8. Measured (green) and modelled (red) organic concentration during the **(a)** RF20 and **(b)** RF23 flights. The concentrations are averaged on the vertical layers of the model and variations around the average are indicated by the horizontal error bars.

the vertical is modelled with 14 layers with interface heights at 0, 30, 60, 100, 150, 200, 300, 500, 750, 1000, 1500, 2400, 3500, 6000, and 12 000 m a.s.l. (Fig. S12). Biogenic emissions are computed using MEGAN (Guenther et al., 2006), and anthropogenic emissions are computed using HTAP-v2 (http://edgar.jrc.ec.europa.eu/htap_v2/, last access: 11 December 2017). Initial and boundary conditions are obtained from a larger-scale simulation (over Europe), as detailed in Chrit et al. (2018). For gaseous chemistry, a carbon-bound approach model is used (CB05; Yarwood et al., 2005). Aerosol dynamics is modelled with a sectional approach (SIREAM; Debry et al., 2007), and for SOA modelling, a surrogate approach is used (Couvidat et al., 2012). The modelling of SOA formation is based on smog chamber experiments, which provide information on SOA yield as a function of organic mass concentration for each precursor using an Odum approach (Odum et al., 1996). Stoichiometric coefficients of SOA surrogates and their saturation vapour pressures are selected to fit data from smog chambers. Candidates for SOA surrogates are estimated from the literature (Couvidat et al., 2012). Biogenic precursors are isoprene, monoterpenes (with α-pinene and limonene as surrogates), and sesquiterpenes, with low-NO_x and high-NO_x oxidation regimes. Isoprene may form two surrogates, amongst which are methyl methyl dihydroxy dihydroperoxide under low NO_x, and methyl glyceric acids under high NO_x. Monoterpenes may form pinonaldehyde, norpinic acid, pinic acid, 3-methyl-1, 2, 3-butanetricarboxylic acid under low-NO_x conditions, and organic nitrate, as well as extremely low-volatility organic carbons (ELVOCs) or highly oxidized multifunctional organic compounds (HOMs) by ozonolysis. Anthropogenic precursors are toluene, xylene, and intermediate or semi-volatile organic compounds (I/SVOCs). Gas-phase emissions of I/SVOCs are estimated by multiplying emissions of primary organic aerosols by a factor 1.5 (Zhu et al., 2016). Partitioning between the gas and aerosol phases is carried out with a secondary organic aerosol processor model (Couvidat and Sartelet, 2015) for organics and inorganic aerosol model ISORROPIA for inorganics (Nenes et al., 1998). Maps of the simulated submicron organic matter (OA_1) are shown in Fig. S12a and b for the two easterly flights RF20 and RF23, respectively.

Figure 8 compares the vertical profiles of measured and modelled OA_1 during the RF20 and the RF23 flights. The concentrations averaged over the vertical layers of the model and the standard deviations around the mean concentrations are shown. The measured concentrations have higher standard deviations than the modelled concentrations due to the coarse horizontal model resolution ($0.125° \times 0.125°$). For both flights there are some differences between the model and the measurements. However, this discrepancy may be due to difficulties in representing the vertical distribution of pollutants above the canopy. Although the mean vertical concentrations of OA_1 tend to be underestimated over 1000 m, they are on average well modelled under 1000 m within the boundary layer for both flights.

Although isoprene emissions are 2.5 times higher than those of monoterpenes and 11.6 times higher than those of sesquiterpenes over that region during the period of simulation, isoprene-derived SOA represents about 15 to 35 % of the simulated OA, which is lower than the monoterpene-derived SOA that represents 35 to 40 %. Sesquiterpene-derived SOA represents about 10 %. Amongst those monoterpene-derived SOAs, 4 to 7 % are monoterpene products (first-generation semi-volatile organic compounds: pinic acid, norpinic acid, and pinonaldehyde), 9 to 14 % are ELVOCs or HOMs, and 17 to 23 % are organic nitrate. In total, biogenic-derived OA represents about 66 to 80 % of OA. The rest is made up by aromatic-derived OA (2 to 3 %) and anthropogenic intermediate and semi-volatile organic compounds (17 to 31 %) (Fig. 9). The contribution of organic nitrate modelled is not reflected in the measurements where less than 5 % of the total measured mass was nitrate aerosol. This difference may be due to hydrolysis not being accounted for in the model. Under ambient conditions hydrolysis could eliminate the organic nitrate functionality, allowing nitric acid to evaporate from the particles (Rindelaub et al., 2016).

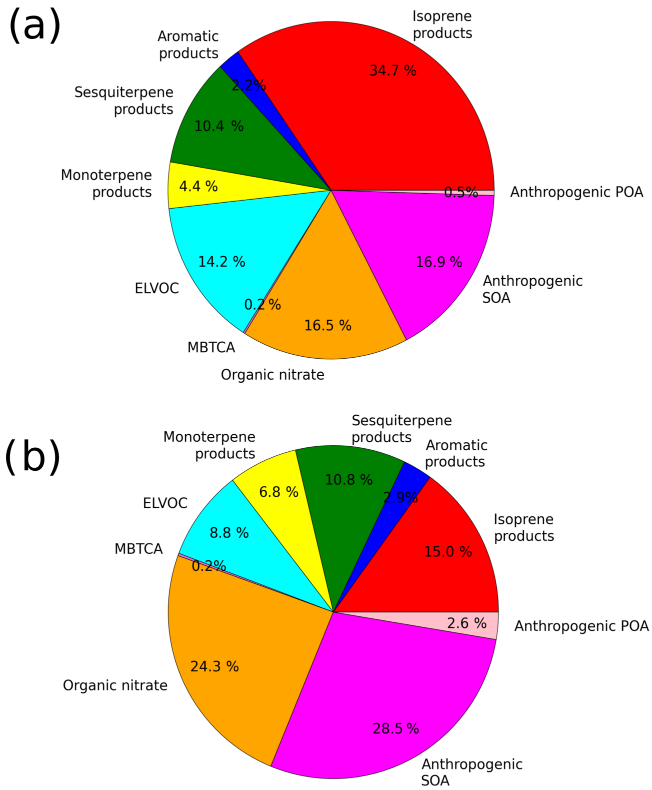

Figure 9. Modelled averaged composition of OA_1 along the flight path during the **(a)** RF20 and **(b)** RF23 flights. This averaged composition is obtained by averaging concentrations along the flight path at altitudes below 1000 m.

The measured organic matter is highly oxidized during both flights with an average measured O : C ratio of 1.05 below 1000 m during the RF20 flight and 1.1 during the RF23 flight. This ratio is very well represented by the model with average values of 1.07 (RF20) and 1.17 (RF23). In the model, these high O : C ratios arise because of organic compounds from isoprene oxidation, which all have an O : C ratio greater than 0.8, as well as some ELVOC compounds (monomers) from monoterpene oxidation. We can conclude from these observations that the low-volatility products (ELVOCs) from monoterpene oxidation as well as isoprene oxidation products may therefore correspond to the measured LOOA concentrations. Although the SOA contribution of anthropogenic VOC precursors is low (Couvidat et al., 2013; Sartelet et al., 2018), the results of the model show a high contribution of anthropogenic compounds (up to 30 %). These anthropogenic compounds could correspond to the regionally transported SOA, potentially identified as MOOA.

4 Conclusion

This paper characterizes aerosol and gas-phase physical and chemical properties over two different forested areas in southern France. During four dedicated flights, aerosol particles and gas-phase composition were measured using a cToF-AMS and a PTR-MS, respectively, with the principle objective of characterizing biogenic emissions. Aerosol particle physical properties were measured using a number of different techniques characterizing particle size and number concentrations. Using a combination of aerosol size distributions coupled with VOC concentrations we observe that although new particle formation seems to occur over all types of vegetation (mainly isoprene-emitting species or mainly monoterpene-emitting species), that low isopreneC / monoterpeneC ratio can favour the formation of fine aerosol particles. These VOC species likely condense on pre-existing particles that can then be chemically analysed.

During eastern flights, in valley areas, high concentrations of organic aerosol and biogenic VOC species were measured (isoprene and its oxidation products MACR + MVK + ISOPOOH). PMF analysis of the organic mass spectra separated two organic factors, namely a more-oxidized organic aerosol (MOOA) and a less-oxidized organic aerosol (LOOA). The MOOA species were strongly associated with SO_4 species whereas the LOOA species were not related to inorganic species but correlated with temporal evolutions of biogenic oxidation products (MACR + MVK + ISOPOOH). Correlation with other precursor biogenic or aromatic VOC species was very weak.

A lack of direct evidence of IEPOX SOA (m/z 82 $C_5H_6O^+$) in the cToF-AMS measurements leads us to conclude that the formation of SOA, following an IEPOX formation route from isoprene precursor species was not dominant during this measurement period. The Polyphemus model determines a contribution of isoprene SOA, formed through alternative pathways, of the order of 15 to 35 %. Therefore, although not possible to accurately identify the formation pathway of the measured SOA, we can, based on its correlation with the oxidation products of isoprene, propose that it is at least partly associated with biogenic isoprene VOC species. The model also illustrates that although the emission of monoterpene and sesquiterpene species is low compared to that of isoprene, the yield of SOA formation from these precursor species is important. This is in agreement with recent observations by Zhang et al. (2018), who showed that SOA is principally formed from monoterpene emissions in the southern USA.

The model results estimate an overall contribution of 66 % biogenic species and approximately 30 % anthropogenic influence to the formation of SOA. The model can successfully replicate the measured OA during the flights, as well as the OA oxidation properties. However, the detailed molecular information obtained in the model (isoprene SOA, monoterpene SOA, organic nitrate) was not easily comparable to measurements. The model resolved organic nitrate contributions up to 17 to 23 %. This high contribution of organic nitrate is not reflected in the cToF-AMS measurements where nitrate contributed less than 5 % to the measured PM_1 mass. This difference is possibly due to nitrate hydrolysis that is not considered in the mode.

This study takes advantage of measurements sampling regional air masses that were gradually enriched with biogenic compounds, allowing us to evaluate the contribution of biogenic SOA in ambient environments. These measurements are compared directly with model simulations, highlighting that there are several atmospheric processes that cannot be neglected by atmospheric models (e.g contribution of ELVOC), as well as emphasizing important processes that need to be implemented into future model simulations (e.g. hydrolysis of organic nitrates).

Data availability. All data used in this work as well as all other data related to the ChArMEx program are available at http://mistrals.sedoo.fr/ChArMEx/, or can be requested directly from the corresponding author (e.freney@uca.fr).

The Supplement related to this article is available online at https://doi.org/10.5194/acp-18-7041-2018-supplement.

Competing interests. The authors declare that they have no conflict of interest.

Special issue statement. This article is part of the special issue "CHemistry and AeRosols Mediterranean EXperiments (ChArMEx) (ACP/AMT inter-journal SI)". It is not associated with a conference.

Acknowledgements. This study received financial support from MISTRALS by ADEME, CEA, INSU, and the project Meteo-France. This research was also funded by the SAFMED (Secondary Aerosol Formation in the Mediterranean) ANR, (grant number ANR-12-BS06-0013-2502). The authors would like to extend a special thanks to the pilots and flight crew from SAFIRE for all their enthusiasm and support during the measurement campaign aboard the ATR42 aircraft. In addition, the authors are very grateful to Eric Hamonou for his logistical help in organizing the campaign, and to Laurence Fleury, Hélène Ferré, and the OMP/SEDOO team, who provided excellent support for aircraft operations through the ChOC web interface set-up and management.

Edited by: Xavier Querol
Reviewed by: Nicolas Marchand and two anonymous referees

References

Adachi, K., Zaizen, Y., Kajino, M., and Igarashi, Y.: Mixing state of regionally transported soot particles and the coating effect on their size and shape at a mountain site in Japan, J. Geophys. Res.-Atmos., 119, 5386–5396, https://doi.org/10.1002/2013JD020880, 2014.

Ait-Helal, W., Borbon, A., Sauvage, S., de Gouw, J. A., Colomb, A., Gros, V., Freutel, F., Crippa, M., Afif, C., Baltensperger, U., Beekmann, M., Doussin, J.-F., Durand-Jolibois, R., Fronval, I., Grand, N., Leonardis, T., Lopez, M., Michoud, V., Miet, K., Perrier, S., Prévôt, A. S. H., Schneider, J., Siour, G., Zapf, P., and Locoge, N.: Volatile and intermediate volatility organic compounds in suburban Paris: variability, origin and importance for SOA formation, Atmos. Chem. Phys., 14, 10439–10464, https://doi.org/10.5194/acp-14-10439-2014, 2014.

Alados-Arboledas, L., Müller, D., Guerrero-Rascado, J. L., Navas-Guzmán, F., Pérez-Ramírez, D., and Olmo, F. J.: Optical and microphysical properties of fresh biomass burning aerosol retrieved by Raman lidar, and star-and sun-photometry, Geophys. Res. Lett., 38, L01807, https://doi.org/10.1029/2010GL045999, 2011.

Allan, J. D., Alfarra, M. R., Bower, K. N., Coe, H., Jayne, J. T., Worsnop, D. R., Aalto, P. P., Kulmala, M., Hyötyläinen, T., Cavalli, F., and Laaksonen, A.: Size and composition measurements of background aerosol and new particle growth in a Finnish forest during QUEST 2 using an Aerodyne Aerosol Mass Spectrometer, Atmos. Chem. Phys., 6, 315–327, https://doi.org/10.5194/acp-6-315-2006, 2006.

Allan, J. D., Morgan, W. T., Darbyshire, E., Flynn, M. J., Williams, P. I., Oram, D. E., Artaxo, P., Brito, J., Lee, J. D., and Coe, H.: Airborne observations of IEPOX-derived isoprene SOA in the Amazon during SAMBBA, Atmos. Chem. Phys., 14, 11393–11407, https://doi.org/10.5194/acp-14-11393-2014, 2014.

Arneth, A., Monson, R. K., Schurgers, G., Niinemets, Ü., and Palmer, P. I.: Why are estimates of global terrestrial isoprene emissions so similar (and why is this not so for monoterpenes)?, Atmos. Chem. Phys., 8, 4605–4620, https://doi.org/10.5194/acp-8-4605-2008, 2008.

Bahreini, R., Dunlea, E. J., Matthew, B. M., Simons, C., Docherty, K. S., DeCarlo, P. F., Jimenez, J. L., Brock, C. A., and Middlebrook, A. M.: Design and operation of a pressure-controlled inlet for airborne sampling with an aerodynamic aerosol lens, Aerosol Sci. Tech., 42, 465–471, https://doi.org/10.1080/02786820802178514, 2008.

Barnaba, F. and Gobbi, G. P.: Aerosol seasonal variability over the Mediterranean region and relative impact of maritime, continental and Saharan dust particles over the basin from MODIS data in the year 2001, Atmos. Chem. Phys., 4, 2367–2391, https://doi.org/10.5194/acp-4-2367-2004, 2004.

Baumgardner, D., Kok, G. L., and Raga, G. B.: On the diurnal variability of particle properties related to light absorbing carbon in Mexico City, Atmos. Chem. Phys., 7, 2517–2526, https://doi.org/10.5194/acp-7-2517-2007, 2007.

Bonn, B., Bourtsoukidis, E., Sun, T. S., Bingemer, H., Rondo, L., Javed, U., Li, J., Axinte, R., Li, X., Brauers, T., Sonderfeld, H., Koppmann, R., Sogachev, A., Jacobi, S., and Spracklen, D. V.: The link between atmospheric radicals and newly formed particles at a spruce forest site in Germany, Atmos. Chem.

Phys., 14, 10823–10843, https://doi.org/10.5194/acp-14-10823-2014, 2014.

Borbon, A., Gilman, J. B., Kuster, W. C., Grand, N., Chevaillier, S., Colomb, A., Dolgorouky, C., Gros, V., Lopez, M., Sarda-Esteve, R., Holloway, J., Stutz, J., Perrussel, O., Petetin, H., McKeen, S., Beekmann, M., Warneke, C., Parrishand, D. D., and de Gouw, J. A.: Emission ratios of anthropogenic VOC in northern mid latitude megacities: observations vs. emission inventories in Los Angeles and Paris, J. Geophys. Res., 118, 2041–2057, 2013.

Bryan, A. M., Bertman, S. B., Carroll, M. A., Dusanter, S., Edwards, G. D., Forkel, R., Griffith, S., Guenther, A. B., Hansen, R. F., Helmig, D., Jobson, B. T., Keutsch, F. N., Lefer, B. L., Pressley, S. N., Shepson, P. B., Stevens, P. S., and Steiner, A. L.: In-canopy gas-phase chemistry during CABINEX 2009: sensitivity of a 1-D canopy model to vertical mixing and isoprene chemistry, Atmos. Chem. Phys., 12, 8829–8849, https://doi.org/10.5194/acp-12-8829-2012, 2012.

Budisulistiorini, S. H., Li, X., Bairai, S. T., Renfro, J., Liu, Y., Liu, Y. J., McKinney, K. A., Martin, S. T., McNeill, V. F., Pye, H. O. T., Nenes, A., Neff, M. E., Stone, E. A., Mueller, S., Knote, C., Shaw, S. L., Zhang, Z., Gold, A., and Surratt, J. D.: Examining the effects of anthropogenic emissions on isoprene-derived secondary organic aerosol formation during the 2013 Southern Oxidant and Aerosol Study (SOAS) at the Look Rock, Tennessee ground site, Atmos. Chem. Phys., 15, 8871–8888, https://doi.org/10.5194/acp-15-8871-2015, 2015.

Capes, G., Murphy, J. G., Reeves, C. E., McQuaid, J. B., Hamilton, J. F., Hopkins, J. R., Crosier, J., Williams, P. I., and Coe, H.: Secondary organic aerosol from biogenic VOCs over West Africa during AMMA, Atmos. Chem. Phys., 9, 3841–3850, https://doi.org/10.5194/acp-9-3841-2009, 2009.

Chrit, M., Sartelet, K., Sciare, J., Pey, J., Marchand, N., Couvidat, F., Sellegri, K., and Beekmann, M.: Modelling organic aerosol concentrations and properties during ChArMEx summer campaigns of 2012 and 2013 in the western Mediterranean region, Atmos. Chem. Phys., 17, 12509–12531, https://doi.org/10.5194/acp-17-12509-2017, 2017.

Chrit, M., Sartelet, K., Sciare, J., Pey, J., Nicolas, J. B., Marchand, N., Freney, E., Sellegri, K., Beekmann, M., and Dulac, F.: Aerosol sources in the western Mediterranean during summertime: A model-based approach, Atmos. Chem. Phys. Discuss., https://doi.org/10.5194/acp-2017-915, in review, 2018.

Couvidat, F. and Sartelet, K.: The Secondary Organic Aerosol Processor (SOAP v1.0) model: a unified model with different ranges of complexity based on the molecular surrogate approach, Geosci. Model Dev., 8, 1111–1138, https://doi.org/10.5194/gmd-8-1111-2015, 2015.

Couvidat, F., Debry, E., Sartelet, K. N., and Seigneur, C.: A hydrophilic/hydrophobic organic (H^2O) aerosol model: Development, evaluation and sensitivity analysis, J. Geophys. Res., 117, D10304, https://doi.org/10.1029/2011JD017214, 2012.

Couvidat, F., Kim, Y., Sartelet, K., Seigneur, C., Marchand, N., and Sciare, J.: Modeling secondary organic aerosol in an urban area: application to Paris, France, Atmos. Chem. Phys., 13, 983–996, https://doi.org/10.5194/acp-13-983-2013, 2013.

Crumeyrolle, S., Schwarzenboeck, A., Roger, J. C., Sellegri, K., Burkhart, J. F., Stohl, A., Gomes, L., Quennehen, B., Roberts, G., Weigel, R., Villani, P., Pichon, J. M., Bourrianne, T., and Laj, P.: Overview of aerosol properties associated with air masses sampled by the ATR-42 during the EUCAARI campaign (2008), Atmos. Chem. Phys., 13, 4877–4893, https://doi.org/10.5194/acp-13-4877-2013, 2013.

Day, D. A., Takahama, S., Gilardoni, S., and Russell, L. M.: Organic composition of single and submicron particles in different regions of western North America and the eastern Pacific during INTEX-B 2006, Atmos. Chem. Phys., 9, 5433–5446, https://doi.org/10.5194/acp-9-5433-2009, 2009.

Debry, E., Fahey, K., Sartelet, K., Sportisse, B., and Tombette, M.: Technical Note: A new SIze REsolved Aerosol Model (SIREAM), Atmos. Chem. Phys., 7, 1537–1547, https://doi.org/10.5194/acp-7-1537-2007, 2007.

Drewnick, F., Hings, S. S., DeCarlo, P. F., Jayne, J. T., Gonin, M., Fuhrer, K., Weimer, S., Jimenez, J. L., Demerjian, K. L., Borrmann, S., Worsnop, D. R.: A new Time-of-Flight Aerosol Mass Spectrometer (ToF-AMS): Instrument Description and First Field Deployment, Aerosol Sci. Tech., 39, 637–658, 2005.

Ganzeveld, L., Eerdekens, G., Feig, G., Fischer, H., Harder, H., Königstedt, R., Kubistin, D., Martinez, M., Meixner, F. X., Scheeren, H. A., Sinha, V., Taraborrelli, D., Williams, J., Vilà-Guerau de Arellano, J., and Lelieveld, J.: Surface and boundary layer exchanges of volatile organic compounds, nitrogen oxides and ozone during the GABRIEL campaign, Atmos. Chem. Phys., 8, 6223–6243, https://doi.org/10.5194/acp-8-6223-2008, 2008.

Gaston, C. J., Riedel, T. P., Zhang, Z., Gold, A., Surratt, J. D., and Thornton, J. A.: Reactive uptake of an isoprene-derived epoxydiol to submicron aerosol particles, Environ. Sci. Technol., 48, 11178–11186, https://doi.org/10.1021/es5034266, 2014.

Guenther, A., Karl, T., Harley, P., Wiedinmyer, C., Palmer, P. I., and Geron, C.: Estimates of global terrestrial isoprene emissions using MEGAN (Model of Emissions of Gases and Aerosols from Nature), Atmos. Chem. Phys., 6, 3181–3210, https://doi.org/10.5194/acp-6-3181-2006, 2006.

Hallquist, M., Wenger, J. C., Baltensperger, U., Rudich, Y., Simpson, D., Claeys, M., Dommen, J., Donahue, N. M., George, C., Goldstein, A. H., Hamilton, J. F., Herrmann, H., Hoffmann, T., Iinuma, Y., Jang, M., Jenkin, M. E., Jimenez, J. L., Kiendler-Scharr, A., Maenhaut, W., McFiggans, G., Mentel, Th. F., Monod, A., Prévôt, A. S. H., Seinfeld, J. H., Surratt, J. D., Szmigielski, R., and Wildt, J.: The formation, properties and impact of secondary organic aerosol: current and emerging issues, Atmos. Chem. Phys., 9, 5155–5236, https://doi.org/10.5194/acp-9-5155-2009, 2009.

Held, A., Nowak, A., Birmili, W., Wiedensohler, A., Forkel, R., and Klemm, O.: Observations of particle formation and growth in a mountainous forest region in central Europe, J. Geophys. Res.-Atmos., 109, D23204, https://doi.org/10.1029/2004JD005346, 2004.

Hu, W. W., Campuzano-Jost, P., Palm, B. B., Day, D. A., Ortega, A. M., Hayes, P. L., Krechmer, J. E., Chen, Q., Kuwata, M., Liu, Y. J., de Sá, S. S., McKinney, K., Martin, S. T., Hu, M., Budisulistiorini, S. H., Riva, M., Surratt, J. D., St. Clair, J. M., Isaacman-Van Wertz, G., Yee, L. D., Goldstein, A. H., Carbone, S., Brito, J., Artaxo, P., de Gouw, J. A., Koss, A., Wisthaler, A., Mikoviny, T., Karl, T., Kaser, L., Jud, W., Hansel, A., Docherty, K. S., Alexander, M. L., Robinson, N. H., Coe, H., Allan, J. D., Canagaratna, M. R., Paulot, F., and Jimenez, J. L.: Characterization of a real-time tracer for isoprene epoxydiols-derived secondary organic aerosol (IEPOX-SOA) from aerosol mass spectrometer measurements, Atmos. Chem. Phys., 15, 11807–11833, https://doi.org/10.5194/acp-15-11807-2015, 2015.

IPCC: Climate Change 2007: The Physical Science Basis, Intergovernmental Panel for Climate Change Working Group I Rep., edited by: Solomon, S., Qin, D., Manning, M., Chen, Z., Marquis, M., Averyt, K. B., Tignor, M., and Miller, H. L., Cambridge University Press, 2007.

Jacobs, M. I., Burke, W. J., and Elrod, M. J.: Kinetics of the reactions of isoprene-derived hydroxynitrates: gas phase epoxide formation and solution phase hydrolysis, Atmos. Chem. Phys., 14, 8933–8946, https://doi.org/10.5194/acp-14-8933-2014, 2014.

Kanawade, V. P., Jobson, B. T., Guenther, A. B., Erupe, M. E., Pressley, S. N., Tripathi, S. N., and Lee, S.-H.: Isoprene suppression of new particle formation in a mixed deciduous forest, Atmos. Chem. Phys., 11, 6013–6027, https://doi.org/10.5194/acp-11-6013-2011, 2011.

Kesselmeier, J. and Staudt, M.: Biogenic volatile organic compounds (VOC): An overview on emission, physiology and ecology, J. Atmos. Chem., 33, 23–88, https://doi.org/10.1023/A:1006127516791, 1999.

Kiendler-Scharr, A., Wildt, J., Dal Maso, M., Hohaus, T., Kleist, E., Mentel, T. F., Tillmann, R., Uerlings, R., Schurr, U., and Wahner, A.: New particle formation in forests inhibited by isoprene emissions, Nature, 461, 381–384, https://doi.org/10.1038/nature08292, 2009.

Kulmala, M., Hämeri, K., Mäkelä, J. M., Aalto, P. P., Pirjola, L., Väkevä, M., Nilsson, E. D., Koponen, I. K., Buzorius, G., Keronen, P., Rannik, Ü, Laakso, L., Vesala, T., Bigg, K., Seidl, W., Forkel, R., Hoffmann, T., Spanke, J., Janson, R., Shimmo, M., Hansson, H.-C., O'Dowd, C., Becker, E., Paatero, J., Teinilä, K., Hillamo, R., Viisanen, Y., Laaksonen, A., Swietlicki, E., Salm, J., Hari, P., Altimir, N., and Weber, R.: Biogenic aerosol formation in the boreal forest, Boreal Environ. Res., 5, 281–297, 2000.

Laakso, L., Merikanto, J., Vakkari, V., Laakso, H., Kulmala, M., Molefe, M., Kgabi, N., Mabaso, D., Carslaw, K. S., Spracklen, D. V., Lee, L. A., Reddington, C. L., and Kerminen, V.-M.: Boundary layer nucleation as a source of new CCN in savannah environment, Atmos. Chem. Phys., 13, 1957–1972, https://doi.org/10.5194/acp-13-1957-2013, 2013.

Lee, A. K. Y., Abbatt, J. P. D., Leaitch, W. R., Li, S.-M., Sjostedt, S. J., Wentzell, J. J. B., Liggio, J., and Macdonald, A. M.: Substantial secondary organic aerosol formation in a coniferous forest: observations of both day- and nighttime chemistry, Atmos. Chem. Phys., 16, 6721–6733, https://doi.org/10.5194/acp-16-6721-2016, 2016.

Lelieveld, J., Butler, T. M., Crowley, J. N., Dillon, T. J., Fischer, H., Ganzeveld, L., Harder, H., Lawrence, M. G., Martinez, M., Taraborrelli, D., and Williams, J.: Atmospheric oxidation capacity sustained by a tropical forest, Nature, 452, 737–740, https://doi.org/10.1038/nature06870, 2008.

Loreto, F., Ciccioli, P., Cecinato, A., Brancaleoni, E., Frattoni, M., Fabozzi, C., and Tricoli, D.: Evidence of the photosynthetic origin of monoterpene emitted by Quercus ilex L. leaves by ^{13}C labelling, Plant Physiol., 110, 1317–1322, https://doi.org/10.1104/pp.110.4.1317, 1996.

Lyamani, H., Olmo, F. J., Alcántara, A., and Alados-Arboledas, L.: Atmospheric aerosols during the 2003 heat wave in southeastern Spain I: Spectral optical depth, Atmos. Environ., 40, 6453–6464, https://doi.org/10.1016/j.atmosenv.2006.04.048, 2006.

Mallet, M., Dubovik, O., Nabat, P., Dulac, F., Kahn, R., Sciare, J., Paronis, D., and Léon, J. F.: Absorption properties of Mediterranean aerosols obtained from multi-year ground-based remote sensing observations, Atmos. Chem. Phys., 13, 9195–9210, https://doi.org/10.5194/acp-13-9195-2013, 2013.

Markowitz, K. M., Flatau, P. J., Ramana, M. V., Crutzen, P. J., and Ramanathan, V.: Absorbing Mediterranean aerosols lead to a large reduction in the solar radiation at the surface, Geophys. Res. Lett., 29, 1968, https://doi.org/10.1029/2002GL015767, 2002.

Martin, S. T., Andreae, M. O., Artaxo, P., Baumgardner, D., Chen, Q., Goldstein, A. H., Guenther, A., Heald, C. L., Mayol-Bracero, O. L., McMurry, P. H., Pauliquevis, T., Pöschl, U., Prather, K. A., Roberts, G. C., Saleska, S. R., Silva Dias, M. A., Spracklen, D. V., Swietlicki, E., and Trebs, I.: Sources and properties of Amazonian aerosol particles, Rev. Geophys., 48, RG2002, https://doi.org/10.1029/2008RG000280, 2010.

Middlebrook, A. N., Bahreini, R., Jimenez, J. L., and Canagaratna, M. R.: Evaluation of composition-dependent collection efficiencies for the Aerodyne aerosol mass spectrometer using field data, Aerosol Sci. Tech., 46, 258–271, https://doi.org/10.1080/02786826.2011.620041, 2012.

Nedelec, P., Cammas, J.-P., Thouret, V., Athier, G., Cousin, J.-M., Legrand, C., Abonnel, C., Lecoeur, F., Cayez, G., and Marizy, C.: An improved infrared carbon monoxide analyser for routine measurements aboard commercial Airbus aircraft: technical validation and first scientific results of the MOZAIC III programme, Atmos. Chem. Phys., 3, 1551–1564, https://doi.org/10.5194/acp-3-1551-2003, 2003.

Nenes, A., Pandis, S. N., and Pilinis, C.: ISORROPIA: A new thermodynamic equilibrium model for multiphase multicomponent inorganic aerosols, Aquat. Geochem., 4, 123–152, https://doi.org/10.1023/A:1009604003981, 1998.

Nguyen, T. B., Coggon, M. M., Bates, K. H., Zhang, X., Schwantes, R. H., Schilling, K. A., Loza, C. L., Flagan, R. C., Wennberg, P. O., and Seinfeld, J. H.: Organic aerosol formation from the reactive uptake of isoprene epoxydiols (IEPOX) onto non-acidified inorganic seeds, Atmos. Chem. Phys., 14, 3497–3510, https://doi.org/10.5194/acp-14-3497-2014, 2014.

Odum, J. R., Hoffmann, T., Bowman, F., Collins, D. C., Flagan, R. H., and Seinfeld, J.: Gas/Particle Partitioning and Secondary Organic Aerosol Yields, Environ. Sci. Tech., 30, https://doi.org/10.1021/es950943, 1996.

Paatero, P. and Tapper, U.: Positive matrix factorization: A non-negative factor model with optimal utilization of error estimates of data values, Environmetrics, 5, 111–126, https://doi.org/10.1002/env.3170050203, 1994.

Palm, B. B., de Sá, S. S., Day, D. A., Campuzano-Jost, P., Hu, W., Seco, R., Sjostedt, S. J., Park, J.-H., Guenther, A. B., Kim, S., Brito, J., Wurm, F., Artaxo, P., Thalman, R., Wang, J., Yee, L. D., Wernis, R., Isaacman-VanWertz, G., Goldstein, A. H., Liu, Y., Springston, S. R., Souza, R., Newburn, M. K., Alexander, M. L., Martin, S. T., and Jimenez, J. L.: Secondary organic aerosol formation from ambient air in an oxidation flow reactor in central Amazonia, Atmos. Chem. Phys., 18, 467–493, https://doi.org/10.5194/acp-18-467-2018, 2018.

Papadimas, C. D., Hatzianastassiou, N., Matsoukas, C., Kanakidou, M., Mihalopoulos, N., and Vardavas, I.: The direct effect of aerosols on solar radiation over the broader

Mediterranean basin, Atmos. Chem. Phys., 12, 7165–7185, https://doi.org/10.5194/acp-12-7165-2012, 2012.

Rindelaub, J. D., Borca, C. H., Hostetler, M. A., Slade, J. H., Lipton, M. A., Slipchenko, L. V., and Shepson, P. B.: The acid-catalyzed hydrolysis of an α-pinene-derived organic nitrate: kinetics, products, reaction mechanisms, and atmospheric impact, Atmos. Chem. Phys., 16, 15425–15432, https://doi.org/10.5194/acp-16-15425-2016, 2016.

Riva, M., Budisulistiorini, S. H., Zhang, Z., Gold, A., and Surratt, J. D.: Chemical characterization of secondary organic aerosol constituents from isoprene ozonolysis in the presence of acidic aerosol, Atmos. Environ., 130, 5–13, 2016.

Robinson, N. H., Hamilton, J. F., Allan, J. D., Langford, B., Oram, D. E., Chen, Q., Docherty, K., Farmer, D. K., Jimenez, J. L., Ward, M. W., Hewitt, C. N., Barley, M. H., Jenkin, M. E., Rickard, A. R., Martin, S. T., McFiggans, G., and Coe, H.: Evidence for a significant proportion of Secondary Organic Aerosol from isoprene above a maritime tropical forest, Atmos. Chem. Phys., 11, 1039–1050, https://doi.org/10.5194/acp-11-1039-2011, 2011.

Sartelet, K. N., Couvidat, F., Seigneur, C., and Roustan, Y.: Impact of biogenic emissions on air quality over Europe and North America, Atmos. Environ., 53, 131–141, https://doi.org/10.1016/j.atmosenv.2011.10.046, 2012.

Sartelet, K., Zhu, S., Moukhtar, S., André, M., André, J. M., Gros, V., Favez, O., Brasseur, A., and Redaelli, M.: Emission of intermediate, semi and low volatile organic compounds from traffic and their impact on secondary organic aerosol concentrations over Greater Paris, Atmos. Environ., 180, 126–137, https://doi.org/10.1016/j.atmosenv.2018.02.031, 2018.

Schwartz, R. E., Russell, L. M., Sjostedt, S. J., Vlasenko, A., Slowik, J. G., Abbatt, J. P. D., Macdonald, A. M., Li, S. M., Liggio, J., Toom-Sauntry, D., and Leaitch, W. R.: Biogenic oxidized organic functional groups in aerosol particles from a mountain forest site and their similarities to laboratory chamber products, Atmos. Chem. Phys., 10, 5075–5088, https://doi.org/10.5194/acp-10-5075-2010, 2010.

Sciare, J., Bardouki, H., Moulin, C., and Mihalopoulos, N.: Aerosol sources and their contribution to the chemical composition of aerosols in the Eastern Mediterranean Sea during summertime, Atmos. Chem. Phys., 3, 291–302, https://doi.org/10.5194/acp-3-291-2003, 2003.

Setyan, A., Song, C., Merkel, M., Knighton, W. B., Onasch, T. B., Canagaratna, M. R., Worsnop, D. R., Wiedensohler, A., Shilling, J. E., and Zhang, Q.: Chemistry of new particle growth in mixed urban and biogenic emissions – insights from CARES, Atmos. Chem. Phys., 14, 6477–6494, https://doi.org/10.5194/acp-14-6477-2014, 2014.

Shilling, J. E., Zaveri, R. A., Fast, J. D., Kleinman, L., Alexander, M. L., Canagaratna, M. R., Fortner, E., Hubbe, J. M., Jayne, J. T., Sedlacek, A., Setyan, A., Springston, S., Worsnop, D. R., and Zhang, Q.: Enhanced SOA formation from mixed anthropogenic and biogenic emissions during the CARES campaign, Atmos. Chem. Phys., 13, 2091–2113, https://doi.org/10.5194/acp-13-2091-2013, 2013.

Sihto, S.-L., Kulmala, M., Kerminen, V.-M., Dal Maso, M., Petäjä, T., Riipinen, I., Korhonen, H., Arnold, F., Janson, R., Boy, M., Laaksonen, A., and Lehtinen, K. E. J.: Atmospheric sulphuric acid and aerosol formation: implications from atmospheric measurements for nucleation and early growth mechanisms, Atmos. Chem. Phys., 6, 4079–4091, https://doi.org/10.5194/acp-6-4079-2006, 2006.

Slowik, J. G., Stroud, C., Bottenheim, J. W., Brickell, P. C., Chang, R. Y.-W., Liggio, J., Makar, P. A., Martin, R. V., Moran, M. D., Shantz, N. C., Sjostedt, S. J., van Donkelaar, A., Vlasenko, A., Wiebe, H. A., Xia, A. G., Zhang, J., Leaitch, W. R., and Abbatt, J. P. D.: Characterization of a large biogenic secondary organic aerosol event from eastern Canadian forests, Atmos. Chem. Phys., 10, 2825–2845, https://doi.org/10.5194/acp-10-2825-2010, 2010.

Spracklen, D. V., Bonn, B., and Carslaw, K. S.: Boreal forests, aerosols and the impacts on clouds and climate, Philos. T. Roy. Soc. Lond. A Mat., 366, 4613–4626, https://doi.org/10.1098/rsta.2008.0201, 2008.

Ulbrich, I. M., Canagaratna, M. R., Zhang, Q., Worsnop, D. R., and Jimenez, J. L.: Interpretation of organic components from Positive Matrix Factorization of aerosol mass spectrometric data, Atmos. Chem. Phys., 9, 2891–2918, https://doi.org/10.5194/acp-9-2891-2009, 2009.

Yarwood, G., Rao, S., Yocke, M., and Whitten, G.: Updates to the carbon bond chemical mechanism: CB05. Rep. RT-0400675, 246 pp., available at: http://www.camx.com/files/cb05_final_report_120805.aspx (last access: 27 March 2017), 2005.

Zannoni, N., Gros, V., Lanza, M., Sarda, R., Bonsang, B., Kalogridis, C., Preunkert, S., Legrand, M., Jambert, C., Boissard, C., and Lathiere, J.: OH reactivity and concentrations of biogenic volatile organic compounds in a Mediterranean forest of downy oak trees, Atmos. Chem. Phys., 16, 1619–1636, https://doi.org/10.5194/acp-16-1619-2016, 2016.

Zhang, H., Yee, L. D., Lee, B. H., Curtis, M. P., Worton, D. R., Isaacman-VanWertz, G., Offenberg, J. H., Lewandowski, M., Kleindienst, T. E., Beaver, M. E., Holder, A. L., Lonneman, W. A., Docherty, K. S., Jaoui, M., Pye, H. O. T., Hu, W., Day, D. D., Campuzano-Jost, P., Jimenez, J., Guo, H., Weber, R. J., de Gouw, J., Koss, A. R, Edgerton, E. S., Brune, W., Mohr, C., Lopez-Hilfiker, F. D., Lutz, A., Kreisberg, N. M., Spielman, S. R., Hering, S., Wilson, K. R., Thornton, J. A, and Goldstein, A. H.: Monoterpene SOA dominate atmospheric fine aerosol, P. Natl. Acad. Sci. USA, 115, 2038–2043, https://doi.org/10.1073/pnas.1717513115, 2018.

Zhang, Y., Tang, L., Sun, Y., Favez, O., Canonaco, F., Albinet, A., Couvidat, F., Liu, D., Jayne, J. T., Wang, Z., Croteau, P. L., Canagaratna, M. R., Zhou, H.-C., Prévôt, A. S. H., and Worsnop, D. R.: Limited formation of isoprene epoxydiols-derived secondary organic aerosol under NO_x-rich environments in Eastern China, Geophys. Res. Lett., 44, 2035–2043, https://doi.org/10.1002/2016GL072368, 2017.

Zhu, S., Sartelet, K., Healy, R., and Wenger, J.: Simulation of particle diversity and mixing state over Greater Paris: A modelmeasurement inter-comparison, Faraday Discuss., 189, 547–566, https://doi.org/10.1039/C5FD00175G, 2016.

Bibliography

Aan de Brugh, J. M. J., Henzing, J. S., Schaap, M., Morgan, W. T., van Heerwaarden, C. C., Weijers, E. P., Coe, H., and Krol, M. C.: Modelling the partitioning of ammonium nitrate in the convective boundary layer, Atmos. Chem. Phys., 12, 3005–3023, doi:10.5194/acp-12-3005-2012, 2012.

Aiken, A., DeCarlo, P., Krol, J., Worsno, D., Huffma, J., Docherty, K., Ulbrich, I., Mohr, C., Kimmel, J., Sueper, D., Sun, Y., Zhang, Q., Trimborn, A., Northway, M., Ziemann, P., Canagaratna, M., Onasch, T., Alfarra, M., Prevot, A., Dommen, J., Duplissy, J., Metzger, A., Baltensperger, U., and Jimenez, J.: O/C and OM/OC Ratios of Primary, Secondary, and Ambient Organic Aerosols with High-Resolution Time-of-Flight Aerosol Mass Spectrometry., Environ. Sci. Technol., 42, 4478–4485, doi:10.1021/es703009q, 2008.

Aksoyoglu, S., Baltensperger, U., and Prévôt, A. S. H.: Contribution of ship emissions to the concentration and deposition of air pollutants in Europe, Atmos. Chem. Phys., 16, 18951906, doi:10.5194/acp-16-1895-2016, 2016.

Albriet, B., Sartelet, K., Lacour, S., Carissimo, B., and Seigneur, C.: Modelling aerosol number distributions from a vehicle exhaust with an aerosol CFD model, Atmos. Environ., 44, 1126 – 1137, doi:10.1016/j.atmosenv.2009.11.025, 2010.

Aphekom: Health impact assessment of short and long-term exposure to ozone and PM in 25 european cities, 2011.

Arndt, J., Sciare, J., Mallet, M., Roberts, G., Marchand, N., Sartelet, K., Sellegri, K., Dulac, F., Healy, R., and Wenger, J.: Sources and mixing state of summertime background aerosol in the northwestern Mediterranean basin, Atmos. Chem. Phys., doi:10.5194/acp-2016-1044, 2017.

Ayres, J., Borm, P., Cassee, F., Castranova, V., Donaldson, K., Ghio, A., Harrison, R., Hider, R., Kelly, F., Kooter, I., Marano, F., Maynard, R., Mudway, I., Nel, A., Sioutas, C., Smith, S., Baeza-Squiban, A., Cho, A., Duggan, S., and Froines, J.: The Reactive Oxidant Potential of Different Types of Aged Atmospheric Particles: An Outdoor Chamber Study, Inhal. Toxicol., 20, 75–99, doi:10.1080/08958370701665517, 2008.

Barth, M., Kim, S.-W., Wang, C., Pickering, K., Ott, L., Stenchikov, G., Leriche, M., Cautenet, S., Pinty, J.-P., Barthe, C., Mari, C., Helsdon, J., Farley, R., Fridlind, A., Ackerman, A., Spiridonov, V., and Telenta, B.: Cloud-scale model intercomparison of chemical constituent transport in deep convection, Atmos. Chem. Phys., 7, 4709–4731, doi:10.5194/acp-7-4709-2007, 2007.

Bean, J. K. and Ruiz, L. H.: Gasparticle partitioning and hydrolysis of organic nitrates formed from the oxidation of α-pinene in environmental chamber experiments, Atmos. Chem. Phys., 16, 2175–2184, doi:10.5194/acp-16-2175-2016, 2016.

Becagli, S., Anello, F., Bommarito, C., Cassola, F., Calzolai, G., Di Iorio, T., di Sarra, A., Gómez-Amo, J.-L., Lucarelli, F., Marconi, M., Meloni, D., Monteleone, F., Nava, S., Pace, G., Severi, M., Sferlazzo, D. M., Traversi, R., and Udisti, R.: Constraining the ship contribution to the aerosol of the central Mediterranean, Atmos. Chem. Phys., 17, 2067–2084, doi:10.5194/acp-17-2067-2017, 2017.

Berg, N., Mellqvist, J., Jalkanen, J.-P., and Balzani, J.: Ship emissions of $SO_2$and NO_2: DOAS measurements from airborne platforms, Atmos. Meas. Tech., 5, 1085–1098, doi:doi:10.5194/amt-5-1085-2012, 2012.

Bergametti, G., Dutot, A.-L., Buat-Ménard, P., Losno, R., and Remoudaki, E.: Seasonal variability of the elemental composition of atmospheric aerosol particles over the northwestern Mediterranean, Tellus, B41, 353361, 1989a.

Bergametti, G., Gomes, L., Remoudaki, E., Desbois, M., Martin, D., and Buat-Ménard, P.: Present transport and deposition patterns of African dusts to the north-western Mediterranean, Kluwer Academic Publishers, p. 227252, 1989b.

Bergström, R., Denier van der Gon, H., Prévôt, A., Yttri, K., and Simpson, D.: Modelling of organic aerosols over Europe (2002-2007) using a volatility basis set (VBS) framework: application of different assumptions regarding the formation of secondary organic aerosol., Atmos. Chem. Phys., 12, 8499–8527, doi:10.5194/acp-12-8499-2012, 2012.

Bessagnet, B., Menut, L., Curci, G., Hodzic, A., Guillaume, B., Liousse, C., Moukhtar, S., Pun, B., Seigneur, C., and Schulz, M.: Regional modeling of carbonaceous aerosols over Europe-focus on secondary organic aerosols, J. Atmos. Chem., 61, 175–202, doi:10.1007/s10874-009-9129-2, 2008.

Bossioli, E., Tombrou, M., Kalogiros, J., Allan, J., Bacak, A., Bezantakos, S., Biskos, G., Coe, H., Jones, B., Kouvarakis, G., N., M., and Percival, C.: Atmospheric composition in the Eastern Mediterranean: Influence of biomass burning during summertime using the WRF-Chem model, Atmos. Environ., 132, 317–331, doi:10.1016/j.atmosenv.2016.03.011, 2016.

Boylan, J. W. and Russell, A. G.: PM and light extinction model performance metrics, goals, and criteria for three-dimensional air quality models, Atmos. Environ., 40, 4946–4959, doi:10.1016/j.atmosenv.2005.09.087, 2006.

Budisulistiorini, S. H., Li, X., Bairai, S. T., Renfro, J., Liu, Y., Liu, Y. J., McKinney, K. A., Martin, S. T., McNeill, V. F., Pye, H. O. T., Nenes, A., Neff, M. E., Stone, E. A., Mueller, S., Knote, C., Shaw, S. L., Zhang, Z., Gold, A., , and Surratt, J. D.: Examining the effects of anthropogenic emissions on isoprene-derived secondary organic aerosol formation during the 2013 Southern Oxidant and Aerosol Study (SOAS) at the Look Rock, Tennessee ground site, Faraday Discuss., 15, 8871–8888, doi:10.5194/acp-15-8871-2015, 2015.

Byun, D. and Ching, J.: Science algorithms of the EPA Models-3 Community Multiscale Air Quality (CMAQ) Modeling System, environmental Protection Agency, Research Triangle Park, NC, 1999.

Byun, D. and Schere, K. L.: Review of the Governing Equations, Computational Algorithms, and Other Components of the Models-3 Community Multiscale Air Quality (CMAQ) Modeling System, Appl. Mech. Rev., 59, 51–77, doi:10.1115/1.2128636, 2006.

Cai, X. and Griffin, R. J.: Secondary aerosol formation from the oxidation of biogenic hydrocarbons by chlorine atoms, J. Geophys. Res., 111, doi:10.1029/2005JD006857, 2006.

Canonaco, F., Slowik, J. G., Baltensperger, U., and Prévôt, A. S. H.: Seasonal differences in oxygenated organic aerosol composition: implications for emissions sources and factor analysis, Atmos. Chem. Phys., 15, 6993–7002, doi:10.5194/acp-15-6993-2015, 2015.

Cappa, C. D. and Jimenez, J. L.: Quantitative estimates of the volatility of ambient organic aerosol, Atmos. Chem. Phys., 10(12), 54095424, doi:10.5194/acp-10-5409-2010, 2010.

Carlton, A. G., Bhave, P. V., Napelenok, S. L., Edney, E. O., Sarwar, G., Pinder, R. W., Pouliot, G. A., and Houyoux, M.: Model representation of secondary organic aerosol in CMAQv4.7, Environ. Sci. Technol., 44, 8553–8560, doi:10.1021/es100636q, 2010.

Chacon-Madrid and Donahue, N. M.: Fragmentation vs. functionalization: chemical aging and organic aerosol formation, Atmos. Chem. Phys., 11, 10 55310 563, doi:10.5194/acp-11-10553-2011, 2011.

Cho, A., Sioutas, C., Miguel, A., Kumagai, Y., Schmitz, D., Singh, M., Eiguren-Fernandez, A., and Froines, J.: Redox activity of airborne particulate matter at different sites in the Los Angeles Basin., Environ. Res., 99, 40–47, doi:10.1016/j.envres.2005.01.003, 2005.

Cholakian, A., Beekmann, M., Colette, A., Coll, I., Siour, G., Sciare, J., Marchand, N., Pey, J., Gros, V., Sauvage, S., Sellegri, K., Colomb, A., Sartelet, K., and Dulac, F.: Simulation of organic aerosols in the western Mediterranean area during the ChArMEx 2013 summer campaign, Atmos. Chem. Phys. Discuss., p. submitted, 2017.

Chrit, M., Sartelet, K., Sciare, J., Pey, J., Marchand, N., Couvidat, F., Sellegri, K., and Beekmann, M.: Modelling organic aerosol concentrations and properties during ChArMEx summer campaigns of 2012 and 2013 in the western Mediterranean region, Atmos. Chem. Phys., 17, 12 509–12 531, doi:10.5194/acp-17-12509-2017, 2017.

Ciarelli, G., Aksoyoglu, S., Crippa, M., Jimenez, J.-L., Nemitz, E., Sellegri, K., ijl, M., Carbone, S., Mohr, C., ODowd, C., Poulain, L., Baltensperger, U., and Prévôt, A. S. H.: Evaluation of European air quality modelled by CAMx including the volatility basis set scheme, Atmos. Chem. Phys., 16, 10 313–10 332, doi:https://doi.org/10.5194/acp-16-10313-2016, 2016.

Ciarelli, G., Aksoyoglu, S., El Haddad, I., Bruns, E. A., Crippa, M., Poulain, L., ijl, M., Carbone, S., Freney, E., ODowd, C., Baltensperger, U., and Prévôt, A. S. H.: Modelling winter organic aerosol at the European scale with CAMx: valuation and source apportionment with a VBS parameterization based on novel wood burning smog chamber experiments, Atmos. Chem. Phys., 17, 7653–7669, doi:10.5194/acp-17-7653-2017, 2017a.

Ciarelli, G., El Haddad, I., Bruns, E., Aksoyoglu, S., Mhler, O., Baltensperger, U., and Prévôt, A. S. H.: Constraining a hybrid volatility basis-set model for aging of wood-burning emissions using smog chamber experiments: a box-model study based on the VBS scheme of the CAMx model (v5.40), Geosci. Model Dev., 10, 2303–2320, doi:10.5194/gmd-10-2303-2017, 2017b.

Claeys, M., Roberts, G., Mallet, M., Arndt, J., Sellegri, K., Sciare, J., Wenger, J., and Sauvage, B.: Optical, physical and chemical properties of aerosols transported to a coastal site in the western Mediterranean: a focus on primary marine aerosols., Atmos. Chem. Phys., 17, 7891–7915, doi:10.5194/acp-17-7891-2017, 2017.

Couvidat, F. and Sartelet, K.: The Secondary Organic Aerosol Processor (SOAP v1.0) model: a unified model with different ranges of complexity based on the molecular surrogate approach, Geosci. Model Dev., 8, 1111–1138, doi:10.5194/gmd-8-1111-2015, 2015.

Couvidat, F. and Seigneur, C.: Modeling secondary organic aerosol formation from isoprene under dry and humid conditions, Atmos. Chem. Phys., 11, 893–909, doi:10.5194/acp-11-893-2011, 2011.

Couvidat, F., Debry, É., Sartelet, K., and Seigneur, C.: A hydrophilic/hydrophobic organic (H^2O) model: Model development, evaluation and sensitivity analysis, J. Geophys. Res., 117, D10 304, doi:10.1029/2011JD017214, 2012.

Couvidat, F., Kim, Y., Sartelet, K., Seigneur, C., Marchand, N., and Sciare, J.: Modeling secondary organic aerosol in an urban area: application to Paris, France, Atmos. Chem. Phys., 13, 983–996, doi:10.5194/acp-13-983-2013, 2013a.

Couvidat, F., Sartelet, K., and Seigneur, C.: Investigating the impact of aqueous-phase chemistry and wet deposition on organic aerosol formation using a molecular surrogate modeling approach, Environ. Sci. Technol., 47, 914–922, doi:10.1021/es3034318, 2013b.

Couvidat, F., Bessagnet, B., Garcia-Vivanco, M., Real, E., Menut, L., and Colette, A.: Development of an inorganic and organic aerosol model (Chimere2017 β v1.0): seasonal and spatial evaluation over Europe., Geosci. Model Dev. Discuss., in review, doi:doi.org/10.5194/gmd-2017-120, 2017.

Crenn, V., Sciare, J., Croteau, P. L., Verlhac, S., Fröhlich, R., Belis, C. A., Aas, W., Äijälä, M., Alastuey, A., Artiñano, B., Baisnée, D., Bonnaire, N., Bressi, M., Canagaratna, M., Canonaco, F., Carbone, C., Cavalli, F., Coz, E., Cubison, M. J., Esser-Gietl, J. K., Green, D. C., Gros, V., Heikkinen, L., Herrmann, H., Lunder, C., Minguillón, M. C., Močnik, G., ODowd, C. D., Ovadnevaite, J., Petit, J.-E., Petralia, E., Poulain, L., Priestman, M., Riffault, V., Ripoll, A., Sarda-Estève, R., Slowik, J. G., Setyan, A., Wiedensohler, A., Baltensperger, U., Prévôt, A. S. H., Jayne, J. T., , and Favez, O.: ACTRIS ACSM intercomparison Part 1: Reproducibility of concentration and fragment results from 13 individual Quadrupole Aerosol Chemical Speciation Monitors (Q-ACSM) and consistency with co-located instruments, Atmos. Meas. Tech., 8, 5063–5087, doi:10.5194/amt-8-5063-2015, 2015.

Crippa, M., Canonaco, F., Lanz, V., Äijälä, M., Allan, J., Carbone, S., Capes, G., Ceburnis, D., Dall'Osto, M., Day, A., DeCarlo, P., Ehn, M., Eriksson, A., Freney, E., Hildebrandt Ruiz, L., Hillamo, R., Jimenez, J., Junninen, H., Kiendler-Scharr, A., Kortelainen, A.-M., Kulmala, M., Laaksonen, A., Mensah, A., Mohr, C., Nemitz, E., O'Dowd, C., Ovadnevaite, J., Pandis, S., Petäja, T., Poulain, L., Saarikoski, S., Sellegri, K., Swietlicki, E., Tiitta, P., Worsnop, D., Baltensperger, U., and Prévôt, A.: Organic aerosol components derived from 25 AMS data sets across Europe using a consistent ME-2 based source apportionment approach., Atmos. Chem. Phys., 14, 6159–6176, doi:10.5194/acp-14-6159-2014, 2014.

Crounse, J. D., Nielsen, L. B., Jrgensen, S., Kjaergaard, H. G., and Wennberg, P. O.: Autoxidation of organic compounds in the atmosphere, J. Phys. Chem. Lett., 4, 3513–3520, doi: 10.1021/jz4019207, 2013.

Darer, A. I., Cole-Filipiak, N. C., OConnor, A. E., and Elrod, M. J.: Formation and stability of atmospherically relevant isoprenederived organosulfates and organonitrates, Environ. Sci. Technol., 45, 18951902, doi:10.1021/es103797z, 2011.

Dawson, M., Xu, J., Griffin, R., and Dabdub, D.: Development of aroCACM/MPMPO 1.0: a model to simulate secondary organic aerosol from aromatic precursors in regional models., Geosci. Model Dev., 9, 2143–2151, doi:10.5194/gmd-9-2143-2016, 2016.

Debry, É., Fahey, K., Sartelet, K., Sportisse, B., and Tombette, M.: Technical Note: A new SIze REsolved Aerosol Model (SIREAM), Atmos. Chem. Phys., 7, 1537–1547, doi:10.5194/acp-7-1537-2007, 2007a.

Debry, É., Fahey, K., Sartelet, K., Sportisse, B., and Tombette, M.: Technical Note: A new SIze REsolved Aerosol Model (SIREAM), Atmos. Chem. Phys., 7, 1537–1547, doi:10.5194/acp-7-1537-2007, 2007b.

Debry, É., Seigneur, C., and Sartelet, K.: Organic aerosols in the air quality platform Polyphemus: oxidation pathways, hydrophilic/hydrophobic partitioning and oligomerization, International Aerosol Modeling Algorithms, univ. of California, Davis, available at: http://mae.ucdavis.edu/wexler/IAMA/ppts/VIIB/debry_iama.pdf, 2007c.

Denier van der Gon, H. A. C., Bergström, R., Fountoukis, C., Johansson, C., Pandis, S., Simpson, D., and Visschedijk, A.: Particulate emissions from residential wood combustion in Europe: revised estimates and an evaluation, Atmos. Chem. Phys., 15, 6503–6519, doi:10.5194/acp-15-6503-2015, 2015.

Denjean, C., Cassola, F., Mazzino, A., Triquet, S., Chevaillier, S., Grand, N., Bourrianne, T., Momboisse, G., Sellegri, K., Schwarzenbock, A., Freney, E., Mallet, M., and Formenti, P.: Size distribution and optical properties of mineral dust aerosols transported in the western Mediterranean., Atmos. Chem. Phys., 16, 1081–1104, doi:10.5194/acp-16-1081-2016, 2016.

Di Biagio, C., Doppler, L., Gaimoz, C., Grand, N., Ancellet, G., Raut, J.-C., Beekmann, M., Borbon, A., Sartelet, K., Atti, J.-L., Ravetta, F., and Formenti, P.: Continental pollution in the western Mediterranean basin: vertical profiles of aerosol and trace gases measured over the sea during TRAQA 2012 and SAFMED 2013, Atmos. Chem. Phys., 15, 9611–9630, doi:10.5194/acp-15-9611-2015, 2015.

Donahue, N., Epstein, S., Pandis, S., and Robinson, A.: A two-dimensional volatility basis set: 1. organic-aerosol mixing thermodynamics, Atmos. Chem. Phys., 11, 3303–3318, doi:10.5194/acp-11-3303-2011, 2011.

Donahue, N. M., Robinson, A. L., Stanier, C. O., and Pandis, S. N.: Coupled partitioning, dilution, and chemical aging of semivolatile organics, Environ. Sci. Technol., 40, 26352643, doi: 10.1021/es052297c, 2006.

Donahue, N. M., Kroll, J. H., Pandis, S. N., and Robinson, A. L.: A two-dimensional volatility basis set Part 2: Diagnostics of organic-aerosol evolution, Atmos. Chem. Phys., 12, 615–634, doi:10.5194/acp-12-615-2012, 2012.

Donahue, N. M., Chuang, W., Epstein, S. A., Kroll, J. H., Worsnop, D. R., Robinson, A. L., Adams, P. J., and Pandis, S. N.: Why do organic aerosols exist? Understanding aerosol lifetimes using the two-dimensional volatility basis set, Environ. Chem., 10, 151–1557, doi: https://doi.org/10.1071/EN13022, 2013.

Duhanian, N. and Roustan, Y.: Below-cloud wet scavenging coefficients for atmospheric gases and particulates, Atmos. Environ., in press, 2011.

Duplissy, J., DeCarlo, P. F., Dommen, J., Alfarra, M. R., Metzger, A., Barmpadimos, I., Prévôt, A. S. H., Weingartner, E., Tritscher, T., Gysel, M., Aiken, A. C., Jimenez, J. L., Canagaratna, M. R., Worsnop, D. R., Collins, D. R., Tomlinson, J., and Baltensperger, U.: Relating hygroscopicity and composition of organic aerosol particulate matter, Atmos. Chem. Phys., 11, 1155–1165, doi:10.5194/acp-11-1155-2011, 2011.

Dzepina, K., Volkamer, R. M., Madronich, S., Tulet, P., Ulbrich, I. M., Zhang, Q., Cappa, C. D., Ziemann, P. J., and Jimenez, J. L.: Evaluation of recently-proposed secondary organic aerosol models for a case study in Mexico City, Atmos. Chem. Phys., 9, 5681–5709, doi: https://doi.org/10.5194/acp-9-5681-2009, 2009.

Eddingsaas, N. C., VanderVelde, D. G., and Wennberg, P. O.: Kinetics and Products of the Acid-Catalyzed Ring-Opening Atmospherically Relevant Butyl Epoxy Alcohols, J. Phys. Chem., 114, 8106–8113, doi:10.1021/jp103907, A 2010.

Ehn, M., Thornton, J., Kleist, E., Sipil, M., Junninen, H., Pullinen, I., Springer, M., Rubach, F., Tillmann, R., Lee, B., Lopez-Hilfiker, F., Andres, S., Acir, I., Rissanen, M., Jokinen, T., Schobesberger, S., Kangasluoma, J., Kontkanen, J., Nieminen, T., Kurtn, T., Nielsen, L. B., Jrgensen, S., Kjaergaard, H. G., Canagaratna, M., Dal Maso, M., Berndt, T., Petj, T., Wahner, A., Kerminen, V., Kulmala, M., Worsnop, D. R., Wildt, J., and Mentel, T. F.: A large source of low-volatility secondary organic aerosol, Nature, 506, 476–479, doi:10.1038/nature13032, 2014.

El Haddad, I., Marchand, N., Wortham, H., Piot, C., Besombes, J.-L., Cozic, J., Chauvel, C., Armengaud, A., Robin, D., and Jaffrezo, J.-L.: Primary sources of PM2.5 organic aerosol in an industrial Mediterranean city, Marseille, Atmos. Chem. Phys., 11, 2039–2058, doi:10.5194/acp-11-2039-2011, 2011.

El Haddad, I., D'Anna, B., Temime-Roussel, B., Nicolas, M., Boreave, A., Favez, O., Voisin, D., Sciare, J., George, C., Jaffrezo, J.-L., Wortham, H., , and Marchand, N.: Towards a better understanding of the origins, chemical composition and aging of oxygenated organic aerosols: case study of a Mediterranean industrialized environment, Marseille, Atmos. Chem. Phys., 13, 7875–7894, doi:10.5194/acp-13-7875-2013, 2013a.

El Haddad, I., D'Anna, B., Temime-Roussel, B., Nicolas, M., Boreave, A., Favez, O., Voisin, D., Sciare, J., George, C., Jaffrezo, J.-L., Wortham, H., , and Marchand, N.: Towards a better understanding of the origins, chemical composition and aging of oxygenated organic aerosols: case study of a Mediterranean industrialized environment, Marseille, Atmos. Chem. Phys., 13, 7875–7894, doi:10.5194/acp-13-7875-2013, 2013b.

El-Zanan, H., Lowenthal, D., Zielinska, B., Chow, J., and Kumar, N.: Determination of the organic aerosol mass to organic carbon ratio in IMPROVE samples., Chemosphere, 60, 480–496, doi:10.1016/j.chemosphere.2005.01.005, 2005.

ENVIRON: Users Guide, Comprehensive Air Quality Model with Extensions (CAMx), Version 5.40, Environ International Corporation, california, USA, 2011.

Ervens, B., Turpin, B. J., , and Weber, R. J.: Secondary organic aerosol formation in cloud droplets and aqueous particles (aqSOA): a review of laboratory, field and model studies, Atmos. Chem. Phys., 11, 11 069–11 102, doi:10.5194/acp-11-11069-2011, 2011.

Fahey, K. M. and Pandis, S. N.: Optimizing model performance: variable size resolution in cloud chemistry modeling, Atmos. Environ., 35, 4471 – 4478, doi:10.1016/S1352-2310(01)00224-2, 2001.

Feng, Y., Penner, J. E., Sillman, S., and Liu, X.: Effects of cloud overlap in photochemical models, J. Geophys. Res., 109, D04 310, doi:10.1029/2003JD004040, 2004.

Finlayson-Pitts, B. J. and Pitts, Jr., J. N.: Chemistry of the upper and lower atmosphere, Academic Press, San Diego, 2000.

Fountoukis, C., Megaritis, A. G., Skyllakou, K., Charalampidis, P. E., Pilinis, C., Denier van der Gon, H. A. C., Crippa, M., Canonaco, F., Mohr, C., Prvt, A. S. H., Allan, J. D., oulain, L., Petj, T., Tiitta, P., Carbone, S., Kiendler-Scharr, A., Nemitz, E., ODowd, C., Swietlicki, E., and Pandis, S. N.: Organic aerosol concentration and composition over -Europe: insights from comparison of regional model predictions with aerosol mass spectrometer factor analysis, Atmos. Chem. Phys., 14, 9061–9076, doi:10.5194/acp-14-9061-2014, 2014.

Fredenslund, A., Jones, R. L., and Prausnitz, J. M.: Group-Contribution Estimation of Activity Coefficients in Nonideal Liquid Mixtures, AIChE J., 21, 1086–1099, 1975.

Freney, E., Sellegri, K., Chrit, M., Adachi, K., Brito, J., Waked, A., Borbon, A., Colomb, A., Dupuy, R., Pichon, J., Bouvier, L., Delon, C., Jambert, C., Durand, P., Bourianne, T., Gaimoz, C., Triquet, S., Féron, A., Beekman, M., Dulac, F., and Sartelet, K.: Aerosol composition and the contribution of SOA formation over Mediterranean forests, Atmos. Chem. Phys. Discuss., in review, doi:doi.org/10.5194/acp-2017-482, 2017.

Fröhlich, R., Cubison, M. J., Slowik, J. G., Bukowiecki, N., Canonaco, F., Croteau, P. L., Gysel, M., Henne, S., Herrmann, E., Jayne, J. T., Steinbacher, M., Worsnop, D. R., Baltensperger, U., and Prévôt, A. S. H.: Fourteen months of on-line measurements of the non-refractory submicron aerosol at the Jungfraujoch (3580 m a.s.l.) chemical composition, origins and organic aerosol sources, Atmos. Chem. Phys., 15, 11 373–11 398, doi:10.5194/acp-15-11373-2015, 2015.

Fry, J. L., Kiendler-Scharr, A., Rollins, A. W., Wooldridge, P. J., Brown, S. S., Fuchs, H., Dub, W., Mensah, A., dal Maso, M., Tillmann, R., Dorn, H.-P., Brauers, T., and Cohen, R. C.: Organic nitrate and secondary organic aerosol yield from NO_3 oxidation of β-pinene evaluated using a gas-phase kinetics/aerosol partitioning model, Atmos. Chem. Phys., 9, 14311449, doi: 10.5194/acp-9-1431-2009, 2009.

Fuzzi, S., Andreae, M., Huebert, B., Kulmala, M., Bond, T., Boy, M., Doherty, S., Guenther, A., Kanakidou, M., Kawamura, K., Kerminen, V.-M., Lohmann, U., Russell, L., and Posch, U.: Critical assessment of the current state of scientific knowledge, terminology, and research needs concerning the role of organic aerosols in the atmosphere, climate, and global change, Atmos. Chem. Phys., p. 20172038, 2006.

Gantt, B., Meskhidze, N., Facchini, M. C., Rinaldi, M., Ceburnis, D., and ODowd, C. D.: Wind speed dependent size-resolved parameterization for the organic mass fraction of sea spray aerosol, Atmos. Chem. Phys., 11, 8777–8790, doi:10.5194/acp-11-8777-2011, 2011.

Gantt, B., Johnson, M. S., Meskhidze, N., Sciare, J., Ovadnevaite, J., Ceburnis, D., and ODowd, C. D.: Model evaluation of marine primary organic aerosol emission schemes, Atmos. Chem. Phys., 12, 8553–8566, doi:10.5194/acp-12-8553-2012, 2012.

GENEMIS: Technical Report, EUROTEC, annual report 1993, 1994.

Gentner, D., Jathar, S., Gordon, T., Bahreini, R., Day, D., El Haddad, I., Hayes, P., Pieber, S., Platt, S., de Gouw, J., Goldstein, A., Harley, R., Jimenez, J., Prévôt, A., and Robinson, A.: Review of Urban Secondary Organic Aerosol Formation from Gasoline and Diesel Motor Vehicle Emissions, Environ. Sci. Technol., 51, 1074–1093, doi:10.1021/acs.est.6b04509, 2017.

Gerasopoulos, E., Zanis, P., Papastefanou, C., Zerefos, C., Ioannidou, A., and Wernli, H.: A complex case study of down to the surface intrusions of persistent stratospheric air over the Eastern Mediterranean, Atmos. Environ., 40, 4113–4125, doi:10.1016/j.atmosenv.2006.03.022, 2006.

Goix, S., Lévêque, T., Xiong, T.-T., Schreck, E., Baeza-Squiban, A., Geret, F., Uzu, G., Austruy, A., and Dumat, C.: Environmental and health impacts of fine and ultrafine metallic particles: Assessment of threat scores, Environ. Res., 133, 185–194, doi:10.1016/j.envres.2014.05.015, 2014.

Grell, G. A., Emeis, S., Stockwell, W. R., Schoenemeyer, T., Forkel, R., Michalakes, J., Knoche, R., and Seidl, W.: Application of a multiscale, coupled MM5/chemistry model to the complex terrain of the VOTALP valley campaign, Atmos. Environ., 34, 1435–1453, doi:10.1016/S1352-2310(99)00402-1, URL `http://www.sciencedirect.com/science/article/pii/S1352231099004021`, 2000.

Grell, G. A., Peckham, S. E., Schmitz, R., McKeen, S. A. Frost, G., Skamaro, W. C., , and Eder, B.: Fully coupled online chemistry within the WRF model, Atmos. Environ., 39, 6957–6975, doi:10.1016/j.atmosenv.2005.04.027, 2005.

Grieshop, A. P., Donahue, N. M., and Robinson, A. L.: Laboratory investigation of photochemical oxidation of organic aerosol from wood fires 2: analysis of aerosol mass spectrometer data, Atmos. Chem. Phys., 9, 22272240, doi:10.5194/acp-9-2227-2009, 2009.

Griffin, R. J., Nguyen, K., Dabdub, D., and Seinfeld, J. H.: A coupled hydrophobic-gydrophilic model for predicting secondary organic aerosol formatio, J. Atmos. Chem., 44, 171–190, doi: 10.1023/A:1022436813699, 2003.

Grosjean, D. and Friedlander, S.: Gas-particle distribution factors for organic and other pollutants in the Los Angeles atmosphere., J. Air Pollut. Control Assoc., 25, 1038–1044, 1975.

Gross, A. and Stockwell, W. R.: Comparison of the EMEP, RADM2 and RACM Mechanisms, J. Atmos. Chem., 44, 151–170, doi:10.1023/A:1022483412112, 2003.

Grythe, H., Strom, J., Krejci, R., Quinn, P., , and Stohl, A.: A review of sea-spray aerosol source functions using a large global set of sea salt aerosol concentration measurements, Atmos. Chem. Phys., 14, 1277–1297, 2014.

Guelle, W., Schulz, M., Balkanski, Y., and Dentener, F.: Influence of the source formulation on modeling the atmospheric global distribution of sea salt aerosol, J. Geophys. Res., 106(D21), 27 509–27 524, doi:10.1029/2001JD900249, 2001.

Guenther, A., Karl, T., Harley, P., Wiedinmyer, C., Palmer, P. I., and Geron, C.: Estimates of global terrestrial isoprene emissions using MEGAN (Model of Emissions of Gases and Aerosols from Nature), Atmos. Chem. Phys., 6, 3181–3210, doi:10.5194/acp-6-3181-2006, 2006.

Hatakeyama, S., Akimoto, H., and Washida, N.: Effect of temperature on the formation of photochemical ozone in a propene NO_x air irradiation system, J. Geophys. Res., 25, 18841890, 1991.

Hayes, P. L., Carlton, A. G., Baker, K. R., Ahmadov, R., Washenfelder, R. A., Alvarez, S., Rappenglck, B., Gilman, J. B., Kuster, W. C., de Gouw, J. A., Zotter, P., Prvt, A. S. H., Szidat, S., Kleindienst, T. E., Offenberg, J. H., Ma, P. K., and Jimenez, J. L.: Modeling the formation and aging of secondary organic aerosols in Los Angeles during CalNex 2010, Atmos. Chem. Phys., 15, 57735801, doi:10.5194/acp-15-5773-2015, 2015.

Hildebrandt, L., Donahue, N. M., and Pandis, S. N.: High formation of secondary organic aerosol from the photo-oxidation of toluene, Atmos. Chem. Phys., 9, 29732986, doi:10.5194/acp-9-2973-2009, 2009.

Hoffmann, T., Odum, J. R., Bowman, F., Collins, D., Klockow, D., Flagan, R. C., and Seinfeld, J. H.: Formation of organic aerosols from the oxidation of biogenic hydrocarbon, J. Atmos. Chem., 26, 189–222, doi:10.1023/A:1005734301837, 1997.

Hoppel, W., Fitzgerald, J., Frick, G., Larson, R., and Mack, E.: Atmospheric aerosol size distributions and optical properties in the marine boundary layer over the Atlantic Ocean, NRL report 9188, 1989.

Horowitz, L. W., Walters, S., Mauzerall, D. L., Emmons, L. K., Rasch, P. J., Granier, C., Tie, X., Lamarque, J.-F., Schultz, M. G., Tyndall, G. S., Orlando, J. J., and Brasseur, G. P.: A global simulation of tropospheric ozone and related tracers: Description and evaluation of MOZART, version 2, J. Geophys. Res., 108, 4784, doi:10.1029/2002JD002853, 2003.

Hoyle, C. R., Boy, M., Donahue, N. M., Fry, J. L., Glasius, M., Guenther, A., Hallar, A. G., Huff Hartz, K., Petters, M. D., Petja, T., Rosenoern, T., and Sullivan, A. P.: A review of the anthropogenic influence on biogenic secondary organic aerosol, Atmos. Chem. Phys., 11, 321–343, doi:10.5194/acp-11-321-2011, 2011.

Hu, C., Lee, Z., and Franz, B.: Chlorophyll-a algorithms for oligotrophic oceans: A novel approach based on three-band reflectance difference, Atmos. Environ., 117, doi:10.1029/2011JC007-395, c01011, 2012.

Hu, W. W., Campuzano-Jost, P., Palm, B. B., Day, D. A., Ortega, A. M., Hayes, P. L., Krechmer, J. E., Chen, Q., Kuwata, M., Liu, Y. J., de S, S. S., McKinney, K., Martin, S. T., Hu, M., Budisulistiorini, S. H., Riva, M., Surratt, J. D., St. Clair, J. M., Isaacman-Van Wertz, G., Yee, L. D., Goldstein, A. H., Carbone, S., Brito, J., Artaxo, P., de Gouw, J. A., Koss, A., Wisthaler, A., Mikoviny, T., Karl, T., Kaser, L., Jud, W., Hansel, A., Docherty, K. S., Alexander, M. L., Robinson, N. H., Coe, H., Allan, J. D., Canagaratna, M. R., Paulot, F., and Jimenez, J. L.: Characterization of a real-time tracer for isoprene epoxydiols-derived secondary organic aerosol (IEPOX-SOA) from aerosol mass spectrometer measurements, Atmos. Chem. Phys., 15, 11 807–11 833, doi:10.5194/acp-15-11807-2015, 2015.

Huffman, J. A., Docherty, K. S., Mohr, C., Cubison, M. J., Ulbrich, I. M., Ziemann, P. J., Onasch, T. B., and Jimenez, J. L.: Chemically resolved volatility measurements of organic aerosol from different sources, Environ. Sci. Technol., 43(14), 53515357, doi:10.1021/Es803539d, 2009.

Jacobson, M. Z.: GATOR-GCMM: A global- through urban-scale air pollution and weather forecast model 1. Model design and treatment of subgrid soil, vegetation, roads, rooftops, water, sea ice, and snow, J. Geophys. Res., 106, 5385–5401, doi:10.1029/2000JD900560, 2001.

Jacobson, M. Z.: Fundamentals of Atmospheric Modeling, Cambridge University Press, 2nd edition, Cambridge, 2005.

Jaeglé, L., Quinn, P. K., Bates, T. S., Alexander, B., and Lin, J.-T.: Global distribution of sea salt aerosols: new constraints from in situ and remote sensing observations, Atmos. Chem. Phys., 11, 3137–3157, doi:10.5194/acp-11-3137-2011, 2011.

Janssens-Maenhout, G., Dentener, F., van Aardenne, J., Monni, S., Pagliari, V., Orlandini, L., Klimont, Z., Kurokawa, J., Akimoto, H., Ohara, T., Wankmller, R., Battye, B., Grano, D., Zuber, A., and Keating, T.: a Harmonized Gridded Air Pollution Emission Dataset Based on National Inventories, european Commission, Joint Research Centre, Institute for Environment and Sustainability (2012) available at http://dx.doi.org/10.2788/14102, 2012.

Jaoui, M. and Kamens, R. M.: Mass balance of gaseous and particulate products analysis from α-pinene, NO_x air in the presence of natural sunlight, J. Geophys. Res., 107, 12 541–12 558, 2001.

Jaoui, M., Kleindienst, T. E., Docherty, K. S., Lewandowski, M., , and Offenberg, J. H.: Secondary organic aerosol formation from the oxidation of a series of sesquiterpenes: α-cedrene, β-caryophyllene, α-humulene and α-farnesene with O_3, OH and NO_3-radicals, Environ. Chem., 10, 178–193, doi:10.1071/EN13025, 2013.

Jathar, S., Gordon, T., Henningan, C., Pye, H., Pouliot, G., Adams, P., Donahue, N., and Robinson, A.: Unspeciated organic emissions from combustion sources and their influence on the secondary organic aerosol budget in the United States. , Proc Natl Acad Sci, 111, 10 473–10 478, doi:10.1073/pnas.1323740111, 2014.

Jathar, S. H., Cappa, C. D., Wexler, A. S., Seinfeld, J. H., and Kleeman, M. J.: Multi-generational oxidation model to simulate secondary organic aerosol in a 3-D air quality model, Geosci. Model Dev., 8, doi:10.5194/gmd-8-2553-2015, 2015.

Jiang, H., Jang, M., Sabo-Attwood, T., and Robinson, S.: Oxidative potential of secondary organic aerosols produced from photooxidation of different hydrocarbons using outdoor chamber under ambient sunlight, Atmos. Environ., 131, 382–389, doi:10.1016/j.atmosenv.2016.02.016, 2016.

Jimenez, J. L., Canagaratna, M. R., Donahue, N. M., Prevot, A. S., Zhang, Q., Kroll, J. H., DeCarlo, P. F., Allan, J. D., Coe, H., Ng, N. L., Aiken, A. C., Docherty, K. D., Ulbrich, I., Grieshop, A. P., Robinson, A. L., Duplissy, J., Smith, J. D., Wilson, K. R., Lanz, V. A., Hueglin, C., Sun, Y. L., Tian, J., Laaksonen, A., Raatikainen, T., Rautiainen, J., Vaattovaara, P., Ehn, M., Kulmala, M., Tomlinson, J. M., Collins, D. R., Cubison, M. J., Dunlea, E. J., Huffman, J. A., Onasch, T. B., Alfarra, M. R., Williams, P. I., Bower, K., Kondo, Y., Schneider, J., Drewnick, F., Borrmann, S., Weimer, S., Demerjian, K., Salcedo, D., Cottrell, L., Griffin, R., Takami, A., Miyoshi, T., Hatakeyama, S., Shimono, A., Sun, J. Y., Zhang, Y. M., Dzepina, K., Kimmel, J. R., Sueper, D., Jayne, J. T., Herndon, S. C., Trimborn, A. M., Williams, L. R., Wood, E. C., Kolb, C. E., Middlebrook, A. M., Baltensperger, U., and Worsnop, D. R.: Evolution of organic aerosols in the atmosphere, Science, 326, 1525–1529, doi:10.1126/science.1180353, 2009.

Jokinen, T., Berndt, T., Makkonen, R., Kerminen, V., Junninen, H., Paasonen, P., Stratmann, F., Herrmann, H., Guenther, A. B., Worsnop, D. R., Kulmala, M., Ehn, M., and Sipilb, M.: Production of extremely low volatile organic compounds from biogenic emissions: Measured yields and atmospheric implications, Proc. Nat. Acad. Sci., 112, 7123–7128, doi:10.1073/pnas.1423977112, 2015.

Kanakidou, M., Seinfeld, J., Pandis, S., Barnes, I., Dentener, F., Facchini, M., Dingenen, R. V., Ervens, B., Nenes, A., Nielsen, C., Swietlicki, E., Putaud, J., Balkanski, Y., Fuzzi, S., Horth, J., Moortgat, G., Winterhalter, R., Myhre, C., Tsigaridis, K., Vignati, E., Stephanou, E., and Wilson, J.: Organic aerosol and global climate modeling: A review, Atmos. Chem. Phys., 5, 10531123, doi:10.5194/acp-5-1053-2005, 2005.

Kim, H., Kim, S., Kim, B.-U., Jin, C.-S., Hong, S., Park, R., Son, S.-W., Bae, C., Bae, M., Song, C.-K., and Stein, A.: Recent increase of surface particulate matter concentrations in the Seoul Metropolitan Area, Korea., Sci. Rep., 7, doi:10.1038/s41598-017-05092-8, 2017.

Kim, Y., Couvidat, F., Sartelet, K., and Seigneur, C.: Comparison of different gas-phase mechanisms and aerosol modules for simulating particulate matter formation, J. Air Waste Manage. Assoc., 61, 1218–1226, doi:10.1080/10473289.2011.603999, 2011a.

Kim, Y., Sartelet, K., and Seigneur, C.: Formation of secondary aerosols: impact of the gas-phase chemical mechanism, Atmos. Chem. Phys., 11, 583–598, doi:10.5194/acp-11-583-2011, 2011b.

Kim, Y., Sartelet, K., Raut, J.-C., and Chazette, P.: Evaluation of the Weather Research and Forecast/urban model over Greater Paris, Bound.-Layer Meteorol., 149, 105–132, doi:10.1007/s10546-013-9838-6, 2013.

Kim, Y., Sartelet, K., Seigneur, C., Charron, A., Besombes, J.-L., Jaffrezo, J.-L., Marchand, N., and Polo, L.: Effect of measurement protocol on organic aerosol measurements of exhaust emissions from gasoline and diesel vehicles, Atmos. Environ., 140, 176–187, doi: 10.1016/j.atmosenv.2016.05.045, 2016.

Koo, B., Knipping, E., and Yarwood, G.: 1.5-Dimensional volatility basis set approach for modeling organic aerosol in CAMx and CMAQ, Atmos. Environ., 95, 158–164, doi: 10.1016/j.atmosenv.2014.06.031, 2014.

Krechmer, J., Coggon, M., Massoli, P., Nguyen, T., Crounse, J., Hu, W., Day, D., Tyndall, G., Henze, D., Rivera-Rios, J., Nowak, J., Kimmel, J., Mauldin, R., Stark, H., Jayne, J., Sipila, M., Junninen, H., St.Clair, J., Zhang, X., Feiner, P., Zhang, L., Miller, D., Brune, W., Keutsch, F., Wennberg, P., Seinfeld, J., Worsnop, D., Jimenez, J., and Canagaratna, M.: Formation of low volatility organic compounds and secondary organic aerosol from isoprene hydroxyhydroperoxide low-NO oxidation, Environ. Sci. Technol., 49, doi:10.1021/acs.est.5b02031, 2015.

Kristensen, K., Cui, T., Zhang, H., Gold, A., Glasius, M., and Surratt, J. D.: Dimers in α-pinene secondary organic aerosol: effect of hydroxyl radical, ozone, relative humidity and aerosol acidity, Atmos. Chem. Phys., 14, 4201–4218, doi:10.5194/acp-14-4201-2014, 2014.

Kroll, J. H., Donahue, N. M., Jimenez, J. L., Kessler, S. H., Canagaratna, M., Wilson, K. R., Altieri, K. E., Mazzoleni, L. R., Wozniak, A. S., Bluhm, H., Mysak, E. R., Smith, J. D., E., K. C., and Worsnop, D. R.: Carbon oxidation state as a metric for describing the chemistry of atmospheric organic aerosol, Nature Chem., 3, 133139, doi:10.1038/NCHEM.948, 2011.

Lelieveld, J., Berresheim, H., Borrmann, S., Crutzen, P. J., Dentener, F. J., Fischer, J., Flatau, P. J., Heland, J., Holzinger, R., Korrmann, R., Lawrence, M. G., Levi, Z., Markowicz, K. M., Mihalopoulos, N., Minikin, A., Ramanathan, V., De Reus, M., Roelofs, G. J., Scheeren, H. A., Sciare, J., Schlager, H., Schultz, M., Seigmund, P., Steil, B., Stephanou, E. G., Steir, P., Traub, M., Warneke, C., Williams, J., and Ziereis, H.: Global air pollution crossroads over the Mediterranean, Science, 298, 794–799, 2002.

Liggio, J. and Li, S.-M.: Organosulfate formation during the uptake of pinonaldehyde on acidic sulfate aerosols, Geophys. Res. Lett., 33, doi:10.1029/2006GL026079, 2006.

Liggio, J., Li, S.-M., , and McLaren, R.: Heterogeneous reactions of glyoxal on particulate matter: Identification of acetals and sulfate esters, Environ. Sci. Technol., 39, 1532–1541, doi: 10.1021/es048375y, 2005.

Lin, J.-T., Martin, R. V., Boersma, K. F., Sneep, M., Stammes, P., Spurr, R., Wang, P., Van Roozendael, M., Clmer, K., and Irie, H.: Retrieving tropospheric nitrogen dioxide from the Ozone Monitoring Instrument: effects of aerosols, surface reflectance anisotropy, and vertical profile of nitrogen dioxide, Atmos. Chem. Phys., 14, 14411461, doi:10.5194/acp-14-1441-2014, 2014.

Lipsky, E. M. and Robinson, A. L.: Effects of dilution on fine particle mass and partitioning of semivolatile organics in diesel exhaust and wood smoke, Environ. Sci. Technol., 40(1), 155162, doi:10.1021/Es050319p, 2006.

Liu, J., DAmbro, E. L., Lee, B. H., Lopez-Hilfiker, F., Zaveri, R., Rivera-Rios, J. C., Keutsch, F. N., Iyer, S., Kurtn, T., Zhang, Z., Gold, A., Surratt, J. D., Shilling, J. E., and Thornton, J. A.: Efficient isoprene secondary organic aerosol formation from a non IEPOX pathway, Environ. Sci. Technol., 50, 98729880, doi:10.1021/acs.est.6b0187, 2016.

Liu, S., Shilling, J. E., Song, C., Hiranuma, N., Zaveri, R. A., and Russell, L.: Hydrolysis of Organonitrate Functional Groups in Aerosol Particle, Aerosol Sci. Technol., 46:12, 1359–1369, doi:10.1080/02786826.2012.716175, 2012.

Mallet, M., Dulac, F., Formenti, P., Nabat, P., Sciare, J., Roberts, G., Pelon, J., Ancellet, G., Tanr, D., Parol, F., di Sarra, A., Alados, L., Arndt, J., Auriol, F., Blarel, L., Bourrianne, T., Brogniez, G., Chazette, P., Chevaillier, S., Claeys, M., DAnna, B., Denjean, C., Derimian, Y., Desboeufs, K., Di Iorio, T., Doussin, J. F., Durand, P., Fron, A., Freney, E., Gaimoz, C., Goloub, P., GÓmez-Amo, J. L., Granados-Muñoz, M. J., Grand, N., Hamonou, E., Jankowiak, I., Jeannot, M., Léon, J.-F., Maillé, M., Mailler, S., Meloni, D., Menut, L., Momboisse, G., Nicolas, J., Podvin, J., Pont, V., Rea, G., Renard, J.-B., Roblou, L., Schepanski, K., Schwarzenboeck, A., Sellegri, K., Sicard, M., Solmon, F., Somot, S., Torres, B., Totems, J., Triquet, S., Verdier, N., Verwaerde, C., Wenger, J., and Zapf, P.: Overview of the chemistryaerosol mediterranean experiment/aerosol direct radiative forcing on the mediterranean climate (charmex/adrimed) summer 2013 campaign, Atmos. Chem. Phys. Discuss., 125(14), 619 615–19 727, doi:10.5194/acpd-15-19615-2015, 2012.

Mallet, M., Dulac, F., Formenti, P., Nabat, P., Sciare, J., Roberts, G., Pelon, J., Ancellet, G., Tanr, D., Parol, F., Denjean, C., Brogniez, G., di Sarra, A., Alados-Arboledas, L., Arndt, J., Auriol, F., Blarel, L., Bourrianne, T., Chazette, P., Chevaillier, S., Claeys, M., D'Anna, B., Derimian, Y., Desboeufs, K., Di Iorio, T., Doussin, J.-F., Durand, P., Fron, A., Freney, E., Gaimoz, C., Goloub, P., Gmez-Amo, J. L., Granados-Muoz, M. J., Grand, N., Hamonou, E., Jankowiak, I., Jeannot, M., Lon, J.-F., Maill, M., Mailler, S., Meloni, D., Menut, L., Momboisse, G., Nicolas, J., Podvin, T., Pont, V., Rea, G., Renard, J.-B., Roblou, L., Schepanski, K., Schwarzenboeck, A., Sellegri, K., Sicard, M., Solmon, F., Somot, S., Torres, B., Totems, J., Triquet, S., Verdier, N., Verwaerde, C., Waquet, F., Wenger, J., and Zapf, P.: Overview of the Chemistry-Aerosol Mediterranean Experiment/Aerosol Direct Radiative Forcing on the Mediterranean Climate (ChArMEx/ADRIMED) summer 2013 campaign, Atmos. Chem. Phys., 16, 455–504, doi:10.5194/acp-16-455-2016, 2016.

Mallet, V. and Sportisse, B.: A comprehensive study of ozone sensitivity with respect to emissions over Europe with a chemistry-transport model, J. Geophys. Res., 110, D22302, doi: 10.1029/2005JD006234, 2005.

Mallet, V. and Sportisse, B.: Uncertainty in a chemistry-transport model due to physical parameterizations and numerical approximations: An ensemble approach applied to ozone modeling, J. Geophys. Res., 111, D01 302, doi:10.1029/2005JD006149, 2006.

Mallet, V., Quélo, D., and Sportisse, B.: Software architecture of an ideal modeling platform in air quality, A first step: Polyphemus, available from http://cerea.enpc.fr/polyphemus/doc/references/mallet_et_al-polyphemus-r1.pdf, 2005.

May, A., Levin, E., Hennigan, C., Riipinen, I., Lee, T., Collett Jr., J., Jimenez, J., Kreidenweis, S., and Robinson, A.: Gas-particle partitioning of primary organic aerosol emissions: 3. Biomass burning., JournalofGeophysicalResearch, 118, 11 327–11 338, doi:10.1002/jgrd.50828, 2013a.

May, A., Presto, A., Hennigan, C., Nguyen, N., Gordon, T., and Robinson, A.: Gas-particle partitioning of primary organic aerosol emissions: (1) Gasoline vehicle exhaust., Atmos. Environ., 77, 128 – 139, doi:10.1016/j.atmosenv.2013.04.060, 2013b.

May, A., Presto, A., Hennigan, C., Nguyen, N., Gordon, T., and Robinson, A.: Gas-Particle Partitioning of Primary Organic Aerosol Emissions: (2) Diesel Vehicles., Environ. Sci. Technol., 47, 8288–8296, doi:10.1021/es400782j, 2013c.

May, A. A., Levin, E. J. T., Hennigan, C. J., Riipinen, I., Lee, T., Collett, J. L., Jimenez, J. L., Kreidenweis, S. M., and Robinson, A. L.: Gas-particle partitioning of primary organic aerosol emissions: 3. Biomass burning, J. Geophys. Res.-Atmos., 118, 11 327–11 338, doi:10.1002/jgrd.50828, 2013d.

Memmesheimer, M., Friese, E., Ebel, A., Jakobs, H. J., Feldmann, H., Kessler, C., and Piekorz, G.: Long-term simulations of particulate matter in Europe on different scales using sequential nesting of a regional model, Int. J. Environm. and Pollution, 22, 108–132, 2004.

Menut, L., Rea, G., Mailler, S., Khvorostyanov, D., and Turquety, S.: Aerosol forecast over the Mediterranean area during July 2013 (ADRIMED/CHARMEX), Atmos. Chem. Phys., 15, 78977911, doi:10.5194/acp-15-7897-2015, 2015.

Michoud, V., Sciare, J., Sauvage, S., Dusanter, S., Léonardis, T., Gros, V., Kalogridis, C., Zannoni, N., Féron, A., Petit, J.-E., Crenn, V., Baisnée, D., Sarda-Estève, R., Bonnaire, N., Marchand, N., DeWitt, H., Pey, J., Colomb, A., Gheusi, F., Szidat, S., Stavroulas, I., Borbon, A., and Locoge, N.: Organic carbon at a remote site of the western Mediterranean Basin: sources and chemistry during the ChArMEx SOP2 field experiment, Atmos. Chem. Phys., 17, 88378865, doi:10.5194/acp-17-8837-2017, 2017.

Millán, M. M., Salvador, R., Mantilla, E., and Kallos, G.: Photooxidant dynamics in the Mediterranean basin in summer: results from European research projects, Geophys. Res. Lett., 102, 88118823, 1997.

Minguillón, M., Perron, N., Querol, X., Szidat, S., Fahrni, S., Alastuey, A., Jimenez, J., Mohr, C., Ortega, A., Day, D., Lanz, V., Wacker, L., Reche, C., Cusack, M., Amato, F., Kiss, G., Hoffer, A., Decesari, S., Moretti, F., Hillamo, R., Teinilä, K., Seco, R., Peñuelas, J., Metzger, A., Schallhart, S., Müller, M., Hansel, A., Burkhart, J., Baltensperger, U., and Prévôt, A.: Fossil versus contemporary sources of fine elemental and organic carbonaceous particulate matter during the DAURE campaign in Northeast Spain., Atmos. Chem. Phys., 11, 12 067–12 084, doi:10.5194/acp-11-12067-2011, 2011.

Minguillón, M., Pérez, N., Marchand, N., Bertrand, A., Temime-Roussel, B., Agrios, K., Szidat, S., van Drooge, B., Sylvestre, A., Alastuey, A., Reche, C., Ripoll, A., Marco, E., Grimalt, J., and Querol, X.: Secondary organic aerosol origin in an urban environment: influence of biogenic and fuel combustion precursors, Faraday Discuss., 189, 337–359, doi:10.1039/c5fd00182j, 2016.

Molteni, U., Bianchi, F., Klein, F., El Haddad, I., Frege, C., Rossi, M., Dommen, J., , and Baltensperger, U.: Formation of highly oxygenated organic molecules from aromatic compounds., Atmos. Chem. Phys., doi:10.5194/acp-2016-1126, 2018.

Monahan, E. C., Spiel, D. E., and Davidson, K. L.: A model of marine aerosol generation via whitecaps and wave disruption, in: Oceanic whitecaps and their role in air-sea exchange processes, pp. 167–174, D. Reidel, Netherlands, 1986.

Monks, P. S., Granier, C., Fuzzi, S., Stohl, A., Williams, M. L., Akimoto, H., Amann, M., Baklanov, A., Baltensperger, U., Bey, I., Blake, N., Blake, R. S., Carslaw, K., Cooper, O. R., Dentener, F., Fowler, D., Fragkou, E., Frost, G. J., Generoso, S., Ginoux, P., Grewe, V., Guenther, A., Hansson, H. C., Henne, S., Hjorth, J., Hofzumahaus, A., Huntrieser, H., Isaksen, I. S. A., Jenkin, M. E., Kaiser, J., Kanakidou, M., Klimont, Z., Kulmala, M., Laj, P., Lawrence, M. G., Lee, J. D., Liousse, C., Maione, M., Mciggans, G., Metzger, A., Mieville, A., Moussiopoulos, N., Orlando, J. J., ODowd, C. D., Palmer, P. I., Parrish, D. D., Petzold, A., Platt, U., Poschl, U., Prévôt, A. S. H., Reeves, C. E., Reimann, S., Rudich, Y., Sellegri, K., Steinbrecher, R., Simpson, D., ten Brinkt, H., Theloke, J., vander Werf, G. R., Vautard, R., Vestreng, V., Vlachokostas, C., and von Glasow, R.: Atmospheric composition change - Global and regional air quality, Atmos. Environ., 43, 5268–5350, doi:10.1016/j.atmosenv.2009.08.021, 2009.

Morris, R., Yarwood, G., Emery, C., Koo, B., and Wilson, G. M.: Development of the CAMx one-atmosphere air quality model to treat ozone, particulate matter, visibility and air toxics and application for State Implementation Plans (SIPs), aWMA specialty conference, Guideline on air quality models: The path forward, available at `http://www.camx.com/publ/pdfs/AWMA_AQGuidelines03_Paper9_CAMx.pdf`, 2003.

Moulin, C., Lambert, C. E., Dayan, U., Masson, V., Ramonet, M., Bousquet, P., Legrand, M., Balkanski, Y., Guelle, W., Marticorena, B., Bergametti, G., and Dulac, F.: Satellite climatology of African dust transport in the Mediterranean atmosphere, J. Geophys. Res., 103(D11), 13 137–13 144, doi:10.1029/98JD00171, 1998.

Murphy, B., Donahue, N., Fountoukis, C., Dall'Osto, M., O'Dowd, C., Kiendler-Scharr, A., and Pandis, S. N.: Functionalization and fragmentation during ambient organic aerosol aging: application of the 2-D volatility basis set to field studies, Atmos. Chem. Phys., 12, 10 797–10 816, doi:10.5194/acp-12-10797-2012, 2012.

Murphy, B., Woody, M., Jimenez, J., Carlton, A., Hayes, P., Liu, S., Ng, N., Russell, L., Setyan, A., Xu, L., Young, J., Zaveri, R., Zhang, Q., and Pye, H.: Semivolatile POA and parameterized total combustion SOA in CMAQv5.2: impacts on source strength and partitioning., Atmos. Chem. Phys., 17, 11 107–11 133, doi:10.5194/acp-17-11107-2017, 2017.

Murphy, B. N., Donahue, N. M., Fountoukis, C., and Pandis, S. N.: Simulating the oxygen content of ambient organic aerosol with the 2D volatility basis set, Atmos. Chem. Phys., 11, 7859–7873, doi:10.5194/acp-11-7859-2011, 2011.

Murphy, D. M., Cziczo, D. J., Froyd, K. D., Hudson, P. K., Matthew, B. M., Middlebrook, A. M., Peltier, R. E., Sullivan, A., Thomson, D. S., and Weber, R. J.: Single-particle mass spectrometry of tropospheric aerosol particles, J. Geophys. Res., 11, 23–32, doi:10.1029/2006JD007340, 2006.

Mutzel, A., Poulain, L., Berndt, T., Iinuma, Y., Rodigast, M., Bge, O., Richters, S., Spindler, G., Sipil, M., Jokinen, T., Kulmala, M., , and Herrmann, H.: Highly oxidized multifunctional organic compounds observed in tropospheric particles: A field and laboratory study, Environ. Sci. Technol., 49, 77547761, doi:10.1021/acs.est.5b00885, 2015.

Mnard, S.: Development of a new Canadian operational air quality forecast model GEM-MACH, national air quality conferences: air quality forecasting, mapping, and monitoring and communicating air quality and communities in motion, Orlando, available at: `http://www.epa.gov/airnow/2007conference/wednesday/menard_s.ppt`, 2007.

Mller, L., Reinnig, M.-C., Naumann, K., Saathoff, H., Mentel, T., Donahue, N. M., and Hoffmann, T.: Formation of 3-methyl-1,2,3-butanetricarboxylic acid via gas phase oxidation of pinonic acid - a mass spectrometric study of SOA aging, Atmos. Chem. Phys., 12, 1483–1496, doi:10.5194/acp-12-1483-2012, 2012.

Nah, T., McVay, A. C., Zhang, X., Boyd, C. M., Seinfeld, J. H., and Ng, N. L.: Influence of seed aerosol surface area and oxidation rate on vapor wall deposition and SOA mass yields: a case study with α-pinene ozonolysis, Atmos. Chem. Phys., 16, 9361–9379, doi:10.5194/acp-16-9361-2016, 2016.

Nenes, A., Pandis, S. N., and Pilinis, C.: ISORROPIA: A new thermodynamic equilibrium model for multiphase multicomponent inorganic aerosols, Aquat. Geochem., 4, 123–152, doi: 10.1023/A:1009604003981, 1998.

Ng, N. L., Chhabra, P. S., Chan, A. W. H., Surratt, J. D., Kroll, J. H., Kwan, A. J., McCabe, D. C., Wennberg, P. O., Sorooshian, A., Murphy, S. M., Dalleska, N. F., Flagan, R. C., and Seinfeld, J. H.: Effect of NO_x level on secondary organic aerosol (SOA) formation from the photooxidation of terpenes, Atmos. Chem. Phys., 7, 5159–5174, doi:10.5194/acp-7-5159-2007, 2007.

Ng, N. L., Herndon, S. C., Trimborn, A., Canagaratna, M. R., Croteau, P. L., Onasch, T. B., Sueper, D., Worsnop, D. R., Zhang, Q., Sun, Y. L., and Jayne, J. T.: An Aerosol Chemical Speciation Monitor (ACSM) for Routine Monitoring of the Composition and Mass Concentrations of Ambient Aerosol, Aerosol Sci. Technol., 45, 780794, doi:10.1080/02786826.2011.560211, 2011.

Nguyen, T. B., Coggon, M. M., Bates, K. H., Zhang, X., Schwantes, R. H., Schilling, K. A., Loza, C. L., Flagan, R. C., Wennberg, P. O., and Seinfeld, J. H.: Organic aerosol formation from the reactive uptake of isoprene epoxydiols (IEPOX) onto non-acidified inorganic seeds, Atmos. Chem. Phys., 14, 3497–3510, doi:10.5194/acp-14-3497-2014, 2014.

Nicolas, J.: Caractérisation physico-chimique de laérosol troposphérique en Méditerranée : sources et devenir, Thse de Doctorat, Univ. Versailles-Saint-Quentin-en-Yvelines, 2013.

Nilsson, E. D., Rannik, U., Buzorius, G., Kulmala, M., and ODowd, C.: Effects of the continental boundary layer evolution, convection, turbulence and entrainment on aerosol formation, Tellus B, 53, 441461, 2001.

Odum, J. R., Hoffmann, T., Bowman, F., Collins, D., Flagan, R. C., and Seinfeld, J. H.: Gas/particle partitioning and secondary organic aerosol yields, Environ. Sci. Technol., 30, 2580–2585, doi:10.1021/es950943+, 1996.

Ots, R., Young, D., Vieno, M., Xu, L., Dunmore, R., Allan, J., Coe, H., Williams, L., Herndon, S., Ng, N., Hamilton, J., Begström, R., Di Marco, C., Nemitz, E., Mackenzie, I., Kuenen, J., Green, D., Reis, S., and Heal, M.: Simulating secondary organic aerosol from missing diesel-related intermediate-volatility organic compound emissions during the Clean Air for London (ClearfLo) campaign., Atmos. Chem. Phys., 16, 6453–6473, doi:10.5194/acp-16-6453-2016, 2016.

ODowd, C. D., Facchini, M. C., Cavalli, F., Ceburnis, D., Mircea, M., Decesari, S., Fuzzi, S., Yoon, Y. J., and Putaud, J. P.: Biogenically driven organic contribution to marine aerosol, Nature, 431, 676–680, doi:10.1038/nature02959, 2004.

ODowd, C. D., Langmann, B., Varghese, S., Scannell, C., Ceburnis, D., and Facchini, M.: A combined organic-inorganic sea-spray source function, Geophys. Res. Lett., 35, doi: 10.1029/2007GL030331, l01801, 2008.

Pankow, J. F.: An absorption model of gas/particle partitioning of organic compounds in the atmosphere, Atmos. Environ., 28, 185–188, doi:10.1016/1352-2310(94)90093-0, 1994.

Passant, N.: Speciation of UK emissions of non-methane volatile organic compounds, AEA Technology, AEAT/ENV/0545, available at: http://uk-air.defra.gov.uk/reports/empire/AEAT_ENV_0545_final_v2.pdf, 2002.

Pilinis, C., Capaldo, K. P., Nenes, A., and Pandis, S. N.: MADM-A new Multicomponent Aerosol Dynamics Model, Aerosol Sci. Technol., 32, 482–502, 2000.

Pope, C.: Invited commentary: particulate matter-mortality exposureresponse relations and threshold, AmJEpidemiol, 152, 407–412, 2000.

Praplan, A. P., Schobesberger, S., Bianchi, F., Rissanen, M. P., Ehn, M., Jokinen, T., Junninen, H., Adamov, A., Amorim, A., Dommen, J., Duplissy, J., Hakala, J., Hansel, A., Heinritzi, M., Kangasluoma, J., Kirkby, J., Krapf, M., Krten, A., Lehtipalo, K., Riccobono, F., Rondo, L., Sarnela, N., Simon, M., Tom, A., Trstl, J., Winkler, P. M., Williamson, C., Ye, P., Curtius, J., Baltensperger, U., Donahue, N. M., Kulmala, M., , and Worsnop, D. R.: Elemental composition and clustering behaviour of α-pinene oxidation products for different oxidation conditions, Atmos. Chem. Phys., 15, 4145–4159, doi:10.5194/acp-15-4145-2015, 2015.

Presto, A. A. and Donahue, N. M.: Investigation of alpha-pinene plus ozone secondary organic aerosol formation at low total aerosol mass, Environ. Sci. Technol., 40, 35393543, 2006.

Pun, B. K., Seigneur, C., and Lohman, K.: Modeling secondary organic aerosol formation via multiphase partitioning with molecular data, Environ. Sci. Technol., 40, 4722–4731, doi: 10.1021/es0522736, 2006.

Putaud, J.-P., Raes, F., Van Dingenen, R., Brueggemann, E. Facchini, M. C., Decesari, S., Fuzzi, S., Gehrig, R., Hueglin, C., Laj, P., Lorbeer, G., Maenhaut, W., Mihalopoulos, N., Mueller, K., Querol, X., Rodriguez, S., Schneider, J., Spindler, G., ten Brink, H., Trseth, K., and Wiedensohler, A. A.: European aerosol phenomenology-2: chemical characteristics of particulate matter at kerbside, urban rural and background sites in Europe, Atmos. Environ., 38, 2579–2595, 2004.

Pye, H., Chan, A. W. H., Barkley, M. P., and Seinfeld, J. H.: Global modeling of organic aerosol: the importance of reactive nitrogen (NO_x and NO_3), Atmos. Chem. Phys., 10, 11 261–11 276, doi:10.5194/acp-10-11261-2010, 2010.

Pye, H., Luecken, D. J., Xu, L., Boyd, C., Ng, N., Baker, K., Ayres, B., Bash, J., Baumann, K., Carter, W., Edgerton, E., Fry, J., Hutzell, W., Schwede, D., and Shepson, P.: Modelling the current and the future roles of particulate organic nitrates in the southeastern United States, Environ. Sci. Technol., 49, 14 195–14 203, doi:10.1021/acs.est.5b03738, 2015.

Pye, H. O. T. and Seinfeld, J. H.: A global perspective on aerosol from low-volatility organic compounds, Atmos. Chem. Phys., 10, 4377–4401, doi:https://doi.org/10.5194/acp-10-4377-2010, 2010.

Rattanavaraha, W., Rosen, E., Zhang, H., Li, Q., Pantong, K., and Kamens, R.: The Reactive Oxidant Potential of Different Types of Aged Atmospheric Particles: An Outdoor Chamber Study, Atmos. Environ., 45, 3848–3855, doi:10.1016/j.atmosenv.2011.004.02, 2011.

Rea, G., Turquety, S., Menut, L., Briant, R., Mailler, S., and Siour, G.: Source contributions to 2012 summertime aerosols in the Euro-Mediterranean region, Atmos. Chem. Phys., 15, 80138036, doi:10.5194/acp-15-8013-2015, 2015.

Rissanen, M., Kurtn, T., Sipil, M., Thornton, J., Kausiala, O., Garmash, O., Kjaergaard, H., Petaja, T., Worsnop, D., Ehn, M., and Kulmala, M.: Effects of chemical complexity on the autoxidation mechanisms of endocyclic alkene ozonolysis products: from Methylcyclohexenes toward understanding α-pinene, J. Phys. Chem., 119, 4633–4650, doi:10.1021/jp510966g, 2015.

Robinson, A. L., Donahue, N. M., Shrivastava, M. K., Weitkamp, E. A., Sage, A. M., Grieshop, A. P., Lane, T. E., Pierce, J. R., and Pandis, S. N.: Rethinking Organic Aerosols: Semivolatile Emissions and Photochemical Aging, Science, 315, 1259–1262, doi:10.1126/science.1133061, 2007a.

Robinson, A. L., Donahue, N. M., Shrivastava, M. K., Weitkamp, E. A., Sage, A. M., Grieshop, A. P., Lane, T. E., Pierce, J. R., and Pandis, S. N.: Rethinking Organic Aerosols: Semivolatile Emissions and Photochemical Aging, Science, 315, 1259–1262, doi:10.1126/science.1133061, 2007b.

Roustan, Y., Pausader, M., and Seigneur, C.: Estimating the effect of on-road vehicle emission controls on future air quality in Paris, France, Atmospheric Environment, 45, 6828–6836, doi:10.1016/j.atmosenv.2010.10.010, URL `http://www.sciencedirect.com/science/article/pii/S1352231010008721`, 2010a.

Roustan, Y., Sartelet, K., Tombette, M., Debry, É., and Sportisse, B.: Simulation of aerosols and gas-phase species over Europe with the Polyphemus system. Part II: Model sensitivity analysis for 2001, Atmos. Environ., 44, 4219–4229, doi:10.1016/j.atmosenv.2010.07.005, 2010b.

Saathoff, H., Naumann, K.-H., Mohler, O., Jonsson, A. M., Hallquist, M., Kiendler-Scharr, A., Mentel, T. F., Tillmann, R., and Schurath, U.: Temperature dependence of yields of secondary organic aerosols from the ozonolysis of α-pinene and limonene, Atmos. Chem. Phys., 9, 15511577, doi:10.5194/acp-9-1551-2009, 2009.

Sartelet, K., Couvidat, F., Seigneur, C., and Roustan, Y.: Impact of biogenic emissions on air quality over Europe and North America, Atmos. Environ., 53, 131–141, 2012.

Sartelet, K. N., Debry, E., Fahey, K., Roustan, Y., Tombette, M., and Sportisse, B.: Simulation of aerosols and related species over Europe with the Polyphemus system. Part I: model-to-data comparison for 2001, Atmos. Environ., 41, 6116–6131, doi:10.1016/j.atmosenv.2007.04.024, 2007.

Saxena, P. and Hildemann, L. M.: Water-soluble organics in atmospheric particles: A critical review of the literature and application of thermodynamics to identify candidate compounds, J. Atmos. Chem., 24, 57109, 1996.

Schaap, M. M., Kunst, A. E., Leinsalu, M., Regidor, E., Ekholm, O., Dzurova, D., Helmert, U., Klumbiene, J., Santana, P., and Mackenbach, J.: Effect of nationwide tobacco control policies on smoking cessation in high and low educated groups in 18 European countries, BMJ, 17(4), 248–255, doi:10.1136/tc.2007.024265, 2008.

Schell, B., Ackermann, I. J., Hass, H., Binkowski, F. S., and Ebel, A.: Modeling the formation of secondary organic aerosol within a comprehensive air quality model system, J. Geophys. Res., 106, 28 275??8293, doi:10.1029/2001JD000384, 2001.

Schwier, A., Sellegri, K., Mas, S., Charrière, B., Pey, J., Rose, C., Temime-Roussel, B., Parin, D., Jaffrezo, J.-L., Picard, D., Sempéré, R., Marchand, N., and DAnna, B.: Primary marine aerosol physical and chemical emissions during a nutriment enrichment experiment in mesocosms of the Mediterranean Sea, Atmos. Chem. Phys. Discuss., doi:10.5194/acp-2017-320, 2017.

Schwier, A. N., Rose, C., Asmi, E., Ebling, A. M., Landing, W. M., Marro, S., Pedrotti, M.-L., Sallon, A., Iuculano, F., Agusti, S., Tsiola, A., Pitta, P., Louis, J., Guieu, C., Gazeau, F., , and Sellegri, K.: Primary marine aerosol emissions from the Mediterranean Sea during pre-bloom and oligotrophic conditions: correlations to seawater chlorophyll a from a mesocosm study, Atmos. Chem. Phys., pp. 7961–7976, doi:10.5194/acp-15-7961-2015, 2015.

Sciare, J., d'Argouges, O., Sarda-Estve, R., Gaimoz, C., Dolgorouky, C., Bonnaire, N., Favez, O., Bonsang, B., and Gros, V.: Large contribution of water-insoluble secondary organic aerosols in the region of Paris (France) during wintertime, J. Geophys. Res., 116, doi:10.1029/2011JD015756, d22203, 2011.

Seinfeld, J. and Pandis, S.: Atmospheric Chemistry and Physics: From Air Pollution to Climate Change, Wiley, New York, 2nd Ed., 2006a.

Seinfeld, J. and Pandis, S.: Atmospheric Chemistry and Physics: From Air Pollution to Climate Change, Wiley, New York, 2nd Ed., 2006b.

Seinfeld, J. H., Erdakos, G. B., Asher, W. E., and Pankow, J. F.: Modeling the formation of secondary organic aerosol (SOA), 2, The predicted effects of relative humidity on aerosol formation in the α-pinene, β-pinene, sabinene, δ^3-carene-, and cyclohexene-ozone systems, Environ. Sci. Technol., 35, 1806–18 171, 2001.

Shilling, J. E., Chen, Q., King, S. M., Rosenoern, T., Kroll, J. H., Worsnop, D. R., , DeCarlo, P. F. Aiken, A. C., Sueper, D., Jimenez, J. L., and Martin, S. T.: Loading-dependent elemental composition of a-pinene SOA particles, Atmos. Chem. Phys., 9, 771782, doi:10.5194/acp-9-771-2009, 2009.

Shrivastava, M., Easter, R. C., Liu, X., Zelenyuk, A., Singh, B., Zhang, K., Ma, P.-L., Chand, D., Ghan, S., Jimenez, J. L., Zhang, Q., Fast, J., Rasch, P. J., and Tiitta, P.: Global transformation and fate of SOA: Implications of low-volatility SOA and gas-phase fragmentation reactions, J. Geophys. Res.-Atmos., 120, 41694195, doi:10.1002/2014JD022563, 2015.

Shrivastava, M., Cappa, C., Fan, J., Goldstein, A., Guenther, A., Jimenez, J., Kuang, C., Laskin, A., Martin, S., Ng, N., Petaja, T., Pierce, J., Rasch, P., Roldin, P., Seinfeld, J., Shilling, J., Smith, J., Thornton, J., Volkamer, R., Wang, J., Worsnop, D., Zaveri, R., Zelenyuk, A., and Zhang, Q.: Recent advances in understanding secondary organic aerosol: Implications for global climate forcing, Rev. Geophys., 55, 509–559, doi:10.1002/2016RG000540, 2017.

Sic, B., El Amraoui, L., Piacentini, A., Marcal, V., Emili, E., Cariolle, D., Prather, M., and Attie, J. L.: Aerosol data assimilation in the chemical transport model MOCAGE during the TRAQA/ChArMEx campaign: aerosol optical depth, Atmos. Meas. Tech., 9, 5535–5554, 2016.

Simpson, D., Winiwarter, W., Börjesson, G., Cinderby, S., Ferreiro, A., Guenther, A., Hewitt, C. N., Janson, R., Aslam, M., Khalil, K., Owen, S., Pierce, T. E., Puxbaum, H., Shearer, M., Skiba, U., Steinbrecher, R., Tarrasón, L., and Öquist, M. G.: Inventorying emissions from nature in Europe, J. Geophys. Res., 104, 8113–8152, 1999.

Skamarock, W., Klemp, J., Dudhia, J., Gill, D., Barker, D., Duda, M., Huang, X., Wang, W., and Powers, J.: A description of the advanced research WRF version 3. NCAR Technical Note, NCAR/TN\ u2013475? STR, 123 pp, 2008.

Sofiev, M., Soares, J., Prank, M., de Leeuw, G., and Kukkonen, J.: A regional-to-global model of emission and transport of sea salt particles in the atmosphere, J. Geophys. Res., 116, D21 302, doi:10.1029/2010JD014713, 2011.

Solazzo, E., Bianconi, R., Hogrefe, C., Curci, G., Tuccella, P., Alyuz, U., Balzarini, A., Baró, R., Bellasio, R., Bieser, J., Brandt, J., Christensen, J., Colette, A., Francis, X., Fraser, A., Vivanco, M., Jiménez-Guerrero, P., Im, U., Manders, A., Nopmongcol, U., Kitwiroon, N., Pirovano, G., Pozzoli, L., Prank, M., Sokhi, R., Unal, A., Yarwood, G., and Galmarini, S.: Evaluation and error apportionment of an ensemble of atmospheric chemistry transport modeling systems: multi-variable temporal and spatial breakdown., Atmos. Chem. Phys., 17, 3001–3054, doi:10.5194/acp-17-3001-2017, 2017.

Sportisse, B.: A review of parameterizations for modelling dry deposition and scavenging of radionuclides, Atmos. Environ., 41, 2683–2698, doi:10.1016/j.atmosenv.2006.11.057, 2007.

Sportisse, B.: Pollution atmosphérique: des processus à la modélisation, Springer-Verlag France, Paris, 2008.

Squizzato, S., Masiol, M., Brunelli, A., Pistollato, S., Tarabotti, E., Rampazzo, G., and B., P.: Factors determining the formation of secondary inorganic aerosol : a case study in the po valley (italy), Atmos. Chem. Phys., 13(4), 19271939, doi:10.5194/ acp-13-1927-2013, 2013.

Stern, R., Kerschbaumer, A., and Reimer, E.: Description of the chemical transport model 'REM-CALGRID', 2007.

Stockwell, C. E., Veres, P. R., Williams, J., and Yokelson, R. J.: Characterization of biomass burning emissions from cooking fires, peat, crop residue, and other fuels with high-resolution proton-transfer-reaction time-of-flight mass spectrometry, Atmos. Chem. Phys., 15, 845–865, doi:10.5194/acp-15-845-2015, 2015.

Stockwell, W. R., Watson, J. G., , Robinson, N. F., and Steiner, Williamand Sylte, W. W.: The ammonium nitrate particle equivalent of NOx emissions for wintertime conditions in central californias san joaquin valley, Atmos. Environ., 34(27), 4711–4717, doi: http://dx.doi.org/10.1016/S1352-2310(00)00148-5, 2000.

Stull, R. B.: An introduction to boundary layer meteorology, Kluwer Academic Publishers, Dordrecht, 1988.

Surratt, J. D., Gómez-González, Y., Chan, A. W. H., Vermeylen, R., Shahgholi, M., Kleindienst, T. E., Edney, E. O., Offenberg, J. H., Lewandowski, M., Jaoui, M., Maenhaut, W., Claeys, M., Flagan, R. C., and Seinfeld, J. H.: Organosulfate formation in biogenic secondary organic aerosol, J. Phys. Chem., 112, 8345–8378, doi:10.1021/jp802310p, 2008.

Surratt, J. D., Chan, A. W. H., Eddingsaas, N. C., Chan, M., Loza, C. L., Kwan, A. J., Hershey, S. P., Flagan, R. C., Wennberg, P. O., and Seinfeld, J. H.: Reactive intermediates revealed in secondary organic aerosol formation from isoprene, Proc. Natl. Acad. Sci., 107, doi: 10.1073pnas.0911114107, 2010.

Svendby, T. M., Lazaridis, M., and Trseth, K.: Temperature dependent secondary organic aerosol formation from terpenes and aromatics, J. Atmos. Chem., 59, 25–46, doi:10.1007/s10874-007-9093-7, 2008.

Szmigielski, R., Surratt, J. D., Gomez-Gonzalez, Y., Van der Veken, P., Kourtchev, I., Vermeylen, R., Blockhuys, F., Jaoui, M., Kleindienst, T. E., Lewandowski, M., Offenberg, J. H., Edney, E. O., Seinfeld, J. H., Maenhaut, W., and Claeys, M.: 3-methyl-1,2,3-butanetricarboxylic acid: An atmospheric tracer for terpene secondary organic aerosol, Geophys. Res. Lett., 34, L24 811, doi:10.1029/2007GL03133, 2007.

Tang, W., Cohan, D. S., Morris, G. A., Byun, D. W., and Luke, W. T.: Influence of vertical mixing uncertainties on ozone simulation in CMAQ, Atmos. Environ., 45, 2898–2909, 2011.

Tang, Y., Carmichael, G. R., Uno, I., Woo, J.-H., Kurata, G., Lefer, B., Shetter, R. E., Huang, H., Anderson, B. E., Avery, M. A., Clarke, A. D., , and Blake, D. R.: Impacts of aerosols and clouds on photolysis frequencies and photochemistry during TRACE-P: 2. Three-dimensional study using a regional chemical transport model, J. Geophys. Res., 108(D21), 8822, doi:10.1029/2002JD003100, 2003.

Troen, I. B. and Mahrt, L.: A simple model of the atmospheric boundary layer; sensitivity to surface evaporation, Bound.-Layer Meteorol., 37, 129–148, doi:10.1007/BF00122760, 1986.

Tsimpidi, A. P., Karydis, V. A., Zavala, M., Lei, W., Molina, L., Ulbrich, I. M., Jimenez, J. L., and Pandis, S. N.: Evaluation of the volatility basis-set approach for the simulation of organic aerosol formation in the Mexico City metropolitan area, Atmos. Chem. Phys., 10, 525546, doi: 10.5194/acp-10-525-2010, 2010.

Tsimpidi, A. P., Karydis, V. A., Pozzer, A., Pandis, S. N., and Lelieveld, J.: ORACLE (v1.0): module to simulate the organic aerosol composition and evolution in the atmosphere, Geosci. Model Dev., 7, 31533172, doi:https://doi.org/10.5194/gmd-7-3153-2014, 2014.

Tuet, W. Y., Chen, Y., Xu, L., Fok, S., Gao, D., Weber, R. J., and Ng, N. L.: Chemical oxidative potential of secondary organic aerosol (SOA) generated from the photooxidation of biogenic and anthropogenic volatile organic compounds, Atmos. Chem. Phys., 17, 839–853, doi:10.5194/acp-17-839-2017, 2017.

Turpin, B. and Lim, H.-J.: Species Contributions to PM2.5 Mass Concentrations: Revisiting Common Assumptions for Estimating Organic Mass., Aerosol Sci. Technol., 35, 602–610, doi: 10.1080/02786820119445, 2001.

Tyrlis, E. and Lelieveld, J.: Aspects of a climatology and dynamics of the summer Etesians., In: EGU General Assembly Conference Abstracts, 14, 2144, [online] Available from: http://adsabs.harvard.edu/abs/2012EGUGA..14.2144T (accessed 11.04.14.), 2012.

von Hessberg, C., von Hessberg, P., Poschl, U., Bilde, M., Nielsen, O. J., and Moortgat, G. K.: Temperature and humidity dependence of secondary organic aerosol yield from the ozonolysis of β-pinene, Atmos. Chem. Phys., 9, 35833599, doi:10.5194/acp-9-3583-2009, 2009.

Wang, H., Easter, R. C., Rasch, P. J., Wang, M., Liu, X., Ghan, S. J., Qian, Y., Yoon, J.-H., Ma, P.-L., and Vinoj, V.: Sensitivity of remote aerosol distributions to representation of cloudaerosol interactions in a global climate model, Geosci. Model Dev., 6, 765–782, doi:10.5194/gmd-6-765-2013, 2013.

Warnke, J., Bandur, R., and Hoffmann, T.: Capillary-HPLC-ESI-MS/MS method for the determination of acidic products from the oxidation of monoterpenes in atmospheric aerosol samples, Analyt. Bioanalyt. Chem., 385, 34–45, doi:10.1007/s00216-006-0340-6, 2006.

Wesely, M.: Parameterization of surface resistances to gaseous dry deposition in regional-scale numerical models, Atmos. Environ., 23, 1293–1304, doi:10.1016/j.atmosenv.2007.10.058, 1989.

Wexler, A. S. and Seinfeld, J. H.: The distribution of ammonium salts among a size and composition dispersed aerosol, Atmos. Environ., 24(5), 1231–1246, doi:10.1016/0960-1686(90)90088-5, 1990.

Witek, M. L., Flatau, P. J., Quinn, P. K., and Westphal, D. L.: Global sea-salt modeling: Results and validation against multicampaign shipboard measurement, J. Geophys. Res., 112, 8215–8229, 2007.

Wolke, R., Hellmuth, O., Knoth, O., Schroder, W., and Heinrich, B.: The chemistry-transport modeling system LMMUSCAT: Description and CityDelta applications. In: Air Pollution Modeling and Its Application XVI (eds C. Borrego and S. Incecik), Proceedings of twenty-sixth NATO/CCMS international technical meeting on air pollution modeling and its applications, Kluver Academic/Plenum Publishers, New York, 2004a.

Wolke, R., Hellmuth, O., Knoth, O., Schroder, W., and Heinrich, B.: The parallel model system LM-MUSCAT for chemistry-transport simulations: Coupling scheme, parallelization and application. In: Parallel Computing: Software Technology, Algorithms, Architectures, and Applications, Elsevier, pp. 363–370, 2004b.

Wong, J. P. S., Lee, A. K. Y., Slowik, J. G., Cziczo, D. J., Leaitch, W. R., Macdonald, A., and Abbatt, J. P. D.: Oxidation of ambient biogenic secondary organic aerosol by hydroxyl radicals: Effects on cloud condensation nuclei activity, Geophys. Res. Lett., 38, 22 805–22 811, doi:10.1029/2011GL04935, 2011.

Woody, M. C., Baker, K. R., Hayes, P. L., Jimenez, J. L., Koo, B., and Pye, H. O. T.: Understanding sources of organic aerosol during CalNex-2010 using the CMAQ-VBS, Atmos. Chem. Phys., 16, 40814100, doi:10.5194/acp-16-4081-2016, 2016.

Xing, L., Fu, T.-M., Cao, J. J., Lee, S. C., Wang, G. H., Ho, K. F., Cheng, M.-C., You, C.-F., and Wang, T. J.: Seasonal and spatial variability of the OM/OC mass ratios and high regional correlation between oxalic acid and zinc in Chinese urban organic aerosols, Atmos. Chem. Phys., 13, 4307–4318, doi:10.5194/acp-13-4307-2013, 2013.

Xu, X., Wang, J., Zeng, J., Spurr, R., Liu, X., Dubovik, O., Li, L., Li, Z., Mishchenko, M., Siniuk, A., and Holben, B.: Retrieval of aerosol microphysical properties from AERONET photopolarimetric measurements. 2: A new research algorithm and case demonstration, J. Geophys. Res., 120, 7079–1098, doi:10.1002/2015JD023113, 2015.

Yang, Q., Gustafson Jr., W. I., Fast, J. D., Wang, H., Easter, R. C., Wang, M., Ghan, S. J., Berg, L. K., Leung, L. R., and Morrison, H.: Impact of natural and anthropogenic aerosols on stratocumulus and precipitation in the Southeast Pacific: a regional modelling study using WRF-Chem, Atmos. Chem. Phys., 12, 8777–8796, doi:10.5194/acp-12-8777-2012, 2012.

Yarwood, G., Rao, S., Yocke, M., and Whitten, G.: Updates to the carbon bond chemical mechanism: CB05. Rep. RT-0400675, p. 246pp, available at http://www.camx.com/files/cb05_final_report_120805.aspx, last access 27 March 2017, 2005.

Zhang, Q., Alfarra, M., Worsnop, D., Allan, J., Coe, H., Canagaratna, M., and Jimenez, J.: Deconvolution and quantification of hydrocarbon-like and oxygenated organic aerosols based on aerosol mass spectrometry., Environ. Sci. Technol., 39, 4938–4952, doi:10.1021/es048568l, 2005a.

Zhang, Q., Worsnop, D., Canagaratna, M., and Jimenez, J.: Hydrocarbon-like and oxygenated organic aerosols in Pittsburgh: insights into sources and processes of organic aerosols., Atmos. Chem. Phys., 5, 3289–3311, doi:10.5194/acp-5-3289-2005, 2005b.

Zhang, R., Khalizov, A. F., Wang, L., Hu, M., and Xu, W.: Nucleation and growth of nanoparticles in the atmosphere, Chem. Rev., 112, 1957–2011, doi:10.1021/cr2001756, 2012.

Zhang, Y., Huang, J.-P., Henze, D. K., and Seinfeld, J. H.: Role of isoprene in secondary organic aerosol formation on a regional scale, J. Geophys. Res., 112, D20207, doi:10.1029/2007JD008675, 2007.

Zhang, Y., Liu, P., Liu, X.-H., Jacobson, M. Z., McMurry, P. H., Yu, F., Yu, S., and Schere, K. L.: A comparative study of nucleation parameterizations: 2. Three-dimensional model application and evaluation, J. Geophys. Res., 115, D20 213, doi:10.1029/2010JD014151, 2010a.

Zhang, Y., McMurry, P. H., Yu, F., and Jacobson, M. Z.: A comparative study of nucleation parameterizations: 1. Examination and evaluation of the formulations, J. Geophys. Res., 115, D20 212, doi:10.1029/2010JD014150, 2010b.

Zhao, Y., Nguyen, N., Presto, A., Hennigan, C., May, A., and Robinson, A.: Intermediate volatility organic compound emissions from on-road diesel vehicles: chemical composition, emission factors, and estimated secondary organic aerosol production., Environ. Sci. Technol., 49, 11 516–11 526, doi:10.1021/acs.est.5b02841, 2015.

Zhao, Y., Nguyen, N., Presto, A., Hennigan, C., May, A., and Robinson, A.: Intermediate volatility organic compound emissions from on-road gasoline vehicles and small off-road gasoline engines., Environ. Sci. Technol., 50, 4554–4563, doi:10.1021/acs.est.5b06247, 2016.

Zhu, S., Sartelet, K., and Seigneur, C.: A size-composition resolved aerosol model for simulating the dynamics of externally mixed particles: SCRAM (v1.0), Geosci. Model Dev., 8, 1595–1612, doi:10.5194/gmd-8-1595-2015, 2015.

Zhu, S., Sartelet, K., Healy, R., and Wenger, J.: Simulation of particle diversity and mixing state over Greater Paris: A model-measurement inter-comparison, Faraday Discuss., 189, 547–566, doi:10.1039/C5FD00175G, 2016.